Using Silicate Mineral Particles for pH Control during *in situ* Bioremediation of Chlorinated Ethene Source Zones

THÈSE N^{O} 5854 (2013)

PRÉSENTÉE LE 13 SEPTEMBRE 2013

À LA FACULTÉ DE L'ENVIRONNEMENT NATUREL, ARCHITECTURAL ET CONSTRUIT
LABORATOIRE DE BIOTECHNOLOGIE ENVIRONNEMENTALE
PROGRAMME DOCTORAL EN ENVIRONNEMENT

ÉCOLE POLYTECHNIQUE FÉDÉRALE DE LAUSANNE

POUR L'OBTENTION DU GRADE DE DOCTEUR ÈS SCIENCES

PAR

Elsa Marina LACROIX

acceptée sur proposition du jury:

Prof. K. Schirmer, présidente du jury
Prof. C. Holliger, Prof. D. A. Barry, directeurs de thèse
Prof. Ph. J. Binning, rapporteur
Prof. T. Kohn, rapporteur
Prof. M. Schroth, rapporteur

ÉCOLE POLYTECHNIQUE
FÉDÉRALE DE LAUSANNE
Suisse
2013

Overview

Résumé

La pollution des sols et des eaux souterraines par les solvants chlorés tels que le trichloroéthylène (TCE) et le perchloroéthylène (PCE) est un problème fréquent dans les pays industrialisés. Les solvants chlorés sont caractérisés par une faible solubilité et une densité supérieure à celle de l'eau. Par conséquent, on les retrouve dans les eaux souterraines sous forme de liquides en phase non-aqueuse, également appelés DNAPL (Dense Non-Aqueous Phase Liquid) qui ont tendance à s'accumuler le long des couches imperméables de l'aquifère. De par leur faible solubilité, les DNAPLs se dissolvent lentement et constituent une source de contamination des eaux qui peut durer pendant des décennies.

Parmi les procédés de traitement des DNAPLs, la bioremédiation *in situ* apparaît comme une alternative prometteuse et économique. Cette technologie utilise l'activité de microorganismes spécialisés capable de transformer les contaminants chlorés en éthène, une molécule non-toxique pour l'environnement. Cette transformation a lieu via un processus anaérobie appelé déhalorepiration. Depuis les années 80, la bioremédiation *in situ* a été appliqué avec succès pour le traitement des panaches de solvants chlorés. En revanche, l'application de cette technologie pour traiter les zones sources (où les polluants sont présents sous forme de DNALP) est relativement récente et s'est principalement développée au cours des 10 dernières années.

Un des problèmes majeurs qui limite l'application de la bioremédiation des zones sources est l'acidification des eaux souterraines, résultant de la déhalorespiration et de la formation d'acides organiques par les bactéries fermentatrices. Les bactéries déhalorespirantes sont inactivées lorsque le pH est inférieur à 5 ou 6. Lorsque la capacité tampon du sol est insuffisante, un apport de matériel tampon est donc nécessaire pour maintenir un pH neutre. La technique habituelle pour contrôler le pH consiste à injecter des solutions contenant un tampon soluble tel que le bicarbonate de sodium. L'inconvénient majeur de ce type de technique est qu'elle requiert de fréquentes injections et une surveillance constante.

Cette thèse a pour objectif de développer une nouvelle méthode pour le contrôle du pH à long-terme. La méthode développée repose sur l'injection dans le sous-sol de tampons solides, constitués de poudre de minéraux silicatés. Les minéraux silicatés présentent des caractéristiques intéressantes en tant qu'agent tampon: leur dissolution est lente en comparaison avec les carbonates et leur vitesse de dissolution ainsi que leur solubilité augmente lorsque le pH devient acide. De plus, ils sont facilement disponibles à bas coût comme matières premières ou résidus de procédés industriels.

Il existe un grand nombre de silicates qui possèdent des caractéristiques très variables en termes de composition, de solubilité et de vitesse de dissolution. Seul certains de ces minéraux présente les caractéristiques adéquates pour être utilisés comme agent tampon. Dans un premier temps, une méthodologie de sélection basé sur des simulations numériques ainsi que sur des considérations cinétiques et thermodynamiques a été développée afin d'identifier les minéraux les plus appropriés. Un modèle géochimique, incluant les principaux processus microbiens ainsi que les phénomènes de dissolution des minéraux a également été développé. Ce modèle constitue un outil utile pour estimer la quantité de minéral nécessaire pour maintenir le pH constant dans la perspective d'une application sur le terrain. Les résultats des simulations ont démontré qu'une dizaine de silicates ont un potentiel

intéressant comme agent tampon. Des expériences en batch réalisé sur cinq minéraux (la nepheline, la fayalite, la forsterite, la diopside et l'andradite) ont permis de valider et d'améliorer le modèle préalablement développé. Ces expériences ont confirmé le potentiel tampon des minéraux sélectionnés et ont également révélé l'importance des précipitations secondaires, un processus qui n'avait pas été inclus dans la première version du modèle. La formation de phase secondaire peut réduire la réactivité des silicates, diminuer la porosité de l'aquifère et entrainer la précipitation de nutriments pour les bactéries. Cette aspect a donc était inclus dans le modèle afin d'être en mesure de prévoir et de limiter ce type de réactions.

L'influence de la dissolution des minéraux silicatés sur les bactéries déhalorespirantes a également été étudiée dans des cultures en batch. Comme prévu par les modélisations, les cinq minéraux (à l'exception de la nepheline) ont permit de maintenir le pH dans la gamme de tolérance pour les trois consortia déhalorespirants testés. Cependant, les résultats ont montré une inhibition des dernières étapes de la déhalorespiration (du *cis*-DCE à l'éthène) en présence des minéraux dans la majorité des expériences. Au regard de ces résultats, il apparait essentiel d'évaluer la compatibilité des minéraux utilisé avec les communautés microbiennes impliqués dans la bioremédiation avant d'envisager leur application sur le terrain.

Par la suite, le potentiel tampon sur le long-terme des trois minéraux les plus prometteurs (la fayalite, la diopside et la forsterite) a été évalué sur le moyen terme (six mois et demi) par des expériences en colonnes à flux continu reproduisant les conditions d'une zone source. Contrairement aux expériences en batchs, la transformation du *cis*-DCE en ethène n'est pas inhibée par la dissolution des minéraux dans ce type de dispositif. Les minéraux appartenant aux groupes des olivines (fayalite et forsterite) ont permis de maintenir un pH constant pendant toute la durée de l'expérience (pH 7.5 pour la forsterite et 6.5 pour la fayalite) et de maintenir l'activité des bactéries déhalorespirantes. En revanche, le potentiel tampon de la diopside a rapidement diminué suite à la formation d'une couche lixiviée peu réactive à la surface du minéral.

Cette thèse a permis de démontrer le potentiel des minéraux silicatés comme agent tampon et de développer une stratégie pour la sélection des minéraux les plus appropriés en fonction des caractéristiques du site contaminé. Cette méthodologie a été testée dans le contexte de la bioremediation *in situ* des solvants chlorés mais peut être appliquée à tout type de technique de remédiation nécessitant des conditions de pH proche de la neutralité.

Mots- clés : acidification des eaux souterraines, bioremediation *in situ*, contrôle du pH, modélisation géochimique, déhalorespiration, minéraux silicatés, solvents chlorés.

Summary

Soil and groundwater pollution by chlorinated solvents such as tricholorethene (TCE) and tetrachloroethene (PCE) is a frequent problem in the industrialized world. Chlorinated solvents, characterized by a low solubility and a density greater than water, form dense non-aqueous phase liquids (DNAPLs) when released in the subsurface. DNAPLs accumulate along low permeability layers and slowly dissolve in groundwater acting as a long-term source of contamination that can last for decades. Remediation of chlorinated solvent DNAPLs is recognized as one of the most challenging problems in the field of environmental remediation. *In situ* bioremediation (ISB) is a promising and cost-effective technology for their removal that relies on the activity of specialized microorganisms able to transform chlorinated compounds to ethene (a non-toxic product) via a stepwise anaerobic process called organohalide respiration (OHR). ISB has been applied successfully for the treatment of dissolved phase plumes since the early 1980's. However, its application for source zones, where contaminants are present as DNAPLs, is relatively recent and has only been developed in the last decade.

One of the major issues limiting source zone ISB is the acidification of the groundwater due to the transformation of chlorinated compounds by organohalide-respiring bacteria (OHRB) and the production of organic acids by fermentative microbial populations. OHRB are inactivated when the pH is below 5-6 and therefore pH buffer amendments are required when the soil buffering capacity is insufficient. In field applications, the most common method used for pH adjustment is the injection of soluble buffers such as sodium bicarbonate. However, this method requires frequent injections and constant monitoring as alkalinity is rapidly consumed. Therefore, there is a need to develop more efficient and long-lasting buffering strategies.

The objective of this thesis was to develop a novel method for long-term control of groundwater pH that relies on the use of ground silicate minerals. Silicate minerals may act as a long-term source of alkalinity release as i) they dissolve slowly compared to carbonates and ii) their dissolution rate and solubility is pH-dependent and increase with acidic pH. In addition, they are easily available at an affordable cost as a raw material or as a by-product of industrial processes.

Silicate minerals are the most common rock forming mineral and constitute a very diverse group with highly variable dissolution rates, solubilities and compositions. Only a restricted numbers of these minerals present appropriate characteristics to act as buffering agents. A screening methodology, based on numerical simulations, thermodynamic and kinetic considerations, was developed to select potential candidates for pH control. A geochemical model including the main microbial processes driving groundwater acidification and silicate mineral dissolution was developed as well. This model provides a useful design tool to estimate the mineral requirement in the perspective of field applications. The results of numerical simulations showed that a dozen silicate minerals have the potential to act as buffering agents.

Abiotic batch experiments were conducted with five silicate minerals (nepheline, fayalite, forsterite, diopside and andradite) to validate and improve the geochemical model. Abiotic experiments

confirmed the buffering potential of these minerals and revealed the importance of secondary precipitation, a process not included in the original formulation of the model. Precipitation of secondary phases can decrease the reactivity of silicates, reduce the aquifer porosity and precipitate nutrients. Therefore, prediction of secondary precipitations was included in the model in order to predict this type of reaction.

The influence of silicate mineral dissolution on OHRB and fermentative bacteria was investigated in batch cultures. As expected, the five silicate minerals (except nepheline) were able to maintain the pH in the tolerance range for the three microbial consortia tested. However, transformation of *cis*-DCE to ethene was completely inhibited in most of the experiments in the presence of minerals. These results showed that compatibility of silicate minerals with the bacterial community involved in *in situ* bioremediation has to be carefully evaluated prior to their use for pH control at a specific site.

Subsequently, the long-term buffering potential of the most promising buffering agents (diopside, fayalite, forsterite) was tested in continuous-flow column studies simulating chloroethene source zone conditions for six and a half month and a half. In contrast to batch experiments, transformation of *cis*-DCE to ethene was not inhibited by mineral dissolution in continuous flow systems. Olivine minerals (such as fayalite and forsterite) appeared as suitable pH buffering agents. They successfully maintained the pH in the neutral range (7.5 for forsterite and 6.5 for fayalite) and sustained the activity of OHRB bacteria. In contrast, the buffering potential of diopside rapidly decreased due to the formation of a less-reactive cation-depleted leached layer at the mineral surface.

This thesis demonstrated the potential of silicate minerals to act as a long-term source of alkalinity release for groundwater pH control. A global strategy for the selection of appropriate buffering agents based on site characteristics was developed. This methodology was applied to the particular case of chlorinated solvent ISB but can be extended to any groundwater remediation technology requiring close to neutral pH conditions.

Keywords: groundwater acidification, *in situ* bioremediation, pH control, geochemical modeling, organohalide respiration, silicate minerals, chlorinated solvents.

List of acronyms

DNAPL: Dense non aqueous phase liquid

CE: Chlorinated ethene

PCE: Tetrachloroethene

TCE: Trichloroethene

DCE: Dichloroethene

VC: Vinyl chloride

PNEC: Predicted non effect concentration

WHO: World Health Organization

USEPA: United States Environment Protection Agency

FOEN: Federal Office for the Environment

ISTT: *In situ* thermal treatment

ISB: *In situ* bioremediation

ERH: Electrical resistance heating

TCH: Thermal conductive heating

OHRB: Organohalide respiring bacteria

OHR: Organohalide respiration

TEAP: Terminal electron acceptor process

TST: Transition state theory

XRF: X-ray fluorescence

BET: Brunauer Emmett Teller

OTU: Operational taxonomic unit

AGW: Artificial groundwater

T-RFLP: Terminal restriction fragment length polymorphism

T-RF: Terminal restriction fragment

PCR: Polymerase chain reaction

DNA: Deoxyribonucleic acid

RNA: Ribonucleic acid

ICP-MS: Inductively coupled plasma mass spectrometry

HPLC: High-performance liquid chromatography

XRD: X-ray diffraction

EDX: Energy-dispersive X-ray spectroscopy

SEM: Scanning electron microscopy

Table of contents

Chapter 1

General introduction

1 General Introduction

1.1 Groundwater contamination with dense non-aqueous phase liquids

1.1.1 General considerations

The water beneath our soil is a valuable resource. Groundwater represents about 96.3 percent of the available freshwater on Earth[1] without taking into account the water accumulated in the form of ice. In Switzerland, about 80% of the water used for drinking and for industry comes from groundwater sources[2]. In the last century, this vital resource has been under pressure due to anthropogenic activities such as agriculture, industrial practices, and urban waste production. As a result, many groundwater reservoirs are now contaminated with a wide variety of chemical compounds. For example, in Europe, approximately 250,000 contaminated sites requiring remediation were identified. It has been estimated that, if the current investigation trends continue, the number of sites needing remediation will increase by 50% by 2025[3]. The environmental and health problems associated with groundwater contamination only started to be recognized in the 1980's. Since then, environmental laws as well as prevention, monitoring and remediation policies have been implemented in industrialized countries in order to limit the impact on aquifers and protect the resource. However, groundwater remediation is a difficult task especially for recalcitrant compounds and research efforts are still needed to develop new remediation techniques and improve existing ones.

1.1.2 Release and migration of dense non-aqueous phase liquids in the subsurface

Soil and groundwater pollution by dense non aqueous phase liquids (DNAPLs) constitutes a persistent and challenging problem in the field of groundwater remediation. DNAPLs are chemicals or mixtures of chemicals characterized by a density greater than water and a low solubility in the aqueous phase (typically hundreds to low thousands of parts per million). Due to these characteristics, when released in the unsaturated or saturated zone, DNAPLs tend to move down vertically in aquifers under the influence of gravity[4]. Because of their low solubility, DNAPLs flow through the saturated zone as a separate liquid phase, until they reach a low-permeable stratum, where a DNAPL pool can be formed. The DNAPL pool can further move laterally in the direction of the lowest point of the low-permeable layer, regardless the direction of groundwater flow. During its vertical migration in the subsurface, a part of the DNAPL gets trapped by capillary forces and forms a discontinuous mass of globules or ganglia[5,6]. This immobile mass of DNAPL is commonly called residual or entrapped DNAPL[7] (see Figure 1.1). The final distribution of the DNAPL in the subsurface is highly heterogeneous and not predictable. It is the result of minute variations in pore size distribution, soil texture, soil structure, and mineralogy. The source zone of a contamination is usually defined as the area in the subsurface where the contaminants are present either in the form of residual or pooled DNAPL.

In practice, except in large releases, DNAPL pools are rarely found and residual DNAPL are the most common form of contamination encountered[8]. DNAPLs immobilized in the subsurface, tend to dissolve slowly in the groundwater and can act as a long-term source of contamination into water or air in the adjacent pores[6,9]. The large contact area between DNAPL and water, especially in residual configuration, increases the amount of contaminants that can be released in the groundwater, forming a plume of dissolved phase contamination.

DNAPLs are widespread. In the United States, the chemicals most commonly encountered belongs to the classes of chlorobenzenes, chloromethanes, polychlorinated biphenyls, halogenated alkanes (tetra- and trichloroethane), halogenated alkenes (tetra- and trichloroethene) and multi component wastes (creosote and coal tar)[8]. Not ordinarily released into the environment as pure chemicals, they are often discharged as a mixture of components containing significant fractions of other organic chemicals, which complicates remediation strategies[4]. In the following sections, the focus will be on the DNAPL containing halogenated alkenes such as tetra- and trichloroethene.

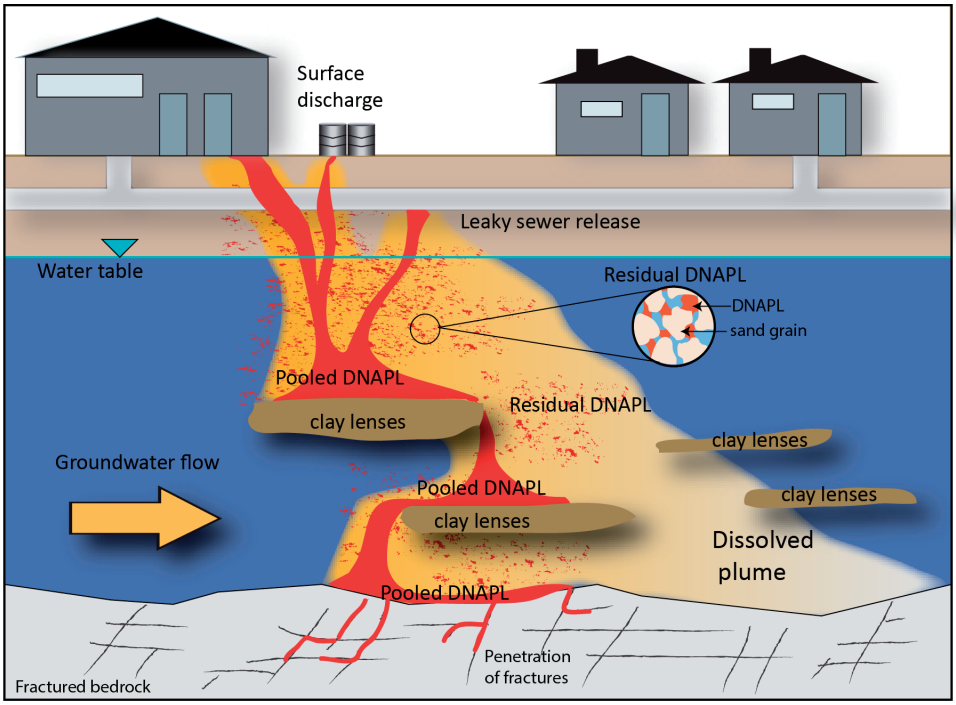

Figure 1.1. Migration of chlorinated solvent DNAPLs in the subsurface following industrial contamination.

1.1.3 Chlorinated ethenes

Chlorinated ethenes (CEs) is a relatively small group of compounds which belongs to the large class of chlorinated hydrocarbons containing both aromatic and aliphatic molecules. CEs include tetrachloroethene (also called perchloroethene, PCE), trichloroethene (TCE), *cis*-1,2 dichloroethene

(*cis*-DCE), *trans*-1,2-dichloroethene (*trans*-DCE), 1,1-dichloroethene (DCE), and vinyl chloride (VC). Higher chlorinated ethenes (PCE and TCE) are generally present in aquifers as a result of spills or poor disposal practices. In contrast, lesser chlorinated ethenes (DCE and VC) are usually encountered as by-products of PCE and TCE biodegradation.

All of these compounds, with the exception of VC, have a density significantly greater than water and tend to form DNAPLs when released in the subsurface[10]. Despite their low solubility in water, dissolution of CE DNAPLs still results in dissolved phase concentrations well above groundwater standards. These compounds are highly toxic and are classified as known or suspected carcinogens[11], therefore their presence in groundwater represents a serious threat for human health and the environment. General physico-chemical properties of CEs are listed in Table 1.1.

Table 1.1. Major physico-chemical properties, ecotoxicological values and drinking water quality standards for chlorinated ethenes.

Chemical	PCE	TCE	1,1-DCE	*cis*-1,2-DCE	*trans*-1,2-DCE	VC
Molecular formula[a]	C_2Cl_4	C_2HCl_3	$C_2H_2Cl_2$	$C_2H_2Cl_2$	$C_2H_2Cl_2$	C_2H_3Cl
Density (g cm^{-3}) at T = 20°C[a]	1.62	1.46	1.21	1.28	1.26	0.91
Solubility (mg l^{-1}) at T = 25°C[a]	150	1100	2500	3500	6300	1600
Koc (mg g^{-1})[b,a]	251	90	65	35	38	8
Vapor pressure at 20°C (Pa)[a]	1900	7960	66500	24000	35300	330000
WHO drinking water guidelines (µg l^{-1})[c]	40	20	30	50	50	0.3
Swiss drinking water guidelines (µg l^{-1})[d]	<1	<1	<1	<1	<1	<1
PNEC (mg l^{-1})[a,e]	0.051	0.115	0.0116	n.d	n.d	0.21

[a] Source: INERIS (http://www.ineris.fr/substances/fr/)

[b] Koc = Soil Organic Carbon-Water Partitioning Coefficient

[c] Source: World Health Organization (http://www.who.int)

[d] Source: Federal Office of the Environment (FOEN), OEaux legislation RS 214.801 (http://www.bafu.admin.ch)

[e] PNEC = Predicted No Effect Concentration

1.1.4 Natural sources of organohalides

Organohalides including chlorinating compounds were long believed to be principally from anthropogenic origin. However, in the past 40 years, the natural occurrence of these molecules in a wide variety of environments has been described. Chlorinated and other halogenated compounds can

be discharged in the environment as a result of biological activities by plants, marine organisms, insects, bacteria or fungi[12]. They are as well produced during geothermic processes such as volcanic eruptions, biomass combustion (firewood) or formation of soils and sediments[13,14]. Recent studies showed that there are more than 3700 organohalogen compounds[15], mainly containing chlorine and bromine, which are naturally produced by biologic or abiotic processes[15,16]. Like many organohalides, CEs can also originate from natural sources: PCE and TCE are formed during volcano activities[12,14] or can be produced by marine micro- and macro-algae[17] while VC can form during abiotic reaction of organic matter in terrestrial soils[18].

1.1.5 Industrial production and uses of chlorinated ethenes

CEs are inflammable as well as apolar compounds, making them excellent degreasing solvents. Thanks to their properties, they have been widely used in industrialized countries since the 1930's in various industrial applications mainly as dry cleaning agent and metal degreaser[10]. Today, PCE is mainly used as a raw material in the chemical synthesis of fluoride hydrocarbons (66% of the production in 2005 in the United States), in textile dry cleaning (12%), as aerosol products for the automotive industry (12%) and as metal cleaning or degreasing agents (8%)[19]. TCE is also widely used as an intermediate for fluorinated hydrocarbons production (73%) and as a metal degreaser in various industrial applications such as metal processing, electronics, printing, paper and textile industries (24%)[20].

1.1.6 Groundwater contamination by chlorinated ethenes, a significant problem in industrialized countries

Widespread industrial use of chlorinated solvents together with poor handling practices over the last century has resulted in extensive contamination of groundwater by these pollutants[21,22]. CEs can enter the groundwater due to careless storage and disposal, deliberate dumping, accidental spillages or leaching following disposal in poorly constructed landfills. Most releases of CEs in the environment occurred between the 1930's and the 1970's, when the potential health effects of CEs were not fully understood and major environmental laws and regulations were yet to be implemented[10]. As a result, PCE and TCE are nowadays among the most frequently encountered organic chemicals in groundwater of industrialized countries[23-26].

According to a survey of the US Environment Protection Agency (USEPA), during the period from 1998 to 2001, total on- and off-site releases of PCE and TCE averaged about 1,820 and 5,000 tons, respectively[27]. These two compounds are among the 29 contaminants most commonly found at USEPA Superfund sites (environmental program established to address abandoned hazardous waste sites). Dry cleaning factories represent an important source of CEs contamination: A recent survey performed by the United State Dry Cleaner Program estimated that 75% of dry cleaner facilities have

caused soil and groundwater contamination by chlorinated solvents[28]. A similar situation exists in Europe. For instance, in Switzerland, the Federal Office for the Environment (FOEN) estimates that around 4,000 sites are contaminated with CEs (http://www.bafu.admin.ch). Similarly, in France, the BASOL database lists 836 sites containing halogenated solvents which are subject to management plans to prevent environmental and health risks (BASOL 2013, http://basol.environnement.gouv.fr).

1.2 Remediation of chlorinated ethenes DNAPLs in groundwater

It is generally accepted that remediation of sites contaminated with DNAPLs presents one of the biggest challenges in the field of environmental remediation[7,29,30]. The characteristics of the DNAPLs (active spreading, slow dissolution in the groundwater and unpredictable migration) make them extremely difficult to localize and quantify using conventional techniques and even more difficult to recover. Traditional approaches such as groundwater pump and treat or soil vapor extraction have been ineffective in reducing contaminant concentrations to regulatory end points[7,31-33]. In the past, containment was often the only solution available to minimize further contamination of the groundwater by DNAPL[7]. However, since the 1990's, a number of innovative technologies have been developed to remediate CEs source zones[29,34]. Each of these methods have their own potential and limitations (for a detailed review see Stroo et al.[29]). Promising technologies for source zone remediation include *in situ* thermal treatment (ISTT), *in situ* chemical oxidation (ISCO), surfactant and co-solvent flushing and *in situ* bioremediation (ISB)[7,29,34]. In the following sections, the principle, advantages and limitations of these techniques are briefly discussed. It is therefore important to consider that, thus far, no perfect solutions were found for DNAPL remediation. At many sites, even aggressive treatment leaves some residual contamination[35-37] and typical criteria required for closure are rarely achieved[38]. A comparison of field performance for these different technologies is given in Figure 1.2.

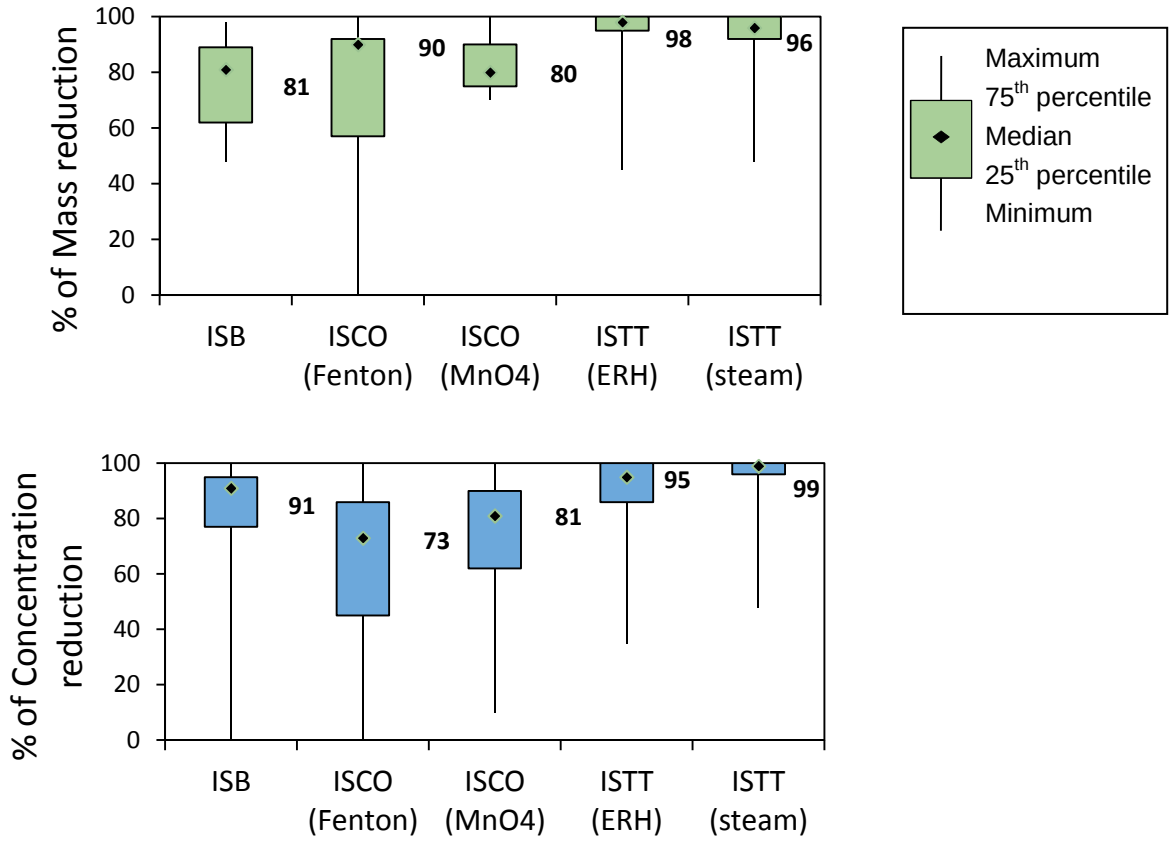

Figure 1.2. Field scale performance of major source zone remediation technologies. Median values, percentiles and range are shown for each technology. ERH refers to electrical resistance heating. Adapted from Stroo et al.[29]

1.2.1 *In situ* thermal treatment

In situ thermal treatment (ISTT) techniques include steam injection, electrical resistance heating (ERH) and thermal conductive heating (TCH)[7,29,34]. All the aforementioned technologies enhance extraction of contaminants through volatilization and desorption by increasing the temperature in the contaminated zone. These treatments have to be coupled with a vapor extraction system above the ground, to recover the toxic vapors.

ISTT has been rapidly adopted as a source zone remediation technology[29]. Although it can be effective with a median reduction in total chloroethenes concentration of roughly 95%[39], it is more expensive and energy-demanding than most other *in situ* technologies[36,40]. In addition, technical limitations exist such as the retention of some fraction material in low-permeability zone of the aquifer[41] and inefficient removal due to the cooling effect (rapid groundwater flux in portion of the subsurface decreases the temperature and hindered volatilization of the contaminants). Other concerns arise from the potential of DNAPL mobilization under the effect of temperature and the risk of extension of the pollution outside the contaminated zone[42].

1.2.2 *In situ* chemical oxidation

In situ chemical oxidation (ISCO) is an aggressive remediation strategy that typically involves the injection of chemical oxidants that chemically convert contaminants to nonhazardous or less toxic compounds through redox reactions. The most commonly used oxidants are potassium permanganate, Fenton's catalyzed hydrogen peroxide, ozone, and sodium persulfate[7,29,34].

ISCO appeared as an attractive technology because it offers fast destruction of the contaminants and do not require aboveground treatment[29]. However complete removal is rarely reached and field applications have produced mixed results[43,44]. A recent survey by Krembs et al. (2010) on 223 chlorinated solvents contaminated sites undergoing ISCO found that drinking water quality standard concentrations were not achieved at any site where DNAPL was present, still alternative clean-up level and site closure were attained for some sites[45]. These difficulties in the application of ISCO for DNAPL can be attributed to several factors such as i) the difficulty of the oxidant compounds to reach low permeability zone of the subsurface due to the short life-time of these molecules, ii) the loss in permeability due to manganese oxide (MnO_2) precipitation when permanganate is used as oxidant, and iii) the release of sorbed contaminants following oxidation of natural organic matter[46].

1.2.3 Surfactant and co-solvent flushing technology

In situ chemical flushing involves the injection and subsequent extraction of chemicals to solubilize and/or mobilize DNAPLs. These chemicals can be co-solvents (e.g., alcohols) or aqueous surfactant solutions. Both act by decreasing the interfacial tension between DNAPL and the chemical flood. Once extracted, the mixture of DNAPL and flushing chemicals needs to be treated above ground and either disposed or returned in the subsurface[7].

Although very effective at a laboratory scale, field applications of this technology have given mixed results[47-49]. One of the main drawbacks is the need for above ground treatment, i.e., recycling and disposable of the extracted fluids, which can be problematic and costly. In addition, technical limitations exist such as the risk of flow by-passing, which limits the total recovery of the DNAPL[29]. The possibility of downward migration of the solubilized plume or the mobilized DNAPL before its extraction[34] is also a potential problem. For all these reasons, recent studies proposed to adopt surfactant and co-solvent flushing combined with other remediation techniques rather than as a primary source zone treatment technology[50,51].

1.2.4 *In situ* bioremediation

1.2.4.1 Definition

ISB refers in general to the use of biological activity to transform contaminants into non harmful products. In the particular case of CEs contaminated sites, ISB relies on the activity of specialized

microorganisms, called organohalide-respiring bacteria (OHRB) that are able to transform chlorinated solvents like PCE and TCE to ethene, a non-toxic volatile product harmless for the environment. This transformation occurs via an anaerobic process called organohalide respiration (OHR) in which OHRB gain energy from the reduction of CEs[22,52]. Details concerning fundamental aspects of OHR as well as organohalide-respiring microorganisms are provided in the section 1.3.

OHR can occur naturally at contaminated sites if the OHRB are present and active in the subsurface. The remediation of contaminants without human intervention is known as natural attenuation. However, this process does not occur at all sites and, when it does, degradation rates are typically low and may not be adequate to reach site closure in a suitable timeframe[10]. To overcome this limitation, engineered ISB schemes were developed in order to optimize conditions promoting microbial degradation. In general, ISB refers to two processes called biostimulation and bioaugmentation. Biostimulation consists of the injection of an electron donor in the subsurface (usually an organic substrate), in order to establish favorable redox conditions and stimulate microbial activity[7,10,53]. Different substrate types can be used such as soluble substrates (pentanol, lactate, propionate, butyrate and oleate)[54-57], slow-release substrates (vegetable oil, emulsified vegetable oil and polylactate ester)[56,58], and solid substrates (mulch and compost)[59]. When the native microbial community at a site does not have the potential to perform complete biodegradation of the contaminants, bioaugmentation, i.e., injection of active microorganisms with the desired biochemical potential in the subsurface, can be implemented.

1.2.4.2 Application of in situ bioremediation to chlorinated ethenes source zone

ISB has been applied successfully for the treatment of dissolved phase plumes since the early 1980's[53]. Application of ISB for source zones is relatively new and has only been developed in the last decade[29]. It has long been believed that ISB was not suitable for DNAPL removal because OHRB would not be able to thrive at high concentrations of CEs typically found in source zones. However, at the end of the 1990's, several studies contradicted this belief, showing that OHRB were active at close-to-saturation PCE concentrations[60-66]. In addition, it has been shown that microbial activity in the vicinity of chlorinated solvent DNAPLs has the potential to enhance DNAPL dissolution[62,66-73]. In the last decade, ISB has been applied at many contaminated field sites containing chlorinated solvent DNAPLs (for a review of case studies see ITRC[74]). A synthesis of performance data performed by Stroo et al.[29] showed that ISB is as effective as other injection-based technologies with a median reduction in CE concentration of 91% (see Figure 1.2).

1.2.4.3 Coupling in situ bioremediation with other more aggressive remediation techniques

Application of ISB alone might not be sufficient at some sites to reach regulatory objectives, for instance at sites with large accumulation of free-phase DNAPL[10]. However, the combination of ISB with other more aggressive technologies appears as an attractive solution[51,59]. Recent studies proposed

to use ISB as a "polishing" step for transforming remaining contaminant mass after application of physico-chemical technologies[75-77]. A comprehensive review on laboratory and field studies supporting the development of such combined strategies was done by Christ et al. (2005)[34]. The results suggest that, if favorable conditions are present, combined strategies can reduce source longevity by as much as an order of magnitude. ISB can be combined with ISTT[78], co-solvent/surfactant flushing[50,79] as well as ISCO[80]. In all these cases, positive synergies have to be considered, for instance, the use of co-solvents as an electron donor. It is also important to evaluate and avoid possible negative effects of other technologies on bioremediation such as sterilization of the subsurface and changes in geochemical conditions like redox and pH[10]. So far, there has been limited research on the potential of combined remediation techniques[19,23], however it seems that surfactant and co-solvent flushing appears to be the most promising treatment for combination with ISB[19].

1.2.4.4 Strengths and limitations of in situ bioremediation for CEs DNAPL remediation

In general, it is recognized that ISB is relatively slow but can be effective, less expensive and less energy demanding than other technologies described above[29]. Another advantage of ISB is that it does not require above-ground treatment of waste such as ISTT or flushing technology because all the contaminants are degraded *in situ*[10]. ISB has a potential for treating low-permeability zones containing residual concentrations. The clean-up of these zones is extremely challenging with other technologies that mostly treat the most transmissive zones. In contrast, with ISB, certain electron donors (such as vegetable oil) can persist and diffuse into the less permeable material over time[39,81,82].

However, the application of ISB for source zone remediation still presents limitations. First, it might not be appropriate for all sites since it is recognized that sites with large accumulation of pooled DNAPL cannot be treated efficiently with ISB[10]. In addition, because ISB is a relatively slow process, it might also not be the best option at sites that require rapid treatment[10]. Another problem associated with ISB are the undesirable side effects on groundwater quality such as increase of biochemical or chemical oxygen demand, increase in dissolved metals, groundwater acidification, methane and hydrogen sulfide generation, and accumulation of carcinogenic intermediate products such as VC[10,29,83]. Although these effects need to be considered carefully, in general, changes in groundwater quality dissipate with time and distance and rarely limit the use of ISB[10,84].

1.3 Biological degradation of CEs

The potential for biological degradation of CEs has been discovered in the early 1980's when environmental problems posed by chlorinated solvents started to be recognized[85]. CEs can be biologically degraded using co-metabolic or metabolic pathways. In co-metabolism reactions, CEs are degraded by fortuitous interactions with enzymes and cofactors (such as vitamin B12, or cofactor F430[86]) produced by the bacteria for other metabolic purposes[85]. Co-metabolic degradation of CEs by

methanogens[87-89], sulfate reducing bacteria[90,91] and homoacetogens[92] was discovered in the 1980's. This process yields very low transformation rates and is nowadays considered as an ubiquitous but inefficient mechanism for CE biodegradation[85] (for a comprehensive review on co-metabolism degradation of CEs see El Fantroussi et al.[89]).

Metabolic degradation of CE can occur through oxidative or reductive processes. Metabolic oxidation refers to the use of CEs as a carbon and energy source. During the oxidation process, CEs are used as electron donors and are converted to CO_2. However, only less chlorinated ethenes (VC and *cis*-DCE) can undergo metabolic oxidation[21]. Oxidation of CEs can occur under both aerobic[93] or anaerobic conditions[94] (for an extensive review on biological oxidation of CE see Bradley and Chapelle[85] and Mattes et al.[95]).

Metabolic reduction of CEs refers to organohalide respiration, a process where CEs are used by bacteria as a terminal electron acceptor for electron transport-based energy conservation under anaerobic conditions[96]. Unlike oxidative processes, OHR can reduce all chlorinated ethenes including PCE and TCE. The discovery of organohalide respiration of CEs was a major breakthrough in the development of ISB. Discovered in the 1990's, bacteria which use OHR rapidly appeared as promising agents for the bioremediation of contaminated sites for the following reasons: (i) their degradation rates are much faster than those encountered during co-metabolism, (ii) they are active under anoxic conditions typically found in the subsurface and (iii) some of them can catalyze the complete transformation from PCE to ethene[91,95,97,98]. OHR is described more in detail in the next section.

1.3.1 Organohalide respiration pathway

During organohalide respiration, PCE is sequentially reduced to TCE, *cis*-DCE (or *trans*-DCE and 1,1-DCE) , VC and the final product ethene. At each reaction step, a chlorine atom is replaced by a hydrogen atom producing hydrochloridric acid as by-product[99] (see Figure 1.3 for the OHR pathway). Among DCE isomers formed during OHR, *cis*-DCE is more prevalent than 1,1-DCE[100].

The first evidence of bacteria able to perform OHR under strict anaerobic conditions was presented by Holliger et al.[101]. This dechlorinating organism, later designated *Dehalobacter restrictus*[102], was able to grow by reduction of PCE and TCE to *cis*-DCE using H_2 as an electron donor. In the 1990's, a number of other organohalide pure cultures able to use CE as electron acceptors were identified[97,101,103-108]. These bacteria belong to many different phyla, such as the *Firmicutes*, *Chloroflexi*, ε- and δ-*Proteobacteria*. All of these microorganisms differ in their electron acceptor and electron donor requirements. Regarding this aspect, OHRB can be classified into two groups; the first one includes versatile microorganisms able to use a broad range of compounds as electron acceptors and electron donors. This group, referred as facultative OHRB, includes isolates that belong to the genera *Anaeromyxobacter*, *Desulfitobacterium*, *Sulfurospirillum*, *Desulfomonile*, *Desulfuromonas*, *Desulfovibrio* and *Geobacter*[22,109]. The second group, called obligate OHRB, contains specialized

bacteria such as *Dehalococcoides* and *Dehalobacter* spp. that strictly require a organohalide compound to gain energy and can only use H_2 as an electron donor[109]. For reviews on the characterization of all the aforementioned OHRB see Smidt and de Vos[109] and Holliger et al.[110].

According to current knowledge, members of *Dehalococcoides* genera are the only microorganism able to drive complete dechlorination of PCE to the non toxic ethene while the OHRB belonging to other genera are only able to reduce PCE to *cis*-DCE[22,95,109]. For this reason, *Dehalococcoides* has been the most studied OHRB and much effort was devoted to understanding its metabolism and to determine its substrate spectrum. *Dehalococcoides ethenogenes mccartyi*[111] was the first identified pure culture able to perform the full transformation of PCE to ethene. However, only the first three steps are metabolic (i.e., energy yielding) while the final dechlorination of VC to ethene is a slow co-metabolic process, leading to transient accumulation of the highly toxic intermediate VC[97,112]. Recently, other isolates able to gain energy from VC dechlorination were identified but they were not able to grow on higher chlorinated compounds. For instance, strain BAV 1 can metabolically reduce *cis*-DCE and VC to ethene but dechlorinates PCE and TCE only cometabolically[113] while strain GT can transform TCE to ethene but cannot grow on PCE[114] (see Figure 1.3). The presence of *Dehalococcoides* has important implications for the application of ISB at chlorinated solvent contaminated sites. Several studies highlighted the correlation between the presence of these bacteria (detected by amplification of the 16S rRNA gene) and the presence of VC and ethene at PCE and TCE contaminated sites[115]. Therefore, the absence of these microorganisms appears as one of the explanations for the incomplete transformation of PCE observed at many sites [116].

However, recent studies suggested than other organohalide respiring microorganisms could be involved in the dechlorination of DCE and VC. For instance, Shani[117] showed the correlation between VC and bacteria closely affiliated to uncultured bacteria of the "Lahn Cluster" at a PCE contaminated site and suggested that members of this cluster might be involved in the reduction of lower CEs. Flynn et al.[118] and Rouzeau-Szynalski[119] showed that *Dehalococcoides* were not detected in an enrichment culture that produced ethene. Rousseau-Szinalski[119] proposed that the phylum *Chloroflexi* might contain other, still unidentified, OHRB able to transform CEs to ethene.

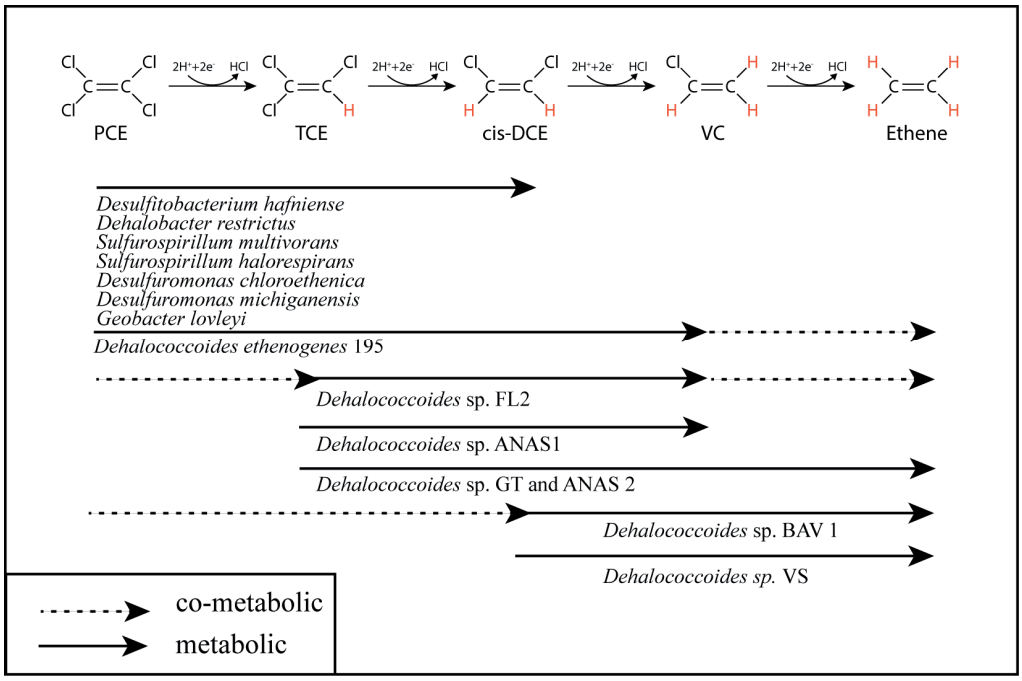

Figure 1.3. Organohalide respiration pathway and organohalide-respiring bacteria. Adapted from Futagami et al.[120].

1.3.2 Environmental factors influencing organohalide respiration

Many environmental factors influence microbial activity of OHRB bacteria. In 2006, Aulenta et al. [22] published a detailed review on this subject. In the following sections, only environmental parameters that are relevant to source zone ISB will be discussed, i.e., high CEs concentrations, redox conditions and pH.

1.3.2.1 Influence of high PCE concentrations

In the past, the potential of ISB for DNAPL removal has been neglected as close to saturation concentrations of chlorinated solvents were believed to be toxic for OHRB[22]. In the last two decades, several laboratory studies contradicted this assumption. However, the potential to tolerate high PCE concentrations differs significantly among OHRB species. Studies showed that pure cultures of *Dehalobacter restrictus*[101], *Desulfuromonas chloroethenica*[105] and *Sulfurospirilum multivorans*[106] were relatively sensitive to high PCE concentrations with an inhibition of PCE dechlorination at concentrations above 0.2, 0.1 and 0.16 mmol l^{-1}, respectively. In contrast, other strains were reported to be able to dechlorinate PCE at saturation (e.g., at about 0.9 mmol l^{-1}) such as *Desulfitobacterium* strain Y51[121], *Enterobacter agglomerans* strain MS-1[107] and *Desulfuromonas michiganensis*[122]. In addition, several mixed cultures were also found to be able to tolerate such conditions[60-62]. Although dechlorination of PCE does occur at high concentrations, dechlorination of *cis*-DCE in presence of high PCE concentrations is more problematic. Indeed, several authors reported inhibition of the transformation of *cis*-DCE to VC and ethene at high PCE concentrations[62,69,123].

1.3.2.2 Influence of redox conditions

It has long been recognized that OHR of CEs occurs under anaerobic conditions (characterized by oxygen concentration below 0.1-0.5 mg l^{-1})[85]. Anaerobic redox conditions are usually further specified and named according to the inorganic compound that acts as a predominant electron acceptor in a given part of the aquifer. Common anaerobic redox conditions in an aquifer, from the less to the more reduced, include nitrate reducing, iron and manganese reducing, sulfate reducing, and methanogenic conditions[124].

A relationship were established between the number of chlorine atoms attached to the ethene backbone of a given CE and the *in situ* redox conditions under which its transformation through OHR is favored. For instance, PCE commonly undergoes conversion to TCE when oxygen has been depleted (under nitrate and iron reducing conditions) while reductive dechlorination of TCE to *cis*-DCE occurs under iron reducing conditions and in more strongly reducing environment[125]. Reduction of *cis*-DCE to VC is generally associated with sulfate reducing and methanogenic conditions[96,125]. Finally, the last step of dechlorination, from VC to ethene, appears to be favored under highly reducing methanogenic conditions[96].

1.3.2.3 Influence of pH

The issue of groundwater acidification encountered during CE bioremediation (discussed in detail in section 1.4) is of particular concern because OHRB, like many other microorganisms, are very sensitive to pH. Several studies investigated the influence of pH on PCE dechlorination rates of pure cultures of OHRB. The results, synthesized in Table 1.2, show that the optimum pH is usually found within the near neutral range, between 6.5 and 7.5 pH units[101,105,106,108,121,122,126-128]. The range of pH tolerance differs among bacterial strains but is overall quite restricted with no PCE dechlorination observed below pH 6 and above pH 9.5. In contrast, mixed cultures appear to tolerate a wider range of pH, especially in the acidic range[129,130]. To date, only a few studies have investigated the influence of pH on PCE dechlorination rates by OHRB consortia. In these studies, the minimum pH at which PCE dechlorination was observed varied from pH 4 to 5.5[129-131]. Although, these studies did not investigate the influence pH exerts on each step of the dechlorination pathway, practitioner knowledge suggests that the transformation of *cis*-DCE to ethene is more sensitive to pH than that for higher chlorinated compounds[132]. It seems that complete dechlorination to ethene do occurs within a pH range between pH 6 and 8.3.

Li[133] investigated the adaptation of a commercial OHRB culture (KB-1™) to acidic conditions by exposure of the consortia to a low pH medium for an extended period of time. After this treatment, the "adapted" culture was able to completely transform VC to ethene at pH 5.7 suggesting that adaptation to acidic conditions might be possible to some extent. Under field conditions, microorganisms seem to be able to adapt to mildly acidic conditions. Indeed, PCE dechlorination and presence of members of

the genus *Dehalococcoides* were observed in moderately acidic groundwater having an average pH of 5[73,134]. However, degradation rates are expected to be much lower under such conditions. In field site applications, it is usually recognized that the pH should be between 5 and 9 to ensure efficient implementation of ISB scheme[53].

Table 1.2. Optimal pH and pH range for OHRB activity.

Bacterial strain	Optimal pH	pH range	Reference
Sulfurospirillum multivorans	7.3-7.6	6.0-8.5	Scholz-Muramatsu et al.[106]; Neumann et al.[126]
Desulfuromonas michiganensis BB1	7.0-7.5	6.8–8.0	Sung et al.[122]
Desulfuromonas chloroethenica	7.4	6.5-7.4	Krumholz[105]
Desulfitobacterium sp. strain Y51	6.5-7.5	6.0-9.5	Suyama et al.[121]
Desulfitobacterium sp. strain PCE1	7.2	6.0-8.8	Gerritse et al.[108]
Desulfitobacterium dehalogenans JW/IU-DC1	7.5	6.0-9.0	Utkin et al.[127]
Dehalobacter restrictus	7.0-7.6	6.5-8.0	Holliger et al.[101]
Desulfomonile tiedjei DCB-1	6.8-7.0	6.5-7.8	DeWeerd et al.[128]
Mixed PCE dechlorinating culture	7.0	4.0-9.5	Zhuang and Pavlostathis[129]
Mixed culture containing *Dehalococcoides*	7.5	5.5-9.5	Ise et al.[131]
Mixed cultures containing *Dehalococcoides*	6.0-6.5	5.1-9.0	Vainberg et al.[130]

1.3.3 OHRB and their interactions with other microbial guilds

ISB in aquifers is a complex microbially mediated process. An understanding of synergistic and competing interactions between OHRB and other microbial guilds present in the aquifer is very important to implement successful ISB schemes. Most known OHRB require hydrogen (H_2) and/or acetate as an electron donor for OHR[135]. Some populations are strictly hydrogenotrophic such as members of *Dehalococcoides*[97] and *Dehalobacter*[102]. *Desulfuromonas* can use acetate but not H_2[105] while other populations are more versatile and can use a variety of electron such as pyruvate, lactate or formate.

As complete dechlorination to ethene can mainly be catalyzed by the strictly hydrogenotrophic *Dehalococcoides* population, H_2 levels appear as key element in the control of ISB[136-138]. The main source of H_2 in groundwater comes from the fermentation of complex organic substrates. Therefore, OHRB depend on the presence and activity of fermentative microbial guilds capable of converting complex substrates into H_2 and acetate. Because of the oligotrophic nature of many groundwater systems, the availability of organic substrates may be limiting under natural conditions and subsurface injection of electron donor is generally required to enhance bacterial activity[22].

However, addition of fermentable substrates may also stimulate the activity of other hydrogenotrophic microorganisms that compete with OHRB for hydrogen such as nitrate-, manganese-, iron-, and sulfate-reducers, as well as methanogens and homoacetogens. The affinity for hydrogen of each of these microbial guilds strongly influences the result of the competition between them. OHRB are characterized by a high affinity for H_2, i.e., a threshold for H_2 utilization lower than 0.9 nM for PCE degradation. Therefore, when the H_2 concentration is low, they can outcompete methanogens and homoacetogens that present higher H_2 thresholds[57,136-138] (see Table 1.3). Based on these observations, significant research efforts were done to control H_2 level in order to minimize competition by methanogens and homoacetogens. One method that gave successful results is the utilization of electron donors that slowly deliver low concentrations of H_2. Slowly fermenting sources of H_2 include electron donors such as polylactate esters, vegetable oil, chitin, wood chips, peat or mulch[56,139-141].

The competition between OHRB, sulfate reducers and iron reducers is more problematic because all these microorganisms are able to thrive at similar H_2 levels[53,142-144]. The effect of sulfate on dechlorination has been the subject of many studies that yielded contradictory results on whether sulfate reduction inhibits PCE dechlorination. Concerning competition with iron reduction, Shani (2013)[145] showed that, at a PCE contaminated site, the competition of iron reducing bacteria with OHRB might have resulted in accumulation of VC. Indeed, the hydrogen threshold for VC reduction is supposed to be higher than the threshold for iron reduction[124] (see Table 1.3).

Thus far, the effect of terminal electron acceptor processes (TEAPs) in the context of source zone DNAPL has not yet been investigated in detail. Several studies on bio-enhanced dissolution of DNAPL by OHRB suggest that methanogens and acetogens are inhibited by high concentrations of CEs[62]. However, another study by Yang and McCarty[56] reported methanogenic activity in a column containing PCE DNAPL suggesting that, within the aquifer, methanogens can colonize niches where PCE concentrations are lower.

Table 1.3. Hydrogen thresholds for each hydrogenotrophic microbial process. Adapted from Luitjen et al.[146].

Process	Hydrogen threshold (nM)
Acetogenesis	>350
Methanogenesis	5-100
Sulfate reduction	1-10
Nitrate reduction	<0.05
Manganese reduction	<0.05
Iron reduction	0.1-0.8
PCE and TCE reduction	0.6-0.9
cis-DCE reduction	0.1-2.5
VC reduction	2-24

1.4 Groundwater acidification during *in situ* bioremediation

One of the major side effects related to ISB of chlorinated solvent source zones is the decrease of groundwater pH. This phenomenon is more likely to occur during remediation of DNAPL due to the larger mass of contaminants present compared with dilute plumes, decrease of pH during PCE degradation has been observed both in laboratory[63,66,71] and field studies. In 2004, a survey conducted by Parsons Corporation[53] investigated the pH changes before and after clean up at 50 chlorinated solvents contaminated sites undergoing ISB. They reported a drop of pH in nearly all the sites after clean up, with most of the values ranging from 5.5 to 7. In about 10 sites, the groundwater pH was lower than 5 and in one case a pH of 3 was observed.

1.4.1 Processes controlling groundwater acidification

Different processes such as mineral dissolution, secondary precipitation and microbial activity influence groundwater pH in the context of chlorinated solvents ISB[147,148] (see Figure 1.4). The two main microbial processes responsible for groundwater acidification are OHR and fermentation of organic substrates[53,63,147-149]. During OHR, each mole of PCE transformed to ethene releases four moles of hydrochloric acid. Fermentation of organic substrates produces acidic products such as CO_2, acetate, and other organic acids. However, acidity produced by fermentation is dependent on the electron donor used, since each of them produces different amounts of acidic products per mole of H_2[147]. Table 1.4 presents the fermentation reactions of the most common electron donors. McCarty et al. (2007) proposed to use sodium formate (HCOONa) as the electron donor to minimize acidification because its fermentation produces sodium bicarbonate, which participates in acidity neutralization[147] and does not produce acetic acid (see Table 1.4).

Table 1.4. Fermentation reactions for common electron donors used in biostimulation (adapted from Robinson et al.[148]).

Electron donor	Fermentation reaction
Linoleic acid	$C_{18}H_{32}O_2 + 16\ H_2O = 14\ H_2 + 9\ CH_3COOH$
Sodium Lactate	$CH_3CHOHCOONa + 2\ H_2O = 2\ H_2 + CH_3COOH + NaHCO_3$
Glucose	$C_6H_{12}O_6 + 2\ H_2O = 4\ H_2 + 2\ CH_3COOH + 2\ CO_2$
Sodium butyrate	$CH_3CH_2CH_2COONa + 2\ H_2O = 2\ H_2 + CH_3COOH + CH3COONa$
Methanol	$CH_3OH + H_2O = 3\ H_2 + CO_2$
Ethanol	$CH_3CH_2OH + H_2O = 2\ H_2 + CH_3COOH$
Sodium formate	$HCOONa + H_2O = NaHCO_3 + H_2$

Competing terminal electron acceptor processes (TEAPs), especially iron and sulfate reduction, also influence groundwater pH both directly and indirectly[148]. Because TEAPs compete with OHR for H_2, they increase the electron donor demand and thus the acidity generated by the production of acetate and CO_2. On the other hand, TEAPs can also increase the alkalinity by releasing hydroxide ions:

Iron reduction $2\ FeOOH_{(s)} + H_2 = 2\ Fe^{2+} + 4\ OH^-$

Sulfate reduction $SO_4^{2-} + 4\ H_2 = H_2S + 2\ OH^- + 2\ H_2O$

Finally, mineral dissolution and precipitation play also an important role in groundwater alkalinity. In natural environments, carbonate minerals are typically the main source of alkalinity in groundwater. In sediments without carbonate, silicate minerals also have the potential to increase groundwater alkalinity, however, because their dissolution is slow compared to carbonate, silicate aquifers are more sensitive towards acidification[150]. Simulations performed by Robinson et al.[148] revealed that, in the timescale of ISB, iron oxide reduction, gypsum and calcite dissolution are the main crystalline processes likely to influence pH.

Only a few detailed studies on the mechanisms controlling groundwater pH during ISB were carried out. McCarty et al. (2007) theoretically evaluated the influence of electron donors and initial groundwater alkalinity on the extent of acidification during ISB[147]. Robinson et al.[148] and Robinson and Barry[151] developed a comprehensive batch geochemical model to estimate the amount of buffer required depending on specific site-conditions. This model, called BUCHLORAC, includes the influence of groundwater composition, TEAPs, site mineralogy as well as gas release. More recently, Brovelli et al.[152] developed a simplified mechanistic model to predict groundwater acidity under field conditions. This model includes, in addition to microbial and geochemical processes, the influence of water flow and subsurface mixing.

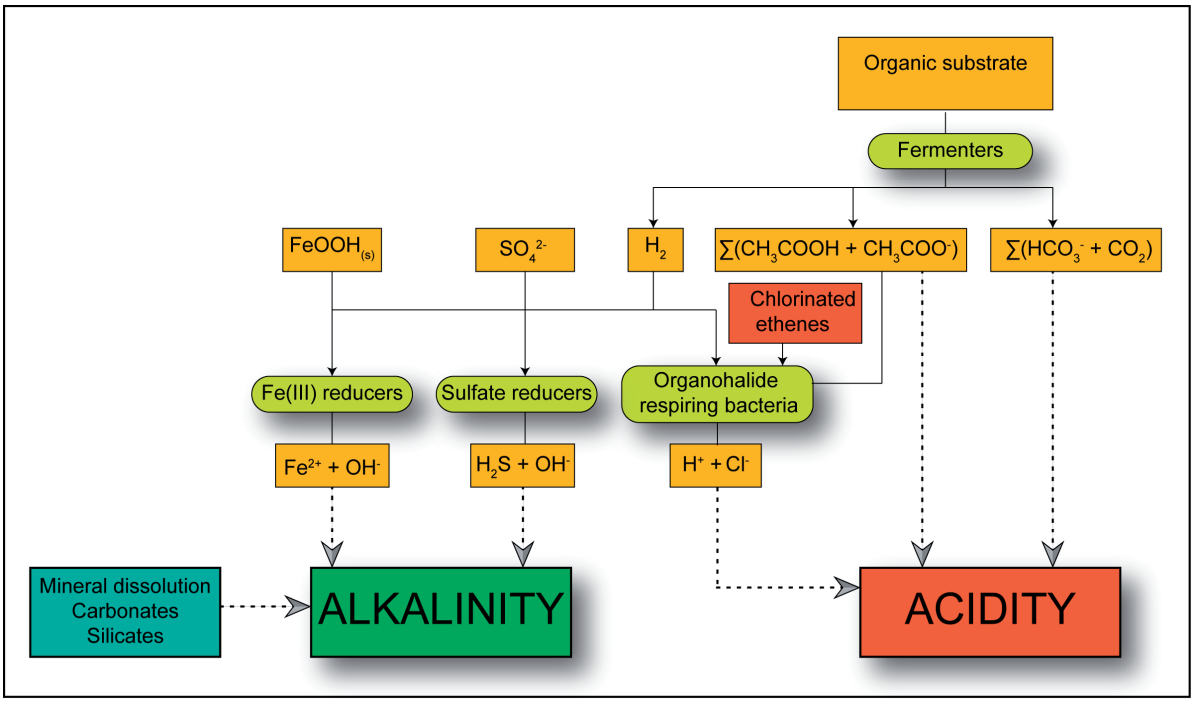

Figure 1.4. Schematic view of the main processes influencing groundwater pH during *in situ* bioremediation of chlorinated ethenes. Adapted from Robinson et al.[148].

1.4.2 Existing pH control strategies

Different methods were developed for raising the pH during ISB. Currently, the most common one is the injection of soluble buffer solutions such as sodium or potassium bicarbonate through the treatment zone[53,147,153]. However, injection of soluble buffers, although effective, has generally only a short term effect because advective groundwater flow quickly removes soluble compounds. Consequently continuous reinjection is required to maintain a neutral pH over time. To overcome this limitation, insoluble solid buffers containing either calcium carbonate (Neutral Zone™ by Remediation and Natural Attenuation Services, Inc.) or magnesium hydroxide particles (AquaBufpH™ by EOS Remediation Products, Inc.) were developed[154]. One possible drawback of using calcium carbonate is the resulting increase in HCO_3^- concentration that can potentially enhance methanogenic and homoacetogenic activities and therefore can increase electron donor demand[155].

Several studies also suggested that increasing the flow rate in the aquifer reduces the acidification problem[152,156]. For this method, the model developed by Brovelli et al.[152] provides a useful tool to determine the optimal pumping rate in order to avoid acidification and to keep the electron donor within the treatment zone.

Laboratory and modeling studies investigated the use of macro-capsules containing KH_2PO_4 buffer encapsulated in a pH-sensitive polymer to control groundwater pH[157-159]. Aelion et al.[158] carried out a field trial to assess the potential of this method to increase the pH within a coal pile runoff acidic

contaminant plume. Although the pH rapidly increased from 3 to 6, the macro-capsules failed to maintain the pH in the neutral range on the long-term and a return to initial acidic conditions was observed after 10 days. Most of these methods require frequent intervention and monitoring, therefore there is a need for developing new long-term pH control strategies for *in situ* remediation of groundwater.

1.5 Potential of silicate minerals for pH control during *in situ* bioremediation

In this thesis, the potential of using silicate mineral powder as a long term source of buffering capacity was investigated. The following sections describe the principal characteristics of these minerals, the mechanism of their dissolution, and their potential for acidity neutralization.

1.5.1 Definition of silicate minerals

Silicate minerals are composed of silica tetrahedrals (SiO_4^{4-}) that are interconnected by interstitial cations such as Ca^{2+}, Fe^{2+}, Fe^{3+}, K^+, Mg^{2+} or Al^{3+}. They represent the most important group of rock-forming minerals and constitute around 95% of the Earth's crust[84]. To date, approximately 600 different silicate minerals have been identified. The most common ones in rock formation belong to the groups of feldspars, amphiboles, pyroxenes, micas, olivines, feldspathoids and zeolites[84].

An important distinction exists between primary and secondary minerals. Primary silicate minerals, such as quartz, pyroxenes or plagioclase formed in igneous and metamorphic rock during the original solidification (or crystallization) of the rock. In contrast, secondary minerals formed at a later period as a result of the weathering of primary minerals. Secondary minerals include clay minerals (such as kaolinite and montmorillonite).

1.5.2 Weathering of silicate minerals in the environment

In natural environments, weathering of silicate minerals is a slow process, still it is recognized as the main source of pH buffering in soil without carbonate minerals[150]. In the last few decades, silicate mineral weathering received much attention because of its role in the global carbon cycle, where this process acts as a sink for CO_2[160]. An increasing number of studies that aimed to understand silicate mineral dissolution and precipitation were carried out in the context of geological sequestration of CO_2[161,162]. The dissolution of primary silicate minerals is generally slow and kinetically controlled[150] and can be either congruent or incongruent. Congruent dissolution means that the ratio of elements appearing in the solution is the same from the ratio in the mineral, i.e., the dissolution is stoichiometric. However, most primary silicate minerals show incongruent dissolution where the element ratio in solution differs from the ratio in the mineral. This type of dissolution is often the result of secondary mineral precipitation or selective dissolution of some weakly bonded constituents of the mineral[150,163].

Silicate minerals present large differences in their dissolution kinetics depending on their crystalline structure, chemical composition and the temperature at which they were formed. In general, minerals that form at the highest temperatures in the soil are the ones that are the more rapidly altered, i.e., which have the fastest dissolution rates. Olivine and Ca-plagioclase are considered as the fastest dissolving minerals while quartz is the most resistant to weathering[164]. Dissolution rates can vary by as much as six orders of magnitude between the fastest and slowest dissolving minerals.

1.5.3 Environmental factors influencing silicate minerals dissolution

Dissolution kinetics of silicate minerals can be described in the framework of the transition state theory (TST)[160]. According to the TST, dissolution rates are controlled by chemical reactions occurring at the surface of dissolving minerals or close to the surface, in the so-called leached layer. Reactants combine to form an activated complex, which break down to form products that enter the solution. The overall rate of the reaction is proportional to the concentration of the activated complexes that in turn is proportional to the product of the reactant concentrations in solution (or ion activity product)[165]. In addition, the overall dissolution rate is a function of temperature, pH, ionic strength and the presence of chelating ligands. Among these parameters, pH and temperature have the greatest influence.

The influence of pH on silicate dissolution rates has been intensively studied for a wide range of minerals. For a detailed review on this topic see Palandri and Kharaka[166]. Regarding the pH dependence, three types of behavior were identified. The dissolution rate of many silicates including feldspar[167,168], muscovite[169] and kaolinite[170] presents a minimum at neutral pH and increases with acidic and basic conditions. Other minerals such as diopside[171] and wollastonite[172] have a maximum rate at acidic pH, which decreases monotonically with increasing pH to pH 12. In the third group of minerals, the dissolution rate increases in the acidic range but remains constant in the basic range. Such behavior has been reported for augite dissolution by Lartigue[173].

Mineral dissolution rates increase as well with temperature and can vary by several orders of magnitude over a 100°C temperature range[174 175]. The temperature dependence of the dissolution rate constants is described empirically by the Arrhenius equation $k = Ae^{-EaRT}$, where k is the dissolution rate constant, A is a pre-exponential frequency factor, E_a is the activation energy, R is the gas constant, and T is the absolute temperature[176].

The effect of ionic strength differs depending on the minerals considered. At neutral to acidic pH, increasing ionic strength increases the dissolution rate of silica[177], quartz[178] and forsterite[179]. In contrast, feldspar dissolution decreases with increasing ionic strength[180]. However, the effect of ionic strength remains negligible compared to the effect of pH for the range of ionic strengths commonly found in groundwater systems[177,179]. The presence of organic acids, such as oxalic, citric or succinic acid can also enhance silicate minerals dissolution as demonstrated by several authors[181-184].

1.5.4 Utilization of silicate minerals for pH control in environmental applications.

It has long been recognized that chemical weathering of silicate minerals has the potential to neutralize acidity. During dissolution, protons are consumed and dissolved species, which contribute to the alkalinity of water, are released[165]. However, only limited studies investigated the potential of silicate minerals to act as acid neutralizing agents for remediation purposes. Kleiv et al.[185] investigated buffering capacities of silicate tailing materials composed of K-feldspar and nepheline from the mining industry. Their results demonstrated that silicate tailing materials present a relatively large buffering capacity. The authors concluded that the use of these minerals as a geochemical barrier might represent a promising alternative. Likens et al.[186] conducted an experiment to evaluate the buffering potential of wollastonite, a calcium silicate mineral, in an anthropogenically acidified stream. They found that wollastonite was highly effective in raising the pH and increasing the acid neutralizing capacity. Another study by Fernandez-Caliani et al.[187] demonstrated that wollastonite might be useful in attenuation of acidity and metal contamination for acid mine drainage. These results suggest that the use of silicate minerals as acid neutralizing agents is a promising technology but additional studies are required to assess the acid neutralization potential of silicate minerals in the context of source zone ISB.

1.6 Objectives and approaches of the thesis

To date, one of the reasons hindering efficient application of ISB at chlorinated solvent source zones is the development of acidic conditions following fermentation of organic substrates and CEs OHR. In this thesis, a new strategy for long-term control of groundwater pH was developed. The potential of suspensions of silicate mineral particles to act as a long-term source of alkalinity release for *in situ* bioremediation was investigated through modeling simulations and experimental work. Silicate minerals appear as promising candidates for pH control due to their kinetic and thermodynamic characteristics: i) their dissolution rate is strongly pH dependent, that is, minerals dissolve faster in acidic conditions, and ii) the solubility is also pH dependent with higher solubility at low pH and limited solubility at neutral and basic pH. These properties allow a more rapid return to nearly neutral conditions while dechlorination is taking place, and increase their lifetime when the groundwater pH is in the neutral range. In the natural environment, silicate dissolution is a slow process, however in an engineered design, reactivity of silicate minerals can be augmented by increasing the reactive surface of particles, i.e., by decreasing the particle size.

In **Chapter 2**, a screening methodology based on thermodynamic considerations and numerical simulations was developed to rank silicate minerals according to their buffering efficiency. A batch geochemical model including microbial processes, groundwater speciation and mineral dissolution was developed. This model was used as a tool to evaluate the buffering capacity of the silicates under various conditions, to understand which criteria are significant in the choice of a buffering agent and to

estimate the quantity of mineral needed according to site conditions. In **Chapter 3**, batch abiotic dissolution experiments were performed with five silicate minerals in order to validate the geochemical model developed previously. The importance of secondary precipitation during abiotic dissolution was revealed as important side process and included in the model. In **Chapter 4**, the interactions between activity of various organohalide-respiring consortia and silicate minerals dissolution were evaluated through batch microcosm experiments. The silicate minerals tested were able to maintain the pH in the tolerance range for the OHRB, however mineral dissolution partially inhibited *cis*-DCE transformation. The influence of pH on microbial community composition and the organohalide respiration rates of each step of the OHR pathway was also evaluated for several OHRB consortia. **Chapter 5** presented the result of a flow-through column study that investigated the long-term buffering capacity of three silicate minerals in porous medium during OHR at high PCE concentrations. The impact of the presence of minerals on the final microbial community repartition along the column was determined. Results showed that the mineral forsterite was efficient at maintaining a neutral pH for more than 6 months and was able to sustain the activity of *Dehalococcoides* bacteria. Finally, in **Chapter 6**, considerations for application and design of this pH control strategy at field scale are discussed.

Chapter 2

Choice of suitable silicate minerals: Screening methodology and modeling approach

2 Choice of suitable silicate minerals: Screening methodology and modeling approach

This chapter was previously published as **Lacroix, E., Brovelli, A., Holliger, C. & Barry, D. A.** Evaluation of silicate minerals for pH control during bioremediation: Application to chlorinated solvents. *Water, Air and Soil Pollution* **223**, 2663-2684, (2012).

Abstract

Accurate control of groundwater pH is of critical importance for *in situ* biological treatment of chlorinated solvents. This study evaluated a novel approach for buffering subsurface pH that relies on the use of silicate minerals as a long-term source of alkalinity. A screening methodology based on thermodynamic considerations and numerical simulations was developed to rank silicate minerals according to their buffering efficiency. A geochemical model including the main microbial processes driving groundwater acidification and silicate mineral dissolution was developed. Kinetic and thermodynamic data for silicate minerals dissolution were compiled. Results indicated that eight minerals (nepheline, fayalite, glaucophane, lizardite, grossular, almandine, cordierite and andradite) could potentially be used as buffering agents for the case considered. A sensitivity analysis was conducted to identify the dominant model parameters and processes. This showed that accurate characterization of mineral kinetic rate constants and solubility are crucial for reliable prediction of the acid-neutralizing capacity. In addition, the model can be used as a design tool to estimate the amount of mineral (total mass and specific surface area) required in field applications.

2.1 Introduction

Groundwater acidification of contaminated sites is a relatively frequent problem. The pH decrease can result from microbial processes[22,53], presence of chemicals (like phenols or acid pesticides) and oxidative dissolution of sulfidic minerals, such as pyrite. Acidification is observed when the natural buffering capacity of ambient groundwater and soil is exceeded[147,148]. Acidity buildup is of particular concern for *in situ* remediation processes such as bioremediation, chemical oxidation and reduction, and *in situ* mobilization-stabilization[148,188,189]. For example, if the pH is too low reaction rates may be reduced or the solubility of the target chemical may be too high or too low. Consequently, the application of such techniques is enhanced by implementation of efficient pH-control strategies.

In situ bioremediation of chlorinated ethenes (CEs) is very sensitive to this issue[63,71,147]. CEs such as perchloroethylene (PCE) and trichloroethylene (TCE) are amongst the most frequently encountered subsurface contaminants due to their extensive use as dry cleaning and metal degreasing agents in many industrial processes[190]. CEs are persistent in the environment and constitute a source of groundwater contamination that may last for decades[53,147]. Enhanced *in situ* anaerobic bioremediation is a promising method to speed up their removal. It involves the stimulation of specialized anaerobic microorganisms that use chlorinated solvents as electron acceptors for energy metabolism through organohalide respiration[56,62]. Stimulation of microbial activity is achieved by delivering an organic substrate into the subsurface, which is fermented to hydrogen, after which it is available as an electron donor for organohalide-respiring bacteria (OHRB)[53]. Organic substrate fermentation and organohalide respiration are both acid-producing processes, the extent of which is directly controlled by the amount of substrate and CEs transformed[53,63,68,149]. For this reason, source zone treatment is more susceptible to acidification than enhanced natural attenuation of dilute plumes due to the larger mass of CEs available[22,148].

Acidic conditions limit microbial degradation due to the inactivation of anaerobic bacteria at low pH. Pure strains of dehalogenating bacteria have a range of pH tolerance between 6 - 6.5 and 8 - 9.5 depending on the bacterial strain[101,105,106,121,122,126], while consortia are slightly more tolerant with a maximum pH range of 4 - 9[130,191]. Fermenting bacteria exhibit a similar behavior with complete inhibition around pH 4 to 5[192,193].

For field applications, the most common methods to control the pH decrease include the circulation of a solution containing dissolved alkaline materials (such as sodium or potassium bicarbonate) in the treatment zone[53,148,194] and the use of water injections to dilute the substrate and the acidity[152]. Constant addition of buffering agent requires frequent injections as alkalinity is rapidly consumed, which probably increases operation costs. In addition, in aquifers with significant concentrations of Ca^{2+}, addition of bicarbonate may lead to precipitation of calcite at neutral pH[195], which hinders further treatment.

The aim of this work was to assess the feasibility of an alternative strategy for pH control, which relies on the use of silicate minerals. Silicate minerals are the most common rock-forming mineral and their weathering is the predominant buffering mechanism in sediments with negligible carbonate content[150]. The dissolution of silicates is accompanied by a release of alkali cations (such as K^+, Na^+, and Mg^{2+}) and by consumption of protons. Both processes can increase groundwater pH. Silicate minerals are appealing buffering agents as

- Dissolution is slow compared with carbonates, and therefore they are long-term sources of alkalinity[150];
- The dissolution rate is pH-dependent, that is, minerals dissolve faster in acidic conditions[160,196]. This enhances their efficacy, as it allows a more rapid return to nearly neutral conditions while dechlorination is taking place, and increases their lifetime when the groundwater pH is in the neutral range;
- The solubility is also pH-dependent with a higher solubility at acidic pH and limited solubility at neutral pH.

In other words, when acidity is produced, minerals dissolve until a near-neutral pH is reached, then dissolution reduces due to thermodynamic constraints. This prevents the increase of groundwater pH in the alkaline range, which is as unfavorable to OHRB as low pH.

Only a limited number of studies evaluated the potential of silicate minerals as acid-neutralizing agents for water remediation. Silicate minerals resulting from industrial processes such as glass and ceramic production were considered, which contained sodium and potassium feldspars, nepheline and wollastonite[185-187]. In all cases, significant buffering capacity was observed and it was concluded that these materials can be used to mitigate water acidity and precipitate/stabilize heavy metals both in the soil[185] and streams[186,187], resulting, for example, from acid mine drainage leaching. The studies conducted so far are, however, limited in the number of minerals and geochemical conditions considered. The objective of this study was to consider a larger spectrum of silicate minerals for acid neutralization than previous work. To this end, a screening methodology for the selection of the most suitable minerals was developed. The methodology was applied to the specific case of *in situ* bioremediation of chlorinated solvents, but can be extended to any decontamination technology requiring near-neutral pH conditions.

2.2 Methods

Silicate dissolution is primarily a surface process, and its dissolution rate depends on the available specific reactive surface area[150,160,196]. Silicate minerals have different thermodynamic and kinetic characteristics and their dissolution rates vary over several orders of magnitude[160]. The methodology used to identify silicate minerals for pH control in the context of *in situ* bioremediation consists of three steps, (i) identification of silicate mineral kinetic parameters, (ii) pre-selection based on

thermodynamic considerations and (iii) numerical simulations to quantify and compare the buffering efficiency of the selected minerals.

A list of 20 silicate minerals was established (Table 2.1) and used as the starting point for the application of the screening methodology described in this work. These minerals were selected because (i) detailed studies on their dissolution kinetics were available in the literature, and (ii) their thermodynamic parameters (solubility constant and enthalpy change) were available and tabulated in existing geochemical databases. To limit the number of numerical simulations, silicate minerals with low reactivity, i.e., a slow dissolution rate in the acidic range (rate constant < 10^{-12} mol m^{-2} s^{-1}) were excluded from the list.

2.2.1 Identification of kinetic parameters

The first step consisted in determining the values of key parameters for mineral dissolution modeling, i.e., thermodynamic and kinetic parameters. Thermodynamic parameters – such as solubility constant K_{eq} and standard enthalpy change of the reaction at 25°C ΔH – can normally be found in thermodynamic databases such as THERMODDEM[197] and MINTEQA2[198] (Table 2.1), whereas kinetic rates were not readily available. For a given temperature and at conditions far from equilibrium, the dissolution rate of most silicates can be expressed by the empirical rate law[196]:

$$r = k_{H^+}\left(10^{-pH}\right)^{n_{H^+}} + k_W + k_{OH^-}\left(10^{-pH}\right)^{-n_{OH^-}} \quad (2.1)$$

where r (mol m^{-2} s^{-1}) is the dissolution rate, k_H^+, k_W and k_{OH}^- (mol m^{-2} s^{-1}) are the rate constants for the acidic, neutral and alkaline ranges, and n_H^+ and n_{OH}^- are the reaction order of proton- and hydroxyl-promoted dissolution. Accurate determination of k_{H+}, k_W, k_{OH-}, n_{H+} and n_{OH-} is critical for geochemical modeling. In order to estimate these values, published data from mineral dissolution experiments were fitted with Eq. 2.1.

For each mineral, two datasets taken from the literature were considered. Only experiments conducted in similar conditions were adopted, i.e., measurements from flow-through reactors, far from equilibrium conditions and at a temperature of 25°C. Moreover, only experiments where steady state conditions were achieved were considered. The estimated parameters (Table 2.2) were compared with those reported by Palandri and Kharaka[166].

Table 2.1. Dissolution reactions and thermodynamic parameters of the selected silicate minerals.

Silicate mineral	Dissolution reaction	Log K_{eq} (T = 25°C) [a]	ΔH [J mol^{-1}] [a]
Albite	$NaAlSi_3O_8 + 4H^+ + 4H_2O = Al^{3+} + Na^+ + 3H_4SiO_4$	4.14	-95 623
Almandine	$Fe_3Al_2Si_3O_{12} + 12H^+ = 2Al^{3+} + 3Fe^{2+} + 3H_4SiO_4$	42.16	-465 683
Andradite	$Ca_3Fe_2Si_3O_{12} + 10H^+ + H_2O = 3Ca^{2+} + 2Fe^{3+} + 3H_4SiO_4$	16.79	-137 101
Anorthite	$Ca(Al_2Si_2)O_8 + 8H^+ = 2Al^{3+} + Ca^{2+} + 2H_4SiO_4$	25.31	-314 358
Chlorite	$Mg_5Al_2Si_3O_{10}(OH)_8 + 16H^+ = 5Mg^{2+} + 2Al^{3+} + 3H_4SiO_4 + 6H_2O$	68.38[b]	-634 275[b]
Cordierite	$Mg_2Al_3(AlSi_5)O_{18} + 16H^+ + 2H_2O = 4Al^{3+} + 2Mg^{2+} + 5H_4SiO_4$	49.41	-660 411
Diopside	$CaMg(SiO_3)_2 + 4H^+ + 2H_2O = Ca^{2+} + Mg^{2+} + 2H_4SiO_4$	21.73	-158 241
Enstatite	$MgSiO_3 + 2H^+ + H_2O = Mg^{2+} + H_4SiO_4$	11.83	-95 552
Fayalite	$Fe_2SiO_4 + 4H^+ = 2Fe^{2+} + H_4SiO_4$	19.02	-159 491
Forsterite	$Mg_2SiO_4 + 4H^+ = 2Mg^{2+} + H_4SiO_4$	28.60	-219 449
Glaucophane	$Na_2(Mg_3Al_2)Si_8O_{22}(OH)_2 + 14H^+ + 8H_2O = 2Al^{3+} + 3Mg^{2+} + 2Na^+ + 8H_4SiO_4$	36.99	-397 394
Grossular	$Ca_3Al_2Si_3O_{12} + 12H^+ = 2Al^{3+} + 3Ca^{2+} + 3H_4SiO_4$	49.36	-449 383
Jadeite	$NaAl(SiO_3)_2 + 4H^+ + 2H_2O = Al^{3+} + Na^+ + 2H_4SiO_4$	7.55	-100 168
Leucite	$KAlSi_2O_6 + 2H_2O + 4H^+ = 2H_4SiO_4 + Al^{3+} + K^+$	6.42 [c]	-92 465[c]
Lizardite	$Mg_3Si_2O_5(OH)_4 + 6H^+ = 3Mg^{2+} + H_2O + 2H_4SiO_4$	32.56	-245 718
Nepheline	$Na(AlSi)O_4 + 4H^+ = Al^{3+} + Na^+ + H_4SiO_4$	14.07	-146 839
Riebeckite	$Na_2(Fe_3Fe_2)Si_8O_{22}(OH)_2 + 14H^+ + 8H2O = 3Fe^{2+} + 2Fe^{3+} + 2Na^+ + 8H_4SiO_4$	-7.81	-18 281
Spodumene	$LiAlSi_2O_6 + 4H^+ = Al^{3+} + Li^+ + 2H_2O + 2SiO_2$	6.99 [d]	-89 181[d]
Tremolite	$(Ca_2Mg_5)Si_8O_{22}(OH)_2 + 14H^+ + 8H_2O = 2Ca^{2+} + 5Mg^{2+} + 8H_4SiO_4$	67.25	-520 914
Wollastonite	$CaSiO_3 + 2H^+ + H_2O = Ca^{2+} + H_4SiO_4$	14.02	-88 220

[a] from THERMODDEM database[197] except where indicated otherwise

[b] from PHREEQC database[199]

[c] from MINTEQA2 database[198]

[d] from LLNL database[200]

Table 2.2. Dissolution rate kinetic parameters of selected silicate minerals obtained by fitting Eq. 2.1 to literature datasets.

Mineral	Acid mechanism		Neutral mechanism	Basic mechanism		Reference of datasets
	Log k_{H^+}	n_{H^+}	Log k_W	Log k_{OH^-}	n_{OH^-}	
	log (mol m^{-2} s^{-1})		log (mol m^{-2} s^{-1})	log (mol m^{-2} s^{-1})		
Albite	-11, -10.16	0.457, 1	-12.4, -12.56	-16.3, -15.6	-0.5,-0.57	Chou and Wollast[201], Knauss and Wolery[167]
Almandine	-5.2	1	-10.7	-13.71	-0.35	Sverdrup[202]
Andradite	-5.2	1	-10.7	-	-	Sverdrup[202]
Chlorite	-10.9,-9.79	0.25, 0.49	-13	-16.79	-0.43	Brandt et al.[209], Lowson[210]
Cordierite	-3.8	1	-11.2	-	-	Sverdrup[202]
Diopside	-8.88, -9.46	0.28,0.41	-11.21, -11.01	-	-	Knauss et al.[174], Golubev et al.[211]
Enstatite	-8.98, -9.02	0.24, 0.6	-12.72	-	-	Schott and Berner[212], Oelkers and Schott[213]
Fayalite	-5.9, -4.8	0.69, 1	-9.5	-	-	Sverdrup[206], Wogelius and Walther[214]
Forsterite	-6.78, -6.70	0.37, 0.74	-10.7, -10.1	-	-	Pokrovsky and Schott[215], Golubev et al.[211]
Glaucophane	-5.6	0.7	-10.1	-	-	Sverdrup[202]
Grossular	-5.1	1	-10.7	-	-	Sverdrup[202]
Jadeite	-8.82, -6	0.7, 0.72	-12, -9.5	-14	-0.3	Sverdrup[206], Hamilton et al.[216]
Leucite	-6	0.7	-9.2	-	-	Sverdrup[202]
Lizardite	-5.7	0.8	-12.4	-	-	Sverdrup[202]
Nepheline	-3.47	0.97	-8.61	-	-	Tole et al.[203]
Riebeckite	-7.7	0.7	-12.2	-	-	Sverdrup[202]
Spodumene	-4.6	0.7	-9.3	-	-	Sverdrup[202]
Tremolite	-11.9, -8.4	0, 0.7	-12.5, -10.6	-	-	Mast and Drever[218], Sverdrup[206]
Wollastonite	-8.72,-7.13	0, 0.28	-	-	-	Weissbart and Rimstidt[166], Golubev et al[211]

2.2.2 Mineral screening based on thermodynamic considerations

Of the 20 silicate minerals selected, a first screening was performed considering solubility. This property depends on the solubility constant, K_{eq}, and on the ion activity product, which is related to proton activity and therefore to pH. The dependency of solubility upon pH is illustrated in Figure 2.1 for five minerals (forsterite, wollastonite, nepheline, fayalite and andradite). Solubility is high in the acidic range and decreases by several orders of magnitude with increasing pH. The relationship, however, differs among minerals. For pH control in the context of *in situ* CE bioremediation, a good buffering agent should have high solubility in the acidic range (pH 4-6) and low solubility in the neutral-basic range (pH 7-9). High solubility for acidic conditions results in a rapid return to neutral conditions while low solubility at high pH (> 7) prevents excessive basification of the groundwater. Solubility in pure water of the 20 selected minerals was computed at pH 5 and pH 8 at a temperature of 20°C using the geochemical code PHREEQC-2 [199] and solubility constants from the MINTEQA2, THERMODDEM and LLNL thermodynamic databases (provided with PHREEQC-2). Minerals with low solubility at pH 5 (< 1 mmol l^{-1}) were excluded from the selection as they do not provide sufficient acid-neutralizing potential. Similarly, minerals with high solubility at pH 8 (above 10 mmol l^{-1}) were excluded, as they are likely to overshoot pH.

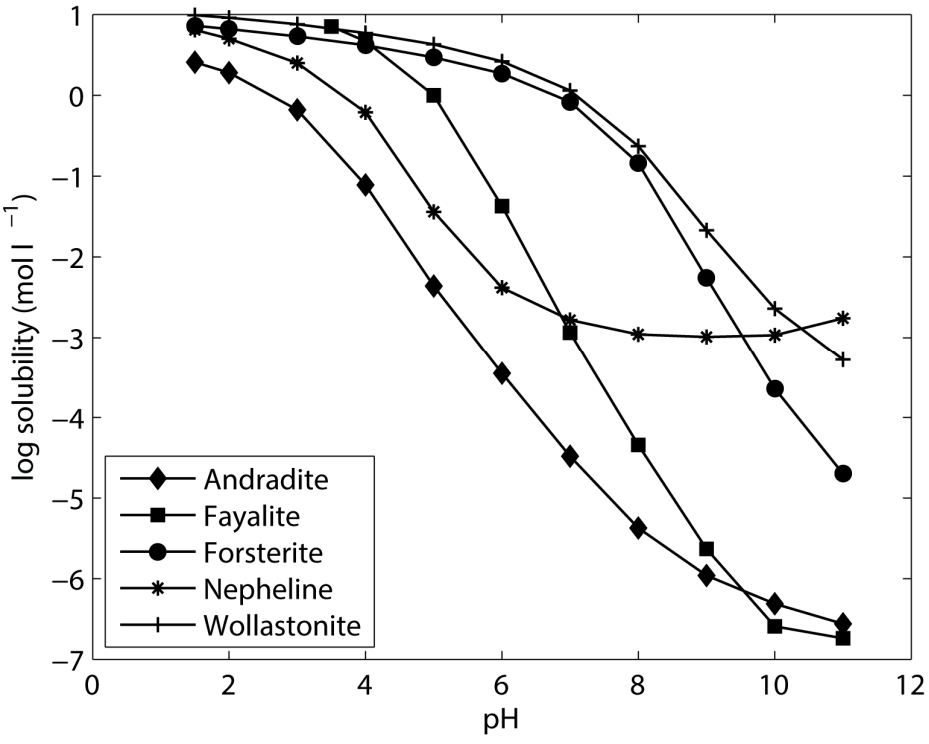

Figure 2.1. Influence of pH on solubility of five silicate minerals (andradite, fayalite, forsterite, nepheline and wollastonite). For all these minerals, solubility decreases with increasing pH.

2.2.3 Numerical model

In order to estimate the acid-neutralization potential of silicate minerals, a batch numerical model was implemented using PHREEQC-2. The model included all relevant acid and alkalinity associated reactions occurring in chlorinated solvent-contaminated aquifers undergoing *in situ* bioremediation, i.e., mineral dissolution, microbial processes and chemical speciation. The model was run in batch mode to simulate a well-stirred reactor. In this work, transport was neglected as it was assumed that groundwater residence time is large compared to the time scale of geochemical and microbial reactions.

2.2.3.1 Acid-generating processes

Two microbial processes are primarily responsible for groundwater acidification during CE bioremediation: fermentation of the soluble organic substrate and organohalide respiration[147,148]. In most *in situ* bioremediation schemes, dissolved hydrogen gas, the electron donor for OHRB, is delivered through fermentation of an organic substrate such as sodium lactate or linoleic acid,

$$\text{Organic substrate} + w H_2O = x CH_3COOH + y H_2 + z CO_2. \quad (2.2)$$

The right-hand side of this equation lists the fermentation products, i.e., hydrogen, acetic acid and carbon dioxide. The stoichiometric coefficients (*w*, *x*, *y*, *z*) are specific to the organic substrate used[147,148,204].

Not all hydrogen produced by fermentation is directed to organohalide respiration, as OHRB must compete with other microbial guilds. In CE source zones, sulfate and iron (III) are the two predominant competing terminal electron acceptors[53,205]. The fraction of hydrogen directed to OHRB not only depends on the amount of iron oxides and sulfate present in the groundwater[53], but also on microbial populations and specific field conditions and is therefore difficult to estimate precisely [103,206]. Following Robinson et al.[148] and Robinson and Barry[151] our model assumes that sulfate and iron oxide are present in excess in the system, and that a fraction f_{min} of hydrogen produced by fermentation is used by OHRB.

Organohalide respiration, i.e., reduction of PCE to ethene is modeled as a sequential reaction involving four steps,

PCE → TCE $\quad C_2Cl_4 + H_2 = C_2HCl_3 + HCl, \quad (2.3)$

TCE → DCE $\quad C_2HCl_3 + H_2 = C_2H_2Cl_2 + HCl, \quad (2.4)$

DCE → VC $\quad C_2H_2Cl_2 + H_2 = C_2H_3Cl + HCl, \quad (2.5)$

VC → Ethene $\quad C_2H_3Cl + H_2 = C_2H_4 + HCl, \quad (2.6)$

where PCE stands for perchloroethylene, TCE for tetrachloroethylene, DCE for dichloroethene and VC for vinyl chloride. If the reaction completes, for each mole of PCE degraded four moles of hydrochloric acid are produced. The goal of the model is to simulate the rate at which acidity is produced and not all complex microbial processes. Therefore, in order to simplify the model and reduce the computational burden, the fermentation rate wa not simulated directly. Instead, the fermentation reaction is combined with organohalide respiration to give the following overall dechlorination stoichiometry for each chloroethene[148]:

$$\text{Organic substrate} + \frac{w}{y\, f_{min}}\text{H}_2\text{O} + \text{CE}_\text{i} = \text{HCl} + \text{CE}_\text{j} + \frac{x}{y\, f_{min}}\text{CH}_3\text{COOH} + \frac{(1-f_{min})}{f_{min}}\text{H}_2 + \frac{z}{y\, f_{min}}\text{CO}_2, \quad (2.7)$$

where CE_i and CE_j are the parent and daughter CEs, respectively.

The following assumptions were made regarding the fermentative and organohalide respiring bacterial guilds:

1. Fermentation is inhibited by high level of hydrogen, as shown by Fennel and Gosset[55]. The fermentation rate is, therefore, controlled by hydrogen consumption by organohalide respiration and by other anaerobic respiration processes;
2. Acetate is not used as an electron donor. Robinson et al.[148] demonstrated that acetate utilization as an electron donor lowers the overall acidity produced, so this represents the worst case in terms of acidity production;
3. The concentration of fermentative biomass is high and remains constant;
4. The impact of pH on microbial activity is similar for fermentative biomass and OHRB;
5. Sufficient organic substrate is provided to ensure complete transformation of the PCE to ethene;
6. The organic substrate dissolution rate exceeds its fermentation rate.

Organohalide respiration rates were modeled using Monod-type kinetic equations including competitive and Haldane inhibition[60,207]. The degradation rate of each chloroethene was computed as

$$R_{\text{PCE reduction}} = \frac{k_{\text{max,PCE}} X C_{\text{PCE}}}{K_{\text{S,PCE}} + C_{\text{PCE}}} f(\text{pH}), \quad (2.8)$$

$$R_{\text{TCE reduction}} = \frac{k_{\max,\text{TCE}} X C_{\text{TCE}}}{K_{\text{S,TCE}}\left(1+\frac{C_{\text{PCE}}}{K_{\text{CI,PCE}}}\right)+C_{\text{TCE}}\left(1+\frac{C_{\text{TCE}}}{K_{\text{HI,TCE}}}\right)} f(\text{pH}), \tag{2.9}$$

$$R_{\text{c-DCE reduction}} = \frac{k_{\max,\text{c-DCE}} X C_{\text{c-DCE}}}{K_{\text{S,DCE}}\left(1+\frac{C_{\text{TCE}}}{K_{\text{CI,TCE}}}\right)+C_{\text{DCE}}\left(1+\frac{C_{\text{c-DCE}}}{K_{\text{HI,c-DCE}}}\right)} f(\text{pH}), \tag{2.10}$$

$$R_{\text{VC reduction}} = \frac{k_{\max,\text{VC}} X C_{\text{VC}}}{K_{\text{S,VC}}\left(1+\frac{C_{\text{TCE}}}{K_{\text{CI,TCE}}}+\frac{C_{\text{c-DCE}}}{K_{\text{CI,c-DCE}}}\right)+C_{\text{VC}}\left(1+\frac{C_{\text{VC}}}{K_{\text{HI,VC}}}\right)} f(\text{pH}), \tag{2.11}$$

and their temporal dynamics is

$$\frac{dC_{\text{PCE}}}{dt} = -R_{\text{PCE reduction}}, \tag{2.12}$$

$$\frac{dC_{\text{TCE}}}{dt} = R_{\text{PCE reduction}} - R_{\text{TCE reduction}}, \tag{2.13}$$

$$\frac{dC_{\text{c-DCE}}}{dt} = R_{\text{TCE reduction}} - R_{\text{c-DCE reduction}}, \tag{2.14}$$

$$\frac{dC_{\text{VC}}}{dt} = R_{\text{c-DCE reduction}} - R_{\text{VC reduction}}, \tag{2.15}$$

$$\frac{dC_{\text{ethene}}}{dt} = R_{\text{VC reduction}}, \tag{2.16}$$

where C_j (mol l^{-1}) is the aqueous concentration and $k_{max,j}$ (mol mg protein^{-1} d^{-1}) is the maximum specific utilization rate of CE j (i.e., j = PCE, TCE, DCE, and VC), X (mg protein l^{-1}) the dechlorinating biomass concentration and $K_{S,j}$ (mol l^{-1}) the half-saturation constant of each chloroethene j, $K_{CI,j}$ (mol l^{-1}) is the competitive inhibition constant and $K_{HI,j}$ the Haldane inhibition constant. f(pH) is a pH inhibition function that is described in detail below (section 2.2.3.2).

Microbial growth is expressed as:

$$\frac{dX}{dt} = -Y\sum_{j=1,4} R_{\text{j reduction}} - k_{\text{d}} X, \tag{2.17}$$

where X (mg protein l^{-1}) is the biomass concentration, Y (mg protein mol Cl released^{-1}) is the growth yield coefficient, $R_{\text{j reduction}}$ (mol l^{-1} d^{-1}) is the reduction rate of CE j and k_d (d^{-1}) is the first-order biomass decay rate. It was assumed that all OHRB populations have the same yield coefficient and decay rate.

2.2.3.2 pH inhibition function

OHRB are highly sensitive to groundwater pH. The dechlorination rate is maximal in the near-neutral range and decreases in the acidic and basic ranges. Several pH inhibition functions have been proposed to describe the pH influence on microbial activity[193,208-210]. In this study, the Gaussian-type function employed by Schepers et al.[209] was used:

$$f\left(\mathrm{pH}\right) = \exp\left[-\frac{\left(\left|\mathrm{pH}_{\mathrm{opt}} - \mathrm{pH}\right|\right)^{n}}{\sigma^{2}}\right], \tag{2.18}$$

where $\mathrm{pH}_{\mathrm{opt}}$ (= 6.7) is the optimal pH, and n and σ are empirical parameters that were estimated by fitting published datasets[130] (Figure 2.2).

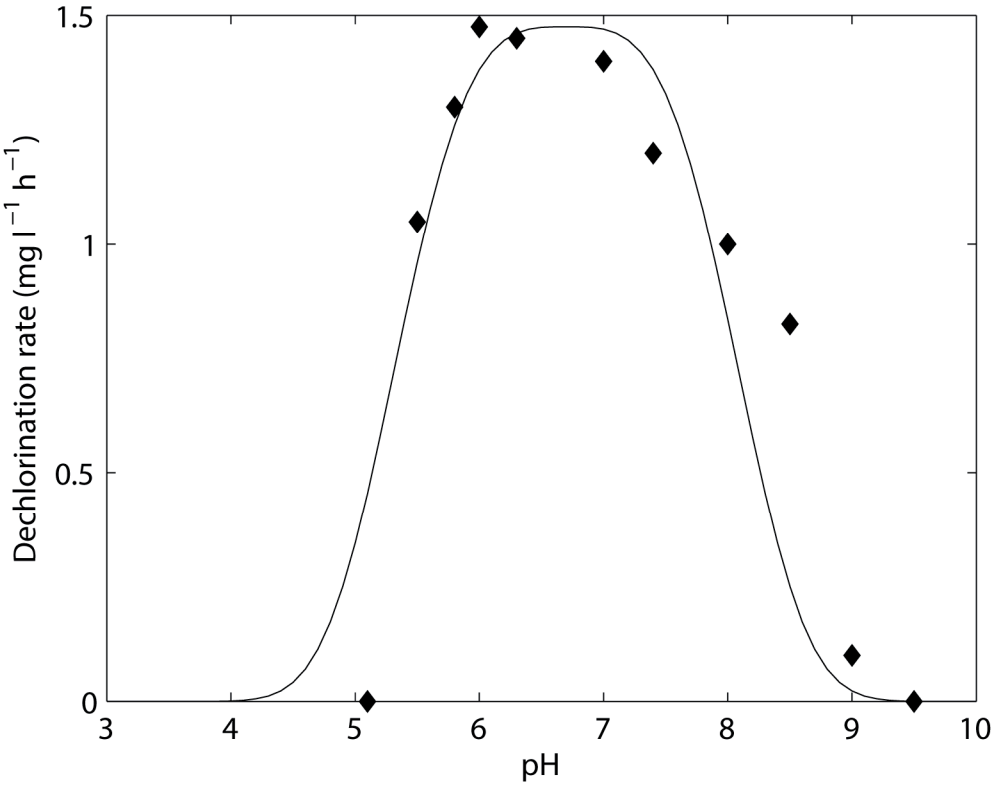

Figure 2.2. pH versus dechlorination rate for a mixed organohalide respiring consortium. The filled diamonds represent the experimental data determined by Vainberg et al.[130] and the line represents the fit of these data with Eq. 2.18.

2.2.3.3 Silicate mineral dissolution

Silicate mineral dissolution is a kinetically controlled process influenced by external factors such as temperature, pressure, pH, thermodynamic affinity and water composition[150,160]. The general form of the rate law for mineral dissolution far from equilibrium proposed by Lasaga[211] was adopted here:

$$R_D = r' \frac{A_0}{V} g(A)(1-\Omega), \tag{2.19}$$

where R_D (mol l^{-1}) is the mineral dissolution rate, r' (mol m^{-2} s^{-1}) is the rate per unit surface area (given by Eq. 2.20), A_0 (m^2) is the initial surface area, V (l) is the solution volume, Ω (-) the mineral saturation index, $g(A)$ (-) is a function which quantifies the changes in reactive surface area as dissolution proceeds.

The rate per unit surface area r' is a function of temperature, pH and groundwater composition and is expressed by:

$$r' = k_{H^+} \frac{\left(10^{-pH}\right)^{n_{H^+}}}{f_{H^+}} \exp\left[-\frac{E_{H^+}}{R}\left(\frac{1}{T}-\frac{1}{298}\right)\right] + \frac{k_W}{f_W} \exp\left[-\frac{E_W}{R}\left(\frac{1}{T}-\frac{1}{298}\right)\right] + k_{OH^-}\left(10^{-pH}\right)^{-n_{OH^-}} \left[-\frac{E_{OH^-}}{R}\left(\frac{1}{T}-\frac{1}{298}\right)\right], \tag{2.20}$$

where E_{H^+}, E_W and E_{OH^-} (J mol^{-1}) are the activation energies for the acid, neutral and basic ranges, R (J K^{-1} mol^{-1}) the universal gas constant, T (K) the absolute temperature and f_{H^+} and f_W are factors accounting for inhibition by ionic species. The energy activation terms used in this study were taken from Palandri and Kharaka[166] and are presented in Table 2.3. The effect of groundwater composition in the acidic and neutral ranges was included through the inhibition factors f_{H^+} and f_W[150]:

$$f_{H^+} = \left(1+\frac{[BC]}{Lim_{BC,H^+}}\right)^{x_{BC}} + \left(1+\frac{[Al^{3+}]}{Lim_{Al,H^+}}\right)^{x_{Al}}, \tag{2.21}$$

$$f_W = \left(1+\frac{[BC]}{Lim_{BC,W}}\right)^{z_{BC}} + \left(1+\frac{[Al^{3+}]}{Lim_{Al,W}}\right)^{z_{Al}}, \tag{2.22}$$

where *Lim* is the threshold activity for solute inhibition, [BC] indicates the sum of activities of the base cations Na^+, K^+ and Mg^{2+}, $[Al^{3+}]$ is the activity of aluminum and exponents x_i and z_i are empirical parameters. The effect of CO_2 on the dissolution rate was not included as it is negligible for partial pressures up to 1 bar[212]. The coefficients *Lim*, x_i and z_i were determined for a limited numbers of minerals by Sverdrup and Warfvinge[213] and Sverdrup[202], and these values were adopted in this work. For most minerals, however, these parameters were not available. As discussed in section 2.3.4.5, the model is only slightly sensitive to these inhibition factors, and therefore they can be neglected in the conditions selected in this study.

The dissolution rate is also controlled by the available reactive surface area, which can change in time as the minerals dissolve (due, for example, to changes in the size and distribution of the crystal

population, selective dissolution, aging of the mineral)[150]. In addition, precipitation of secondary mineral phases may coat the surface of the dissolving mineral[214,215]. Reactive surface area is, however, not measurable. Also, it is difficult to correlate to the total surface area because, for instance, dissolution occurs only at certain sites on the mineral surface[216]. Moreover, the reactive surface area might undergo variations of several orders of magnitude during dissolution[217]. Different models based on geometrical considerations have been proposed to relate changes in reactive surface area to mineral dissolution[218-220]. In this study, the approach of Lichtner[218] was adopted,

$$g(A) = \left(\frac{m}{m_0} \right)^{\alpha}, \tag{2.23}$$

where m_0 (mol) is the initial amount of mineral, m (mol) is the current amount of undissolved mineral and α is an exponent that depends on crystal shape, grain size distribution[150,221] and relative rates of dissolution on different surfaces[222]. For a mono-disperse population of uniformly dissolving spheres or cubes α = 0.67, while α = 3.4 for a lognormal grain size distribution. Since this parameter is unknown and variable, α = 0.67 was arbitrarily chosen for the simulations conducted in this work and a sensitivity analysis was performed to assess its impact on model results.

Kinetic rate constants determined in laboratory experiments commonly exceed the mineral weathering rates observed in the field[223,224]. Discrepancies were attributed to stirring in laboratory studies[225,226], inaccurate estimation of the mineral surface in aquifers[217] and different characteristics of the mineral surfaces in the laboratory compared to field conditions[227]. To correct dissolution rates obtained in the laboratory, following Vangrinsven and Vanriemsdijk[228] a safety factor, D, was introduced,

$$R_{\mathrm{D}}' = \frac{R_{\mathrm{D}}}{D}, \tag{2.24}$$

where R_{D} (mol l^{-1}) is the total mineral dissolution rate obtained from continuous stirred flow reactor experiments and R_{D}' is the corrected value. Vangrinsven and Vanriemsdijk[228] compared mineral dissolution rates in a number of different experiments and found $D \approx 15$ between dissolution rates determined in batch and in porous medium column experiments. This value was adopted in this work.

Precipitation of secondary minerals was not included due to the lack of a reliable modeling approach. Precipitation of a new mineral phase occurs when the saturation index exceeds a critical level, which is different for each mineral and in most cases is unknown[229]. Moreover, the definition of the initial surface area or of the nucleation sites is extremely difficult[160,229].

Table 2.3. Activation energy terms of silicate mineral dissolution in acid, neutral and basic range.

Silicate mineral	Activation energy		
	E_{H^+} (kJ mol^{-1})	E_W (kJ mol^{-1})	E_{OH^-} (kJ mol^{-1})
Albite	65	69.8	71
Almandine	94.4	103.8	37.8
Andradite	94.41	103.8	n.d.[b]
Anorthite	16.6	17.8	n.d.
Chlorite	88.0	88.0	88.0
Cordierite	113.3	28.3	n.d.
Diopside	96.1	40.6	n.d.
Enstatite	80.0	80.0	n.d.
Fayalite	94.4	94.4	n.d.
Forsterite	67.2	79.0	n.d.
Glaucophane	85.0	94.4	n.d.
Grossular	85.0	103.8	n.d.
Jadeite	132.2	94.4	n.d.
Leucite	132.2	75.5	56.6
Lizardite	75.5	56.6	n.d.
Nepheline	62.9	65.4	37.8
Riebeckite	56.6	47.2	n.d.
Spodumene	94.4	66.1	n.d.
Tremolite	18.9	94.4	n.d.
Wollastonite	54.7	54.7	n.d.

[a] Data are from Palandri and Kharaka[166].

[b] n.d. = not determined

2.2.4 Numerical simulations

2.2.4.1 Definition of base conditions

The model developed above was set up to simulate conditions of a typical groundwater undergoing *in situ* bioremediation. The conditions used were:

- The groundwater composition was defined using major constituents of a typical site contaminated with chlorinated solvents: K^+, 0.2 mmol l^{-1}; Mg^{2+}, 2.3 mmol l^{-1}; Ca^{2+}, 7.2 mmol l^{-1}; Na^+, 5.9 mmol l^{-1}; Cl^- 0.2, mmol l^{-1}; SO_4^{2-}, 10.4 mmol l^{-1}; CO_3^{2-}, 5.1 mmol l^{-1}; pH, 6.8[204];
- The temperature was set to 20°C: This value corresponds to the upper limit for groundwater temperature, which is usually between 10 and 20°C[53]. This value was

chosen because microbial rates are much higher at 20°C than at 10°C[101,129], consequently so is acidity production. In other words, this is the worst-case condition in term of acidity production;

- The water was in equilibrium with a free phase of pure PCE (1.5 mmol l^{-1}). The solubility limit of PCE was set to 0.9 mmol l^{-1} [230];
- The factor f_{min} was set to 0.4, a typical value for field conditions[53];
- The organic fermentable substrate used was linoleic acid, which is a major component of vegetable oil, a substrate often injected in field applications[53]. Linoleic acid is fermented to hydrogen and acetate following the reaction :

  $C_{18}H_{32}O_2 + 16H_2O = 14H_2 + 9CH_3COOH$; (2.25)
- The microbial kinetic parameters (maximum specific utilization rates, half-saturation constants, competitive and Haldane inhibition constants) were taken from Yu and Semprini[60] for the PM culture, a mixed consortium able to convert PCE to ethene even at high PCE concentration. These kinetic parameters were determined at 20°C. All microbial processes model parameters used in the base case simulations are listed in Table 2.4;
- It was assumed that the natural buffering capacity of soil and groundwater was already consumed, again this is the worst-case scenario.

Three cases were considered:

Case A: The pH was fixed at the optimal value for organohalide respiration (pH = 6.7). The goal was to determine the time needed to complete degradation without pH inhibition.

Case B: This simulation was used to quantify the maximum dechlorination efficiency without addition of an external buffer.

Case C: In this simulation, fayalite was added to the system. The goal was to ascertain the effect on pH and therefore on PCE degradation efficiency. A total of 10 g of mineral with a specific surface area of 30 m^2 g^{-1} was used. Using the formula defined by Borkovec et al.[231], which incorporates the effect of surface roughness, this corresponds to a powder with grain size around 1.5 μm.

Results were analyzed considering the time required converting 99% of the initial PCE mass to ethene ($t_{99\%}$). This metric is directly linked to the buffering effect as the only parameter influencing the dehalogenation rate is pH: A rapid dechlorination (high $t_{99\%}$) reflects a good buffering capacity of the mineral. $t_{99\%}$ of case C above (named $t_{BC,99\%}$) was used as a reference value in the sensitivity analysis.

Table 2.4. Parameters for the microbial dechlorination model.

Parameter and units	Value
Maximum degradation rates [μmol mg-protein^{-1} d^{-1}] [a]	
$k_{PCE,max}$	13.3
$k_{TCE,max}$	124
$K_{c\text{-}DCE,max}$	22
$k_{VC,max}$	2.4
Half velocity constants [μmol l^{-1}] [a]	
$K_{s,PCE}$	3.9
$K_{s,TCE}$	2.8
$K_{s,c\text{-}DCE}$	1.9
$K_{s,VC}$	602
Haldane inhibition constants [μmol l^{-1}] [a]	
$K_{HI,PCE}$	900
$K_{HI,c\text{-}DCE}$	6000
$K_{HI,VC}$	7000
Competitive inhibition constants [μmol l^{-1}] [a]	
$K_{CI,PCE}$	3.86
$K_{CI,TCE}$	2.76
$K_{CI,c\text{-}DCE}$	1.90
$K_{CI,VC}$	602.00
Biomass yields [mg-protein/μmol Cl$^-$] [b]	
Y	4.8×10^{-3}
First-order decay constant [d^{-1}] [c]	
k_d	2×10^{-2}
pH inhibition function parameters [d]	
n [-]	3.5
σ [pH units]	2.1
pH_{opt} [pH units]	6.7
Fraction of H_2 used for organohalide respiration [-] [e]	
f_{min}	0.35

[a] Yu and Semprini[60]

[b] MaymoGatell et al.[97]

[c] Fennell and Gossett[55]

[d] Parameters fitted from data of Zhuang and Pavlostathis[129]

[e] Average value between 0.2 and 0.5[53]

2.2.4.2 Global sensitivity analysis

A global sensitivity analysis was conducted to ascertain the contribution of each parameter influencing mineral dissolution rate. This leads to identification of (i) insensitive parameters for model reduction and (ii) sensitive parameters that require a more accurate characterization. The analysis also improved the understanding of the model behavior and clarified the interactions among parameters. For each parameter considered, the range of variability found in the literature was used: the model was run using the two extreme values while keeping the other parameters fixed. The description of all the cases and the values of the parameters used for the simulation are given in Table 2.6. Cases 1 to 5 focus on the influence of the mineral dissolution kinetic parameters (k_{H^+}, k_W, k_{OH^-}, n_{H^+} and n_{OH^-}) and activation energy terms (E_{H^+} and E_W). The importance of the security factor D was investigated in case 6. The influence of the thermodynamic parameters K_{eq} and ΔH was evaluated in cases 7 and 8, respectively. To get a better understanding of the model behavior, some parameters were evaluated together, in particular the kinetic rate constants k_{H+} and k_W (case 2) and the energy activation terms, E_{H^+} and E_W (case 5). In addition to model parameters, simulations were run to ascertain the effect of other important variables. The effect of temperature was evaluated in case 9 where the model was run for 10 and 15°C. The inhibition of ionic species on mineral dissolution (case 10) and the representation of the reactive surface area changes (case 11) were also considered. In this latter case, the parameter α was changed from 0.67 (uniform grain size distribution) to 3.4 (log normal distribution of the grains).

The $t_{s99\%}$ obtained from each run was compared to $t_{BC,99\%}$ and the difference $\Delta t_{99\%} = t_{s99\%} - t_{BC99\%}$ was computed. A high $\Delta t_{99\%}$ indicates a marked contribution of the parameter to the model output and vice-versa.

2.2.4.3 Mineral ranking

The acid neutralizing potential and lifetime of the minerals selected during the preliminary screening were also quantified, considering the $t_{99\%}$ metric and the mass of mineral consumed per mol of PCE degraded. For each mineral, the appropriate thermodynamic and kinetic data were included in the model and are listed in Tables 2.1, 2.2 and 2.3. The same amount of mineral (50 mmol l^{-1} and surface area of 300 m^2 of mineral l^{-1} of solution) was considered in all simulations. This amount corresponds to 10 grams of mineral with a particle size of 1.5 µm per liter. The results were used to rank the minerals according to their suitability for field application as buffering agents.

2.3 Results and Discussion

2.3.1 Determination of kinetic and thermodynamic parameters

Tables 2.1, 2.2 and 2.3 report the results of the literature review conducted to collect the available kinetic and thermodynamic parameters for the 20 silicate minerals considered in this work. The

stoichiometry of each dissolution reaction is also reported (Table 2.1), as it can be used to quantify the buffering potential of each mineral through the number of protons consumed per mole of dissolution. This value varies among the minerals, from 16 moles of protons per mole of dissolved mineral (cordierite, chlorite) to 2 moles of protons per mole of dissolved mineral (enstatite, wollastonite). Mineral dissolution kinetic parameters identified using Eq. 2.1 are listed in Table 2.2. For most minerals, the dissolution parameters in the alkaline range (k_{OH^-} and n_{OH^-}) could not be determined as most studies only considered the acid-neutral range. Even though the datasets considered were produced from experiments in similar conditions, large differences between them were found. These led to uncertainties in the determination of the parameters as large as 3 orders of magnitude for k_{H^+} and 2 orders of magnitude for k_W. These large ranges are likely due to one or more of the following: uncertainties in estimates of the available reactive surface area[216,232,233], differences in the experimental design and solid phase preparation such as stirring rate[225], grinding method, or differences in the initial structure and composition of the mineral[166]. When datasets for the same mineral were significantly different, a range of values was determined (Table 2.2). As an illustration, Figure 2.3 shows the results of the fit for the mineral diopside. Two datasets were used[171,212] to determine the kinetic parameters. Fitting of the parameters was done for each dataset. As a result, two values were obtained for each parameter and the upper and lower limits of the kinetic equation were computed (Figure 2.3).

All minerals considered have a pH-dependent dissolution rate with the reaction order of proton-promoted dissolution n_{H^+} between 0.14 and 1 (average value). Comparison of kinetic parameters showed high variability. In the acidic range, the kinetic constant k_{H^+} varies over 7 orders of magnitude, the fastest and slowest minerals being nepheline and albite, respectively. The kinetic constant in the neutral range k_W shows a slightly smaller variation (4 orders of magnitude between nepheline and albite).

The kinetic constants determined in this work fall in the range reported by Palandri and Kharaka[166] for the majority of the minerals. A mismatch was found in seven cases, and was attributed to different criteria used to select the datasets. In particular, in contrast to the compilation of Palandri and Kharaka[166], in this study only datasets using a similar experimental setup and conditions were considered.

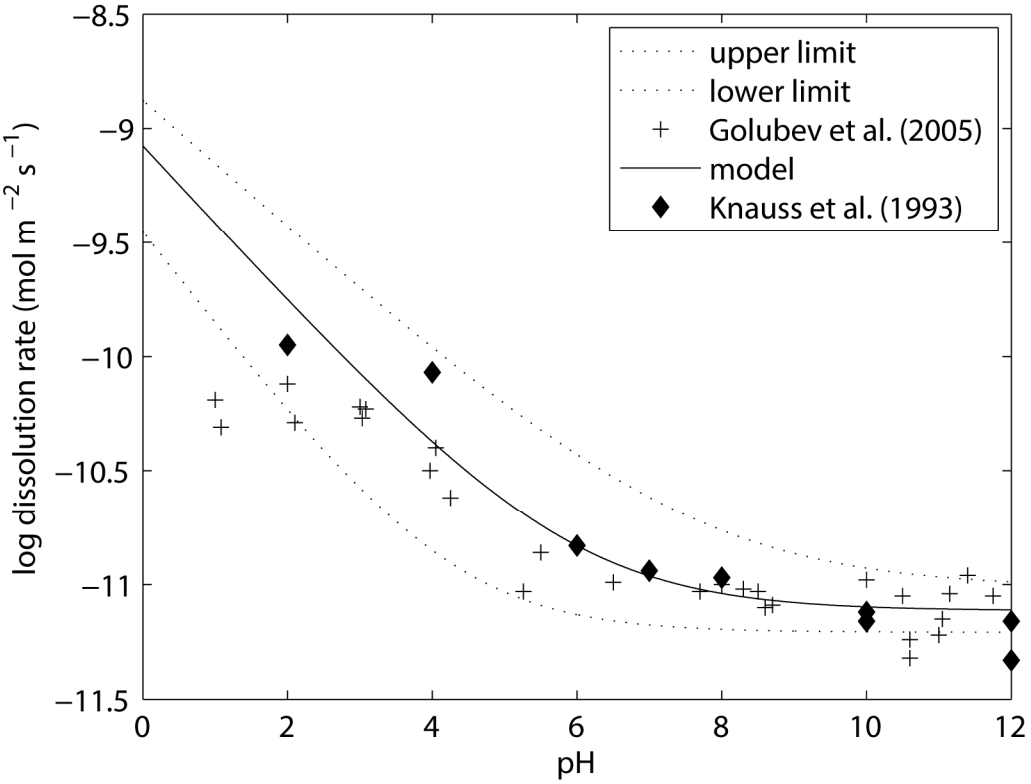

Figure 2.3. Diopside dissolution rate versus pH. The points represent the data obtained by Golubev et al.[212] and Knauss et al.[171]. The lines were obtained by fitting these datasets to Eq. 2.1. For each dataset a different value of the three parameters k_{H+}, n_{H+} and k_W was obtained. Therefore, two values were available for each parameter. The continuous line was computed with the average value while the dotted lines were computed with the minimal and maximal values.

2.3.2 Mineral screening based on thermodynamic considerations

The values of the solubility in the acid range at pH 5 and in the basic range at pH 8 are presented in Figure 2.4. Minerals with a solubility higher than 10 mmol l^{-1} are likely to lead to an increase of pH above 9, which is inhibitory to OHRB[129,130] and therefore they were excluded. On the other hand, in the acidic range solubility should be sufficient to avoid limitation of mineral dissolution due to thermodynamic constraints. The minerals selected present a wide range of solubility at pH 5 and 20°C ranging from 4.3 mol l^{-1} for wollastonite to 8.45×10^{-5} mol l^{-1} for riebeckite. All minerals with solubility lower than 1 mmol l^{-1} were excluded. Minerals were classified in three classes according to their change in solubility as a function of pH (Table 2.5).

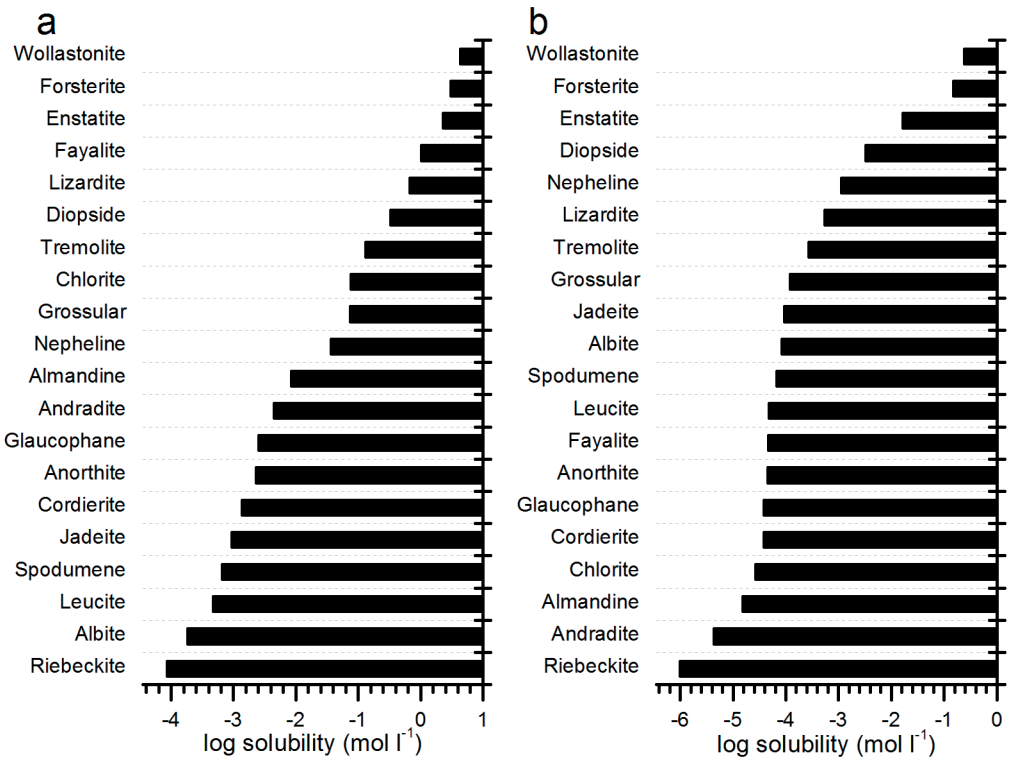

Figure 2.4. Logarithm of mineral solubility at pH 5 (a) and pH 8 (b) for the 20 selected silicate minerals. These solubility values were calculated at 20°C in pure water. The solubility values vary by several orders of magnitude among minerals.

Table 2.5. Mineral classification based on the solubilities in acid and alkaline conditions. Minerals belonging to class 1 have a solubility at pH 8 that exceeds 10 mmol l^{-1}, while minerals belonging to class 2 have a solubility at pH 5 below 1 mmol l^{-1}. Minerals from the third class have a suitable solubility to be used as buffering agent (solubility above 1 mmol l^{-1} at pH 5 and below 10 mmol l^{-1} at pH 8).

Class 1 Excessive solubility at pH 8	Class 2 Insufficient solubility at pH 5	Class 3 Appropriate solubility at pH 5 and 8
Wollastonite	Riebeckite	Cordierite
Forsterite	Albite	Anorthite
Enstatite	Leucite	Glaucophane
	Spodumene	Andradite
	Jadeite	Almandine
		Nepheline
		Grossular
		Chlorite
		Tremolite
		Diopside
		Lizardite
		Fayalite

2.3.3 Base simulations

Base simulations demonstrated the positive impact of the addition of silicate mineral on groundwater pH and on the activity of OHRB. If the influence of pH on dechlorination is neglected, degradation of 99% of 1.5 mmol l^{-1} of PCE to ethene occurs in 17 d ($t_{99\%}$) with transient accumulation of VC and to a smaller extent of DCE and TCE (Figure 2.5a). Until day 2 the PCE concentration is equal to 0.9 mmol l^{-1} (PCE solubility). After 2 d, the separate PCE phase was dissolved and the aqueous PCE concentration started to decrease.

When the feedback of pH on OHRB activity is considered, without an external source of alkalinity, the pH dropped below 4.5 after 9 d, stopping the dechlorination (Figure 2.5b). Degradation of PCE was incomplete and, after 18 d, only 64% of the initial mass was transformed to DCE and VC. When dechlorination ceased, 4.6 mmol of acetate and 2.7 mmol of hydrochloric acid had been produced, indicating that the two processes contribute in a similar extent to groundwater acidification. This simulation highlights the need of an external buffer during enhanced bioremediation of CEs when the natural soil buffering capacity is small.

The addition of fayalite had a positive impact on the CE degradation rates, with $t_{99\%}$ = 25 d (Figure 2.5c). The pH initially dropped to 5.1 due to rapid conversion of PCE to VC because dechlorination was faster than mineral dissolution. Afterwards, the pH returned to close to neutral as the transformation of VC to ethene is slower than the previous dechlorination steps (see maximum degradation rates in Table 2.4) and because acidic conditions further reduced the activity of OHRB. At the end of the simulation, 7 mmol of fayalite were consumed. When PCE removal was completed, the pH remained stable at 6.87 and mineral dissolution ceased since solubility of fayalite is very low at neutral pH (Figure 2.1). This simulation suggested that, for the conditions considered, fayalite is a good candidate for groundwater buffering as pH remains close to neutral. Moreover, only the quantity required to buffer the acidity produced was used, and the rest remained in the system. This suggests that fayalite is also a good long-term source of alkalinity.

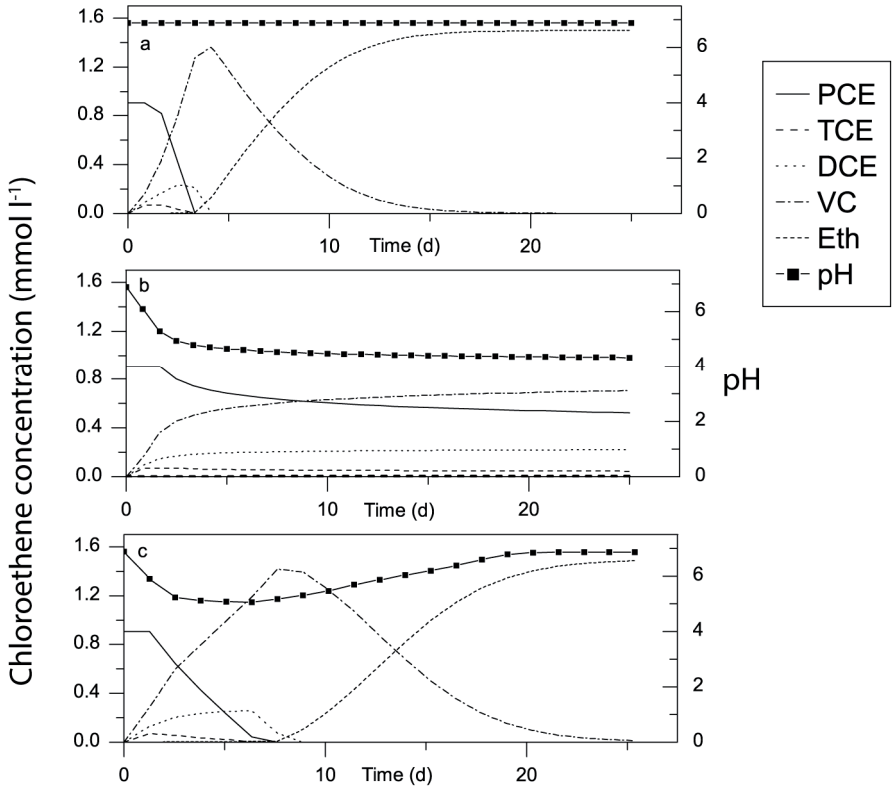

Figure 2.5. Dechlorination pattern and pH evolution for the case A (pH constant at its optimal value) (a), case B (pH inhibition) (b) and case C (introduction of 300 m^2 l^{-1} of fayalite) (c).

2.3.4 Global sensitivity analyses

2.3.4.1 Influence of mineral dissolution rate parameters

The results of the global sensitivity analysis are presented in the Table 2.6. The kinetic rate parameters in the alkaline range (k_{OH}^- and n_{OH}^-) have no influence on the degradation rate ($\Delta t_{99\%} = 0$) (cases 1 and 4). The reason is that water remains in the acid-neutral pH range for the entire simulation period. Therefore, the lack of available data for these parameters does not limit model application. Conversely, k_H^+ and k_W have a significant impact on the model response. A five-fold decrease of k_H^+ and k_W (case 2.2) increased $t_{99\%}$ to 52.3 d (twice as long as the base case). When these two parameters were an order of magnitude smaller than in the base case (case 2.3), 99% degradation of PCE was not achieved. Hence, k_H^+ and k_W directly control the mineral dissolution rate: When they are too low compared with the CE degradation rate, the pH drops rapidly inhibiting bacterial activity. Similarly, the security factor D has a significant impact on the model output (case 6). An increase of D from 15 to 50 increased $t_{99\%}$ by 29.6 d.

2.3.4.2 Influence of activation energy

The influence of the activation energy terms E_{H^+} and E_W on the model response is very limited. E_{H^+} was varied between 18.9 to 132 kJ mol^{-1} and E_W between 51 and 104 kJ mol^{-1}, corresponding to the minimum and maximum values observed for the 20 selected minerals (case 5). The resulting $\Delta t_{99\%}$ was equal to -0.2 d (minimal values of the activation energy) and 2.7 d (maximal values of activation energy). Activation energy controls the changes in the mineral dissolution rate when temperature is different from 25°C. The simulations reported here considered a temperature of 20°C fairly close to the reference value, which partially explains the weak sensitivity. Further numerical simulations with lower temperatures (e.g., 10°C) indicated that, for typical groundwater temperatures, the influence of activation energies remains limited.

2.3.4.3 Influence of solubility constant

Riebeckite has the smallest solubility constant among the minerals considered (log K_{eq} = -7.81). For this value (case 7.1), the target 99% PCE degradation is not reached as the solution rapidly equilibrates with the mineral phase and dissolution halts. Only a total of 0.16 mmol of mineral dissolved within 25 d (compared to 7 mmol l^{-1} for the base case). Conversely, an increase of the solubility constant up to 68.4 (value for chlorite) reduced $t_{99\%}$ to its minimum value, i.e., 17 d (case 7.2), which corresponds to an optimal pH over the entire simulation period. In this case, the solution always remained far from equilibrium with the mineral phase and mineral dissolution was only controlled by kinetics.

2.3.4.4 Influence of temperature

A 10°C decrease in temperature increased $t_{99\%}$ to 62.9 d (2.5 fold increase) (case 9.1). In the simulations, temperature changes affect the mineral dissolution rates and solubility constants. The influence of temperature on the dechlorination rate was instead not taken into account and the same parameters for biological transformations estimated at 20°C were used. The reason for this approximation was the lack of information about the extent of reduction of the dechlorination rate with temperature for the PM consortium. Zhuang and Pavlostathis[129] studied the influence of temperature on a OHRB mixed culture and showed that the rate was approximately halved reducing the temperature from 20 to 15°C. On the other hand, a change in ambient temperature from 20 to 15°C leads to a decrease of the mineral dissolution rate of fayalite by a factor of 1.8 (Eq. 2.20). This suggests that, in the temperature range 10-20°C, the change in dechlorination rate will be similar to the change in dissolution rate and buffering capacity of the mineral, with little or no effect on the ability of the mineral to counterbalance the acidity produced. The $t_{99\%}$ value will increase nevertheless, as the rate at which CEs are transformed is reduced at lower temperatures.

2.3.4.5 Cation inhibition function

The goal of case 10 was to evaluate the importance of the base cations inhibition terms f_{H^+} and f_W in Eq. 2.20. As discussed previously, these parameters are available for few minerals only and it was therefore important to ascertain the resulting error on model predictions. For the groundwater composition considered in this simulations, the decrease in dechlorination efficiency when the inhibition terms are considered is relatively small, $\Delta t_{99\%} = 4.4$ d. This value should be compared with that resulting from the uncertainty in the kinetic rate parameters k_{H^+} and k_W, which is five or more times larger ($\Delta t_{99\%} > 20$ d). As a result, the two inhibition terms can be neglected for the conditions used. For higher concentrations of Al^{3+}, Na^+, K^+ and Mg^{2+}, this choice should be tested further. For example, additional calculations showed that, for the case where the sum of the activities of the base cations exceeds 20 mmol l^{-1}, the dissolution rate of K-feldspar is halved.

2.3.4.6 Surface area evolution

Case 11 investigated the effect of changing the parameter α in Eq. 2.23, that is, the equation governing the change in reactive surface area as mineral dissolution proceeds. The parameter was changed from 0.67 – which corresponds to a monodisperse population of spherical grains – to 3.4, the value for a lognormal grain size distribution. Simulation results showed a $\Delta t_{99\%} = 1.9$ d. It was then concluded that this parameter has little influence, and uncertainties in its determination introduce only a small change in simulation results.

2.3.4.7 Summary of global sensitivity analyses

Results of global sensitivity analyses demonstrated that the most influent parameters are the solubility constant, K_{eq}, and the kinetic dissolution rate constants in the acidic and neutral range k_{H^+} and k_W. The security factor D also influenced significantly the model response. Experimental determination of the kinetic rate constants is associated with a high level of uncertainty as discussed before. Therefore, additional efforts should be spent to characterize better those parameters, in particular in field conditions. With current knowledge this method can still be successful but it might be necessary to overestimate the amount of mineral to be injected, to guarantee sufficient buffering capacity.

Table 2.6. Result of global sensitivity analysis. Case-specific parameters/conditions used and value of $t_{s99\%}$ and $\Delta t_{99\%}$.

Case	Parameters	Units	Base case value	Sensitivity value		
1			BC value	Case 1.1	Case 1.2	
	log k_{OH}^-	log (mol m^{-2} s^{-1})	-	-16.3	-13.7	
	Results					
	$t_{s99\%}$			25	25	
	$\Delta t_{99\%}$			0	0	
2			BC value	Case 2.1	Case 2.2	Case 2.3
	log k_W	log (mol m^{-2} s^{-1})	-5.35	-4.85	-5.85	-6.35
	log k_H^+	log (mol m^{-2} s^{-1})	-9.5	-9	-10	-10.5
	Results					
	$t_{s99\%}$			17	52.3	Not reached
	$\Delta t_{99\%}$			-8	27.3	-
3			BC value	Case 3.1	Case 3.2	
	n_H^+	-	0.85	0.28	1	
	Results					
	$t_{s99\%}$			17	30.6	
	$\Delta t_{99\%}$			-8	5.6	
4			BC value	Case 4.1	Case 4.2	
	n_{OH}^-	-	0.85	0	1	
	Results					
	$t_{s99\%}$			25	25	
	$\Delta t_{99\%}$			0	0	
5			BC value	Case 5.1	Case 5.2	
	E_W	(kJ mol^{-1})	94.4	51	104	
	E_H^+	(kJ mol^{-1})	94.4	18.9	132	
	Results					
	$t_{s99\%}$			24.8	27.7	
	$\Delta t_{99\%}$			-0.2	2.7	
6			BC value	Case 6.1	Case 6.2	
	Security factor D	-	15	1	50	
	Results					
	$t_{s99\%}$			17	54.6	
	$\Delta t_{99\%}$			-8	29.6	
7			BC value	Case 7.1	Case 7.2	Case 7.3
	Solubility constant K_{eq}	-	19.02	-7.8	68.4	1
	Results					
	$t_{s99\%}$			not reached	17	43
	$\Delta t_{99\%}$			-	-8	18
8			BC value	Case 8.1	Case 8.2	
	Standard enthalpy ΔH	(J mol^{-1})	159 491	88 220	1 965 817	
	Results					
	$t_{s99\%}$			25	25	
	$\Delta t_{99\%}$			0	0	
9			BC value	Case 9.1	Case 9.2	
	Temperature	(°C)	20	10	15	
	Results					
	$t_{s99\%}$			62.9	36.4	
	$\Delta t_{99\%}$			37.9	11.4	
10			BC conditions	Case 10.1		
	Ionic species inhibition f_H^+/f_W		f_{H+} =1 ; f_W =1			
	lim BC	-		200		
	xBC			0.3		
	Results					
	$t_{s99\%}$			29		
	$\Delta t_{99\%}$			4		

Table 2.6 (part 2)

Case	Parameters	Units	Base case value	Sensitivity value
11			BC conditions	Case 11.1
	Surface area evolution α	-	0.67	3.4
	Results			
	$t_{s99\%}$			26.9
	$\Delta t_{99\%}$			1.9

2.3.5 Comparison among minerals

Additional simulations were used to rank the twelve minerals previously selected on the basis of their solubility in the acid/alkaline pH range (i.e., those belonging to class 3 in Table 2.5). The minerals were ordered considering the time required to reach 99% degradation of the initial PCE mass, i.e., the more suitable minerals had lower $t_{99\%}$ values. Results are reported in Table 2.7. Of the twelve minerals tested, five (anorthite, chlorite, diopside, tremolite and enstatite) had a dissolution rate that was too low to counterbalance acidity produced by the dechlorination. As a result, the target 99% PCE degradation was not reached and byproducts (mainly vinyl chloride) accumulated. Thus, these minerals were excluded from the list of candidate buffers. The kinetic constants k_H^+ and k_W for these minerals were less than 10^{-8} mol m^{-2} s^{-1} and 10^{-11} mol m^{-2} s^{-1}, respectively. Among the remaining eight minerals, $t_{99\%}$ varied from 21 d (nepheline) to 54 d (andradite). The minerals with smaller $t_{99\%}$ (< 30 d), namely nepheline, fayalite, glaucophane and lizardite, are the best candidates as acid-neutralizing agents. This result is partially corroborated by Kleiv and Sandvik[185], who recognized the buffering properties of nepheline. The amount of mineral consumed to buffer the same amount of PCE was also computed (Table 2.7). Only relatively small variations were found, ranging from 0.32 to 0.97 g mineral consumed per mmol of PCE transformed. According to simulation results, dechlorination of 1.5 mmol of PCE will consume 0.7 to 1.5 g l^{-1} of mineral for a period of approximately one month, depending on the mineral used.

Table 2.7. Results of the screening methodology. Nepheline has the smallest $t_{99\%}$ and is therefore the best candidate as buffering agent.

Silicate mineral	$t_{99\%}$	Grams of mineral per mmol of PCE transformed
Nepheline	21	0.54
Fayalite	24.8	0.97
Glaucophane	29.8	0.51
Lizardite	29.8	0.45
Grossular	35	0.50
Almandine	46.8	0.74
Cordierite	48.6	0.32
andradite	53.8	0.49
Anorthite	not reached	-
Chlorite	not reached	-
Diopside	not reached	-
Tremolite	not reached	-
Enstatite	not reached	-

2.4 Conclusions

The importance of groundwater pH control for enhanced *in situ* bioremediation of CEs as well as other remediation technologies is well recognized. A batch biogeochemical model was implemented to evaluate the use of silicate minerals as buffering agents during the treatment of contaminated sites. To the best of our knowledge, this is the first study focusing on the use of silicate mineral powder in aquifers. Although in this work the technology was applied to the specific case of CE bioremediation, the geochemical model could be applied to other remediation processes requiring maintenance of neutral pH. As it stands, the model can be used as a design tool to calculate the amount of mineral needed. This requires knowledge of the initial mass of CEs.

Eight potentially suitable minerals were identified through the screening methodology. The other silicate minerals were excluded as their dissolution kinetic was too low to neutralize the acidity produced by the biological processes. The most promising candidate was nepheline, due to its relatively rapid dissolution rate. This result extends the work of Kleiv and Sandvik[185], who proposed its use as a buffering agent for heavy metal stabilization. The minerals considered in this study can be easily found on the market, as they are used in industrial processes (such as glass making, ceramics, abrasive) or in mine tailings, and are therefore relatively inexpensive. In the context of field application, the local availability of the mineral should also be assessed. The minerals considered in this study are distributed worldwide and mineralogical databases (e.g., www.mindat.org) can be used to identify local deposits and availability.

A sensitivity analyses was conducted to identify the parameters that control the model response and therefore need accurate characterization. It was observed that the most influential parameters are the mineral dissolution rate constants in the acidic and neutral ranges, k_{H^+} and k_W, the reaction order for protons promoted dissolution, n_{H^+}, and the solubility constant K_{eq}. Due to the large uncertainties associated with the determination of the kinetic rate constants, the results of the sensitivity analysis suggested that model predictions should be further verified. Groundwater temperature is also important, as it controls both the rate of acidity production and the buffering capacity of the mineral.

The model includes the main geochemical and microbial processes that control pH evolution. Interactions between minerals and microorganisms were, however, neglected due to the lack of reliable data. Possible feedbacks include the microbial enhancement of mineral weathering rates[234-236] and the inhibition of bacteria by trace elements release during mineral dissolution[237]. The other important process not included in the model is the possible passivation of the mineral reactive surface due to secondary phase precipitation, which would decrease the dissolution rate and buffering capacity. Microcosm experiments to validate the model and ascertain the importance of the different modeling assumptions are presented in the following chapters.

Chapter 3

Geochemical model improvement and validation: Abiotic batch experiments

3 Geochemical model improvement and validation: Abiotic batch experiments

Abstract

Accurate control of groundwater pH is of critical importance for *in situ* biological treatment of chlorinated solvents. The use of ground silicate minerals mixed with groundwater is an appealing buffering strategy as silicate minerals may act as long-term sources of alkalinity. A geochemical model for evaluation of the pH buffering capacity of such minerals was developed in Chapter 2. The model included the main microbial processes driving groundwater acidification as well as mineral dissolution. In the present study, abiotic mineral dissolution experiments were conducted with five silicate minerals (andradite, diopside, fayalite, forsterite, nepheline) to validate the model. These five minerals increased the pH from acidic to neutral and slightly basic values. The model was revised and improved to better represent the experimental observations. In particular, the experiments revealed the importance of secondary mineral precipitation on the buffering potential of silicates, a process not included in the original formulation. The main secondary phases likely to precipitate were identified through model calibration, as well as the degree of saturation at which they formed. The predictions of the revised geochemical model were in good agreement with the observations, with a correlation coefficient higher than 0.9 in most cases. This study confirmed the potential of silicate minerals to act as pH control agents and showed the reliability of the geochemical model, which can be used as a design tool for field applications.

3.1 Introduction

In Chapter 2, a geochemical model to assess the potential of silicate minerals for groundwater pH control was developed[238]. The simulations showed that certain silicate minerals have suitable kinetic and solubility characteristics to act as long-term alkalinity sources in contaminated aquifers. The objective of this study was to validate model predictions experimentally and extend these results. In Chapter 2, it was shown that kinetic parameters in the acidic and neutral range as well as solubility constants are key parameters for accurate estimation of the buffering potential of minerals. As kinetic constants estimation can vary by 2 to 3 orders of magnitude between different datasets taken from the literature, the present study aimed to provide an estimation of these parameters for the mineral samples used in this work. The influence of groundwater composition on the mineral dissolution and solubility was also investigated. To do so, a series of batch-scale abiotic experiments as carried out with the candidate minerals identified previously.Two minerals that were not selected by the modeling approach in Chapter 2 (diopside, forsterite) were however tested in this study as they presented a buffering potential based on the results of a preliminary scoping experiment carried out on ten minerals (results not shown).

3.2 Materials and Methods

3.2.1 Experimental design

Bulk mineral samples were purchased from Dr. F. Krantz Rheinisches Mineralien-Kontor Gmbh and Co. Kg (Bonn, Germany). Five silicate minerals were used: andradite ($Ca_3Fe_2Si_3O_{12}$, from Erzgebirge, Sachsen, Germany), diopside ($CaMg(SiO_3)_2$, Outukumpu, Finland), fayalite (Fe_2SiO_4, Billiton, Indonesia), forsterite (Mg_2SiO_4, Aheim, Northfjord, Norway) and nepheline ($NaAlSiO_4$, Stoledalen, Norway). These minerals were selected based on results of Chapter 2 and some preliminary scoping experiments.

The minerals were crushed with a hydraulic press and ground with an agate disc mill. The mineral powder was rinsed and sonicated (2×5 min in ethanol then 5 min in milliQ pore water) to remove fine particles. Previous dissolution experiments showed that mineral samples treated in this way displayed initial parabolic kinetics. This was attributed to the rapid dissolution of fine particles[181]. To avoid this experimental artifact, mineral samples were further washed for 24 h in milliQ water as proposed by Barker et al.[236] and dried overnight at 60°C. The minerals were dry-sterilized by heating to 150°C for 3 h. Chemical compositions were determined by X-ray fluorescence analysis with an XRF spectrometer Philips PW2400. The specific surface area of the cleaned mineral powder was determined by the multi-point nitrogen adsorption BET (Brunauer–Emmett–Teller) method with a Quantachrome Nova surface area analyzer. Abiotic mineral dissolution experiments were conducted in anaerobic conditions in 0.5-l glass bottles. Each bottle was amended with 150 ml of sterile anoxic solution and 5 g of sterile

mineral. The gas phase was replaced by 100% nitrogen. Two types of solution were used: A solution of degassed milliQ water (Millipore) acidified to pH 5 with HCl (named HCl solution in the following) and an anoxic artificial groundwater solution (AGW) with the following composition: 109 mg l^{-1} of $K_2HPO_4 . 3H_2O$, 75 mg l^{-1} of NH_4HCO_3, 223 mg l^{-1} of $Na_2S . 9H_2O$, 2 mg l^{-1} of $CaCl_2 . 2H_2O$, 1.9 mg l^{-1} of $MgCl_2 . 6H_2O$, 111 mg l^{-1} of CH_3COOH, 14 mg l^{-1} of HCl. The bottles were incubated in the dark at 30°C on an overhead shaker at 20 rpm. At regular time intervals, 1.5 ml samples were withdrawn for pH measurements and analyses of selected elements (Mg, Si, Na, Ca, Al, Fe and K). The experiments were continued until both pH and the concentration of the total amount of elements in solution reached equilibrium.

3.2.2 Analytical methods

Total element concentrations of Mg, Na, Si, Al, Ca, Fe and K were determined by inductively coupled plasma atomic emission spectroscopy with an ICPE-9000 (Shimadzu, United States). The pH was measured with an InLab® Micro electrode and a SevenEasy™ pH-meter (Mettler Toledo, Switzerland).

3.2.3 Calculation of solubility constants

The solubility product constant (K_{eq}) for each mineral was obtained from the dissolution experiment using the methodology of Xiong et al.[239]. The computation of K_{eq} for diopside is presented as an illustrative example. The diopside dissolution reaction is:

$$CaMg(SiO_3)_2 + 4H^+ + 2H_2O = Ca^{2+} + Mg^{2+} + 2H_4SiO_4 \quad (3.1)$$

The equilibrium quotient (log Q) for reaction (3.1) can be computed from the activities of the species in solution:

$$\log\ Q = \log\left(\frac{a_{Mg^{2+}} a_{Ca^{2+}} \left(a_{H_4SiO_4}\right)^2}{\left(a_{H^+}\right)^4} \right), \quad (3.2)$$

where a_i is the activity of species i. At equilibrium, log Q equals log K_{eq}. The geochemical code PHREEQC-2[199] and the MINTEQA2 database[198] were used to infer the activities of the ions in solution using the total element concentrations measured and the water composition. The apparent K_{eq} was determined at 30°C. In order to allow comparison with literature data, K_{eq} at 25°C was calculated using the van't Hoff equation:

$$\ln\left(\frac{K_{spT_2}}{K_{spT_1}} \right) = \frac{\Delta H^\circ}{R}\left(\frac{1}{T_1} - \frac{1}{T_2} \right), \quad (3.3)$$

where K_{eqT} (-) is the solubility constant at temperature T, $\Delta H°$ (kJ mol^{-1}) is the standard enthalpy change, R (J mol^{-1} K^{-1}) is the universal gas constant and T (K) is the temperature.

3.2.4 Estimation of the kinetic rate constants

The two kinetic rate constants k_{H+} and k_W for the different minerals were estimated from the results of the mineral dissolution experiments. Mineral dissolution rates (mol m^{-2} s^{-1}) were calculated at each time step for conditions far from equilibrium, i.e., at the beginning of each experiment (until day 10) as:

$$R_{exp} = \frac{\Delta C_{Si} V}{m A n_{Si} \Delta t}, \tag{3.4}$$

where R_{exp} is the dissolution rate determined experimentally, ΔC_{Si} (mol l^{-1}) is the change in aqueous silica concentration between two time steps, V (l) is the volume of solution, n_{Si} is the stoichiometric coefficient of Si in the mineral formula, m (g) is the mass of mineral, A (m^2 g^{-1}) is the specific surface area and Δt (s) is the time increment. The data were corrected for volume variations occurring due to sampling. Dissolution rates were plotted versus pH. The pH was calculated as arithmetic mean of the pH between two time steps. The approximated rates computed from the experiments were fitted with an empirical rate law for mineral dissolution[160],

$$R = k_{H^+} (a_{H^+})^{n_{H+}} + k_W. \tag{3.5}$$

3.2.5 Modeling approach

Predictions from the geochemical model developed in Chapter 2 were compared to the experimental observations. The model was however slightly modified, as follows. First, microbial processes were not included because only abiotic mineral dissolution was considered in the experiments. Second, the mineral dissolution equation was simplified. In particular, the effect of groundwater composition in the acidic and neutral ranges, denoted by the inhibition factors f_{H+} and f_W[150], was not included since the values of f_{H+} and f_W were not available for the minerals tested in this study, and because the model is only slightly sensitive to these parameters for the conditions considered (see Chapter 2). Similarly, the rate expression in the basic range was also neglected as here the processes occured in acidic and neutral conditions. After these modifications, the resulting mineral dissolution equation was:

$$R_{Diss} = \left[k_{H^+} \left(10^{-pH}\right)^{n_{H^+}} \exp\left(-T_{inf} E_{H^+}\right) + k_W \exp\left(-T_{inf} E_W\right) \right] \frac{A_0}{V} \left(\frac{m}{m_0} \right)^{\frac{2}{3}} (1-\Omega), \tag{3.6}$$

where $T_{inf} = (T^{-1} - 298^{-1})/R$, R_{Diss} (mol m^{-2} s^{-1}) is the dissolution rate, k_{H^+} and k_W (mol m^{-2} s^{-1}) are the rate constants for the acidic and neutral ranges, n_{H^+} (-) is the reaction order of the proton-promoted dissolution, E_{H^+} and E_W (J mol^{-1}) are the activation energies for the neutral and basic ranges,

respectively, R (J K^{-1} mol^{-1}) is the universal gas constant, T (K) is the absolute temperature, A_0 (m^2) is the initial surface area, V (l) is the solution volume, Ω (-) is the mineral saturation index, and m and m_0 are, respectively, the current and initial mass of mineral. Third, precipitation of secondary phases was allowed after reaching a given target saturation. The threshold saturation indexes ranged between 0 and 9, and were determined by fitting the model to the observations. All simulations were performed with the geochemical code PHREEQC-2[199] and the database MINTEQA2[198].

3.3 Results and Discussion

3.3.1 Mineral buffering capacity

The evolution of pH during abiotic mineral dissolution in both anaerobic AGW and HCl solution is presented in Figure 3.1. All the minerals tested were able to increase the pH from 5 to neutral or slightly basic values within 1 to 7 d. The final pH obtained at equilibrium, $pH_{eq,}$ represents the pH above which the primary silicate mineral precipitates and below which it dissolves for the experimental conditions tested. pH_{eq} is important because it indicates whether mineral dissolution may result in pH overshooting, i.e., a final pH in the basic range. Basic conditions (pH > 9) are as unfavorable to OHRB as acidic conditions. For the experiments with AGW, the pH_{eq} of nepheline and fayalite was between 6.5 and 7 while that of diopside, forsterite and andradite was between 8 and 8.6.

For OHRB consortia, complete degradation of PCE to ethene occurs between pH 6.0 and 8.3[132] whereas partial degradation of PCE to *cis*-DCE occurs in a broader pH range of 5 to 9-10[129,130,132]. The pH values determined in this study fall in the range of tolerance of the microorganisms, although the pH_{eq} value of andradite (8.5) and forsterite (8.65) were slightly outside the optimal range for complete degradation.

Figure 3.1 shows that water composition had a significant impact on pH_{eq}. In fact, in the experiments where the HCl solution was used, the pH_{eq} values were consistently higher than those obtained for AGW (9 to 9.5 for diopside, forsterite and andradite and close to 7.3 for nepheline and fayalite). The reason is that AGW is a complex solution that has some buffering capacity, whereas for the pure HCl solution a small increase in the concentration of base cations increases the pH abruptly. Consequently, the HCl solution is not representative of groundwater conditions and pH overshooting above pH 9-9.5 is a worst case situation that is unlikely to occur in practice. This indicates that a realistic water composition must be considered when designing a field application.

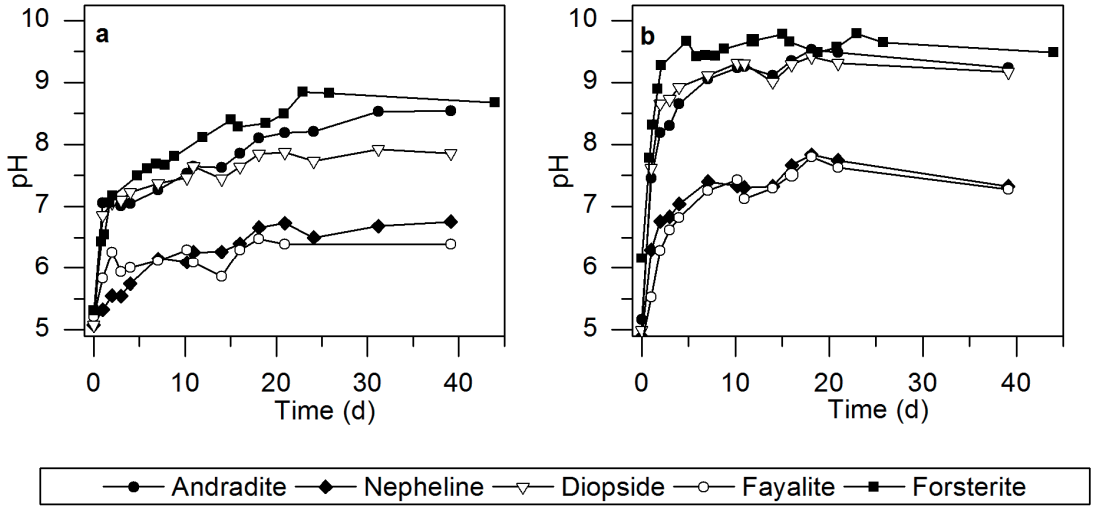

Figure 3.1. pH evolution during abiotic mineral dissolution in AGW (a) and HCl solution (b) for the five minerals tested.

3.3.2 Solubility constants and kinetic parameters

The solubility product constant controls the extent of mineral dissolution and was found to be a key parameter for identifying the appropriate buffering mineral in a given application (see Chapter 2). The apparent log K_{eq} at 25°C (Table 3.1) ranged from 11.2 ± 0.15 for nepheline to 28.8 ± 0.05 for forsterite and was correlated with $pH_{eq.}$ Higher K_{eq} values correspond to higher values of pH_{eq}. The solubility of nepheline and fayalite was low compared to that of diopside and forsterite. The K_{eq} value for andradite ($Ca_3Fe_2Si_3O_{12}$) could not be computed because the total dissolved iron concentration was below the detection limit due to secondary precipitation of ferric iron at slightly basic pH. It was also observed that the apparent K_{eq} value was slightly higher in the HCl solution than in the AGW. Some authors have reported variations of K_{eq} with pH for other minerals such as iron oxides and aragonite[240,241], with K_{eq} values increasing with pH. This is consistent with our results. Another possible explanation for the different K_{eq} values found for AGW and HCl is that the solubility product in AGW is controlled by the solubility of secondary phases (which precipitate) and not by the solubility of the primary silicate mineral. The secondary phases likely to form in AGW are discussed below. The differences between the K_{eq} values determined in this study and those reported in the literature are up to four orders of magnitude. These differences may appear large, but are in fact in the range of variability observed among different studies on a specific mineral[242-244]. Possible explanations for the discrepancies are the use of different methodologies to calculate the activities[244], the presence of impurities in the natural samples[242], and the pH at which K_{eq} is determined[241].

Table 3.1. Apparent solubility product constants determined experimentally and comparison with data from geochemical databases (MINTEQA2,[198], LLNL[200], THERMODDEM[197]). K_{eq} values were experimentally determined at 30°C and corrected for temperature using the van't Hoff equation. The solubility product constant of andradite could not be determined because the iron concentration was below the detection limit. The solubility product constant of nepheline could not be determined in AGW because aluminum was below the detection limit.

		K_{eq} (at 25°C)		
Mineral	Dissolution equation	HCl solution	AGW	Literature
Andradite	$Ca_3Fe_2Si_3O_{12} + 12H^+ = 3Ca^{2+} + 2Fe^{3+} + 3\ H_4SiO_4$	n.d.	n.d.	[16.8; 33.4]
Diopside	$CaMg(SiO_3)_2 + 4H^+ + 2H_2O = Ca^{2+} + Mg^{2+} + 2H_4SiO_4$	23.7±0.25	20±0.6	[19.8; 21.7]
Fayalite	$Fe_2SiO_4 + 4H^+ = 2Fe^{2+} + H_4SiO_4$	16.6±0.25	14.7 ±0.1	[19; 19.1]
Forsterite	$Mg_2SiO_4 + 4H^+ = 2Mg^{2+} + H_4SiO_4$	28.8±0.05	26.9±0.25	[27.8; 28.6]
Nepheline	$NaAlSiO_4 + 4H^+ = Al^{3+} + Na^+ + H_4SiO_4$	11.2±0.15	n.d.	[13.8; 14]

n.d.: not determined

Other important parameters are the dissolution rate constants in the acidic and neutral ranges. The estimated parameters from the experiments are listed in Table 3.2. When determined by fitting experimental data, the parameter n_{H+} in Eq. 3.5 was found to be sensitive to data in the acidic range. However, in our experiments, the pH mostly ranged between 6 and 10. For this reason, n_{H+} was fixed to a typical value taken from the literature and only k_{H+} and k_W were calibrated. The model was fitted to the data using a non-linear least squares method and the trust region algorithm, as implemented in MATLAB (www.mathworks.com) (Figure 3.2). For each parameter, a range of values was identified using the 95% interval confidence bounds obtained from the fitting procedure. The estimates of k_{H+} are within the literature ranges for all minerals except nepheline, for which the dissolution kinetics were slower compared to those measured by Tole, Lasaga, Pantano and White et al.[203]. The values of k_W are lower but close to literature values (within an order of magnitude) for diopside, forsterite and andradite. A greater difference was found for fayalite and nepheline, for which k_W is around two orders of magnitude smaller than the literature values. As already observed for the solubility constant, such differences are common and are due to the conditions used in the different studies, such as variation in experimental design and mineral preparation, mineral composition, degree of cation disorder, degree of crystallinity, variation in frequency and distribution of crystal defects[166], and inexact estimation of the reactive surface area[233,245,246]. In addition, for fayalite and nepheline, only one dataset for each mineral was found in the literature to evaluate the kinetics. From this, it was concluded that before selecting a mineral for pH control, it is useful to perform some laboratory experiments to determine more precisely the kinetic parameters in the experimental conditions and with the mineral of interest, rather than relying only on literature data.

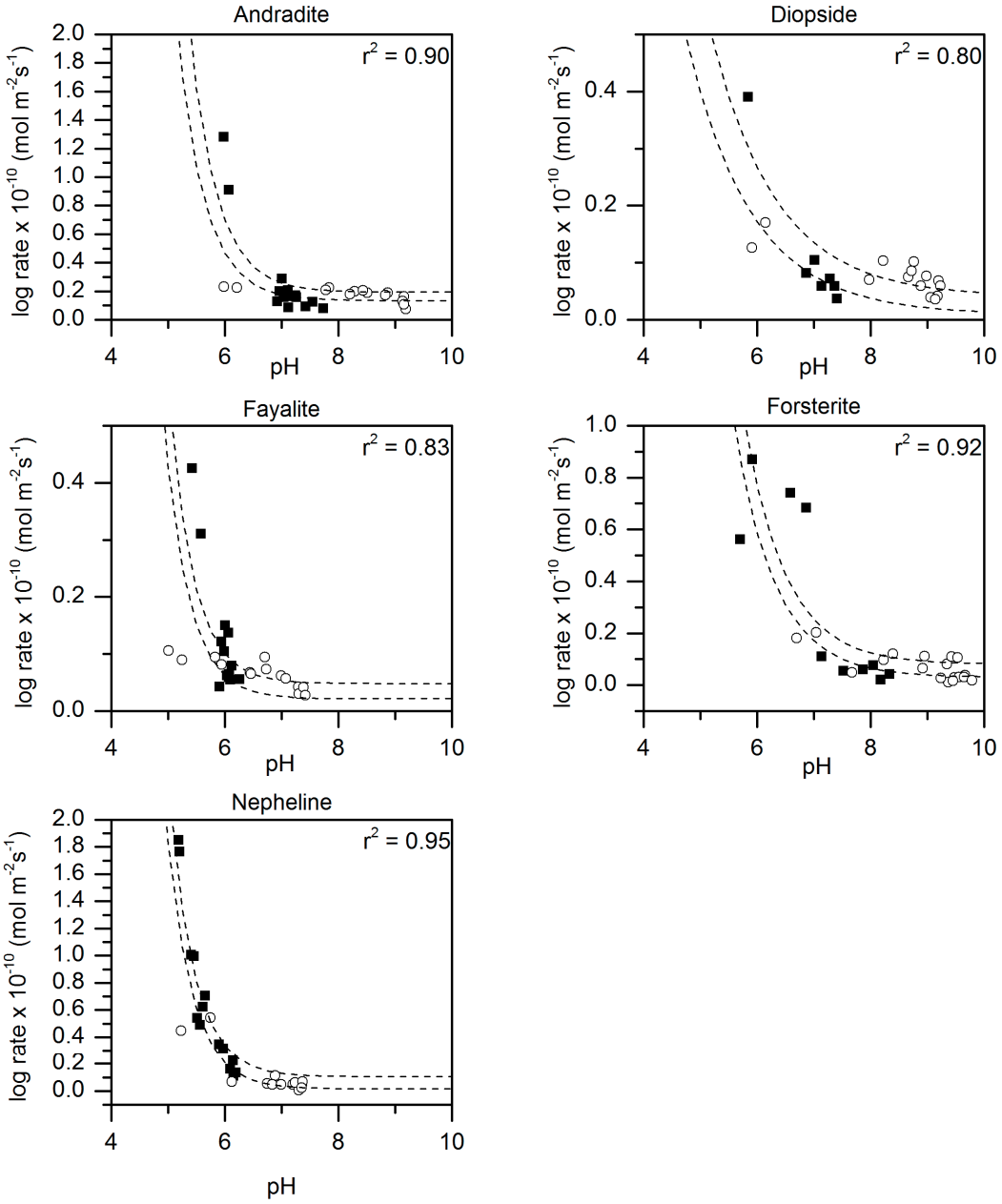

Figure 3.2. Normalized dissolution rate in the HCl solution (○) and artificial groundwater solution (AGW) (■) during the first 10 d of the mineral dissolution experiments. The lines represent the fit of Eq. 3.5 to the data (lower and upper 95% confidence bounds). The correlation coefficients (r^2) are indicated. The fitted parameters are listed in Table 3.2

Table 3.2. Range of rate constants in the acidic and neutral ranges at 25°C determined in this study for the five minerals tested and comparison with values from other studies. The kinetic constants were determined experimentally at 30°C and corrected for temperature using the van't Hoff equation.

Mineral	This study		Other studies		
	log k_{H^+}	log k_W	log k_{H^+}	log k_W	References
Andradite	[-5.4,-5.2]	[-11.2,-11.0]	-5.2	-10.7	Sverdrup[202]
Diopside	[-8.8, -8.6]	[-12.1, -11.5]	[-8.9, -9.5]	[-11.2, -11]	Knauss et al.[171,212], Golubev et al. [216]
Fayalite	[-5.7, 5.6]	[-11.9, -11.6]	[-5.9, -4.8]	-9.5	Sverdrup[206],Wogelius and Walther[214]
Forsterite	[-6.9,-6.8]	[-11.7, -11.3]	[-6.8, 6.7]	[-10.7, -10.1]	Pokrovsky and Schott[215], Golubev et al.[211]
Nepheline	[-5.1, -5]	[-12, -11.2]	-3.5	-8.6	Tole et al.[203]

3.3.3 Model validation

The results of the abiotic dissolution of minerals in AGW were used to validate and extend the geochemical model previously developed[238]. Modeling of abiotic mineral dissolution was done using K_{eq} as determined experimentally (Table 3.1), the fitted kinetic parameters (Table 3.2), and the stoichiometry coefficients of each mineral deduced from the results of XRF analyses (Table A3.1 in Appendix). An exhaustive list of parameters used for the numerical simulations is presented in Table A3.2 (Appendix). Total elements concentrations and pH evolution over time during dissolution in AGW are presented in Figure 3.3 together with the modeling predictions.

The results showed that mineral dissolution was clearly incongruent (Figure 3.3), i.e., non-stoichiometric. Incongruent dissolution can be the result of preferential release of a specific cation and/or secondary phase precipitation. Prediction of secondary mineral precipitation based only on geochemical modeling is challenging because data are scarce[166,247]. In addition, the degree of saturation needed for a mineral to precipitate is different for each mineral and is in most cases unknown[229].

Simulations were first performed without forcing mineral precipitation. The supersaturated minerals were noted and recorded. Not all supersaturated minerals were assumed to precipitate. Rather, the changes in the concentrations of major elements (e.g., diminution of concentration over time or non-stoichiometric release of an ion) were used to deduce which of the supersaturated minerals identified by the simulations did actually precipitate. In addition, a literature review was performed to identify which secondary minerals are commonly observed in conditions similar to those of our experiments (T = 30°C, atmospheric pressure, anaerobic conditions). Once these phases were identified, the model was modified to allow precipitation. The target saturation index for precipitation was identified fitting the experimental data. After including secondary phase precipitation, model predictions were in good

agreement with the experimental results (Figure 3.3 and Table 3.3) with most correlation coefficients above 0.9. This indicates that the model was able to predict mineral dissolution rates and the subsequent water chemistry changes. Although the model provides acceptable fits to the observations, at the beginning of the experiments, during day 1, a strong preferential release of calcium ions was observed for calcium-bearing minerals (andradite and diopside). This behavior, which has been observed in numerous other studies during dissolution of freshly ground mineral powder, was not reproduced by the model. It might be due to the localization of calcium in weakly bound sites in the mineral structure[171]. It was chosen not to adapt the model to reproduce this rapid release of calcium, as it would involve artificially adding an appropriate mineral without any obvious benefit other than reproducing the short-time data. Instead, for andradite and diopside, simulations were performed starting at day 1, after completion of the initial dissolution spike.

As already indicated, secondary phase precipitation affected the mineral dissolution patterns predicted by the geochemical model. Since the rate-dependent (kinetic) behavior of mineral precipitation is unknown, it was assumed that equilibrium precipitation occurred after reaching a threshold saturation index. Several possible secondary phases were identified. For calcium-bearing silicates, a decrease of calcium concentration was observed above pH 7.5. This drop of calcium in solution correlated with a decrease in the concentration of PO_4^{3-} at the end of the experiment (results not shown), thus suggesting precipitation of hydroxyapatite ($Ca_5(PO_4)_3OH$). This hypothesis is corroborated by numerous studies showing that in geochemical environments such as soils and sediments, hydroxyapatite is often the most thermodynamically stable solid phase predicted to control activities of Ca^{2+} and PO_4^{3-} [248]. Note that hydroxyapatite is usually formed in the pH range 7.4 to 8.4[249,250], which is relevant for our experiments.

For nepheline (aluminum bearing), the Al^{3+} concentration was below the detection limit. Simulations showed that this was consistent with precipitation of aluminum phosphate ($AlPO_4$) or aluminum hydroxides, such as gibbsite ($Al(OH)_3$). Precipitation of $AlPO_4$ was supported by the phosphate measurements that were below the detection limit at the end of the experiment. Precipitation of gibbsite and its $Al(OH)_3$ polymorphs was also found previously, where it was shown that these solid phases readily precipitate under a wide variety of experimental conditions[251].

For fayalite, andradite, forsterite and diopside, which all contained iron, simulations showed that precipitation of iron sulfide (FeS) in the form of mackinawite explained the low iron concentration observed (often below the detection limit). Several studies reported that, in experiments carried out in similar conditions to ours (i.e., similar T and pH), FeS is the first solid phase to precipitate in natural anoxic Fe-S systems[252-254]. Precipitation of hematite (Fe_2O_3) was also predicted. In the experiment with fayalite, precipitation of vivianite, an iron-phosphate complex ($Fe_3(PO_4)_2{:}8H_2O$), possibly occurred according to modeling predictions and phosphate measurements. In the case of forsterite dissolution, precipitation of magnesium and silica was observed toward the end of the experiment when the pH

was above 8.7, which was attributed to precipitation of talc ($Mg_3Si_4O_{10}(OH)_2$). This is consistent with the recent a study of Tosca et al.[255], showing that talc precipitation at 25°C occurs only if the pH is greater than 8.7. Magnesite ($MgCO_3$) precipitation was also predicted during forsterite dissolution, a process that often occurs in natural environments[161].

In the nepheline dissolution experiment, the main difference between model and data is the sodium concentration. The AGW initially had a high sodium concentration, which decreased over time, suggesting precipitation to a sodium-bearing mineral. However, the geochemical model (using the MINTEQA2 database) did not predict any supersaturated Na-mineral phases. A possible explanation is the precipitation of solid $NaAlPO_4$. For this salt, literature data (solubility constants, precipitation conditions, etc.) are very scarce, and insufficient for modeling purposes. Consequently, Na precipitation was not included in the model.

A summary of the minerals which were allowed to precipitate and the threshold saturation indexes are listed in Table A3.3 (Appendix) for the five minerals studied. Minerals that were predicted to precipitate along with the mass of precipitate are presented in Table 3.4. Table A3.4 (Appendix) lists the dissolution equations and solubility constants of the secondary minerals considered. These results indicate that, at least for the five minerals tested, precipitation of secondary phases must be considered when the minerals are dissolved in a complex solution (e.g., containing a variety of nutrients). Precipitation of secondary mineral phases can have several impacts, (i) it influences the solution pH and usually reduces the pH_{eq}, (ii) it affects the availability of nutrients needed for microbial metabolism (such as in the cases of phosphate precipitation), (iii) secondary phases can change the hydraulic conductivity by decreasing the porosity and connectivity of the pore-space and (iv) it can reduce the reactivity of the silicate minerals by formation of coatings at the mineral surface.

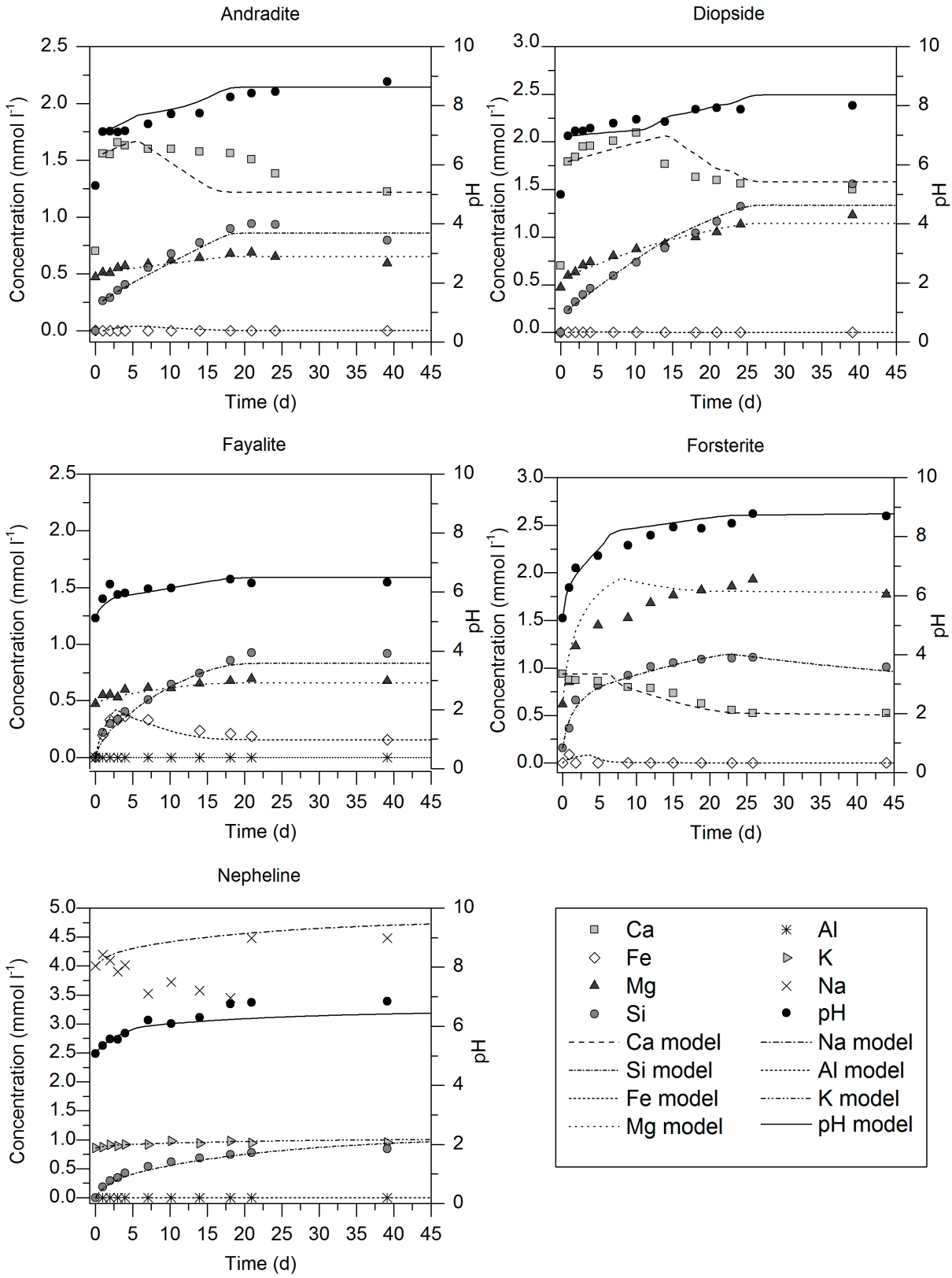

Figure 3.3. Evolution of pH and major total amount of elements (Ca, Fe, Mg, Si, Al, K and Na) over time during abiotic mineral dissolution in AGW. For each mineral, all the main elements present in the mineral sample were plotted. For the experiment with forsterite, Ca^{2+} although not present in the mineral, is plotted to show the precipitation of calcium over time. The lines represent the prediction of the geochemical model

Table 3.3. Correlation coefficients for the observations versus model predictions for mineral dissolution during AGW

	Forsterite	Diopside	Fayalite	Nepheline	Andradite
pH	0.99	0.93	0.88	0.97	0.96
Si	0.99	0.98	0.99	0.99	0.99
Mg	0.92	0.98	0.96		0.90
Ca	0.96	0.72			0.67
Fe			0.94		
K				0.90	
Na				0.05	

Table 3.4. List of minerals assumed to precipitate and predicted mass of mineral precipitated.

Primary mineral	Secondary precipitates	Mass (mg)
Andradite	Hydroxyapatite ($Ca_5(PO_4)_3OH$)	11.37
	Mackinawite (FeS)	2.18
Diopside	Hydroxyapatite ($Ca_5(PO_4)_3OH$)	9.38
	Hematite (Fe_2O_3)	0.98
Fayalite	$AlPO_4$	3.81
	Mackinawite (FeS)	11.23
	Vivianite ($Fe_3(PO_4)_2$:$8H_2O$)	6.73
Forsterite	Hydroxyapatite ($Ca_5(PO_4)_3OH$)	6.57
	Mackinawite (FeS)	2.25
	Magnesite ($MgCO_3$)	8.44
	Talc ($Mg_3Si_4O_{10}(OH)_2$)	4.85
Nepheline	$AlPO_4$	8.23
	Gibbsite(C) ($Al(OH)_3$)	6.06

3.4 Conclusions

The experiments conducted in this study provided additional insights into the dissolution/precipitation mechanisms of silicate minerals, and led to an extension (precipitation of secondary phases) of our previously reported geochemical model. The revised geochemical model was able to predict well the evolution of both pH and water chemistry during mineral dissolution. The experimental results confirmed the potential of the silicate minerals tested (andradite, diopside, fayalite, forsterite and nepheline) to prevent groundwater acidification and to maintain the pH close to neutral (i.e., between 7 and 8.6). The experiments enabled us to infer the kinetic and solubility product constants for the five minerals considered, information that is crucial for the successful application of the model.

Nepheline and fayalite were found to be more suitable for applications requiring the pH to remain in the 6 to 6.5 range, while forsterite, andradite and diopside are more suitable for the 7.5 to 8.5 range. As mentioned, the results of the experiments and the comparison with model predictions highlighted the importance of secondary mineral precipitation in the evolution of the solution pH and composition, and ultimately on mineral dissolution. The phases that most likely precipitate during primary silicate mineral dissolution in anaerobic conditions were also identified for the experimental conditions considered.

Finally, this study highlights the influence of groundwater composition on the buffering efficiency of silicate minerals and particularly on the equilibrium pH. The geochemical model developed is a useful tool for selecting the most appropriate buffering mineral for given environmental parameters such as temperature and pore-water composition. For application to (long-term) field remediation schemes, further studies should be conducted to evaluate the buffering efficiency of the considered minerals on longer time scales (see Chapter 5) and to evaluate the interactions between silicate mineral dissolution and OHRB (see Chapter 3).

3.5 Appendix

Table A3.1. Stoichiometric coefficients for the minerals used for modeling simulations determined from the results of XRF analyses (Table A3.5).

	Si	Al	Fe	Mg	Ca	Na	K
Diopside	2.00	-	0.12	1.02	0.75	-	-
Fayalite	1	0.25	1.53	0.23	-	-	-
Andradite	1	-	0.28	0.24	0.70	-	-
Nepheline	1	0.91	-	-	-	0.74	0.14
Forsterite	1	-	0.14	1.83	-	-	-

Table A3.2. List of parameters used for modeling mineral dissolution in AGW.

	Andradite	Diopside	Fayalite	Forsterite	Nepheline
$K_{eq\ T=25°C}$	16	22	15.3	26.9	11.1
$k_{H+\ T=25°C}$	-5.25	-8.7	-5.5	-6.8	-5
$k_{W\ T=25°C}$	-11.25	-11.8	-11.8	-11.8	-11.2
$n_{H+\ T=25°C}$	0.9	0.38	1	0.6	0.97
Ew	103.8	40.6	94.4	79	62.9
E_{H+}	94.41	96.1	94.4	67.2	65.4
Total surface area in batch (m^2)	1.63	5.115	8.745	7.4	1.79

Table A3.3. Minerals allowed to precipitate in the model and the saturation index (Ω_t) at which precipitation occurred.

Primary mineral	Secondary mineral phases	Ω_t
Andradite	Hydroxyapatite ($Ca_5(PO_4)_3OH$)	0.0
	Mackinawite (FeS)	2.2
	Hematite (Fe_2O_3)	0.0
	Greigite (Fe_3S_4)	3.0
	Vivianite ($Fe_3(PO_4)_2$:$8H_2O$)	2.0
Diopside	Hydroxyapatite ($Ca_5(PO_4)_3OH$)	0.0
	Mackinawite (FeS)	2.2
	Hematite (Fe_2O_3)	0.0
	Greigite (Fe_3S_4)	3.0
Fayalite	$AlPO_4$	0.0
	Mackinawite (FeS)	2.2
	Hematite (Fe_2O_3)	0.0
	Greigite (Fe_3S_4)	3.0
	Vivianite ($Fe_3(PO_4)_2$:$8H_2O$)	2.0
Forsterite	Hydroxyapatite ($Ca_5(PO_4)_3OH$)	0.0
	Mackinawite (FeS)	2.2
	Hematite (Fe_2O_3)	0.0
	Greigite (Fe_3S_4)	3.0
	Vivianite ($Fe_3(PO_4)_2$:$8H_2O$)	2.0
	Magnesite ($MgCO_3$)	0.0
	Talc ($Mg_3Si_4O_{10}(OH)_2$)	8.9
Nepheline	Gibbsite(C) ($Al(OH)_3$)	1.0
	$AlPO_4$	0.0
	$Al(OH)_3$(a)	0.0

Table A3.4. Precipitation reactions used in the model for prediction of secondary phase precipitation.

Mineral	Precipitation reaction	log K_{eq}	ΔH (kcal)
Hydroxyapatite	$Ca_5(PO_4)_3OH + H^+ = 5Ca^{2+} + 3PO_4^{3-} + H_2O$	-32.5	unknown
Mackinawite	$FeS + H^+ = Fe^{+2} + HS^-$	-4.6	unknown
Hematite	$Fe_2O_3 + 6H^+ = 2Fe^{+3} + 3H_2O$	-4	-30.8
Greigite	$Fe_3S_4 + 4H^+ = 2Fe^{+3} + Fe^{+2} + 4HS^-$	-45	unknown
Vivianite	$Fe_3(PO_4)2{:}8H_2O = 3Fe^{+2} + 2PO_4^{-3} + 8H_2O$	-36	unknown
Magnesite	$MgCO_3 = Mg^{2+} + CO_3^{2-}$	-8	-6.2
Talc	$Mg_3Si_4O_{10}(OH)_2 + 4H_2O + 6H^+ = 3Mg^{2+}+4H_4SiO_4$	23	-35
$AlPO_4$	$AlPO_4 + 2H^+ = Al^{3+} + H_2PO_4^-$	-9	unknown
Gibbsite(C)	$Al(OH)_3 + 3H^+ = Al^{3+} + 3H_2O$	8.8	-22.8
$Al(OH)_3$(a)	$Al(OH)_3 + 3H^+ = Al^{3+} + 3H_2O$	10.4	-27

Table A3.5. Major elements composition of mineral samples determined by XRF.

	Major elements (wt / wt %)											
Sample	SiO_2	TiO_2	Al_2O_3	Fe_2O_3	MnO	MgO	CaO	Na_2O	K_2O	P_2O_5	Cr_2O_3	NiO
Andradite	42.75	0.08	2.48	16.14	0.66	6.96	27.77	0.47	0.00	0.16	0.00	0.00
Diopside	53.95	0.01	0.82	4.40	0.10	18.49	18.87	0.12	0.00	0.03	0.16	0.09
Fayalite	29.14	0.53	6.06	59.22	2.15	4.58	1.35	0.08	0.47	0.45	0.01	0.01
Forsterite	40.68	0.01	0.61	7.49	0.1	49.94	0.01	0.00	0.00	0.01	0.44	0.34
Nepheline	43.05	0.01	33.34	0.33	0.00	0.00	0.56	16.48	4.88	0.01	0.00	0.00

Chapter 4

Use of silicate minerals for pH control during reductive dechlorination of chloroethenes in batch cultures of different microbial consortia

---

4 Use of silicate minerals for pH control during reductive dechlorination of chloroethenes in batch cultures of different microbial consortia

Abstract

In chloroethene-contaminated sites undergoing *in situ* bioremediation, groundwater acidification is a frequent problem, especially in the source zone, and buffering strategies have to be implemented to maintain the pH in the neutral range and sustain bacterial activity. A potential alternative to conventional soluble buffers is silicate mineral particles as a long-term source of alkalinity. In previous studies, the buffering potential of these minerals was evaluated based on abiotic dissolution tests and geochemical modeling. In the present study, the buffering potential of five silicate minerals was tested in batch cultures amended with tetra- and *cis*-1,2-dichloroethene (*cis*-DCE), and inoculated with different organohalide-respiring consortia. The consortia showed significant differences in sensitivities towards acidic pH for the different dechlorination steps in cultivation media with soluble buffering agents. Molecular analysis indicated that *Dehalococcoides* spp. that was present in all consortia, were the most pH sensitive organohalide-respiring guild members compared to *Sulfurospirillum* spp. and *Dehalobacter* spp. In batch cultures with silicate mineral particles as pH buffer, four of the five minerals tested were able to maintain the pH in the appropriate range for reductive dechlorination of chloroethenes. However, dechlorination was almost always incomplete with *cis*-DCE as the end product indicating an inhibition effect of silicate minerals and/or its dissolution products on reductive dechlorination of *cis*-DCE. Its dechlorination to ethene was only observed in one consortium amended with ground fayalite. These results showed that despite the theoretical pH buffering potential of silicate mineral particles, compatibility with the bacterial community involved in *in situ* bioremediation has to be carefully evaluated prior to their use for pH control at a specific site.

4.1 Introduction

In chloroethene-contaminated sites undergoing *in situ* bioremediation, groundwater acidification is a frequent problem[53,63,68,149]. The extent of groundwater acidification is related to the amount of substrate transformed and to the natural buffering capacity of the soil. Due to the larger mass of pollutant present, acidification is more likely to occur in the vicinity of the chlorinated ethene source zone[22,148]. The tolerance of OHRB to low pH has been studied for pure cultures[101,105,106,108,121,122,126-128] and some OHRB consortia[129,130]. It has been shown that OHRB are inactivated under acidic conditions and therefore pH buffer amendments are required when the initial pH is too low or when the soil buffering capacity is insufficient[53,148,256]. The buffering capacity of ground silicate minerals for pH control during groundwater remediation has previously been demonstrated by geochemical modeling (see Chapter 2) and abiotic mineral dissolution experiments (see Chapter 3). According to the results of Chapter 3, five silicate minerals (diopside, forsterite, fayalite, nepheline and andradite) have promising groundwater buffering capacity. In the present study, the use of powders of these silicate minerals as buffering agents in actively dechlorinating batch cultures of consortia containing different OHRB was tested. Special emphasis was put on the effect of pH and the presence of a silicate mineral buffer on each step of PCE dechlorination to ethene.

4.2 Materials and Methods

4.2.1 Chemicals

All chemicals were analytical grade and used without purification. Tetrachloroethene (PCE) (99%) and n-hexadecane (99%) were obtained respectively from Acros Organics and Merck. Due to the possible presence of inhibiting compounds in synthetic *cis*-DCE, biogenic *cis*-DCE prepared following Maymo-Gatell et al.[112] was used, with *Desulfitobacterium hafniense* strain TCE1 used as a *cis*-DCE producer. All gases (N_2, CO_2, H_2) were supplied by Messer Schweiz AG, Switzerland.

4.2.2 Organohalide-respiring consortia

The five organohalide-respiring consortia used in this study, SL2-PCEa, SL2-PCEb, AQ-1, AQ-5 and PM were isolated from chlorinated ethene-contaminated aquifers and enriched and maintained in the laboratory for several years. Details of the enrichment process were described by Szynalski[257] for SL2-PCEa, SL2-PCEb, AQ-1 and AQ-5 and by Yu[258] for the PM culture. The consortia AQ-5, SL2-PCEa and PM have the ability to dechlorinate PCE to ethene completely. SL2-PCEb is a subculture of SL2-PCEa and dechlorinates PCE only to *cis*-DCE. Consortium AQ-1 dechlorinates *cis*-DCE to ethene but cannot grow on PCE or TCE.

4.2.3 Effect of pH on the OHR rate

The influence of mildly acidic to neutral pH on the OHR rates was determined for the five consortia described above. Duplicate batch tests were conducted in 500-ml serum bottles containing 200 ml of anaerobic growth medium. For each consortium, six different pH values were tested from pH 5 to pH 7.5 with a stepwise increment of 0.5 pH units. Tests at pH > 7.5 were not possible due to precipitation of calcium phosphate, which made phosphate unavailable for bacterial growth and activity. The anaerobic growth medium used was similar to one described previously[101] with the following modifications: $NaH_2PO_4.2H_2O$ and $NaHCO_3$ were replaced by zwitterionic buffers: 2-(*N*-morpholino) ethanesulfonic acid (MES) at 100 mmol l^{-1} for pH 5 to 6.5 and 3-(N-morpholino) propanesulfonic acid (MOPS) at 100 mmol l^{-1} for pH 7 to 7.5. The initial pH was adjusted by addition of NaOH or HCl. The bottles were sealed with Viton rubber stoppers and the gas phase of the bottles was replaced with 100% hydrogen (for SL2-PCEa and SL2-PCEb) or 100% of nitrogen (for AQ-1, AQ-5 and PM) using a gas exchange system. To provide the chloroethenes, a two-liquid phase system[102] was used with PCE and *cis*-DCE dissolved in hexadecane. The nominal chloroethene concentration in the medium was 5 mM, except for consortium PM where it was 1.25 mM. Acetate (final concentration 2 mM) was added as a carbon source for SL2-PCEa and SL2-PCEb from concentrated stock solutions. Consortia AQ-1 and AQ-5 were amended weekly with an electron donor mixture of ethanol, propionate and butyrate (0.66 mM each per week) and consortium PM with 1.2 mM lactate per week. The cultures were inoculated with 8 ml of pre-culture and incubated at 30°C in the dark without agitation. Measurements of pH and the chloroethene concentrations were performed on a regular basis. Finally, experimental observations were fitted to the equation:

$$R_{D,i} = r_{max,i} f(\mathrm{pH}), \tag{4.1}$$

where $R_{D,i}$ is the degradation rate of the chloroethene i, $r_{max,i}$ is the maximum degradation rate and f(pH) is the inhibition function pH (see Eq. 4.3).

4.2.4 Molecular detection of OHRB

Terminal Restriction Fragment Length Polymorphism (T-RFLP) analyses were conducted to evaluate the microbial community structure of the consortia SL2-PCEa, SL2-PCEb, AQ-1 and AQ-5. The analyses were performed at the end of the experiments conducted to investigate the influence of pH on OHR rates. DNA extraction and T-RFLP analysis were carried on cells from a 20-ml culture aliquot as described previously[259] with the following modifications: For each sample, three T-RFLP analyses with three restriction enzymes (Hae III, HhaI and Msp I, Promega) were conducted. The affiliation of T-RFs to known OHRB was achieved by using a semi-specific T-RFLP method using a semi-specific PCR with the non-specific primer Eub-8F and a specific reverse primer for the genus of interest. Reverse primers were taken from Smits et al.[260] for *Dehalobacter restrictus*, Adrian et al.[261] for

Dehalococcoides spp., Lanthier et al.[262] for *Desulfitobacterium* spp, and Daprato et al.[263] for *Sulfurospirillum* spp. Pure cultures and highly enriched consortia of known composition were used as positive controls. The semi-specific T-RFLP analyses were conducted in parallel with three restriction enzymes Hae III, Hha I and Msp I in order to obtain three T-RFs corresponding to one genus (see Table A4.1 in the Appendix).

4.2.5 Minerals preparation and characterization

Bulk mineral samples of the five silicate minerals tested were purchased from Dr. F. Krantz Rheinisches Mineralien-Kontor Gmbh and Co. Kg (Bonn, Germany): andradite ($Ca_3Fe_2Si_3O_{12}$, from Erzgebirge, Sachsen, Germany), diopside ($CaMg(SiO_3)_2$, Outukumpu, Finland), fayalite (Fe_2SiO_4, Billiton, Indonesia), forsterite (Mg_2SiO_4, Aheim, Northfjord, Norway) and nepheline ($NaAlSiO_4$, Stoledalen, Norway). These minerals were chosen as they were identified as suitable buffering agents in the study described in Chapter 3. The minerals were prepared as described in Chapter 3 section 3.2.1. Chemical compositions and specific surface area were determined as described before in section 3.2.1. Trace elements were analyzed by laser ablation inductively coupled plasma mass spectrometry (ICP-MS) with a quadrupole spectrometer Elan 6100 DRC.

4.2.6 Evaluation of buffering capacity of silicate minerals in biotic experiment

Biotic experiments to investigate the acid neutralizing capacity of silicate minerals during OHR of chlorinated compounds were performed with the three consortia, SL2-PCEa, SL2-PCEb and AQ-1. AQ-5 and PM consortia were not used because they showed activity in a too narrow pH range (for AQ-5) or because it was difficult to obtain reproducible results with the growth medium used in this experiment (for PM). Duplicate batch tests were conducted in 120-ml serum bottles containing 50 ml of sterile anaerobic growth medium, modified from Holliger et al.[101] to reduce the soluble buffering capacity so that the main source of pH buffering was the mineral powder. The following modifications were made: $K_2HPO_4.3\ H_2O$ at 0.49 mM, NH_4HCO_3 at 0.98 mM, and removal of $NaH_2PO_4.2H_2O$ and $NaHCO_3$. A small amount of bicarbonate and phosphate was kept in the medium to cover the metabolic needs of the bacteria. For consortium AQ-1, it had been shown in a preliminary study (results not shown) that the low-buffered medium ionic strength was too low and inhibited *cis*-DCE degradation. Therefore, for this consortium, the ionic strength of the anaerobic medium was raised by increasing the concentration of $MgCl_2$, $CaCl_2$ and NaCl to 4.4, 7.0 and 19.5 mmol l^{-1} respectively. Electron donors, carbon sources and chloroethenes were amended as described above. The nominal chloroethene concentration in the medium was 5 mM of PCE for SL2-PCEb, 2.5 mM of PCE for SL2-PCEa and 0.6 mM of *cis*-DCE for AQ-1. For AQ-1, the microcosms were amended with 5 ml of the electron donor mixture (ethanol, propionate, butyrate) on day 0 with no re-amendment during the experiment. The mineral powder was introduced in sterile conditions in the batch cultures before gas exchange and addition of the reducing agent. The amounts of sterile mineral powder added to each

batch culture were based on preliminary results of screening experiments and geochemical simulations described below. The amount of mineral, listed in Table A4.2 (Appendix), was chosen so as to maintain the pH in the tolerance range for each consortium. The five minerals chosen were tested with consortium SL2-PCEb. For experiments with SL2-PCEa and AQ-1, nepheline was excluded because results with SL2-PCEb showed that its buffering capacity was insufficient in the given experimental conditions. Two types of controls without mineral powder were performed, (i) a "positive" control with a standard medium as described previously[101] and (ii) a "negative" control with the low-buffered medium described above. The batch cultures were incubated in the dark at 30°C on an overhead shaker at 20 rpm. Measurements of pH, chloroethenes, volatile fatty acids (acetate, propionate, and butyrate), ethanol and total elements concentrations were performed on a regular basis. Analytical measurements were performed until complete transformation of chloroethenes to ethene or *cis*-DCE (for SL2-PCEb) or until dechlorination ceased due to inhibition.

4.2.7 Analytical methods

PCE, TCE, *cis*-DCE, VC and ethene were analyzed by gas chromatography with a GC Varian Star 3400CX equipped with a GS-GasPro column (30 m by 0.32 mm; J&W Scientific, MSP Friedly & Co, Koeniz, Switzerland) coupled to a flame ionization detector. One hundred microliters of gas samples were collected from the headspace with a Hamilton gastight syringe (Leno, NV) and analyzed on the GC with a 1.3 ml min^{-1} flow of nitrogen carrier gas. The initial temperature was 45°C; the column was kept at 45°C for 3 min, and then the temperature was raised to 75°C at a rate of 15°C min^{-1} and then to 200°C at a rate of 25°C min^{-1} and finally kept at 200°C for 5 min. pH and total concentration of Mg, Si, Ca, and Fe were determined as described in Chapter 3 section 3.2.2. Volatile fatty acids and ethanol concentration were measured with a high performance liquid chromatograph (HPLC) equipped with an organic acid ion exclusion column ORH-801 (Transgenomics, UK) and a refraction index detector (HPLC Jasco Co-2060 Plus, Omnilab, Germany). Samples for HPLC analyses were prepared as follows: 1 ml of diluted sample (× 10) was mixed with 125 µl of barium hydroxide ($Ba(OH)_2$) and 125 µl zinc sulfate ($ZnSO_4$) in a 2 ml cryotube. The mixture was centrifuged for 1 min at 10,000 × g and the supernatant was withdrawn and filtered at 0.2 µm.

4.2.8 Modeling approach

A geochemical model was used to determine the amount of mineral needed to maintain the pH neutral during the biodegradation of a given amount of chloroethenes. Numerical simulations were performed with the geochemical software PHREEQC-2[199] and with the database MINTEQA2[198] using a modified version of the geochemical model described in Chapter 2. The amount of mineral needed was chosen such that the cations released by mineral dissolution counterbalanced acidity production by bacterial activity. Chloroethene transformations were modeled by a simplified Monod-type kinetics, which did

not take biomass growth into account because growth parameters were unknown for the consortia used in this study:

$$R_i = \frac{k_{max,i} C_i}{K_{S,i}\left(1+\frac{C_j}{K_{I,j}}\right)+C_i} f(\mathrm{pH}), \tag{4.2}$$

where R_i is the degradation rate of the chloroethene i, C_i (mol l^{-1}) is the aqueous concentration of the chloroethene i, C_j (mol l^{-1}) is the concentration of the chloroethene parent compound, $K_{I,j}$ (mol l^{-1}) is the competitive inhibition coefficient of the chloroethene compound on the dechlorination of its daughter compound, $k_{max,i}$ (d^{-1}) is the apparent maximum utilization rate of the chloroethenes i and $K_{S,i}$ (mol l^{-1}) is the apparent half-saturation constant of the chloroethene i. The parameters $k_{max,i}$ and $K_{S,i}$ were fitted on results of previous experiments (data not shown) and are listed in Table A4.3 (Appendix). The pH inhibition function f(pH) was expressed as[209]:

$$f(\mathrm{pH}) = \exp\left[-\frac{\left(\left|\mathrm{pH}_{opt}-\mathrm{pH}\right|\right)^n}{\sigma^2}\right], \tag{4.3}$$

where pH_{opt} is the optimal pH, and n and σ are empirical parameters that were estimated by fitting Eq. 4.1 and 4.3 to experimental observations. Partitioning of chloroethenes between the hexadecane, gas and water phases was expressed as:

$$M = V_w C_w + V_g C_g + V_h C_h = C_w (V_w + V_g H_{cc} + V_h K_{h\text{-}w}), \tag{4.4}$$

where M (mol) is the total mass of chloroethenes in the system; C_w, C_g and C_h (mol l^{-1}) are the concentrations of the chloroethenes in the aqueous, gas and hexadecane phases, respectively, V_w ,V_g and V_h are the volumes of the three phases, H_{cc} (-) is Henry's constant for partitioning between the aqueous and gas phases, and $K_{h\text{-}w}$ (-) is the water-hexadecane partition coefficient. The parameters used in this equation are listed in Table A4.4 (Appendix).

The mineral dissolution rate was expressed as[160,166]:

$$R_{Diss} = \left[k_{H^+}\left(10^{-\mathrm{pH}}\right)^{n_{H^+}} \exp\left(-T_{inf} E_{H^+}\right) + k_W \exp\left(-T_{inf} E_W\right)\right] \frac{A_0}{V}\left(\frac{m}{m_0}\right)^{\frac{2}{3}} (1-\Omega), \tag{4.5}$$

$$\text{with } T_{inf} = \frac{1}{R}\left(\frac{1}{T}-\frac{1}{298}\right),$$

where R_{Diss} (mol m^{-2} s^{-1}) is the mineral dissolution rate, k_{H^+} and k_W (mol m^{-2} s^{-1}) are the rate constants for the acidic and neutral ranges, respectively, n_{H^+} (-) is the reaction order of proton-promoted dissolution, E_{H^+} and E_W (J mol^{-1}) are the activation energies for the neutral and basic ranges,

respectively, R (J K^{-1} mol^{-1}) the universal gas constant, T (K) the absolute temperature, A_0 (m^2) is the initial surface area, V (l) is the solution volume, Ω (-) the mineral saturation index, m and m_0 are, respectively, the actual and initial mass of mineral.

The following hypotheses were made, (i) the reactive surface area is equal to the measured BET surface area, and (ii) no passivation of mineral surfaces occurred. The values of all the parameters related with mineral dissolution are listed in Table A4.5 (Appendix).

4.3 Results

4.3.1 Influence of pH on OHR rates

Five organohalide-respiring consortia were used to test the influence of pH on OHR rates. The incubation period of these tests was 23 d for consortium SL2-PCEb, 91 d for PM and 110 d for the other three consortia. A small pH drift (between 0.3 to 1 pH units) was always observed due to insufficient buffering capacity of the zwitterionic buffer. To overcome the impact of pH drift on data analysis, OHR rates were calculated between two time steps during which pH variations were negligible. The dechlorination patterns under standard conditions (i.e., at pH 7) were different for the five consortia tested: SL2-PCEb transformed PCE to *cis*-DCE without transient accumulation of TCE, SL2-PCEa dechlorinated PCE to ethene with transient accumulation of *cis*-DCE and VC, PM dechlorinated PCE to ethene with a transient accumulation of VC, and AQ-1 transformed *cis*-DCE to ethene with transient VC accumulation. The dechlorination pattern of AQ-5 was particularly interesting because PCE was transformed to ethene without accumulation of intermediate products (Figure 4.1). The pH sensitivity of OHR rates exhibited significant differences between consortia and between each step of the OHR pathway (Figure 4.2). The parameters of the pH inhibition function (Eq. 4.3) for each consortium are listed in Table 4.1. The degradation of the lesser chlorinated compounds was more sensitive towards acidic pH. During the experiment conducted with SL2-PCEa, *cis*-DCE was formed down to pH 4.8, VC down to pH 5.3 and ethene down to pH 5.9. The tolerance towards acidic pH conditions was also variable between the five consortia. SL2-PCEb and SL2-PCEa were the most tolerant while AQ-5 was extremely sensitive to acidic conditions. For this consortium, the lowest pH at which dechlorination was observed was 6.15 and a small change in pH had a strong impact on the dechlorination pattern. At pH 7, AQ-5 transformed PCE directly to ethene without accumulation of intermediate products while at pH 6.5, accumulation of *cis*-DCE was observed and no formation of ethene (Figure 4.1).

Table 4.1. Fitted parameters of the pH inhibition function (Eq. 4.3) and goodness-of-fit (r^2) for the five consortia SL2-PCEa, SL2-PCEb, AQ-1, AQ-5 and PM.

Consortium	Dechlorination step	pH_{opt}	σ	n	r^2
SL2-PCEa	PCE to *cis*-DCE	7.0	1.0	2.2	0.95
	cis-DCE to VC	6.6	1.0	4.0	1.00
	VC to ethene	6.5	0.6	4.0	0.99
SL2-PCEb	PCE to *cis*-DCE	6.4	0.8	3.0	0.60
AQ-1	*cis*-DCE to VC	7.4	1.1	2.2	0.95
	VC to ethene	7.0	0.8	3.0	0.48
AQ-5	PCE to ethene	6.7	0.5	1.3	0.97
PM	PCE to VC	6.8	0.7	3.0	0.87
	VC to ethene	6.8	0.62	4.0	0.99

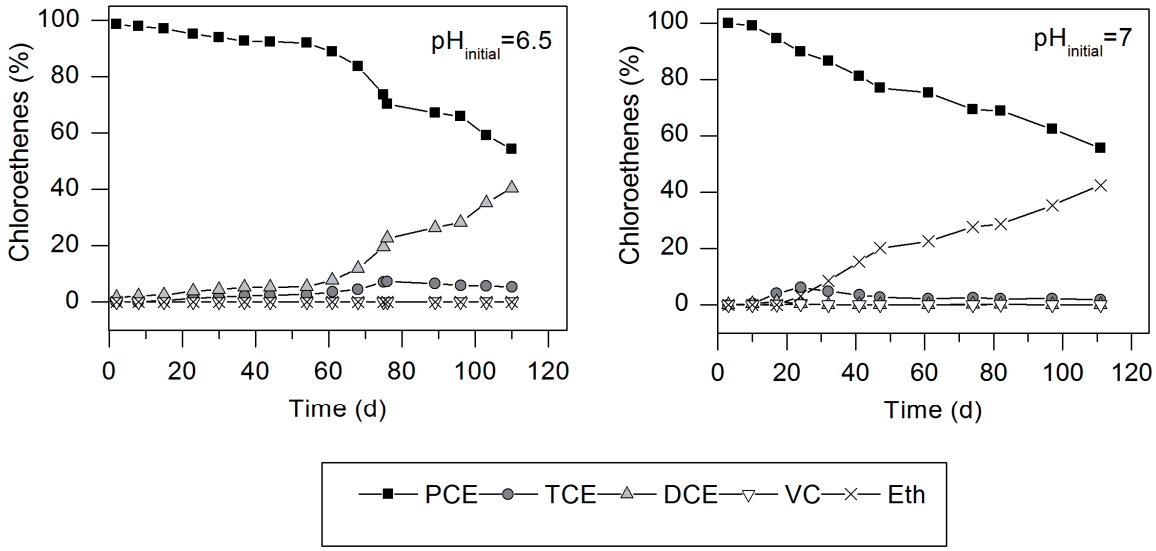

Figure 4.1. Dechlorination of PCE by cultures of consortium AQ-5 at initial pH values of 6.5 and 7.0.

4.3.2 Sensitivity of different OHRB

All consortia except SL2-PCEb contained *Dehalococcoides*. Consortia SL2-PCEa and SL2-PCEb both contained a population identified as *Sulfurospirillum* spp.[264] and consortium AQ-5 a population affiliated to *Dehalobacter* spp. The T-RFLP profiles obtained at the end of the experiment showed that the two consortia containing more than one OHRB – SL2-PCEa and AQ-5 – had a different predominant OHRB at the end of the experiment, which correlated with the dechlorination end product observed. SL2-PCEa was dominated at pH 5 and 5.5 with *cis*-DCE as the dechlorination product by *Sulfurospirillum* spp. (78% ± 7% at pH 5) while at pH 6 to 7.5 *Dehalococcoides* spp. was

the most abundant OHRB (77.5% ± 1% at pH 7.5) and ethene as the dechlorination product. In the consortium AQ-5, *Dehalobacter* spp. was predominant at pH 6.5 (74% ± 1%) while *Dehalococcoides* spp. was predominant at pH 7 (76% ± 4.5%) at the end of the experiment.

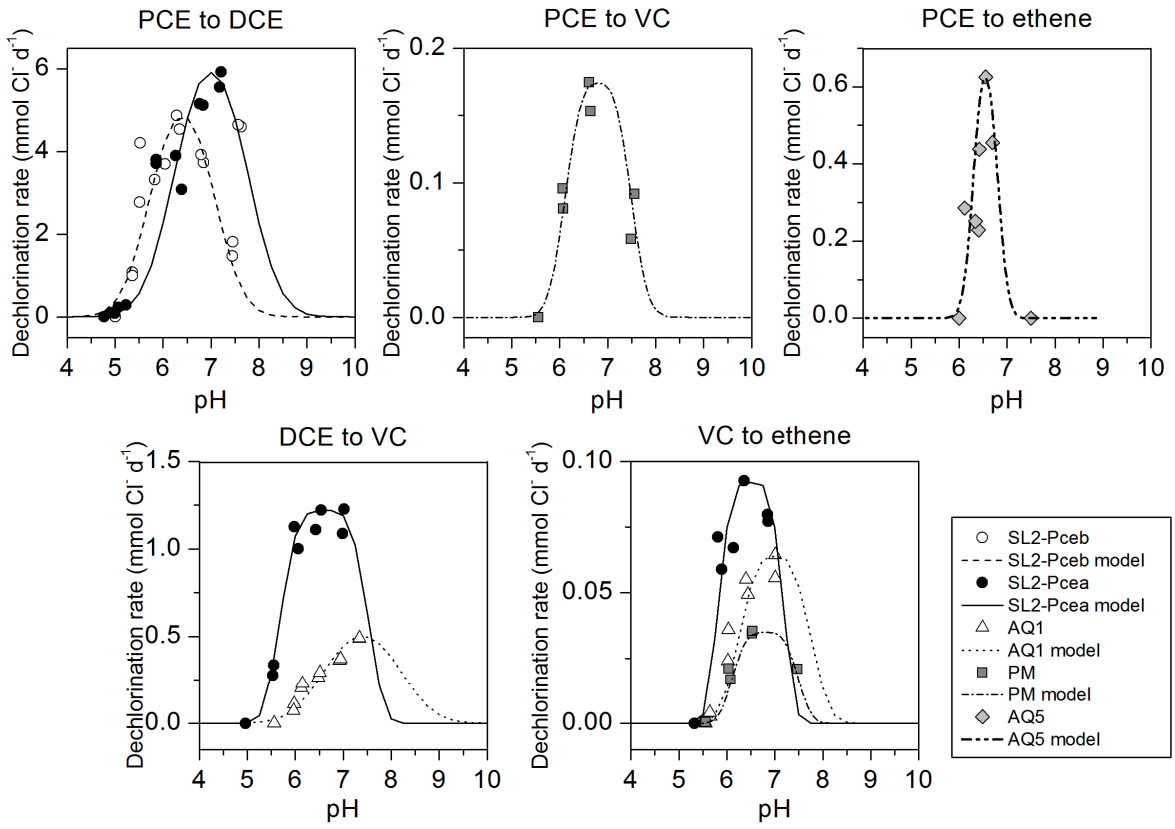

Figure 4.2. Effect of pH on organohalide respiration rate for each step of the PCE dechlorination pathway and for the five consortia tested. The lines represent the fit of the experimental data to Eq. 4.1 and 4.3.

4.3.3 Acid neutralizing capacity of silicate minerals during growth of OHRB

Figure 4.3 shows the evolution of pH in the batch cultures containing minerals and OHRB. In positive controls, the pH remained rather constant in the range of 7.2 to 7.7. On the contrary, in the negative control, OHR and fermentation activities resulted in a pH decrease down to the pH-inhibition value for OHRB (Figure 4.4). In batch cultures containing silicate mineral powders, the pH remained in a range that was above the acidic limit below which OHR activity of the consortia was inhibited. One exception was nepheline that which was only tested with consortium SL2-PCEb (Figure 4.3). In cultures of SL2-PCEa and SL2-PCEb, the pH was maintained between 5.5 and 7.5 by andradite, fayalite, forsterite and diopside. In cultures of AQ-1, the pH was maintained between 6.5 and 7.2 with fayalite whereas it increased to values of around 8.3 in cultures with forsterite and diopside, respectively.

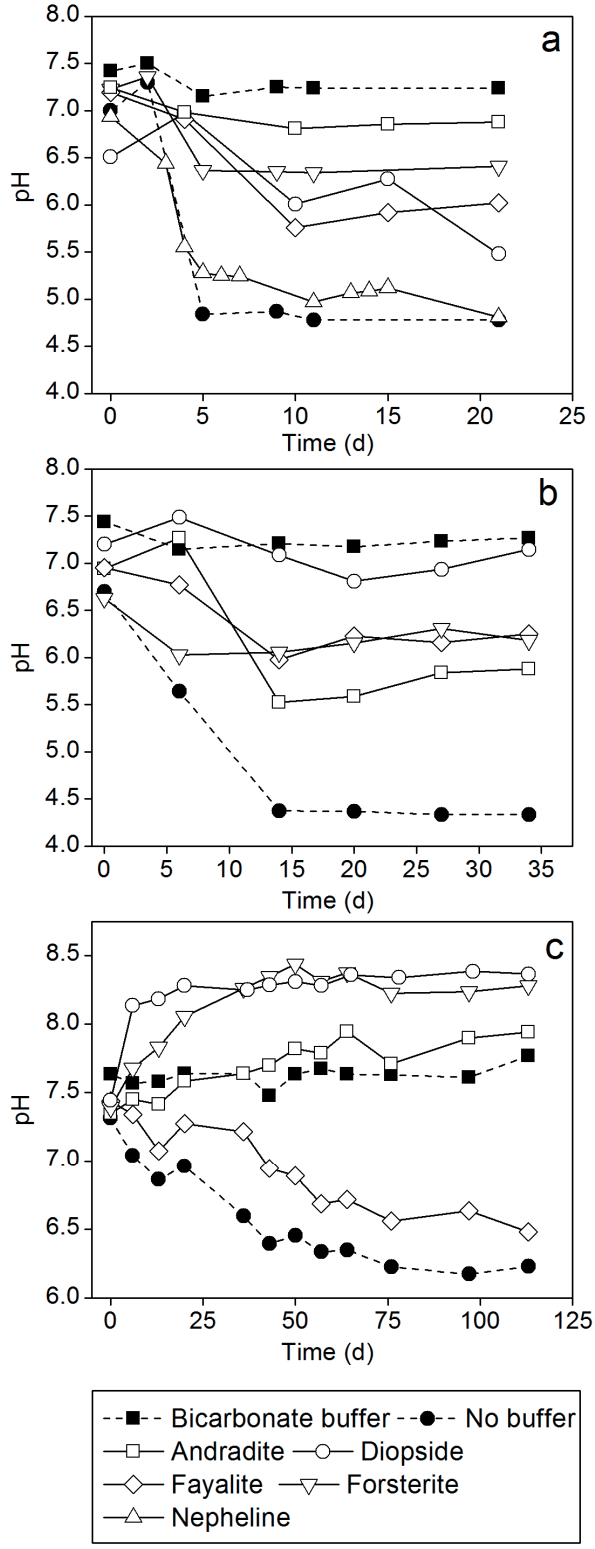

Figure 4.3. Evolution of pH in cultures of consortia Sl2-PCEb (a), SL2-PCEa (b), and AQ-1 (c) with PCE or *cis*-DCE as electron acceptors and different ground silicate minerals as buffering agents.

4.3.4 OHR and fermentation activity with silicate minerals as pH buffering agents

Dechlorination of PCE, which was tested with the consortia SL2-PCEa and SL2-PCEb, occurred with all silicate minerals evaluated. In the case of nepheline where the pH dropped below inhibitory levels, dechlorination was incomplete and stopped after 13 d of incubation. A total of 60% was present as *cis*-DCE, the rest as TCE and PCE. With andradite, PCE to *cis*-DCE dechlorination was also partially inhibited both in SL2-PCEa and SL2-PCEb. Although the pH remained in a range where no inhibition should occur with the minerals andradite, diopside, fayalite and forsterite, dechlorination ceased at *cis*-DCE within cultures of SL2-PCEa, which is normally able to produce ethene (Figure 4.4). The evolution of dechlorination products with time in SL2-PCEa culture amended with fayalite is given on Figure 4.4c as an illustrative example, similar patterns were observed for the other minerals. In the presence of silicate minerals as the buffering agent, the evolution of dechlorination products shows that *cis*-DCE production was complete after 14 d of incubation. No activity was observed during the following 20 d. In the positive control, PCE was completely dechlorinated to ethene after 34 d of incubation. Similarly to the results of SL2-PCEa, *cis*-DCE was not dechlorinated in cultures of consortium AQ-1 in the presence of silicate minerals with the exception of fayalite, where dechlorination was comparable to the positive control (Figures 4.4 and 4.5). In the case of diopside and forsterite, the elevated pH might have been the reason for no dechlorination activity. However, in the case of andradite, the pH remained around 7.5, which should not have an inhibitory influence on dechlorination of *cis*-DCE. The consortium AQ-1 was cultivated with a mixture of the electron donors ethanol, propionate, and butyrate. Ethanol was normally preferentially used by the fermentative syntrophs and transformation of ethanol to acetate was observed in the positive and negative controls, and in cultures amended with fayalite. Ethanol consumption was extremely limited in presence of diopside and forsterite (only 0.1 mmol l^{-1} of acetate produced) where the pH was rather high. Surprisingly, ethanol fermentation was also limited in the presence of andradite where the pH remained in the neutral range.

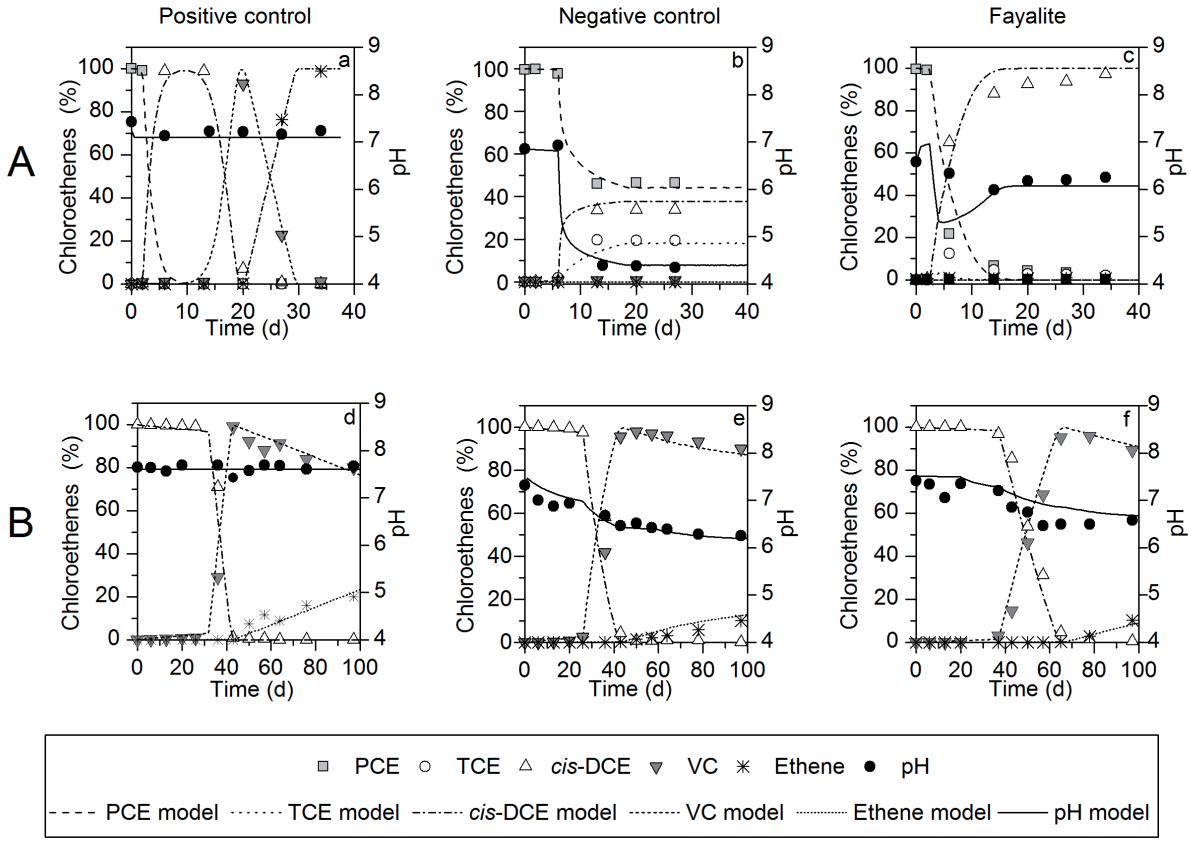

Figure 4.4. Dechlorination pattern and pH evolution for the batch cultures with soluble buffer (positive control) (a and d), without buffer (negative control) (b and e), and with fayalite (c and f) for the two consortia, SL2-PCEa (A) and AQ-1 (B). The lines represent the modeling predictions. For Figure 4.4f, the *kmax,i* values for *cis*-DCE and VC were divided by two to fit the data since in the presence of fayalite, degradation rates were slower than the control.

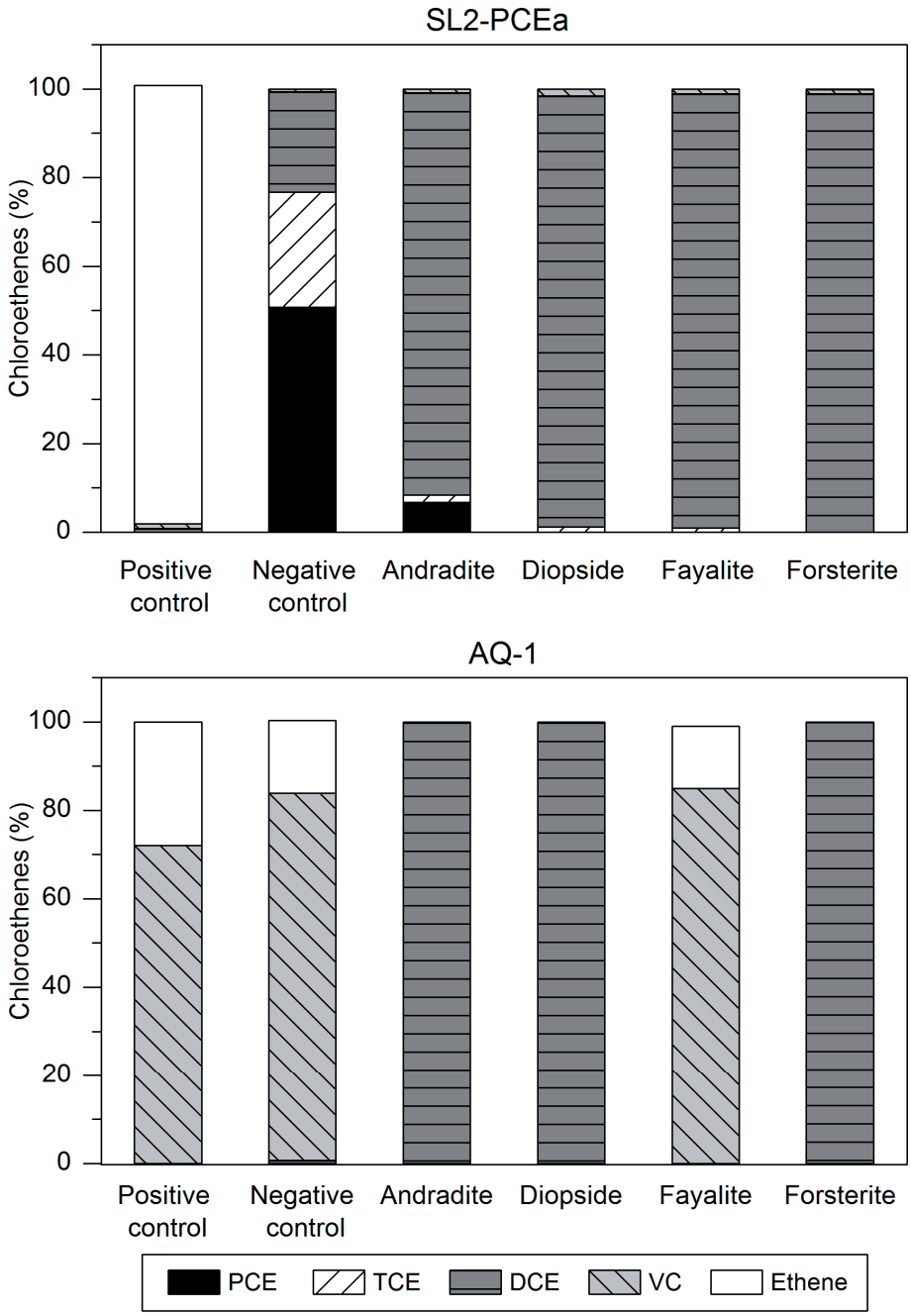

Figure 4.5. Proportion of dechlorination products at the end of the incubation period of cultures inoculated with consortia SL2-PCEa and AQ-1, and amended with different ground silicate minerals. Incubation lasted 34 d for SL2-PCEa and 97 d for AQ-1.

4.3.5 Mineral dissolution during PCE dechlorination

The evolution of concentrations of total elements that were released during mineral dissolution is presented in Figure A4.1 (Appendix) for experiments with consortium SL2-PCEa. The experimental data were compared to the results of numerical simulations performed with the geochemical model. As listed in Table A4.5, kinetic parameters as well as solubility constants were available from previous

work (Chapter 3). The correlation coefficients for the fits were quite high for most elements (Table A4.6, Appendix). Fayalite and forsterite minerals a congruent dissolution, i.e., a stoichiometric release of the elements contained in the mineral. For calcium-containing minerals (andradite and diopside), the dissolution was not stoichiometric and preferential calcium release in the early stage of the experiment was observed. Preferential Ca-release in the early stage of diopside dissolution was previously reported in several studies[171,265,266] and could be attributed to the localization of calcium in weakly bound sites in the mineral structure[171,267]. In order to reproduce the data with the numerical model, an artificial calcium-releasing phase was added to the system for andradite and diopside, which led to a better fit of the experimental observations. For all minerals tested, it was observed that mineral dissolution was triggered by acidity production due to the dependence of mineral solubility and dissolution rate on pH. Similarly, mineral dissolution ceased or was reduced when dechlorination, and thus the acidity production, was finished. Surprisingly, the apparent solubility product of forsterite and diopside when equilibrium was reached was lower than the values from the literature[197] and from previous abiotic mineral dissolution experiments (Chapter 3). To fit the experimental data with the geochemical model, log K_{eq} was reduced from 24 to 19 for forsterite and from 20 to 16.5 for diopside. The reason for these results is unclear. One possible explanation is the dependency of the solubility product upon pH[240,241]. Specifically it was found that the solubility product decreases with decreasing pH. Although reduced, the solubility of forsterite and diopside was still sufficient to counterbalance the acidity produced and to maintain the pH in the neutral range. In the andradite experiment, the iron concentration was low or even below the detection limit, indicating precipitation of iron oxides or iron sulfides as secondary phases.

4.4 Discussion

4.4.1 Influence of pH on OHR activity

This study showed that mixed cultures of OHRB present higher tolerance towards acidic pH conditions than pure cultures of OHRB. The lowest pH at which PCE dechlorination was observed in preceding studies with pure cultures of OHRB ranged from 6 for *Desulfitobacterium* spp.[108,121,127] to 6.5 for *Sulfurospirillum multivorans*[106,126], *Dehalobacter restrictus*[101], and *Desulfuromonas chloroethenica*[105]. In the consortia used in this study, PCE dechlorination was observed down to pH 4.8 (SL2-PCEa). In previous studies on mixed OHRB cultures, PCE degradation was observed down to a minimum pH of 4 to 5.5 for OHR of PCE[129,130]. Similarly, OHRB seem to tolerate a broader pH range at field sites where evidence of OHR with PCE and presence of members of the genus *Dehalococcoides* have been observed in moderately acidic groundwater having a pH of 5[73,134].

Noticeable differences in pH sensitivity were evident between the different steps of the PCE dechlorination pathway. The last steps from *cis*-DCE to ethene were more sensitive towards acidic pH than the transformation of PCE to *cis*-DCE. This pattern can be explained by the different sensitivity

of the different OHRB involved in PCE dechlorination. Consortium AQ-5 is mainly composed of a population of *Dehalobacter* spp. that dechlorinated PCE to *cis*-DCE and a population of *Dehalococcoides* spp. able to form ethene. At pH 7.0 where ethene was formed, *Dehalococcoides* spp. was the predominant population at the end of the experiment while at pH 6.5, *Dehalobacter* spp. was predominant and *cis*-DCE was the dechlorination end product, indicating that the former population was extremely pH sensitive unlike the latter. For consortium SL2-PCEa, composed of *Sulfurospirillum* spp. and *Dehalococcoides* spp., the latter was also not detected in cultures with acidic pH where PCE dechlorination ceased at *cis*-DCE. These results indicate that bacteria belonging to the genus *Dehalococcoides* are more sensitive towards acidic pH, which is in agreement with practitioner knowledge and with a study of Rowlands[132] that showed that the range of complete degradation from PCE to ethene was observed between pH 6 and 8.3, whereas partial degradation of PCE to *cis*-DCE and VC occurred in a broader pH range of 5 to 9 in mixed consortia. In addition, Loffler et al.[268] showed that pure culture of *Dehalococcocoides* are active only between pH 6.5 and 8.0. The five consortia tested in this study presented different tolerances towards acidic pH. SL2-PCEa was the most tolerant consortium with transformation of VC to ethene down to pH 5.9 while AQ-5 presented a very narrow tolerance range (production of ethene down to pH 6.4). These two consortia both contained members of the genus *Dehalococcoides* but probably different strains. Identification of *Dehalococcoides* strains tolerant to mildly acidic pH might be of interest for bioaugmentation application. In addition, it is apparently of importance to know the pH sensitivity of the OHRB guild present at a specific site in order to design the appropriate bioremediation approach and to assure that the success of the remediation approach is not hampered due to pH inhibition. The mere detection of presence of *Dehalococcoides* spp. does not provide sufficient information and laboratory tests could help to get the necessary information.

4.4.2 Suitability of silicate minerals as pH buffering agents during OHR of chloroethenes

The results of cultures amended with ground silicate minerals confirmed the potential of the latter as acid-neutralizing agents. Previous studies using numerical simulations (see Chapter 2) and abiotic dissolution experiments (see Chapter 3) already indicated that these minerals could be used as pH buffers. Four out of the five minerals tested (andradite, fayalite, forsterite and diopside) were able to maintain the pH above the value causing inhibition of dechlorination. Dissolution of the fifth mineral nepheline was limited by its relatively low solubility (log K_{eq} = 14.2 at T = 25°C[198]) and by the initial high concentration of Na in the medium that limited further dissolution throught the common ion effect. For these reasons, saturation with respect to nepheline was rapidly achieved, and the acid-neutralizing capacity was limited. In contrast, in the absence of acidification activity, as in cultures of consortium AQ-1, dissolution of diopside (log K_{eq}, = 21.73 at T = 25°C) and forsterite (log K_{eq} = 28.6 at T = 25°C) was too rapid even at pH above 7.0 and resulted in a pH above 8.0. Development of

slightly basic pH conditions was due to the higher solubility of these minerals at neutral pH and also to the long lag phase (about 30 d) prior to dechlorination. As already mentioned in the Materials and Methods section (4.2.3), phosphate precipitated with calcium at pH above 8.0 making this essential nutrient unavailable for bacterial growth. In geochemical environments, formation of calcium phosphate complexes such as hydroxyapatite ($Ca_5(PO4)_3OH$) was observed in the pH range of 7.4 to 8.4 by several authors[248-250], but precipitation of calcium-phosphate complexes might not be a problem in an environment where phosphate is not limiting. Precipitation of phosphorous might also be a problem at pH < 7.5 if the silicate mineral contains aluminum. This kind of phosphorous precipitation has been reported to occur under low redox conditions at pH > 5.0[269,270] and aluminum salts are commonly used for phosphate removal in wastewater treatment[271]. Hence, aluminum-bearing minerals, such as nepheline, do not appear as a promising means of pH control for groundwater undergoing *in situ* bioremediation.

In addition to the negative influence of insufficient or excessive solubility of silicate minerals on chloroethene dechlorination leading to too low or too high pHs, there are also other possible mechanisms that can impede chloroethene dechlorination. Andradite was capable of maintaining pH in the suitable range and still dechlorination was not complete. Moreover, andradite partially inhibited the first step of the dechlorination from PCE to *cis*-DCE. Additional experiments, demonstrated that the extent of PCE dechlorination inhibition was proportional to the amount of andradite dissolved (results not shown). This observation could be due to the presence of an oxidizing component in the mineral. Indeed, andradite is the only mineral tested in this study that contained Fe(III)[272]. Ferric iron is a recognized oxidizing agent and addition of Fe(III) is known to increase the redox potential of anaerobic solutions[273,274]. In the experiment conducted in this study, it was observed that the growth medium containing resazurin was turning from colorless to pink a few days after the experiment started in andradite-amended cultures. Resazurin is a redox indicator that is colorless at a redox potential ≤ 100 mV and pink under more oxidizing conditions[275]. To confirm the increase of redox potential by andradite dissolution, additional abiotic tests were conducted with andradite in a reduced growth medium for 40 d. The redox potential increased from -300 to +108 mV, confirming the oxidizing effect of andradite. OHRB are strict anaerobic microorganisms[276] and it is likely that release of Fe(III) during andradite dissolution raised the redox potential until a value that was unsuitable for OHR activity. Our results suggest that the presence of redox-active compounds inside the minerals have to be considered carefully prior to selecting a buffering agent. For iron-containing minerals, the oxidation state of iron should be evaluated and ferric iron-containing minerals should not be used if the remediation strategy requires a low redox potential to proceed.

The experiments with the consortia SL2-PCEa and AQ-1 indicated that the transformation of *cis*-DCE to ethene was more sensitive to mineral dissolution than the transformation of PCE to *cis*-DCE. Significant formation of VC and ethene was only observed in a culture of AQ-1 amended with

fayalite. Since in both consortia *Dehalococcoides* spp. seemed to be responsible for *cis*-DCE and VC dechlorination, the results indicated that OHRB of this genus are quite sensitive to effects that silicate mineral dissolution might have on biological activity. As mentioned above, silicate mineral dissolution might result in an increase of the redox potential due to the release of an oxidizing agent but also due to the precipitation of the reducing compound such as sulfide. Upon mineral dissolution, the redox potential might have remained in the suitable range for the transformation of PCE to *cis*-DCE but might have been too high for the transformation from *cis*-DCE to ethene. Indeed, it is known that dechlorination of PCE or TCE to *cis*-DCE is possible under mildly reducing conditions whereas transformation of *cis*-DCE to VC and VC to ethene requires more strongly reducing conditions[125]. Abiotic experiments with the five minerals tested in this study showed that dissolution of fayalite, forsterite and andradite increased the redox potential within 40 d from -300 mV to -67.7, 82, and 108 mV, respectively, while diopside and nepheline had no effect on this parameter. The redox potential in the presence of fayalite might have been sufficiently low for the *Dehalococcoides* population of consortium AQ-1 to perform *cis*-DCE dechlorination.

Another possible explanation for the absence of *cis*-DCE dechlorination involves heavy metal ions that are released upon silicate mineral dissolution and accumulate, and thus might become toxic. ICP-MS analyses conducted on the minerals tested showed that they all contained traces of potentially toxic elements such as vanadium, chromium, cobalt, nickel, zinc, gallium, arsenic, rubidium, strontium, zirconium, barium, cerium, lead, titanium and manganese (Table A4.7 in Appendix). To date, there are no studies on the toxicity of these metals on PCE-dechlorinating bacteria. However, metal toxicity studies have been conducted with other bacteria involved in halogenated compound biodegradation, but they are limited to a restricted number of organic compounds (trichloroaniline, 2-chlorophenol, 3-chlorobenzoate, hexachlorobenzene, pentachlorophenol) and metals (mercury, lead, zinc, copper, chromium and cadmium)[277]. The lowest metal concentrations reported to cause inhibition of anaerobic biodegradation vary from 0.01 mg l^{-1} (inhibition of trichloroaniline degradation by Cd^{2+})[278] to 20 mg l^{-1} (inhibition of 2-chlorophenol and 3-chlorobenzoate transformation by Cu^{2+})[279].

4.5 Conclusion

Although this study has shown that silicate minerals are suitable buffering agents for counteracting acidity production during chloroethene dechlorination, different aspects have to be taken into consideration for choosing the best suited mineral. The inhibition of *cis*-DCE transformation observed in most of the experiments was perhaps a consequence of the experimental approach chosen. Indeed, in a batch system, nutriment depletion and accumulation of toxic or redox active compounds is increasing with time. In contrast, under field conditions, these effects are less likely to occur, due to the renewal of the pore water through groundwater flow. This study showed that Fe^{3+} bearing minerals (such as andradite) are not suitable for pH control of a remediation strategy requiring reduced

conditions. Similarly, Al^{3+}-bearing minerals are not appropriate due to their potential to complex phosphate under mildly acidic and neutral conditions. These results showed the importance of mineral composition when selecting silicate minerals for pH control of remediation strategies involving bacterial activity.

4.6 Appendix

Table A4.1. Length of T-RFLP fragments (in base pairs, bp) corresponding to known organohalide respiring genera determined by semi-specific T-RFLP with the three restrictions enzymes Hae III, Hha I and Msp I.

Genera	fragment size (bp)		
	Hae III	Hha I	Msp I
Sulfurospirillum spp.	252	90	463
Dehalococcoides spp.	165[(1)] / 244 [(2)]	194	507 [(3)]
Dehalobacter spp.	212	229	137
Desulfitobacterium spp.[(4)]	300/306/324	99/111/125	226/230/249

[(1)] Fragment size corresponding to the *Dehalococcoides* strain present in the SL2-PCEa consortium.

[(2)] Fragment size corresponding to the *Dehalococcoides* strain present in consortium AQ-5.

[(3)] There is no restriction site for the restriction enzyme MspI in the fragment amplified. The fragment length corresponds to the undigested fragment.

[(4)] The genus *Desulfitobacterium* has six different copies of the 16sRNA gene which have a relatively close sequence. When digested, these six copies gave three fragments of different sizes.

Table A4.2 Experimental conditions used in the biotic experiments amended with minerals.

Consortium	Electron donor	Electron acceptor	Mineral	Mass (g)	Specific surface area ($m^2\ g^{-1}$)
SL2-PCEb	Hydrogen	PCE	Andradite	4	0.4
		$C_{PCE(aqueous)}$:	Diopside	4	1.55
		0.02 mmol l^{-1}	Fayalite	4	1.136
		Total C_{PCE}:	Forsterite	0.7	4.41
		5 mmol l^{-1}	Nepheline	7.02	0.36
SL2-PCEa	Hydrogen	PCE	Andradite	2	0.4
		$C_{PCE(aqueous)}$:	Diopside	2	1.55
		0.02 mmol l^{-1}	Fayalite	2	1.14
		Total C_{PCE}:	Forsterite	0.25	2.73
		2.5 mmol l^{-1}			
AQ-1	Ethanol, butyrate propionate at 2.8 mmol l^{-1}	*cis*-DCE	Andradite	4.01	0.40
		$C_{cis\text{-}DCE(aqueous)}$:	Diopside	6.2	0.77
		0.02 mmol l^{-1}	Fayalite	9.06	0.75
		Total $C_{cis\text{-}DCE}$:	Forsterite	1.58	0.86
		0.6 mmol l^{-1}			

Table A4.3. Microbial kinetics parameters used in the geochemical model for the consortium SL2-PCEa.

Parameter	SL2-PCEa	AQ-1
$k_{max,\ PCE}$ (mol $l^{-1}s^{-1}$)	5.5×10^{-8}	-
$k_{max,TCE}$ (mol $l^{-1}s^{-1}$)	5.5×10^{-8}	-
$k_{max,cis\text{-}DCE}$ (mol $l^{-1}s^{-1}$)	1.1×10^{-8}	0.7×10^{-9}
$k_{max,VC}$ (mol $l^{-1}s^{-1}$)	3.2×10^{-9}	0.4×10^{-10}
$K_{S,PCE}$ (mol l^{-1})	1.3×10^{-5}	-
$K_{S,TCE}$ (mol l^{-1})	9.0×10^{-7}	-
$K_{S,DCE}$ (mol l^{-1})	9.0×10^{-7}	9.0×10^{-7}
$K_{S,VC}$ (mol l^{-1})	9.0×10^{-7}	9.0×10^{-8}
$K_{I,PCE}$ (mol l^{-1})	1.0×10^{-12}	-
$K_{I,DCE}$ (mol l^{-1})	1.0×10^{-12}	1.0×10^{-12}

Table A4.4. Water-hexadecane partition coefficient and dimensionless Henry's law constants (C_{gas}/C_{aq}) of PCE, TCE, *cis*-DCE, vinyl chloride and ethene used in this model.

Compound	H_{cc} (T= 30°C)[(1)]	$K_{h\text{-}w}$[(2)]
PCE	0.93	4466
TCE	0.5	478
cis-DCE	0.19	87
VC	1.28	23
Ethene	6.52	15

(1) Data from Gossett[280] for PCE, TCE, *cis*-DCE and ethene and from US EPA[281] for VC

(2) Data from Abraham et al.[282] for PCE, TCE, *cis*-DCE and ethene. For VC, the water-hexadecane partition coefficient was found in literature and the octanol-water partition coefficient was used instead [283].

Table A4.5. List of parameters used for modeling mineral dissolution in presence of the consortium SL2-PCEa.

Parameter	Andradite	Diopside	Fayalite	Forsterite
$K_{eq\ T=25°C}$ (1)	16	16.5	16.6	18
$k_{H+\ T=25°C}$	-5.25	-8.7	-5.5	-6.8
$k_{W\ T=25°C}$	-11.25	-11.8	-11.8	-11.8
$n_{H+\ T=25°C}$	0.9	0.38	1	0.6
E_w	103.8	40.6	94.4	79
E_{H+}	94.41	96.1	94.4	67.2

(1) These parameters were modified to fit the data. All the other parameters were from the results of abiotic batch experiment performed with the same mineral samples (Chapter 3).
(2) From Plandri and Kharaka (2004) [166].

Table A4.6. Correlation coefficients for the observations versus model predictions for the mineral dissolution in SL2-PCEa batch cultures (Figure A4.1).

	Fe	Si	Mg	Ca	pH
Fayalite	0.96	0.98	-	-	0.21
Forsterite	-	0.93	0.99	-	0.54
Andradite	0.74	0.9	-	0.84	0.86
Diopside		0.93	0.92	0.98	0.88

Table A4.7. Trace elements present in the minerals measured by ICP-MS (in ppm).

	V	Cr	Co	Ni	Zn	Ga	As	Rb	Sr	Zr	Ba	Ce	W	Pb	TiO_2	MnO
Fayalite	2.2	2.3	1.7	1.8	2.1	1.1	1.3	1.5	1.4	2.1	2.7	1.5	2.2	1.6	3.8	4.3
Andradite	1.4	1.8	1.8	1.0	4.1	0.7	2.0	0.0	0.8	1.4	0.5	0.9	2.4	2.0	2.9	3.8
Nepheline	1.1	1.9	1.7	0.0	1.5	1.5	0.0	1.9	1.4	0.5	1.2	0.2	2.5	0.9	1.7	1.5
Diopside	1.6	3.1	1.8	2.9	2.2	0.3	0.0	0.0	1.3	0.0	0.2	0.0	2.1	0.9	1.8	3.0
forsterite	1.4	3.4	2.1	3.4	1.6	0.0	0.2	0.0	0.1	0.0	0.5	0.0	1.4	0.0	0.8	3.0

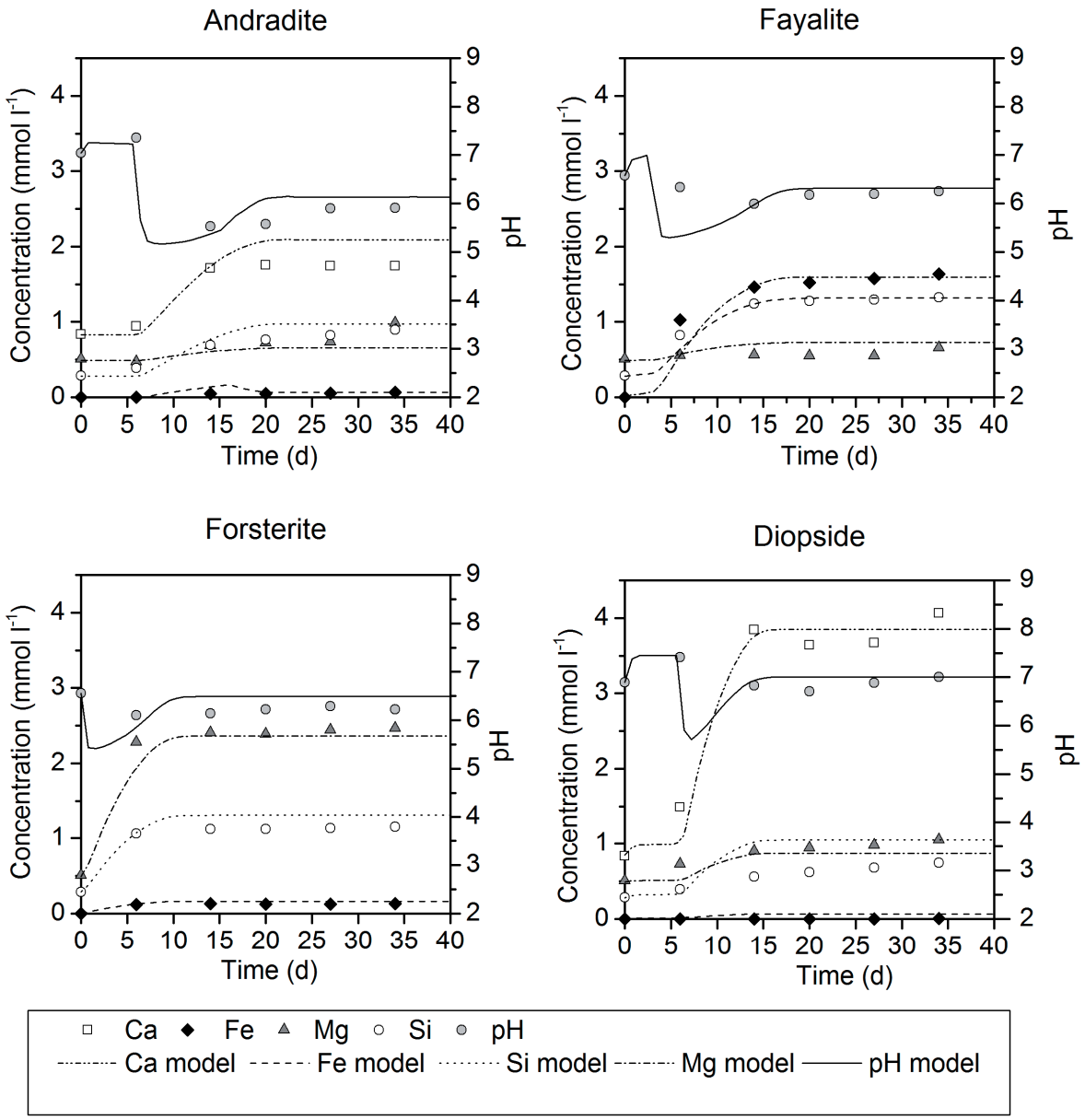

Figure A4.1. Evolution of pH, Ca, Fe, Mg and Si over time in SL2-PCEa experiment in the presence of andradite, fayalite, forsterite and diopside. The lines represent the predictions of the geochemical model.

Chapter 5

Evaluation of long-term acid neutralizing capacity of silicate minerals for PCE bioremediation in continuous-flow columns

5 Evaluation of long-term acid neutralizing capacity of silicate minerals for PCE bioremediation in continuous-flow columns

Abstract

The buffering potential of silicate minerals for chloroethene-contaminated sites undergoing *in situ* bioremediation was demonstrated by numerical simulations and batch experiments in the previous chapters. In the present study, the buffering potential of three silicate minerals (diopside, fayalite and forsterite) was evaluated in a porous medium in flow through column experiments over a period of 6.5 months. The columns were operated with PCE concentrations close to saturation and inoculated with the organohalide respiring consortium SDC-9™, which is able to dechlorinate PCE at such concentrations. In the absence of buffering agents, fermentation and organohalide respiration drove the pH close to 6.1 and PCE dechlorination was fully inhibited. Forsterite and fayalite were able to maintain the pH close to 7.5 and 6.5, respectively, and to sustain production of VC and ethene. Diopside gradually lost its buffering capacity during the first 84 days due to the formation of a low reactive leached layer. Among the three minerals tested, forsterite was identified as the best buffering agent. Indeed, the column amended with this mineral presented the best PCE removal performance and the highest relative abundance of *Dehalococcoides*.

5.1 Introduction

In the preceding chapters, numerical simulations and abiotic and biotic batch experiments showed that silicate minerals may act as buffering agents for *in situ* bioremediation of chloroethenes. However, batch experiments presented several limitations: (i) they were conducted on a short time scale and (ii) mineral and solution were constantly mixed, which potentially increases the reactivity of the mineral[228]. In addition, several studies reported that initial dissolution rates of freshly ground silicate minerals are often faster than long-term steady state dissolution rates[171,223]. The time to reach steady state can vary between minerals and was found to be up to 113 days for diopside[267] and up to 4 years for plagioclase[223]. Another problem associated with batch setups is the accumulation of toxic elements released from mineral dissolution that might have been responsible for inhibition of *cis*-DCE transformation as described in Chapter 4. To overcome the limitations associated with batch setup and to study the mineral buffering potential on a longer time scale and under more realistic conditions, flow-through column experiments were conducted. Preceding studies suggested that columns studies are preferred to batch studies due to minimal disturbance of the solid phase and a more realistic mineral/water interface[228]. Three minerals, previously identified as potential buffering agents, were selected for the column experiment: diopside ($CaMg(SiO_3)_2$), fayalite (Fe_2SiO_4) and forsterite (Mg_2SiO_4). The columns were inoculated with the organohalide-respiring consortium SDC-9™ and operated with PCE concentrations close to saturation in order to reproduce the conditions typically found in the vicinity of chloroethene source zones. The goal of the study was to determine the long-term dissolution rate and buffering potential of the selected minerals and to determine the impact of mineral dissolution on OHRB presence and activity in a porous medium.

5.2 Materials and Methods

5.2.1 Organohalide respiring consortium

The columns were inoculated with the organohalide respiring consortium SDC-9™ commercially available from Shaw Environmental Inc. (Baton Rouge, Louisiana, USA). This mixed culture was isolated by enrichment culturing of samples from a chlorinated solvent-contaminated aquifer in southern California as described by Vainberg et al.[130]. The consortium contained a population of *Dehalococcoides* able to transform PCE to ethene and to tolerate PCE concentrations that were close to saturation (0.9 mM). Prior to column inoculation, the SDC-9™ consortium was cultivated on a reduced anaerobic medium, the composition of which is given in Table A5.1 (Appendix) and amended with lactate at 12 mmol l^{-1} and PCE at 0.9 mmol l^{-1}.

5.2.2 Mineral preparation and characterization

Three minerals were used in this study: diopside ($CaMg(SiO_3)_2$, Outukumpu, Finland), forsterite (Mg_2SiO_4, Aheim, Northfjord, Norway), and fayalite (Fe_2SiO_4, Billiton, Indonesia). The mineral powders were prepared as described in Chapter 3 section 3.2.1. Chemical composition and specific surface area were analyzed as described in sections 3.2.1 and 4.2.5. Identification of crystalline structures present in the samples was done by X-Ray diffraction (XRD) with a Thermo X'tra powder diffractometer equipped with a Peltier-cooled Si(Li) solid state detector.

5.2.3 Column packing

This study was conducted in 25 cm tall, 3.5 cm diameter, glass columns with sampling ports at the inlet and the outlet. Five columns were constructed, columns 1 and 2 (respectively the positive and negative control) were filled with coarse quartz sand sieved between 200 and 315 µm and washed in MilliQ water (Millipore) during 24 hours. Columns 3, 4, and 5 were filled with a mixture of coarse quartz sand and 50-100 µm silicate minerals powder. These three columns contained respectively 60 g of diopside (corresponding to a initial total surface area of 88 m^2), 62 g of forsterite (44 m^2) and 57 g of fayalite (49 m^2). The mineral grain size was defined so as to keep the mineral particles immobilized within the quartz sand matrix and the amount of mineral was defined based on numerical simulations (see Chapter 2). Before packing, quartz sand and mineral powder were mixed manually to allow a homogenized distribution of the minerals within the columns. Wet packing was done inside an anoxic glove box with an atmosphere composed of 8% H_2 and 92% N_2. The solid matrix was mixed with the liquid phase composed of fresh anaerobic medium without PCE and SDC-9™ culture in a ratio of 1:1 allowing a uniform distribution of the biomass inside the columns. The pore volumes of the columns were equal to 128 ml for columns 1 and 2, 125 ml for columns 3 and 4, and 117 ml for column 5.

5.2.4 Experimental set up

After packing, the columns were mounted and installed outside the glove box at room temperature (temperature was constant between 20 and 24 °C during the experiment). A schematic diagram of the experimental setup is presented in Figure 5.1. The columns were operated in upflow mode with all the lines to and from the columns composed of Teflon PTFE (diameter of 1.5 mm; Maag Technic AG, Dübendorf, Switzerland) for the semi-rigid parts and of Viton™ (diameter of 0.8 mm; Fischer Scientific, Wohlen, Switzerland) for the flexible parts. The system had three 1-l glass bottle reservoirs containing the influent medium. The reservoir bottles were sealed with Viton™ rubber stoppers and pressurized to 0.1 bar with nitrogen to prevent air leaking into the reservoir. The influent solution was pumped from the reservoirs to the columns with peristaltic pumps (Lambda PreciFlow, Lambda Laboratory Instruments, Switzerland). The reservoir bottles were stirred at low speed (~ 30 rpm) with a magnetic stir bar throughout the experiment to ensure the medium in the bottles remained well

mixed. The reservoir bottles were maintained in sterile conditions during the experiment. When the columns were operated in upflow mode, the concentration of the nutrients in the influent medium was reduced by a factor of five compared to the medium used for batch cultures except for the reducing agent $Na_2S.9H_2O$ present at a concentration of 2 mmol l^{-1}. In column 1 (positive control), the pH was kept constant with 97 mmol l^{-1} of 3-(N-morpholino) propanesulfonic acid (MOPS). In column 2 (negative control), the influent solution had a reduced buffering capacity with only 0.4 mmol l^{-1} of phosphate and 0.19 mmol l^{-1} of bicarbonate. Columns 3, 4, and 5 were operated with the same low-buffered influent solution as column 2 so that the main source of pH buffering was the mineral dissolution. The medium contained resazurin as a redox indicator in order to verify the redox state of the solution (resazurin is colorless in anaerobic conditions and turns pink when the redox is above 100 mV[284]). A detailed composition of the media used in this study is given in Table A5.1.

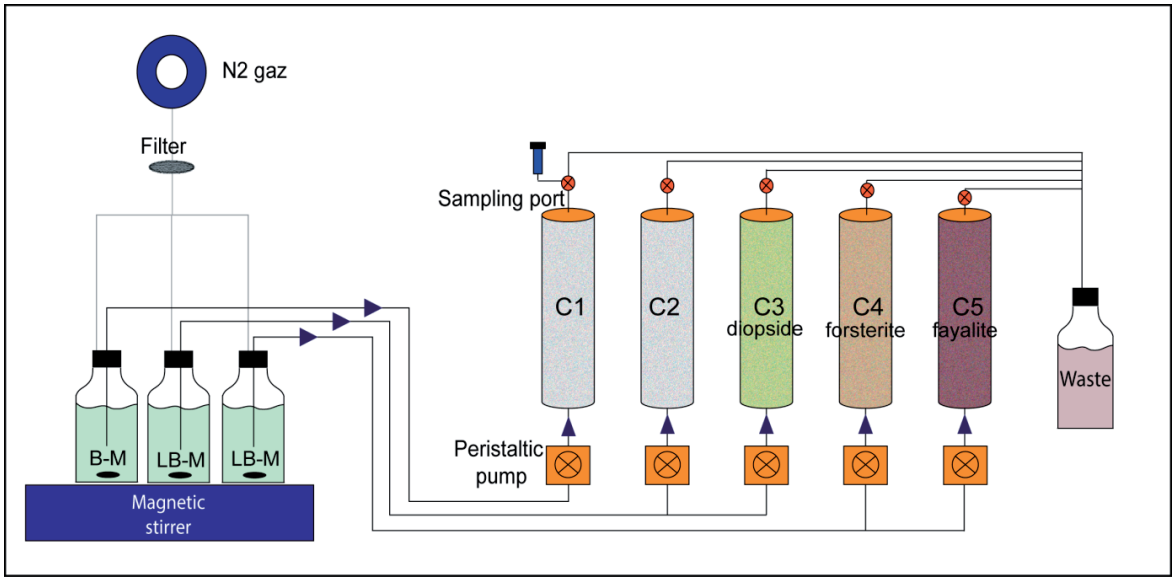

Figure 5.1. Schematic view of the experimental setup. B-M: buffered medium, LB-M: low buffered medium.

5.2.5 Experimental stages

After packing the column, one pore volume of fresh anaerobic medium containing PCE at saturation concentration and MOPS at 97 mmol l^{-1} (medium B in Table A5.1) was pumped in each column during 24 hours. Then, the flow was stopped and the columns were operated in batch mode to allow colonization of the columns by the biomass. The batch phase lasted 12 d for columns 1, 2 and 4, 7 d for column 5, and 6 d for column 3. After this batch phase, the columns were operated in upflow mode with a hydraulic retention time of 3 d. The values of the flow rate were fixed at 43 ml d^{-1} for columns 1 and 2, 41.5 ml d^{-1} for columns 3 and 4, and 39 ml d^{-1} for column 5, and were kept constant during the duration of the experiment. During the first 105 d (later referred to as phase 1), influent solutions were amended with PCE at saturation concentration (i.e., 0.9 mmol l^{-1}) and sodium lactate at 16 mmol l^{-1}.

The influent solution was prepared by addition of neat PCE in excess in the reservoir bottle compared to the PCE solubility limit (addition of 0.6 ml of neat PCE to 742 ml of media). Non-aqueous PCE remained at the bottom of the reservoir thus indicating the solution was saturated. From day 105 to 147 (later referred to as phase 2), the concentration of PCE and lactate were reduced by a factor of three (0. 33 mmol l^{-1} of PCE and 5.33 mmol l^{-1} of lactate). To maintain a constant PCE concentration at 0.33 mmol l^{-1} throughout the experiment, the reservoir bottles were amended with 10 ml of hexadecane in which PCE was dissolved at a concentration of 1.5 mol l^{-1}. From day 157 to the end of experiment (later referred to as phase 3), the concentration of lactate was increased to 16 mmol l^{-1} and the PCE concentration was kept at 0.33 mmol l^{-1}. The experiment was conducted during 176 d for columns 1 and 2 and for 194 d for columns 3, 4 and 5. A more detailed description of the experimental stages is available in Table A5.2 (Appendix).

5.2.6 Sampling

Twice a week, the effluent sampling ports were monitored for PCE, TCE, DCE isomers, VC, ethene, pH, volatile fatty acids (acetate, propionate), lactate, methane, phosphate, and total calcium, magnesium, iron and silica. Samples were frequently withdrawn in reservoir bottles for lactate and PCE analysis in order to verify that no degradation occurred before the influent entered the column. Aliquots of 5 ml aqueous samples were withdrawn with a 10 ml gastight glass syringe (Eterna Matic, Sanitex, Switzerland). During sampling, the flow rate was increased to about 600 ml d^{-1} to reduce the time required for sample collection and minimize the losses of volatile compounds.The redox potential of the effluent was measured towards the end of the experiment on days 165 and 176.

5.2.7 Tracer test

Bromide tracer tests were performed at the end of the study to allow non-destructive determination of porosity reduction and detection of possible shortcuts. The tracer tests were performed by injecting a solution of NaBr at 0.5 mmol l^{-1} during a pulse of 16 h. The columns were operated at the same flow rate used for normal column operation. Samples were taken at a regular time interval at the column outlets to measure bromide concentration. Breakthrough curves were analyzed with the CXFIT code in Excel[285].

5.2.8 Analytical methods

Chloroethenes, ethene, and methane were analyzed by headspace gas chromatography. For headspace analysis, 3 ml of the effluent sample collected with a gastight glass syringe was injected into a 15 ml empty glass vial sealed with a Viton™ stopper. The analysis of the headspace was realized after 20 min of equilibration between the aqueous and the gas phase as described previously (Chapter 4, section 4.2.7). Acetate, propionate and lactate analyses were performed by high performance liquid chromatography (HPLC) as described previously (Chapter 4, section 4.2.7). Total elements resulting

from mineral dissolution (Ca, Fe, Si and Mg) were analyzed by inductively coupled plasma atomic emission spectroscopy as described previously (Chapter 3, section 3.2.2). Prior to analysis, the samples were filtered at 0.2 µm and acidified with 10 µl of nitric acid at 99%. Anion concentrations (bromide and phosphate) were determined using an ion chromatograph (Column ICS-3000-B, Dionex AG, Switzerland). The pH was measured directly after sampling as described previously (Chapter 3, section 3.2.2). Redox potential was measured with a redox meter (Metrohm ion analysis) using an air-tight redox cell.

5.2.9 Column dissection

At the end of the study, the columns were sectioned into 2.5 cm thick slices. The columns containing silicate minerals (columns 3, 4 and 5) were dissected under anoxic conditions in a glovebox to avoid oxidation of the mineral powder. Only the inner part of the slices (diameter of 2.6 cm) was sampled to avoid cross contamination between slices. Half of the solid material was introduced in a 50-ml Falcon™ tube for DNA extraction and stored at -40°C. The other half was rinsed three times with degassed anaerobic MilliQ water (Millipore) and dried at 35°C degrees inside the glove box for 24 h. Dried samples were then introduced in air-proof glass flasks and were stored at room temperature for mineral characterization.

5.2.10 Molecular biology analyses

5.2.10.1 DNA extraction

The PowerSoil™ DNA Extraction Kit (MoBio Laboratories, USA) was used for DNA extraction according to the manufacturer's instructions with the following modifications: after addition of solution C1, samples were heated 2 x 5 min at 70°C and lysis of cells was completed in a Bead-Beater (2 x 30s). Aliquots of 0.4 g of wet solid column material of each section were used for the extraction. The extracted DNA was quantified and its quality assessed with a Nanodrop spectrophotometer (Nanodrop®, ND-1000, Thermo Fisher Scientific, USA).

5.2.10.2 T-RFLP

Microbial community composition of each column section was assessed using Terminal Restriction Fragment Length Polymorphism (T-RFLP). Each analysis was carried out in triplicates. PCR products were generated with a combination of FAM-labelled Eub8f and Univ518r primers as follows: 50 µl PCR reactions were composed of 5 µl 5x colorless Go Taq buffer (Promega), 2 µl of both primer at 10 µM, 4 µl of 10mM dNTPs, 0.25 µl of GoTaq DNA polymerase (Promega), 26 µl of sterilized MilliQ water (Millipore) and 5 µl of template DNA (1ng μl^{-1}). PCR amplifications were conducted in a PTC200 Peltier Thermal Cycler (MJ Research) as follows: initial denaturing step at 95°C (10 min), followed by 25 cycles of 1 min denaturation at 95°C, 45 s annealing at 56°C, 1 min elongation at 72°C

and a final elongation step of 10 min at 72°C. Migration of PCR products on 1.5% agarose gel were carried out to confirm the specificity of the amplification reaction. PCR products were purified with the MSB® Spin PCRapace (Stratec Molecular GmbH, Germany) according to the manufacturer's instructions. Purified PCR products were diluted to obtain 100 ng of DNA per 10 µl mix. The 10 µl mix contained 8.5 µl of diluted DNA, 0.5 µl of the restriction enzyme Hae III (10 U μl^{-1} Promega) and 1 µl of 10x Buffer C. The mix was incubated at 37°C for 1 h. One µl of digested sample was mixed with 8.5 µl of HiDi formamid (ABI) and 0.5 µl of GS600-LIZ standard (ABI). Samples were denatured by heating to 95°C for 2 min followed by cooling on ice for 5 min. The denatured samples were loaded onto an ABI 3130xl DNA capillary sequencer equipped with 50 cm long capillaries (80 µm inner diameter) and POP 7 electrophoresis matrix (POP-7™ polymer, Genetic Analyzers). The electrophoresis conditions and electropherograms analysis were conducted as described by Rossi et al.[259].

5.2.10.3 Quantitative PCR (qPCR)

A unique reference plasmid named pDHC was used as a standard for targeting both eubacterial and *Dehalococcoides*-specific 16S rRNA gene. This plasmid was obtained by cloning a 847-bp fragment of *Dehalococcoides* 16S gene amplified from SDC-9 total DNA with primers DHC-161-F (5'-GTGATGGGCTGACATAAGTCGGTTC-3') and DHC-1007-R (5'-GCAAACTCCTGACTTAA CAGGTCG-3') in a PCR reaction containing: 66.5 µl of MilliQ water (Millipore), 10 µl of 10x PCR buffer S (Peqlab), 3 µl of dNTPs at 2.5 mM, 5 µl of 10 µM primer and 0.5 µl of Taq polymerase at 5 U μl^{-1} (Peqlab). One µl of DNA at 1 ng μl^{-1} was added as a template. The PCR program was designed as follows: 5 min of initial denaturation at 95°C, 30 cycles of amplification with each cycle including 45 s denaturation at 95°C, 45 s of primer annealing at 52°C, and 90 s of elongation at 72°C; a 10 min step of final elongation at 72°C was added at the end. The PCR product was purified with the PCR purification Kit (Qiagen) and ligated into the vector pGEM-T Easy (Promega) following the manufacturer's instructions. The resulting plasmid was transformed into $CaCl_2$-competent *E. coli* DH5 α cells using standard heat shock protocol. Transformants were selected by colony PCR and verified by sequencing using an in-house facility as described previously[286]. A positive transformant harboring pDHC was cultivated for plasmid extraction using the Qiaquick Miniprep Kit (Qiagen). One µg of plasmid DNA was linearized by digestion with the restriction enzyme *Sca*I (Promega), dephosphorylated by shrimp alkaline phosphatase (TaKaRa) and finally purified using the PCR purification kit (Qiagen). DNA concentration was measured with a NanoDrop ND-1000 apparatus. Standards for qPCR were prepared by serial dilution from $4.01 \cdot 10^8$ to 10^1 plasmid copies μl^{-1}. Runs of qPCR consisted of the standard dilution series and samples in triplicates. The 10 µl qPCR reaction mixture was composed of 5 µl of KAPA SYBR® FAST Universal 2X qPCR Master Mix, 0.2 µl of each primer at 10 µM, 2.1 µl of sterile water and 2.5 µl of DNA template. The following primers were used: primers DHC-691-F (5'-GGTTTTCTAGGTTGTCA-3') and DHC-958-R (5'-

GCATGTCAAATCTTGGT-3') targeting the genus *Dehalococcoides* specifically, and primers EUB-338-F (5'-ACTCCTACGGGAGGCAGCAG-3') and EUB-520-R (5'-ATTACCGCGGCTGCTGGT-3') for eubacterial 16S genes. The program consisted of 15 min of initial denaturation at 94°C, followed by 40 cycles of 30 s denaturation at 94°C, 20 s primer annealing at 60°C, and 30 s of elongation at 72°C after which acquisition of the fluorescence was done. A melt curve ranging from 50 to 99°C was added at the end for quality assessment. The reaction was run in the RotorGene RG3000 machine (Corbett Research).

Data were analyzed using the RotorGene 6 software with a fluorescence threshold fixed at 0.25. For each primer set, at least three independent qPCR runs (each including triplicates of standards) were considered to establish the relation between fluorescence at cycle threshold (CT) and gene copy number (cn). Based on Eq. 5.1, the parameters for targeting DHC and EUB 16S rRNA genes are given in Table 5.1. For samples, standard deviations based on triplicate measurement were kept below 3% of the average CT value.

$$cn = 10^{[(CT-B)/M]} \quad (5.1)$$

Table 5.1. Parameters for qPCR.

Parameters	DHC	EUB
B	32.883 ± 1.068	31.500 ± 0.780
M	-3.467 ± 0.064	-3.350 ± 0.109
Efficiency	0.943	0.990
r^2	0.998	0.997

5.2.10.4 Pyrosequencing

Normalized extracted DNA from the ten slices of each column were pooled in order to obtain a sample representative of the global microbial diversity of each column. A 16S rRNA gene PCR amplification was carried out with the same primers and same conditions as the one used for the T-RFLP and the samples were sent to Research and Testing Laboratory LLC (Lubbock, TX,USA) for bTEFAP 16S diversity analysis on at least 3,000 pyrosequencing reads following the procedure published by Sun et al.[287]. Affiliation of operational taxonomic units (OTUs) detected by T-RFLP was done using the Pyro-TRF-ID software developed by Weissbrodt et al.[288].

5.2.11 Mineral characterization after column dissection

Formation of potential new crystalline structures was investigated by XRD as described in section 5.2.2. Characterization of changes in the surface structure and chemical composition was done by scanning electron microscopy (SEM) and energy dispersive X-ray (EDX) analysis with a XLF-30

scanning electron microscope (Phillips) equipped with a energy dispersive X-ray spectrometer for semi-quantitative element analysis (EDAX Si(Li) EDX detector). The mineral powders were coated with a carbon layer prior to EDX analyses. SEM and EDX analyses were conducted only on the first slice (from the inlet) of the columns, while XRD was conducted on all slices.

5.2.12 Calculation of mineral dissolution rate

The release rates of Si, Ca, Mg and Fe for the silicate minerals were calculated using:

$$r_i = \frac{QC_i}{Sv_i}, \tag{5.2}$$

where r_i is the release rate of element i (mol m^{-2} s^{-1}) normalized for mineral stoichiometry, Q is the volumetric flow rate (l s^{-1}), C_i is the effluent concentration of element i (mol l^{-1}) corrected for background concentration, S is the initial surface area of the mineral in the column (m^2), and v_i is the stoichiometric coefficient of element i in the mineral formula.

5.3 Results

5.3.1 pH evolution

The experiment was divided into three phases characterized by different electron donor and acceptor concentrations corresponding to different levels of acidification. The major microbial process leading to acidification was the fermentation of lactate to propionate and acetate. Production of HCl by organohalide respiration of chlorinated compounds also resulted in acidification but to a smaller extent. As a consequence, phases 1 and 3 were characterized by higher levels of acidification than phase 2. The evolution of pH in the effluents of the five columns is presented on Figure 5.2 and the average pH values during each phase are listed in Table 5.2.

In column 1 (positive control), the pH was kept stable at 7.0 ± 0.1 during phases 1 and 3 and at 7.2 ± 0.1 during phase 2 due to the presence of a zwitterionic buffer. Column 1 represented a good reference in order to evaluate the extent of PCE dechlorination when the pH was maintained at the optimal value for the consortium SDC-9™.

In column 2 (negative control), the pH decreased just after the beginning of phase 1 due to microbial activity. Within 20 days, the pH dropped from 6.88 to 6.14. An average pH of 6.23 ± 0.1 was observed during phases 1 and 3, and of 6.72 ± 0.2 during phase 2.

In column 3 (amended with diopside), mineral dissolution maintained the pH above 6.5 during the first 84 d of the experiment. However, during this period a constant decrease of effluent pH was observed from 7.5 on day 15 to 6.5 on day 84. Between day 84 and 88, the pH decreased sharply and reached the same level as in the negative control (pH = 6.16). From day 88 on, the pH was below that

of the negative control column with an average of 6.59 (±0.18) during phase 2 and of 6.13 (±0.06) during phase 3.

In column 4 (amended with forsterite), the pH was constant at 7.6 ± 0.2 during phases 1 and 3 and at 7.85 ± 0.1 during phase 2. The capacity of mineral dissolution to maintain the pH above 7 was constant during the whole experiment. A slight pH drop to 7.1 was observed between days 56 and 70 correlated to the increase in *cis*-DCE production (see section 5.3.3).

In column 5 (amended with fayalite), the pH was kept constant around 6.5 ± 0.2 during phase 1 and 3 and at 6.7 ± 0.1 during phase 2. Between day 74 and day 81, the pH increased up to 7 but this observation was the result of an experimental error. During these seven days, there was no lactate in the influent, and therefore acidifying fermentation activity was absent during this period.

Table 5.2. Average pH and standard deviations in the effluent during each experimental phases in the five columns.

Column	Condition	Phase 1	Phase 2	Phase3
Column 1	Positive control	7.00 ± 0.12	7.25 ± 0.10	7.19 ± 0.04
Column 2	Negative control	6.23 ± 0.09	6.72 ± 0.21	6.23 ± 0.08
Column 3	Diopside $CaMg(SiO_3)_2$	6.70 ± 0.34	6.59 ± 0.18	6.13 ± 0.06
Column 4	Forsterite Mg_2SiO_4	7.54 ± 0.22	7.85 ± 0.08	7.63 ± 0.10
Column 5	Fayalite Fe_2SiO_4	6.50 ± 0.20	6.72 ± 0.12	6.43 ± 0.08

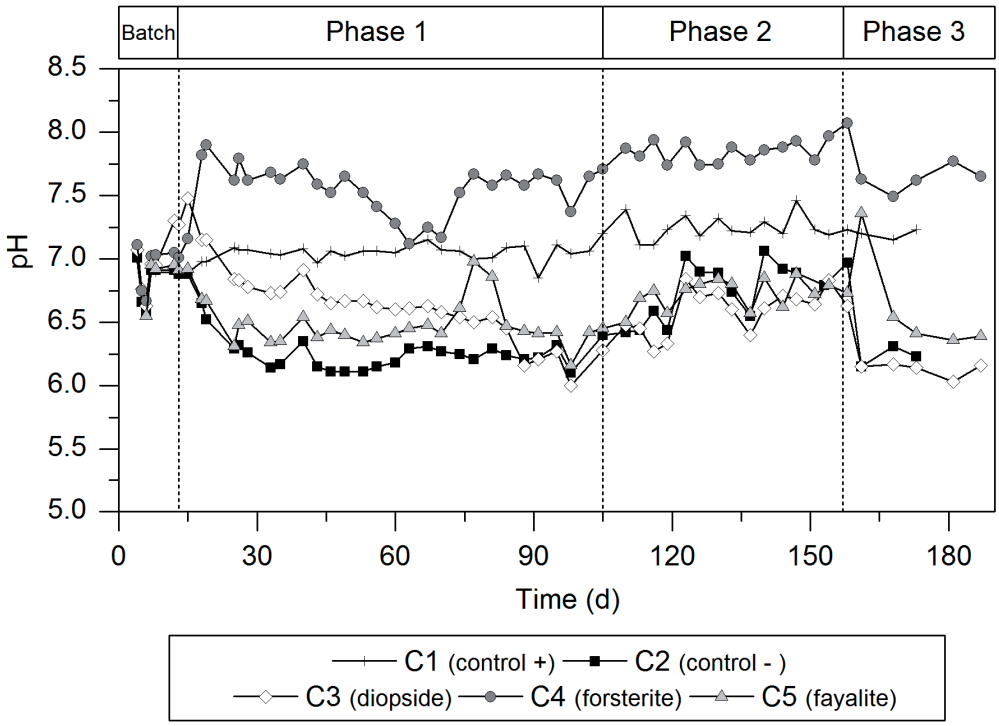

Figure 5.2. Evolution of the pH in the effluents of the five columns.

5.3.2 Electron donor fermentation

In the five columns, lactate was fermented to propionate and acetate. The ratio acetate:propionate at the column outlet during each experimental phase is given in Table 5.3 and the evolution of the VFAs and lactate concentrations over time is presented in Figure 5.3. Lactate fermentation was not influenced by the differences of pH between columns, with similar fermentation pattern for column 1 (average pH = 7) and column 2 (average pH = 6.2). Differences were observed in the proportion of acetate and propionate between columns, with higher proportion of acetate produced in columns containing minerals (columns 3, 4 and 5) compared to controls columns (columns 1 and 2).

Table 5.3. Average ratio of acetate:propionate concentrations during each phase at the outlet of the five columns.

	Acetate:Propionate		
	Phase 1	Phase 2	Phase 3
Column 1	1:1.45	1:1.06	1:1.45
Column 2	1:1.41	1:1.15	1:1.67
Column 3	1:1.25	1:0.97	1:1.69
Column 4	1:1.06	1:0.89	1:1.39
Column 5	1:1.23	1:0.84	1:1.43

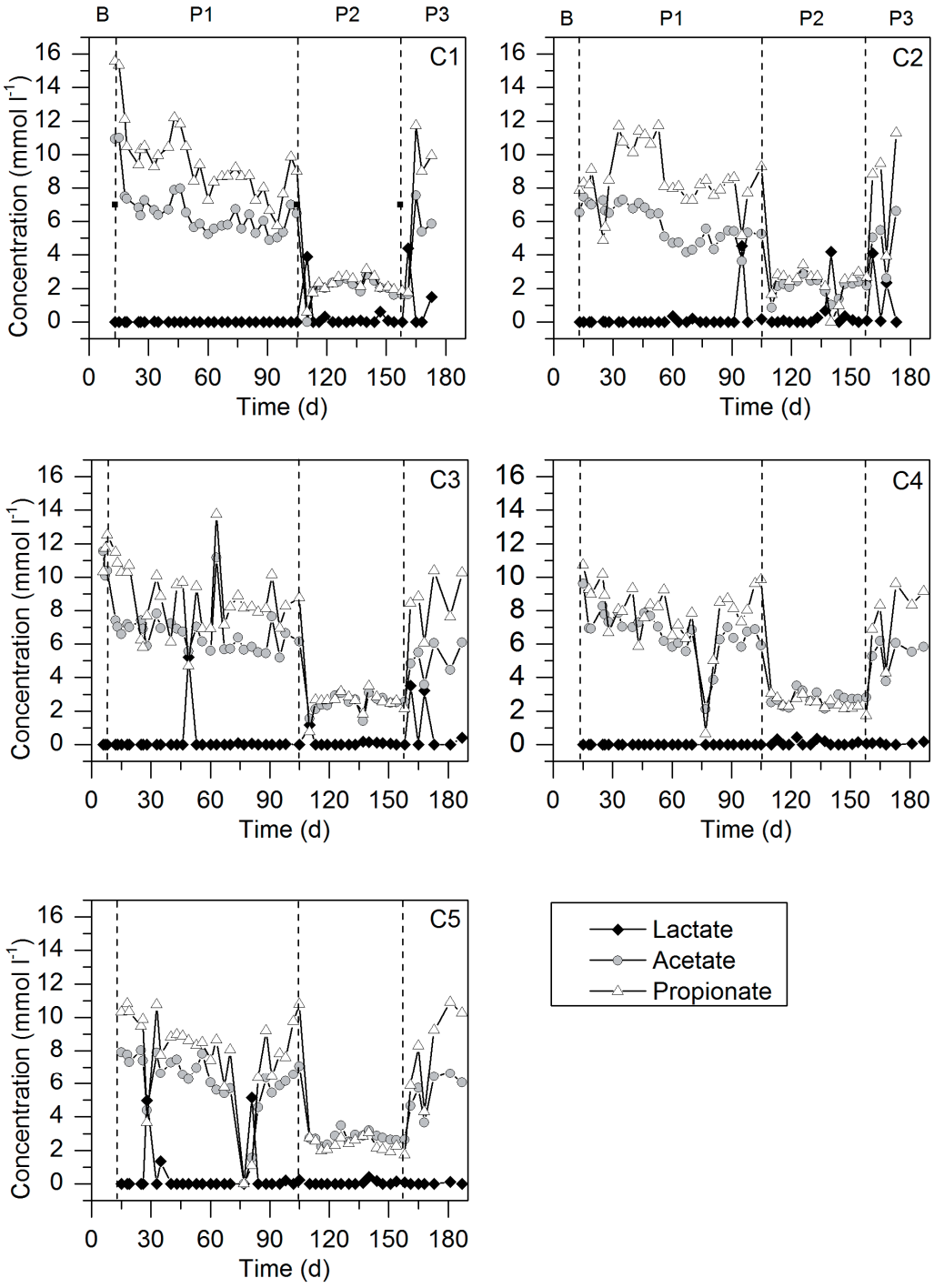

Figure 5.3. Evolution of lactate, propionate and acetate concentrations at the column outlet in the five columns (B: batch phase; P1, 2 and 3: phases 1, 2 and 3; C1, C2, C3, C4, C5: columns 1, 2, 3, 4, and 5).

5.3.3 PCE organohalide respiration

The activity of OHRB was monitored by measuring the concentration of PCE and its dechlorination products in the column effluents (Figure 5.4 for columns 1 and 2 and Figure 5.5 for columns 3, 4 and

5). PCE dechlorination activity was rather unstable during the first 40-50 days of the experiment in columns 1, 3 and 4. On day 22, the flow was stopped in these columns for 3 days due to technical problems. his perturbation might have induced a negative effect on the bacterial activity. Different dechlorination patterns were observed in each column.

In column 1, PCE dechlorination did not start readily after column installation and significant PCE dechlorination was only observed after a lag phase of 20 d. After 40 d, PCE was completely converted to *cis*-DCE. VC started to be produced after 60 d and ethene after 74 d. From the start of phase 2 and onwards, the effluent was mainly composed of a mixture of ethene, VC and *cis*-DCE and it was only towards the very end of the experiment (day 168) that quasi complete dechlorination to ethene was observed (98% of ethene on day 173).

In column 2, degradation of PCE started readily during the batch phase with initial production of VC and ethene. However, after 25 d, organohalide respiration activity decreased and PCE started to accumulate in the effluent and after day 60, transformation of PCE was fully inhibited. Decrease of OHR activity was correlated with the decrease of pH down to 6.2. During phase 2, a rebound of OHR activity was observed with partial dechlorination of PCE to *cis*-DCE (up to 74% of *cis*-DCE).

In column 3, dechlorination started readily after the mounting of the column with production of VC, *cis*-DCE and ethene during the first 60 d. For the rest of the experiment, the dechlorination products were mainly *cis*-DCE and to a smaller extent VC but no more ethene was produced. Although the pH was at the same level as in the negative control after 88 d, the extent of PCE dechlorination was higher.

In column 4, dechlorination started readily but complete disappearance of PCE was only observed after 60 d. Significant VC production started after 84 d followed on day 95 by significant ethene production. From day 95 onwards, VC and ethene concentration increased and a maximum of 91% of ethene was reached on day 137. In the last 20 d of the experiment, the effluent concentration remained quite stable with the average composition: ethene (34%), VC (32%) and *cis*-DCE (28%).

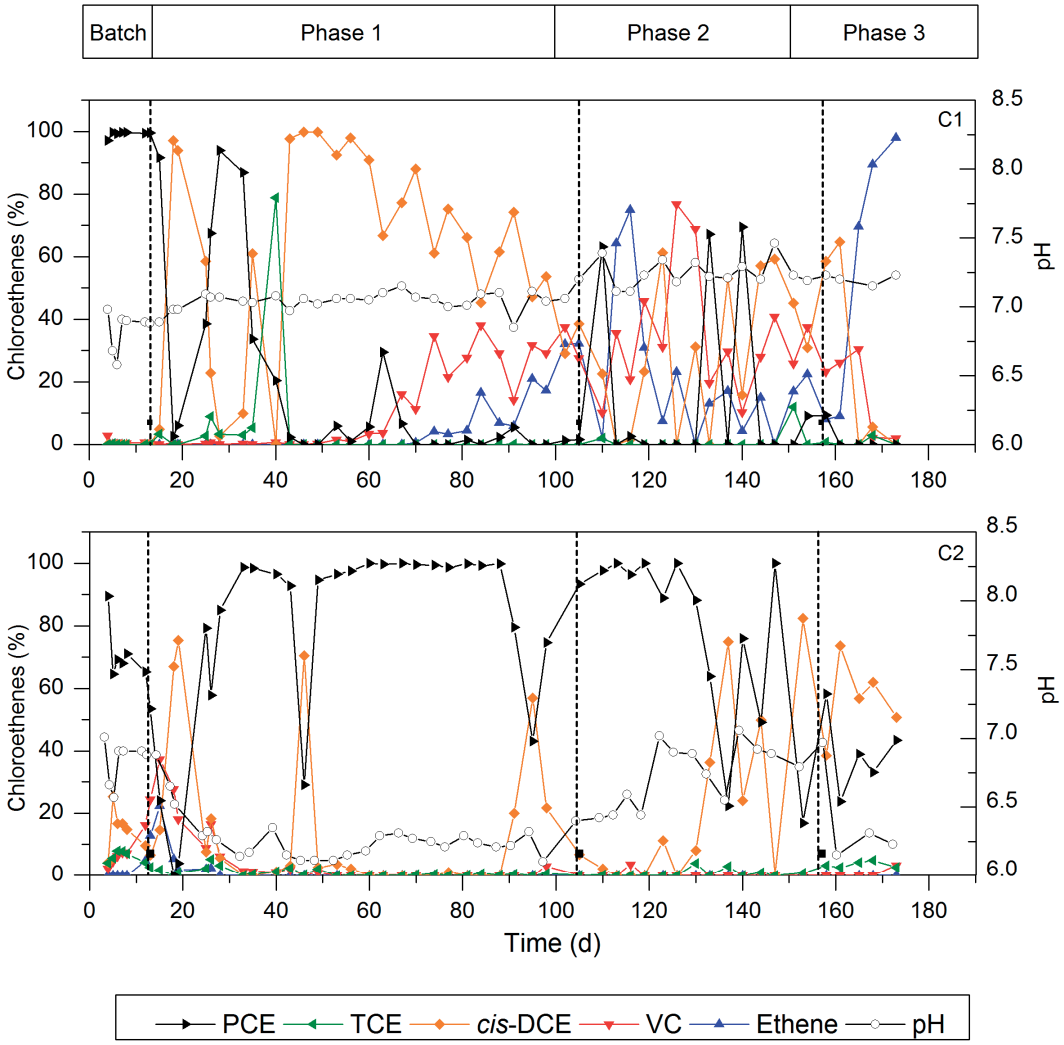

Figure 5.4. Evolution of pH and relative concentration of PCE, TCE, *cis*-DCE, VC and ethene in the effluent of columns 1 (C1) and 2 (C2) (positive and negative control).

In column 5, during the first 80 d, PCE dechlorination was extremely limited and 90 to 95% of the initial PCE was not degraded. After day 80, PCE suddenly started to be dechlorinated to *cis*-DCE. At day 133, ethene and VC started to be produced with a maximum of 77% of ethene on day 161. Similarly to column 4, during the last 20 d, the effluent was mainly composed of a mixture of ethene (22%), VC (32%) and *cis*-DCE (38%).

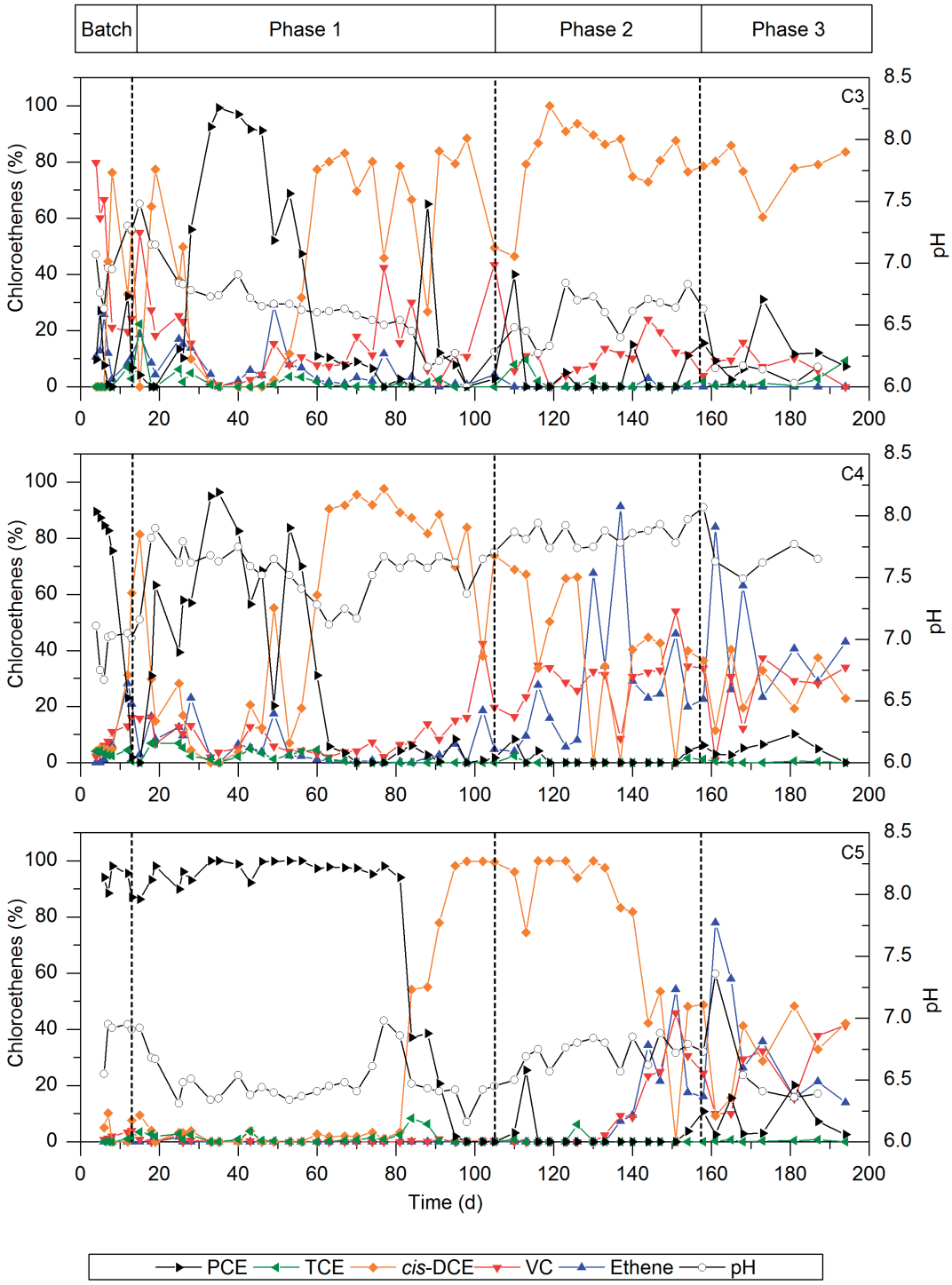

Figure 5.5. Evolution of pH and relative concentration of PCE, TCE, *cis*-DCE, VC and ethene in the effluents of columns 3 (C3), 4 (C4), and 5 (C5) amended with diopside, forsterite, and fayalite, respectively.

5.3.4 Evolution of dissolved phosphate

Initial concentrations of phosphate in the reservoir were equal to 0.8 mmol l^{-1} for column 1 and 0.4 mmol l^{-1} for the four other columns. The same concentrations were observed in the effluent of columns 1 to 4 indicating that the amount of phosphate consumed by the bacteria was small and within the error

range of the analytical measure. However, in the effluent of column 5, phosphate concentrations were between 0 and 0.15 mmol l^{-1} suggesting precipitation of dissolved phosphate inside the column.

5.3.5 Redox potential

Redox potential measurements performed on day 176 showed that the effluent presented low redox values between -363 mV for column 4 to -234 mV for column 5. In columns 1, 2 and 3 the redox potential was comprised between -285 and -282 mV.

5.3.6 Mineral dissolution rates

Mineral dissolution was monitored by following the evolution of Si, Ca, Mg and Fe total element concentrations in the column effluents. The evolution of dissolution rates calculated with Eq. 5.2 is presented in Figure 5.6. Measurements were also taken in the effluents of the control columns to evaluate background concentrations for mineral dissolution rate corrections. In columns 1 and 2, Ca and Mg concentrations were constant at about 0.14 ± 0.04 and 0.09 ± 0.018 mmol l^{-1}, respectively. Low concentrations of Si (0.026 ± 0.019 mmol l^{-1}) resulting from quartz dissolution were also detected.

In column 3, diopside dissolution was initially incongruent, with a preferential release of Ca during the first 84 d. Ca-based dissolution rates were on average 7.5-times higher than Si- and Mg-based dissolution rate (Figure 5.6). Between day 84 and day 91, a sharp decrease of Ca release was observed with a reduction of Ca concentration by a factor of 10. In addition, during the first 100 d, Si, Ca, and Mg-based dissolution rates decreased linearly with time with a reduction of the Si-based dissolution rate from 3.06 x 10^{-12} mol m^{-2} s^{-1} to 8 x 10^{-13} mol m^{-2} s^{-1}. After 100 d, a steady state was achieved and constant dissolution rates during each phase were observed.

In column 4, forsterite dissolution was congruent from the beginning of the experiment. In addition, dissolution rates were constant during each phase of the experiment.

In column 5, fayalite dissolution was incongruent during the whole experiment with very low release of Fe. Iron-based dissolution rates were between 1 to 3 orders of magnitude lower than Si-based rates. These results indicated iron precipitation inside the column. Iron precipitation appeared to be pH dependent with Fe concentrations below detection limit when the pH was above 6.5.

In the three columns, mineral dissolution rates were enhanced by acidification. Between phase 1 and 2 where the level of acidification was reduced by a factor of 3, Si-dissolution rates were simultaneously reduced by 37%, 39%, and 21% for diopside, forsterite, and fayalite, respectively.

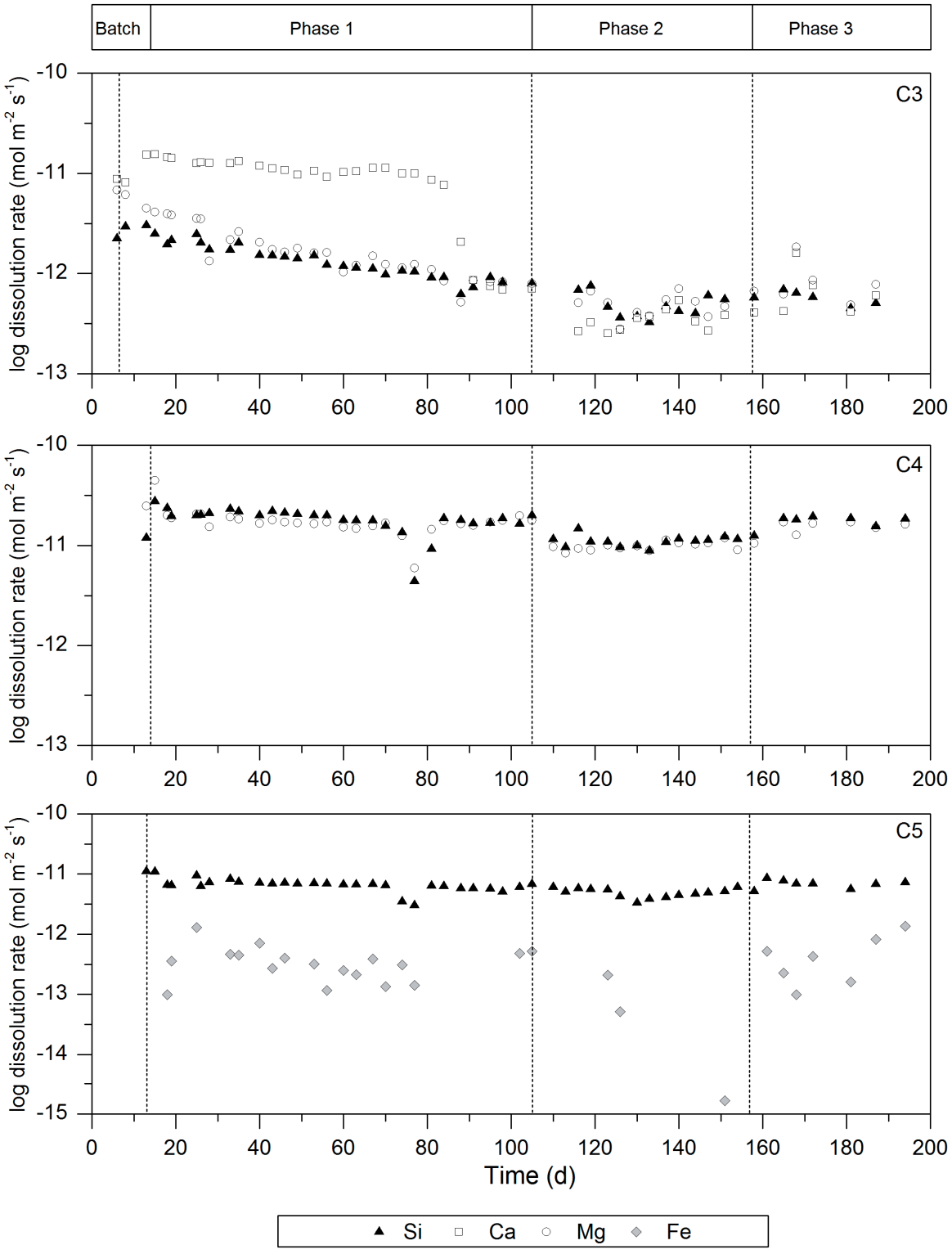

Figure 5.6. Evolution of mineral dissolution rates based on Si, Mg, Ca, and Fe total element concentrations in the effluents of columns 3 (C3), 4 (C4) and 5 (C5).

5.3.7 Tracer test

The breakthrough curves of the tracer test performed at the end of the experiment are presented in Figure A5.1 (Appendix). The shape of the curves showed the absence of preferential flow path inside

the columns. In columns 2, 4, and 5, the hydraulic residence time at the end appeared to be shorter (2.6 days) than the initial residence time of 3 days suggesting a decrease of porosity in these columns (based on comparison of the data with CXFIT predictions).

5.3.8 Changes of mineral structure and formation of secondary phases

5.3.8.1 Mineral phases before dissolution

XRD analyses conducted prior to dissolution (Figure 5.7) revealed that the samples were not pure and contained traces of other mineral phases.

Diopside contained traces of pargasite ($NaCa_2(Mg,Fe^{2+})_4Al(Si_6Al_2)O_{22}(OH)_2$) and talc ($Mg_3Si_4O_{10}(OH)_2$), forsterite contained traces of talc and chlorite $(Mg,Fe,Li)_6AlSi_3O_{10}(OH)$, fayalite contained traces of biotite ($K(Mg,Fe)_3AlSi_3O_{10}(F,OH)_2$). Analyses of the chemical composition of the samples by XRF (Chapter 3, Table A3.5, Appendix) showed that these contaminant phases contributed less than 10% of the mineral samples. SEM and EDX analyses also revealed that forsterite and fayalite samples contained iron oxide particles.

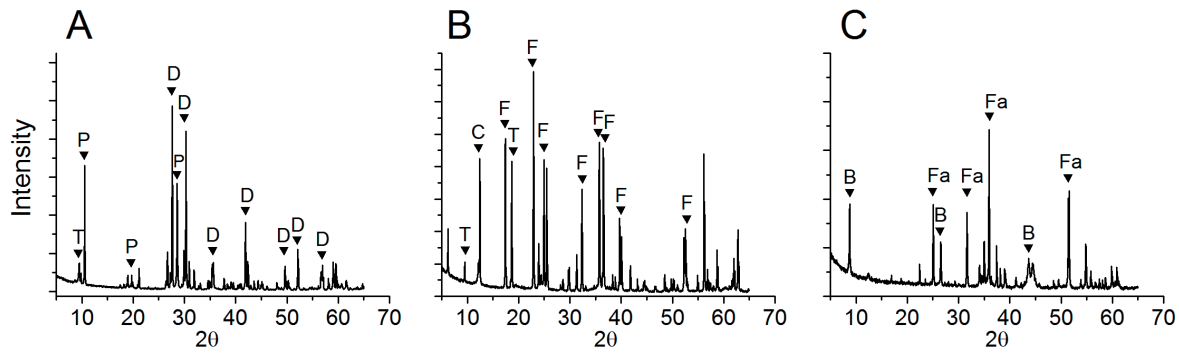

Figure 5.7. XRD analyses of diopside (A), forsterite (B) and fayalite (C) samples prior to dissolution. The mineral peaks were labeled as diopside (D), pargasite (P), talc (T), forsterite (F), chlorite (C), biotite (B) and fayalite (Fa).

5.3.8.2 Mineral phases after dissolution

XRD analyses, conducted after mineral dissolution, showed that the column material contained quartz and the mineral phases described above. No new mineral phases were detected suggesting the absence of crystalline secondary precipitation. In order to evaluate the formation of amorphous precipitates, SEM and EDX analyses (on at least 15 points) were conducted. No secondary precipitates were observed at the surface of diopside and forsterite at the end of the experiment (Figures 5.8 and 5.9). On the surface of forsterite particles, etch pits resulting from dissolution were observed (Figures 5.9 c and d). The chemical composition of diopside determined by EDX showed that all calcium initially present at the mineral surface disappeared at the end of the experiment (Table 5.4). The proportion of

Ca in the mineral after dissolution was below 0.04% in all points analyzed. In contrast, the chemical composition of forsterite showed little variation before and after dissolution (Table 5.4). Comparison between SEM pictures of fayalite before and after dissolution showed that quartz and fayalite particles were coated with secondary precipitates at the end of the experiment (Figure 5.10). These secondary precipitates were identified as iron sulfide (FeS) by EDX analyses (Table 5.4).

Table 5.4. Average chemical composition of the surface layer of diopside, forsterite and fayalite particles before and after dissolution determined by EDX.

	Atomic composition (molal %)					
Element	Diopside		Forsterite		Fayalite	
	Before dissolution	After dissolution	Before dissolution	After dissolution	Before dissolution	After dissolution
O	60.68	55.23	59.34	53.96	63.00	68.80
Al	0	0	0	0	2.71	0
Mg	6.86	20.64	20.24	25.78	2.77	0.11
Si	20.58	20.86	17.18	14.24	17.95	4.00
Ca	10.19	0.04	0	0	0	0
S	0	0	0	0	0.06	13.57
Fe	1.38	2.92	2.92	5.18	13.25	13.09

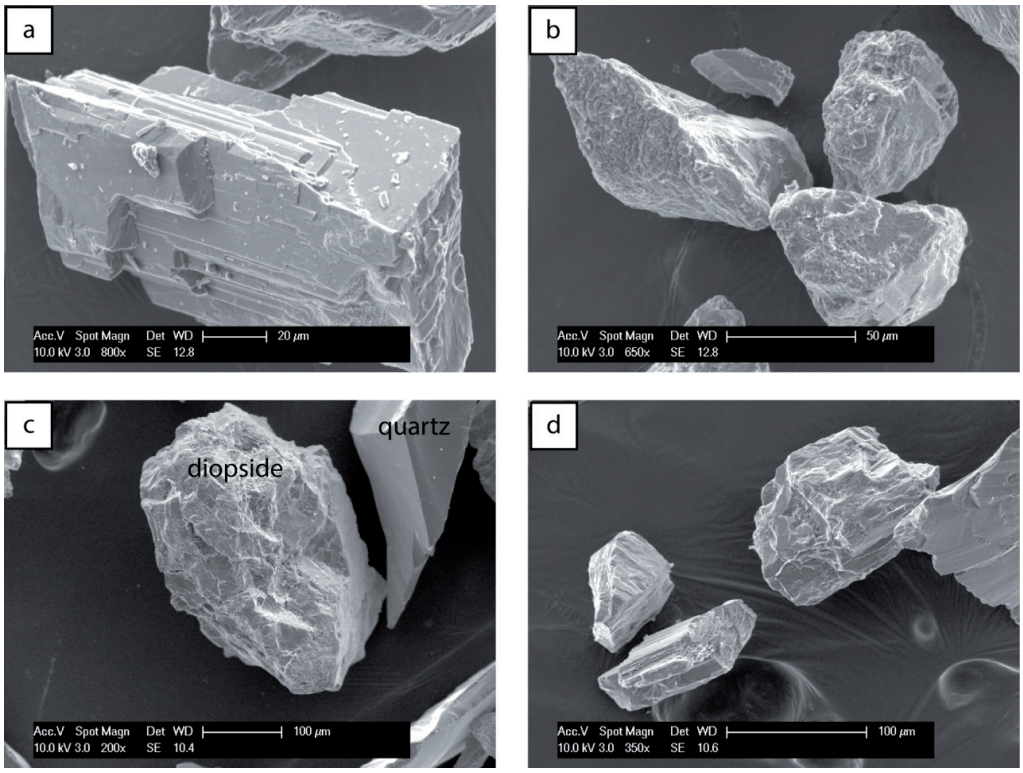

Figure 5.8. SEM pictures of diopside before (a and b) and after the experiment (c and d). A particle of quartz is present in picture c. No formation of secondary precipitates was observed on the surface.

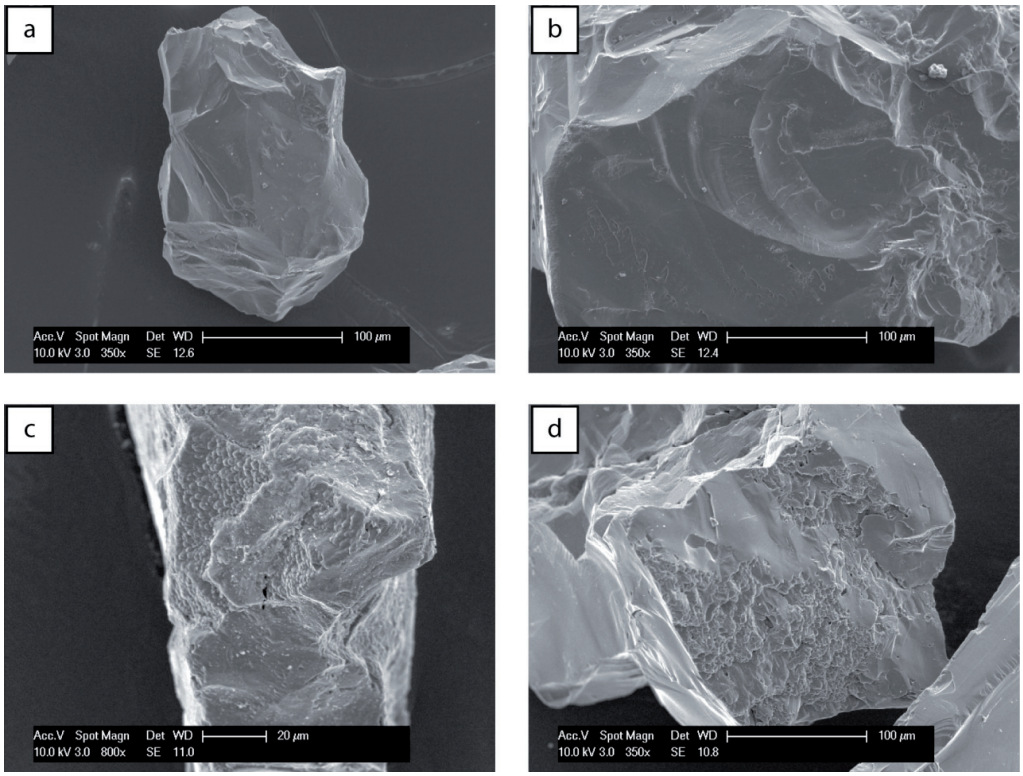

Figure 5.9. SEM pictures of forsterite particles before (a and b) and after the experiment (c and d). Formation of dissolution etch pits are clearly visible at the surface of forsterite in picture d.

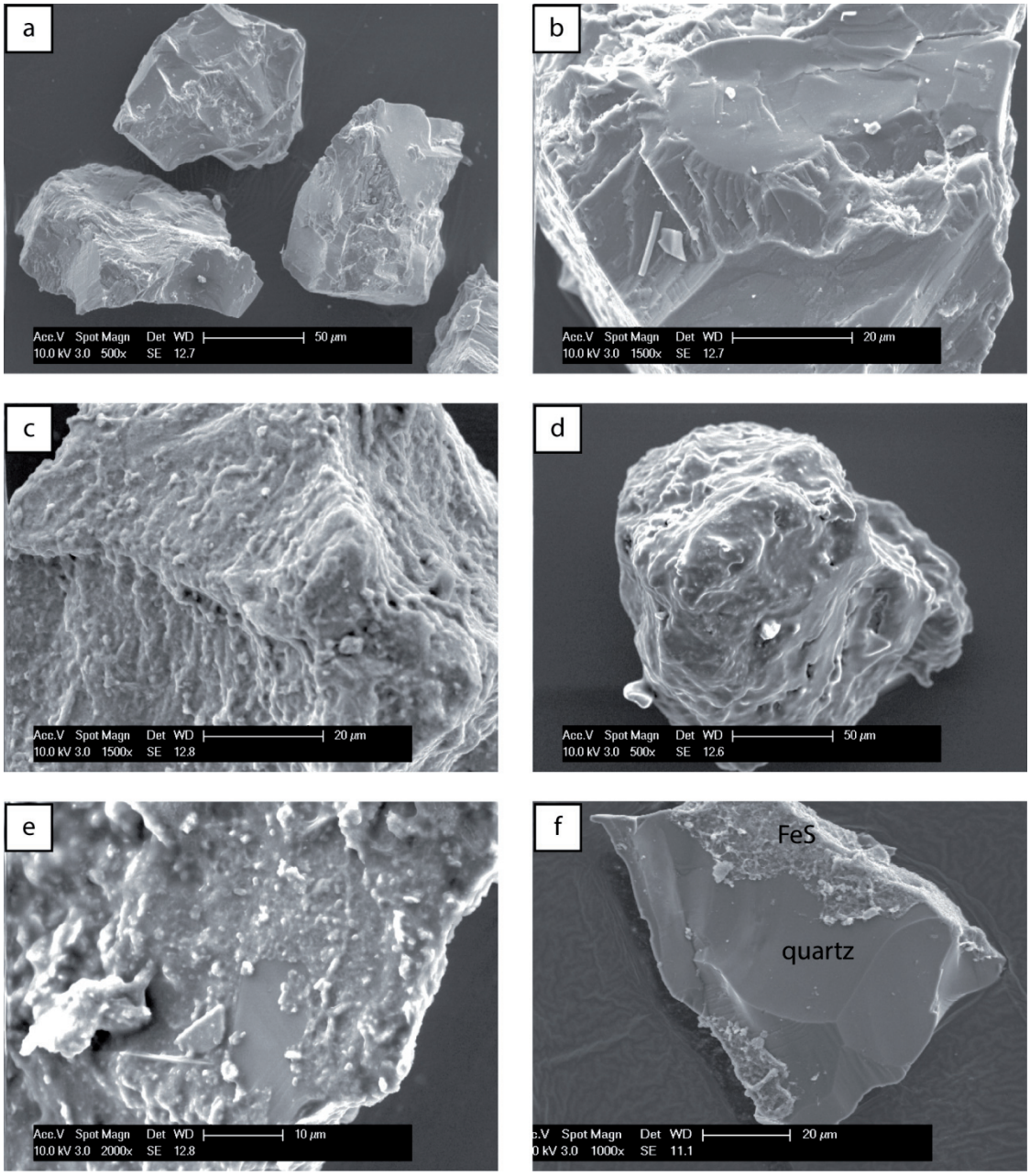

Figure 5.10. SEM pictures of fayalite particles before (a and b) and after the experiment (c, d, e and f). Picture f represents a quartz particle coated with iron sulfide. Fayalite particles on pictures c and d are completely covered by iron sulfide precipitates.

5.3.9 Microbial community analyses

After column dissection, DNA was extracted from each slice and quantification of *Dehalococcoides* and total eubacterial 16S rRNA gene copies was performed by q-PCR. The composition of the microbial community in the columns and in the initial SDC-9™ culture was determined by a combination of T-RFLP, pyrosequencing, and PyroTRF-ID as described by Weissbrodt et al.[288]. In this study, operational taxonomic units (OTUs) usually used to describe T-RFLP analyses are referred as experimental terminal-restriction fragments (eT-RFs).

5.3.9.1 Microbial community composition of the consortium SDC-9™

The major eT-RFs and their corresponding affiliation identified in the SDC-9™ culture are presented in Table 5.5. The consortium was mainly composed of *Desulfovibrio* spp. (35.8%, e-TRFs 70, 195 and 196), *Dehalococcoides* spp. (13.6%, eT-RF 245) and a population affiliated to the order of *Bacteroidales* (17.8%, eT-RF 404).

Table 5.5. Identification of predominant eT-RFs (> 3%) present in SDC-9™ culture used to inoculate the columns using PyroTRF-ID software.

eT-RF[a] (bp)	dT-RF[b] (bp)	Phylogenetic affiliation[c]	Counts[d]	Fraction of T-RF (%)[e]	Accession number	Normalized SW score[f]
70	76	S: *Desulfovibrio desulfuricans*	418	94	DQ517287	0.985
195	194	G: *Desulfovibrio*	41	100	FJ393061	0.835
196	195	G: *Desulfovibrio*	7	100	GQ503855	0.784
200	204	F: *Veillonellaceae*	32	100	FJ674057	0.835
245	248	G: *Dehalococcoides*	128	84.76	GU139321	1.000
		G: *Cloacibacillus*	16	10.59	CU463952	1.000
290	295	G: *Desulfovibrio*	4	100	EU980605	0.446
404	408	O: *Bacteroidales*	134	100	EU981245	0.985

[a] Experimental Terminal-Restriction Fragment (eT-RF) determined by T-RFLP analysis.

[b] Digital Terminal-Restriction Fragment determined with the PyroTRF-ID software.

[c] Predominant phylotype contributing to the eT-RF obtained after comparison with the Greengenes database of 16S rRNA sequences (O: order, F: family, G: genus, S: species).

[d] Number of sequences from the pyrosequencing dataset affiliated to a same microbial population.

[e] Different bacterial populations can contribute to the same eT-RF. This column gives the relative contribution of each population to the target eT-RF. Only the bacterial groups representing a major contribution are reported here, which explains why the total contribution is sometimes below 100%.

[f] The SW (Smith-Waterman) score is indicative of the similarity between sequences obtained by pyrosequencing and sequences from the Greengenes database. The SW score is normalized by the read length and represents an estimation of the percentage of sequence identity (Weissbrodt et al.[288] for details).

5.3.9.2 Predominant microbial population in the columns

The evolution of bacterial community composition along the column flow path at the end of the experiment is presented in Figure 5.11 (for columns 1 and 2) and 5.12 (for columns 3, 4 and 5). The closest bacterial affiliations of eT-RFs detected in each column are presented in Table 5.6. The predominant bacterial phylotypes identified in the columns were *Proteus vulgaris*, *Citrobacter* spp, *Clostridium* spp., *Dehalococcoides* spp., *Oscillospira* spp., *Sulfurospirillum* spp., *Propionicimonas* spp. and *Desulfovibrio* spp. The relative abundance of these predominant phylotypes along the column flow path is presented in Figure 5.13. Surprisingly, these predominant groups, except *Dehalococcoides* spp. and *Desulfovibrio* spp., were below the detection limit in the original bacterial culture SDC-9™ suggesting that these populations were positively selected during the column experiment.

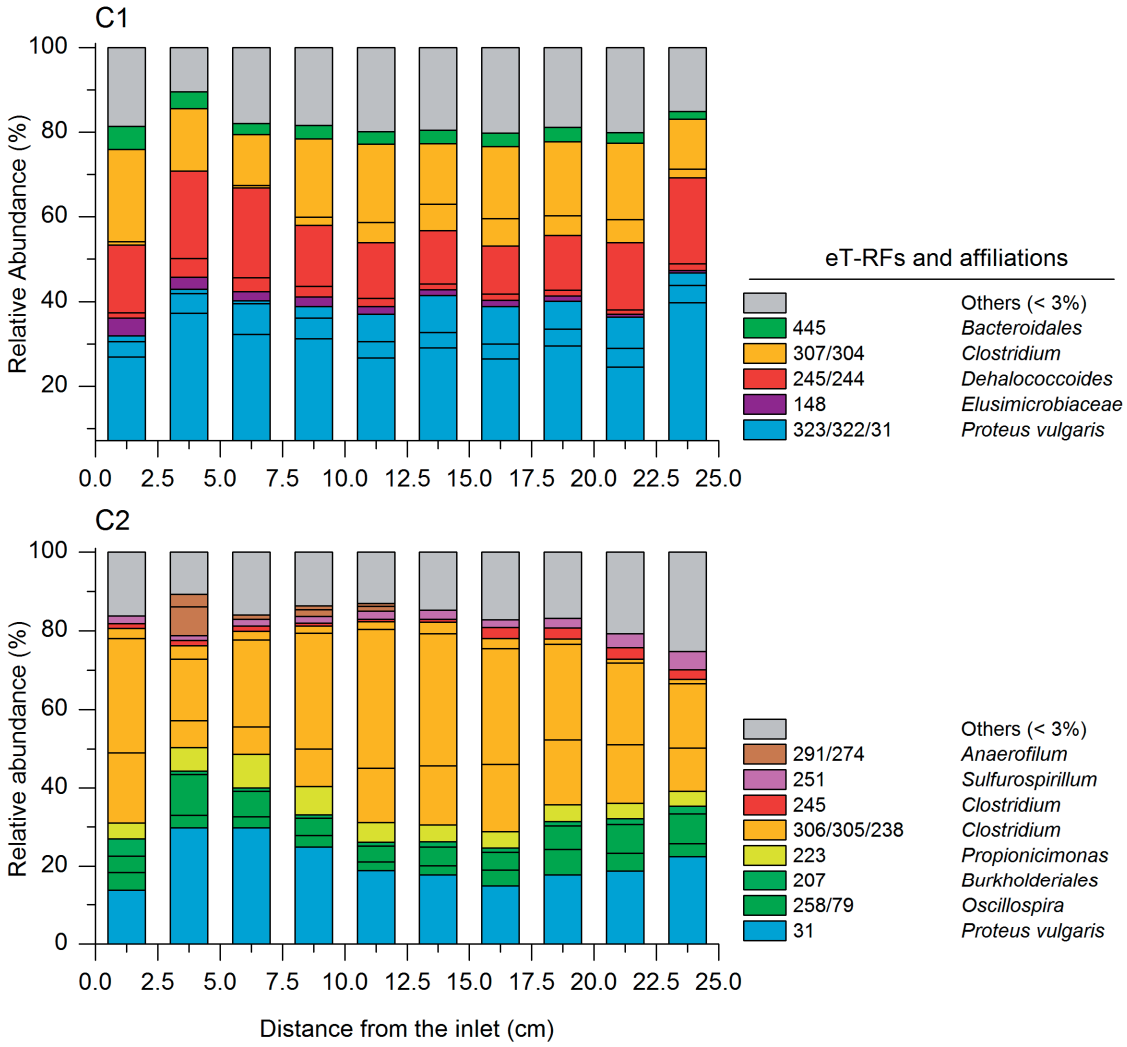

Figure 5.11. Predominant bacterial populations (contribution > 3%) analyzed by T-RFLP along the flow path of columns 1 (C1) and 2 (C2) at the end of the experiment. The closest bacterial affiliations of the eT-RFs were obtained by pyrosequencing and PyroTRF-ID analysis. When several bacterial populations contribute to one single eT-RF, the bacterial population with the highest contribution is given.

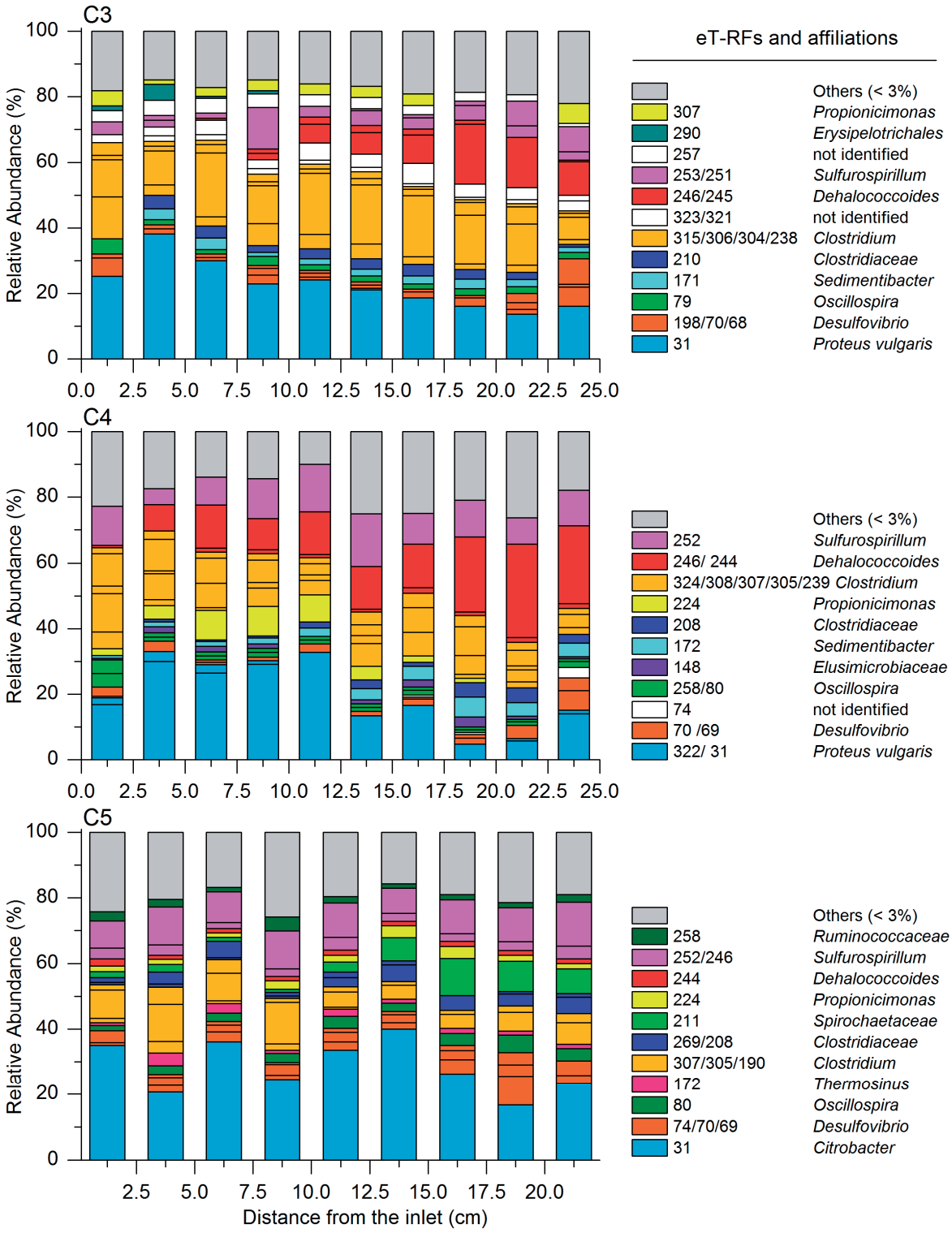

Figure 5.12. Predominant bacterial populations (contribution > 3%) analyzed by T-RFLP along the flow path of columns 3 (C3), 4 (C4) and 5 (C5) at the end of the experiment. The closest bacterial affiliations of the eT-RFs were obtained by pyrosequencing and PyroTRF-ID analysis. When several bacterial populations contribute to one single eT-RF, the bacterial population with the highest contribution is given.

5.3.9.3 Microbial communities along the flow path of the five experimental columns

The T-RFLP profiles presented strong differences in between columns as shown in Figures 5.11 and 5.12. Some bacterial populations (e.g. *Propionicimonas* spp., *Oscillospira* spp., *Sulfurospirillum* spp.) were present in high proportions in one column and not detected in another. A common feature between the five columns was the predominance of the eT-RF 31 that was mainly affiliated to *Proteus vulgaris* and to some extent also to *Citrobacter* spp. in columns 4 and 5.

Fluctuations of microbial community composition along the flow path were observed in columns with minerals (columns 3, 4 and 5) whereas in the controls (columns 1 and 2) the microbial community composition was rather stable. In columns 3 and 4, a decrease of *Proteus vulgaris* and an increase of *Dehalococcoides* spp. were observed towards the column outflow. In addition, differences in total microbial diversity were observed between columns: control columns 1 and 2 presented a lower richness (37 and 42 different eT-RFs, respectively) than columns 3, 4 and 5 (63, 60, and 61 eT-RFs, respectively).

5.3.9.4 Relative abundance of Dehalococcoides

Relative abundance of *Dehalococcoides* (Figures 5.13A and 5.14) exhibited strong differences between the five columns. In column 1, *Dehalococcoides* spp. were present in a relative abundance comprised between 13 to 25%. In contrast, the relative abundance was very low (between 0.04 to 1.32%) in column 2. In columns 3 and 4, amended with diopside and forsterite respectively, a gradient along the column flow path was observed. *Dehalococcoides* genes copies increased from less than 1% to about 15% (column 3) and 30% (column 4) towards the column outflow. Finally, in column 5 amended with fayalite, low and constant relative abundances were observed along the column between 1 to 2.2%.

5.3.9.5 Relative abundance of Sulfurospirillum

Besides *Dehalococcoides*, another organohalide-respiring population, *Sulfurospirillum* spp., was present in the columns. Figure 5.13 shows that *Sulfurospirillum* spp. was present in higher proportion in columns containing minerals than in the control columns, with an average relative abundance of 4.3, 10.7, and 10.4% for columns 3, 4, and 5, respectively.

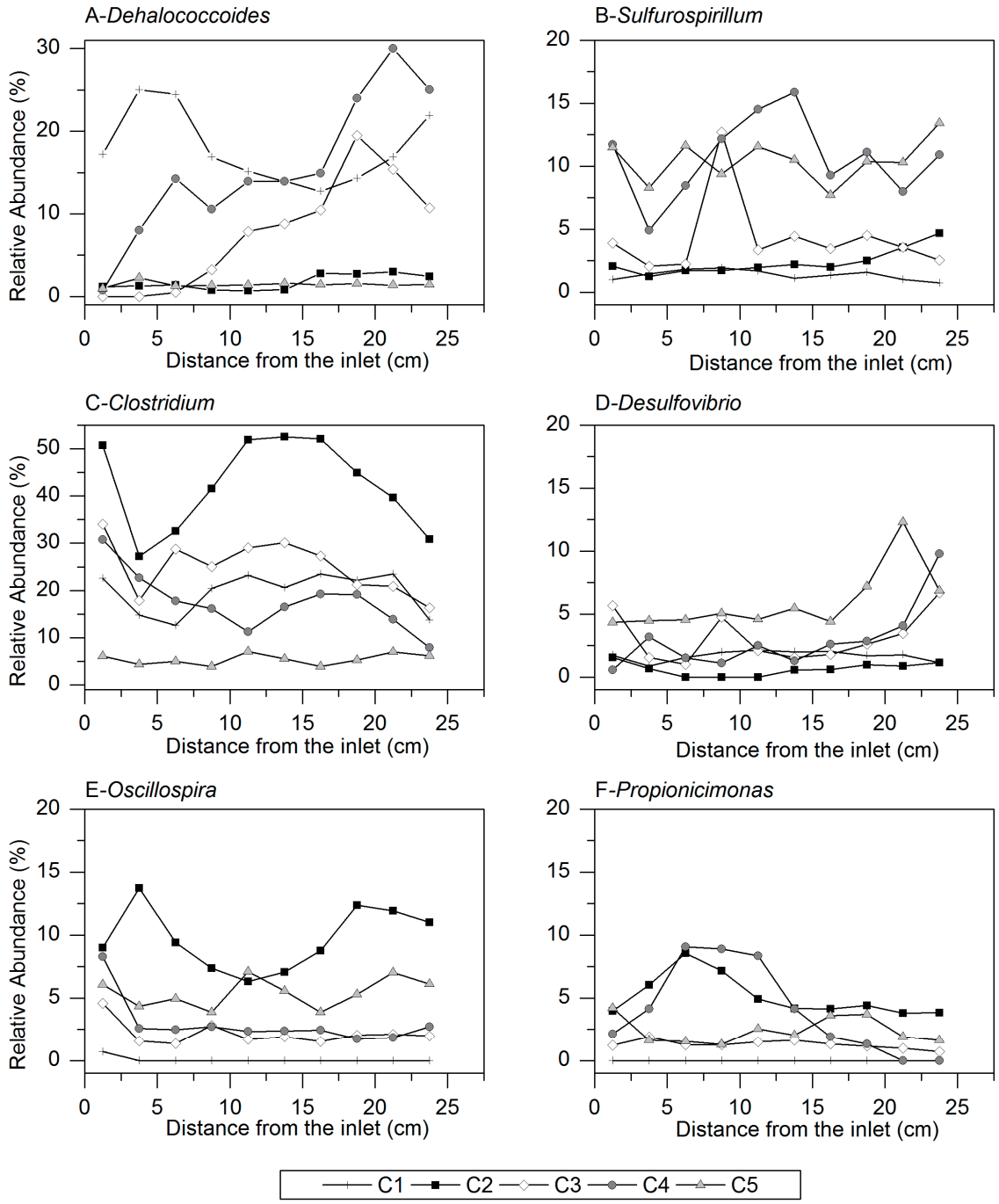

Figure 5.13. Relative abundance of the predominant microbial populations along the column length. Relative abundances were calculated from T-RFLP profiles. In A, the relative abundances for column 2 are overestimated because *Dehalococcoides* contributes only to 6.8% to the eT-RF 245. A better estimation of *Dehalococcoides* relative abundances in column 2 is given by the result of the q-PCR analyses (Figure 5.14).

5.3.9.6 Validation of T-RFLP by qPCR for Dehalococcoides quantification

In order to validate the semi-quantitative character of the T-RFLP results, the relative abundance determined by qPCR (ratio of 16S rRNA *Dehalococcoides* gene copies over 16S rRNA total eubacteria gene copies) were compared with the relative abundance of the eT-RFs affiliated with

Dehalococcoides spp. (from T-RFLP profiles) (Figure 5.14). T-RFLP and q-PCR results were very similar suggesting that the conditions applied here for T-RFLP provided a good estimate of the relative abundance of microbial populations. In column 2, *Dehalococcoides* contributed only to 6.8% to the eT-RF 245 (see Table 5.6) and therefore, relative abundances determined by T-RFLP were over-estimated. For the other columns, only one data point in column 4 showed a big difference of relative abundance between the two methods. In view of the good match for all other data points, this point was considered as an outlier with an overestimation by qPCR.

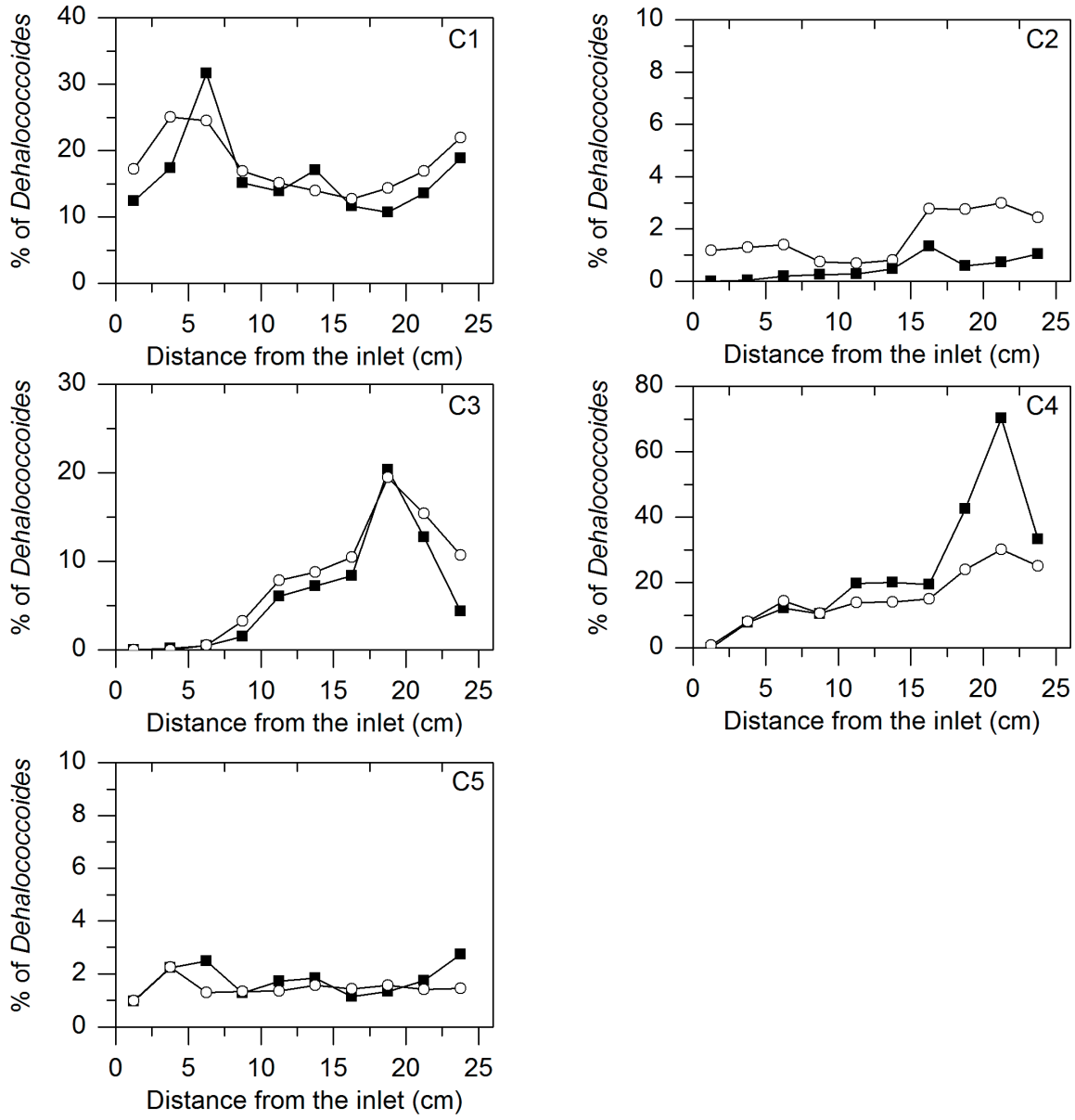

Figure 5.14. Comparison of the relative abundance of *Dehalococcoides* observed along the column flow path at the end of the experiment analyzed by T-RFLP (○) and qPCR (■) (C1, C2, C3, C4, C5: columns 1, 2, 3, 4, and 5).

Table 5.6. Identification of predominant eT-RFs (> 3%) present in each column using PyroTRF-ID software.

eT-RF[a] (bp)	dT-RF[b](bp)	Phylogenetic affiliation[c]	Counts[d]	Fraction of T-RF (%)[e]	Accession number	Normalized SW score[f]
		Column 1				
31	35	S: *Proteus vulgaris*	2478	93.79	X07652	0.962
148	152	F: *Elusimicrobiaceae*	35	100	GQ448655	0.692
244	247	G: *Dehalococcoides*	1191	96.28	GU139321	0.985
		F:*Dethiosulfovibrionaceae*	42	3.39	FJ167482	0.905
245	248	G: *Dehalococcoides*	81	98.780	AJ853547	0.830
304	309	G: *Clostridium*	402	100	AJ576348	0.748
307	310	G: *Clostridium*	197	96.09	AJ576348	0.620
		G: *Desulfitobacterium*	8	3.90	U68528	0.536
322	325	S: *Proteus vulgaris*	27	90	X07652	0.900
323	331	S: *Proteus vulgaris*	25	100	X07652	0.813
445	450	O: *Bacteroidales*	28	100	AB243814	0.907
		Column 2				
31	39	S: *Proteus vulgaris*	2183	96.08	AY167943	0.977
79	85	G: *Oscillospira*	25	75.75	FJ625862	0.889
		G: *Clostridium*	6	18.18	AY667250	0.649
207	212	F: *Burkholderiales*	5	71.42	EU499695	0.714
223	228	F: *Propionicimonas*	49	100	GQ066679	0.923
238	242	G: *Clostridium*	211	98.59	X77841	0.874
245	248	G: *Clostridium*	25	56.81	X77841	0.740
		G: *Cloacibacillus*	16	36.36	CU463952	1.000
		G: *Dehalococcoides*	3	6.81	GU139321	0.992
251	253-254	G: *Sulfurospirillum*	16	100	GQ377111	0.983
258	262	G: *Oscillospira*	10	62.5	EU463672	0.541
		F: *Ruminococcaceae*	4	25	EU777235	0.541
274	278	G: *Anaerofilum*	12	100	AF150697	0.730
291	291	G: *Anaerofilum*	12	85.71	AF150697	0.595
305	307-308	G: *Clostridium*	210	100	AY667250	0.860
306	309-310	G: *Clostridium*	34	100	GQ503859	0.725

Table 5.6 (Part 2)

eT-RF[a] (bp)	dT-RF (bp)[b]	Phylogenetic affiliation[c]	Counts[d]	Fraction of T-RF (%)[e]	Accession number	Normalized SW score[f]
			Column 3			
31	39	S: *Proteus vulgaris*	149	51.9	AY167953	0.960
0.96		G: *Citrobacter*	51	17.42	GQ416169	0.924
		F: *Porphyromonadaceae*	50	17.42	GQ461629	0.885
		G: *Dysgonomonas*	21	7.31	FJ823922	0.545
68-70	76	S: *Desulfovibrio desulfuricans*	35	87.5	AF427913	0.991
79	85	G: *Oscillospira*	22	100	FJ625862	0.914
171	176	G: *Sedimentibacter*	2	100	AY766466	0.893
198	202	S: *Desulfovibrio desulfuricans*	1	100	DQ984659	0.975
210	214-215	F: *Spirochaetaceae*	1	100	EF515354	0.931
		G: *Trichococcus*	1	100	GU136579	0.989
238	242	G: *Clostridium*	136	100	X77841	0.882
245	247	G: *Dehalococcoides*	25	86.2	AF388549	0.985
246	248	G: *Dehalococcoides*	8	100	AF388549	0.824
251	255-256	G: *Sulfurospirillum*	2	40	GQ377111	0.735
		G: *Desulfovibrio*	1	20	DQ517287	0.393
		F: *Catabacteriaceae*	1	40	CU925891	0.883
253	258	O: *Bacteroidales*	1	50	EU037360	0.737
		G: *Sulfurospirillum*	1	50	FJ799153	0.686
253	259	F: *Erysipelotrichaceae*	3	100	FJ681450	0.492
290	295	O: *Erysipelotrichales*	3	100	EU771320	0.565
304	307-308	G: *Clostridium*	66	100	AB298756	0.700
306	309	G: *Clostridium*	6	100	AB298756	0.532
307	310	G: *Clostridium*	18	85.77	FJ799151	0.786
315	320	G: *Clostridium*	7	100	AY667250	0.593

Table 5.6 (Part 3)

eT-RF[a] (bp)	dT-RF (bp)	Phylogenetic affiliation[c]	Counts[d]	Fraction of T-RF (%)[e]	Accession number	Normalized SW score[f]
		Column 4				
31	39	S: *Proteus vulgaris*	449	54.95	X07652	0.970
		G: *Citrobacter*	245	29.98	EU704201	0.945
		F: *Porphyromonadaceae*	60	7.34	GQ461629	0.931
69-70	76	S: *Desulfovibrio desulfuricans*	25	78.12	EU980606	0.985
	76	G: *Propionicimonas*	6	18.75	GQ066440	0.711
80	85	G: *Oscillospira*	27	96.42	FJ625862	0.967
148	152	F: *Elusimicrobiaceae*	4	100	GQ448655	0.694
172	179	G: *Sedimentibacter*	5	83.33	AB237719	0.883
208		F: *Clostridiaceae*	34	91.89	FJ672824	0.991
224	227	G: *Propionicimonas*	156	98.11	GQ066564	0.943
224	228	G: *Propionicimonas*	29	96.66	GQ066564	0.794
239	242	G: *Clostridium*	27	100	AB237713	0.757
244	247	G: *Dehalococcoides*	341	99.41	GU139321	0.985
246	248	G: *Dehalococcoides*	95	81.89	GU139324	0.746
		F: *Synergistaceae*	19	16.37	AB237713	0.757
252	253-254	G: *Sulfurospirillum*	87	96	FJ799153	0.977
258	261	G: *Oscillospira*	11	73.33	EU463672	0.477
305	308	G: *Clostridium*	41	100	AY667250	0.857
307-308	309-310	G: *Clostridium*	168	97.67	AJ576348	0.763
		G: *Desulfitobacterium*	4	2.32	U40078	0.597
322	325	S: *Proteus vulgaris*	8	100	EU710747	0.882
324	331	G: *Clostridium*	19	95	AJ576348	0.538

Table 5.6 (Part 4)

eT-RF[a] (bp)	dT-RF (bp)	Phylogenetic affiliation[c]	Counts[d]	Fraction of T-RF (%)[e]	Accession number	Normalized SW score[f]
		Column 5				
31	39	G: *Citrobacter*	351	43.65	GQ461629	0.755
		S: *Proteus vulgaris*	261	32.46	AY167936	0.968
		F: *Porphyromonadaceae*	83	10.32	GQ461629	0.755
69-70	76	S: *Desulfovibrio desulfuricans*	57	86.36	AF427913	0.970
		G: *Desulfitobacterium*	3	4.54	AF297871	0.571
		G: *Sulfurospirillum*	3	4.54	GQ377111	0.614
80	85	G: *Oscillospira*	9	90	FJ625862	0.871
172	176	G: *Thermosinus*	5	100	GU454918	0.800
190	194	G: *Clostridium*	4	80	GQ011067	0.789
208	212	F: *Clostridiaceae*	15	71.42	FJ672824	0.974
		G: *Desulfitobacterium*	6	28.57	AF357919	0.750
211	215	F: *Spirochaetaceae*	11	78.57	AJ009476	0.812
		F: *Synergistaceae*	3	21.42	CU927653	0.421;
224	228	G: *Propionicimonas*	66	95.65	GQ066679	1.000
244	248	G: *Dehalococcoides*	35	74.46	GU139321	0.985
		F: *Synergistaceae*	11	23.40	FN563349	0.890
246	249	G: *Sulfurospirillum*	15	88.23	GQ377111	0.712
252	253-254	G: *Sulfurospirillum*	28	100	FJ799153	0.985
258	262-263	F: *Ruminococcaceae*	7	58.33	EU842755	0.540
	263	F: *Porphyromonadaceae*	5	41.66	GU476602	0.743
269	273	F: *Clostridiaceae*	11	68.75	FJ671294	0.687
		F: *Ruminococcaceae*	3	18.75	AJ488075	0.667
305	307-308	G: *Clostridium*	48	94.11	FJ799151	0.815
307	309-310	G: *Clostridium*	34	100	GQ503859	0.757

[a] Experimental Terminal-Restriction Fragment (eT-RF) determined by T-RFLP analysis.

[b] Digital Terminal-Restriction Fragment determined with the PyroTRF-ID software.

[c] Predominant phylotype contributing to the T-RF obtained after comparison with the Greengenes database of 16S rRNA sequences (O: order, F: family, G: genus, S: species).

[d] Number of sequences from the pyrosequencing dataset affiliated to a same microbial population.

[e] Different bacterial populations can contribute to the same T-RF. This column gives the relative contribution of each population to the target T-RF. Only the bacterial groups representing a major contribution are reported here, which explains why the total contribution is sometimes below 100%.

[f] The SW (Smith-Waterman) score is indicative of the similarity between sequences obtained by pyrosequencing and sequences from the Greengenes database. SW score is normalized by the read length and represents an estimation of the percentage of sequence identity (Weissbrodt et al.[288]).

5.4 Discussion

5.4.1 Influence of pH on electron donor fermentation and PCE dechlorination

The average effluent pH varied from 6.2 in columns 2 and 3 to 7.8 in column 4. No differences in lactate fermentation kinetics were observed within this range of pH with complete lactate transformation occurring in all columns. These results are consistent with previous studies showing that fermentation to acetate and propionate occurred in the range of 4.5 to 8.5[289]. In contrast, organohalide respiration of chloroethenes was highly affected by pH variations. In the negative control, PCE dechlorination was, as expected, completely inhibited at pH 6.2. Moreover, in the four other columns, significant ethene production (i.e., superior to 20%) was observed only for pH above 6.7. These results are in agreement with a previous experiment where SDC-9™ was cultivated at different pH under saturated PCE concentrations (Figure A5.2, Appendix) and where no PCE dechlorination was observed at pH 6 and below. Contradictory results were reported by Vainberg et al.[130] who observed inhibition of PCE degradation by SDC9™ at pH 5 and close to maximum PCE dechlorination rates at pH 6. However, these assays were conducted at low PCE concentrations (0.06 mmol l^{-1}), which might explain the discrepancies with the results of the present study.

5.4.2 Performance of the system for PCE removal

Complete dechlorination of PCE to 100% ethene was only observed in the positive control toward the very end of the experiment (day 168). These results suggest that, even under optimal pH conditions, the experimental conditions (residence time, electron donor concentration) might not have been optimal to observe full dechlorination from PCE to ethene. Another explanation is that the experiment should have been conducted longer to reach steady state in column 1.

In the columns with minerals, which were operated about 20 d longer, steady state PCE dechlorination (i.e., constant concentration of dechlorination sub-products over time) were observed during the last weeks from day 165 on. In order to compare the dechlorination efficiency between each column, a performance metric was defined as the average concentration of chloride produced during the steady state phase. This metric was plotted versus the average effluent pH within the same period for each column (Figure 5.15). The best dechlorination performances were observed for column 1, followed by columns 4 and 5. All columns containing minerals presented better performance than the control without buffer (column 2), but not as good as the positive control (column 1). A clear correlation appeared between the pH and the extent of dechlorination, with an optimal PCE degradation at pH 7.2 (column 1).

Surprisingly, column 3 presented better performance than column 2 although its pH was lower. This result can be attributed to the fact that neutral conditions were maintained in column 3 during the first 84 d. In contrast to column 2, acidification occurred gradually in column 3 (due to progressive loss of

the diopside buffering capacity) allowing acclimatization of OHRB to slightly acidic conditions. These results are corroborated with a study of Li[133] who showed better acclimatization of the organohalide-respiring consortium KB-1™ to acidic pH by stepwise pH decrease rather than sudden acidification.

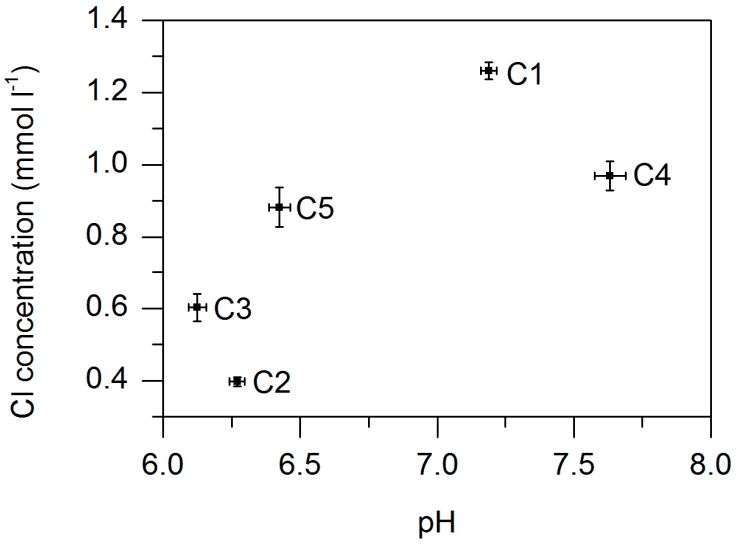

Figure 5.15. Extent of PCE dechlorination expressed as average Cl^- concentration produced versus average pH during the steady-state phase (day 165 onward). C1, C2, C3, C4, C5: columns 1, 2, 3, 4, and 5.

5.4.3 Mineral dissolution

The three minerals tested in this study presented very different buffering capacities: forsterite was able to maintain the pH between 7.6 and 7.85 during the whole experiment, fayalite maintained the pH between 6.45 and 6.7, and diopside gradually lost its buffering capacity during the first 84 days. Investigation of mineral dissolution patterns and of changes in mineral composition during the experiment allowed a better understanding of these different behaviors.

In each column, the effluent was under-saturated with respect to the silicate mineral studied. Saturation indexes, calculated with the software PHREEQC-2[199] and the MINTEQ v4.0[198] database, were equal to -7.5, -5.8 and -4.6 for diopside, forsterite and fayalite, respectively.

5.4.3.1 Forsterite dissolution

Stoichiometric releases of Mg and Si during forsterite dissolution observed in this experiment were in agreement with most laboratory studies carried out at 25°C in the same pH range[179,212,290].

5.4.3.2 Fayalite dissolution

Incongruent fayalite dissolution with preferential Si release compared to Fe was due to the formation of secondary phases. EDX analyses and SEM pictures at the end of the experiment revealed that iron

sulfide (FeS) precipitates were formed at the surface of fayalite and quartz particles following the reaction:

$$Fe^{2+} + H_2S \rightarrow FeS + 2H^+ \qquad \log K_{eq} = -2.95 \text{ (from MINTEQ v4.0 database}^{198}\text{)} \qquad (5.3)$$

Iron sulfide phases were not detected by XRD indicating the amorphous nature of these precipitates. According to the reaction above, iron sulfide solubility decreases with increasing pH explaining why the extent of precipitation was higher when the pH was above 6.5. This result is consistent with several studies that reported rapid FeS precipitation under conditions similar to those present in the columns of this study (i.e., similar T, pH and redox potential)[252-254,291]. Furthermore, indications of FeS precipitation were already observed in batch dissolution experiments with fayalite (see Chapter 3). Precipitation of the reducing agent (HS^-) could explain why the redox potential in column 5 was slightly higher than in the other columns. The constant Si dissolution rate suggested that FeS precipitation did not modify the reactivity of the fayalite surface on the time scale of the experiment.

Effluent phosphate concentrations indicated that iron phosphate precipitation occurred in this column as well. Although solid phosphate phases were not detected by SEM/EDX analyses in the first section, precipitates might have formed in the part of the columns towards the outflow. Under the pH conditions observed in this study, precipitation of phosphate by Fe(III) present in the iron oxide particles (Fe_2O_3) or Fe(II) are likely as reported by previous studies[292-294]. Because the phosphate requirement for bacteria was relatively low in the columns, precipitation of a fraction of phosphate might not have been a problem. However, it is important to avoid removal of all phosphate present.

5.4.3.3 Diopside dissolution

During the first 88 d, the diopside dissolution rate decreased linearly and preferential Ca release was observed. Such a decrease of mineral dissolution rates over time is generally attributed to secondary precipitation on mineral surfaces or the presence of a diffusion-inhibiting leached layer[201,295]. In this study, SEM and EDX analyses excluded the formation of secondary precipitation. In addition, the Ca-depletion in the mineral surface layer after dissolution suggested the formation of a leached layer.

In other diopside dissolution studies carried out in mixed flow reactors under same pH and temperature conditions, preferential Ca release was also reported. However, in these studies, dissolution became congruent after a few days to two weeks[171,212]. Chen and Brantley[267] conducted a long-term diopside dissolution experiment and showed that steady state was achieved only after 112 days at pH 3.55 and 25°C. They observed a preferential release of Ca and Mg in the early stage but no preferential release of Ca over Mg. To our knowledge, the particular diopside dissolution pattern observed in the present study has not been reported previously. The reason for these discrepancies remains unclear but can be attributed to the type of experiment (column with immobilized mineral versus mixed flow reactor), the anoxic conditions, and/or the presence of bacterial activity. According to the leached layer model, diopside dissolution could have occurred in three steps: i) cations exchange

between H^+ and Ca^{2+} and formation of a Si-rich Ca-depleted leached layer, ii) silica polymerization and formation of a less reactive vitreous silica, and iii) dissolution of the leached layer at a reduced rate. This mechanism was proposed by Casey et al.[296] and Weissbart and Rimstidt[163] to explain the dissolution of chain silicates.

5.4.3.4 Mass of mineral dissolved during the experiment

The total mass of silicate mineral dissolved and leaving the system during the experiment was calculated by integration of dissolved concentrations measured in the effluent. The amount of mineral consumed, as a percentage of the initial mass, was equal to 1.28%, 0.9% and 0.26% for forsterite, diopside, and fayalite, respectively. The small amount of mineral consumed demonstrates the potential of silicates to reduce the amount of buffering material required compared to traditional soluble buffers.

5.4.3.5 Influence of pH on mineral dissolution

As expected from modeling and previous batch experiments (see Chapters 2 and 4), mineral dissolution was enhanced by the acidity produced by microbial activity, with higher dissolution rates when acidity was increased. These results confirmed the potential of silicate to respond quickly to variations of acidification in porous medium. This characteristic of the silicate minerals allow them to dissolve only when buffering capacity is needed and avoids waste of the buffering material.

5.4.3.6 Comparison of the mineral dissolution rates between batch and column experiments

A preceding study reported discrepancies between mineral dissolution rates determined in head-over-end mixed batches and in porous medium column experiments[228]. The mineral dissolution rate determined in flow-through columns filled with porous media is likely to be more relevant to field conditions. However, this type of study is more complex and time consuming and ideally one should be able to extrapolate dissolution rates obtained from batch experiments. To do so, mineral dissolution rates in the columns (in phase 1) were compared with dissolution rates calculated from kinetic parameters determined in Chapter 3 via abiotic batch experiments (Table 5.7). For the sake of consistency and to avoid misinterpretation due to secondary precipitation, only the Si-based dissolution rates were taken into account. The difference between dissolution rates in column and batch did not exceed 0.3 orders of magnitude for fayalite and forsterite. Higher differences were observed for diopside, especially toward the end of the experiment were its dissolution rate in the column was almost one order of magnitude lower than in the batch. In conclusion, except for diopside, batch experiments as conducted in Chapter 3 provides a good approximation of mineral dissolution rate in porous media.

Table 5.7. Range of dissolution rate at the column outlet during phase 1 compare to dissolution rate at pH 6 calculated with the kinetic parameters estimated from abiotic batch experiments.

	Log rate (mol m^{-2} s^{-1})	
	Columns	Batch
Diopside	[-12.08 ; -11.6]	-11.18
Forsterite	[-10.78 ; -10.70]	-10.58
Fayalite	[-11.29 ; -11.08]	-11.6

5.4.4 Microbial communities

5.4.4.1 Microbial populations involved in lactate fermentation and hydrogen production

Studies on lactate fermentation under anaerobic conditions[55,297,298] showed that lactate can be fermented following two metabolic pathways as presented in reactions A and B in Table 5.8. Fermentation of lactate via the methylmalonyl-coA or acrylyl-coA pathway (reaction A) produces acetate and propionate at a 1:2 ratio and is thermodynamically favorable with a negative ΔG_0'[298]. In contrast, fermentation of lactate to hydrogen and acetate (reaction B) is energetically less favorable and can only proceed if H_2 partial pressure is kept low. This reaction occurred via synthrophic interactions between fermentative and hydrogenotrophic populations. Under certain conditions, propionate formed during reaction A can be further transformed to acetate and H_2 by synthrophic propionate-oxidizing bacteria (reaction C). Similarly to mechanism B, propionate oxidation requires H_2 scavenging populations to make the reaction thermodynamically possible[299,300].

Table 5.8. Reaction potentially involved in lactate and propionate transformation and their standard Gibbs free energy values.

	Reaction	ΔG_0' (kJ/mol)
A	$lactate^- \rightarrow 1/3\ acetate^- + 2/3\ propionate + 1/3\ HCO_3^- + 1/3\ H^+$	-56.7[a]
B	$lactate^- + 2H_2O \rightarrow acetate^- + HCO_3^- + H^+ + 2\ H_2$	-4.2[b]
C	$propionate^- + 3H_2O \rightarrow acetate^- + HCO_3^- + H^+ + 3\ H_2$	+76[c]

[a] Seeliger et al. (2012)[298]

[b] Elferink et al. (1994)[301]

[c] Muller et al. (2010)[302]

In the microbial communities present at the end of the experiment, no known propionate-oxidizing populations were detected suggesting that the H_2 required for organohalide respiration was produced by reaction B rather than reaction C. The observed acetate-over-propionate ratio in the effluent suggested that some of the lactate was fermented following reaction A and the rest following reaction B. *Desulfovibrio* spp. were most probably involved in synthrophic hydrogen production (reaction B) as already described by Bryant et al.[297] while *Propionicimonas* spp. were likely responsible for fermentation of lactate to propionate and acetate (reaction A) as observed in other studies[289,303].

Members of the genera *Clostridium* and *Citrobacter* were earlier described as lactate fermenters[298,304-306] and can also be involved in both reactions A and B. *Proteus vulgaris*, which was predominant in all columns, is also able to grow on lactate[307,308] but the exact metabolic pathway is not well characterized.

5.4.4.2 Hydrogen production and terminal electron acceptor processes

Based on the acetate-over-propionate ratio and the stoichiometry of reactions A and B, an estimation of the concentration of hydrogen produced, $C_{H2,}$ was calculated as follows:

$$C_{H_2} = 2\left[C_{\text{acetate}} - \frac{C_{\text{propionate}}}{2} \right]. \quad (5.4)$$

The theoretical hydrogen production was compared with the theoretical hydrogen demand required for OHR, calculated on the basis of chloroethene concentrations. The results, presented in Figure 5.16, showed that the estimated hydrogen production was above the hydrogen required by OHR, indicating that a fraction of hydrogen was channeled toward other terminal electron acceptor processes (TEAPs). Hydrogen production presented relatively high fluctuations during phase 1 and became more stable in phase 2 and 3. In these last phases, the fraction of hydrogen channeled towards TEAPs was higher in columns containing forsterite and fayalite than in the other columns. Three potential TEAPs were identified. In column 1, during the first 123 d, methane was detected by gas chromatography (not quantified), which indicated the occurrence of methanogenesis. In all columns, consumption of hydrogen by homoacetogenesis was possible; potential homoacetogens included a population affiliated to the family *Spirochataceae* and to the genus *Clostridum*[309,310]. Finally, iron reduction could have occurred in columns 4 and 5 where iron oxide (Fe_2O_3) particles were present (as detected by EDX, see section 5.3.8.1). Indeed, several species of *Desulfovibrio* spp. (present in columns 4 and 5) were reported to reduce insoluble Fe(III) oxides under anaerobic conditions[311].

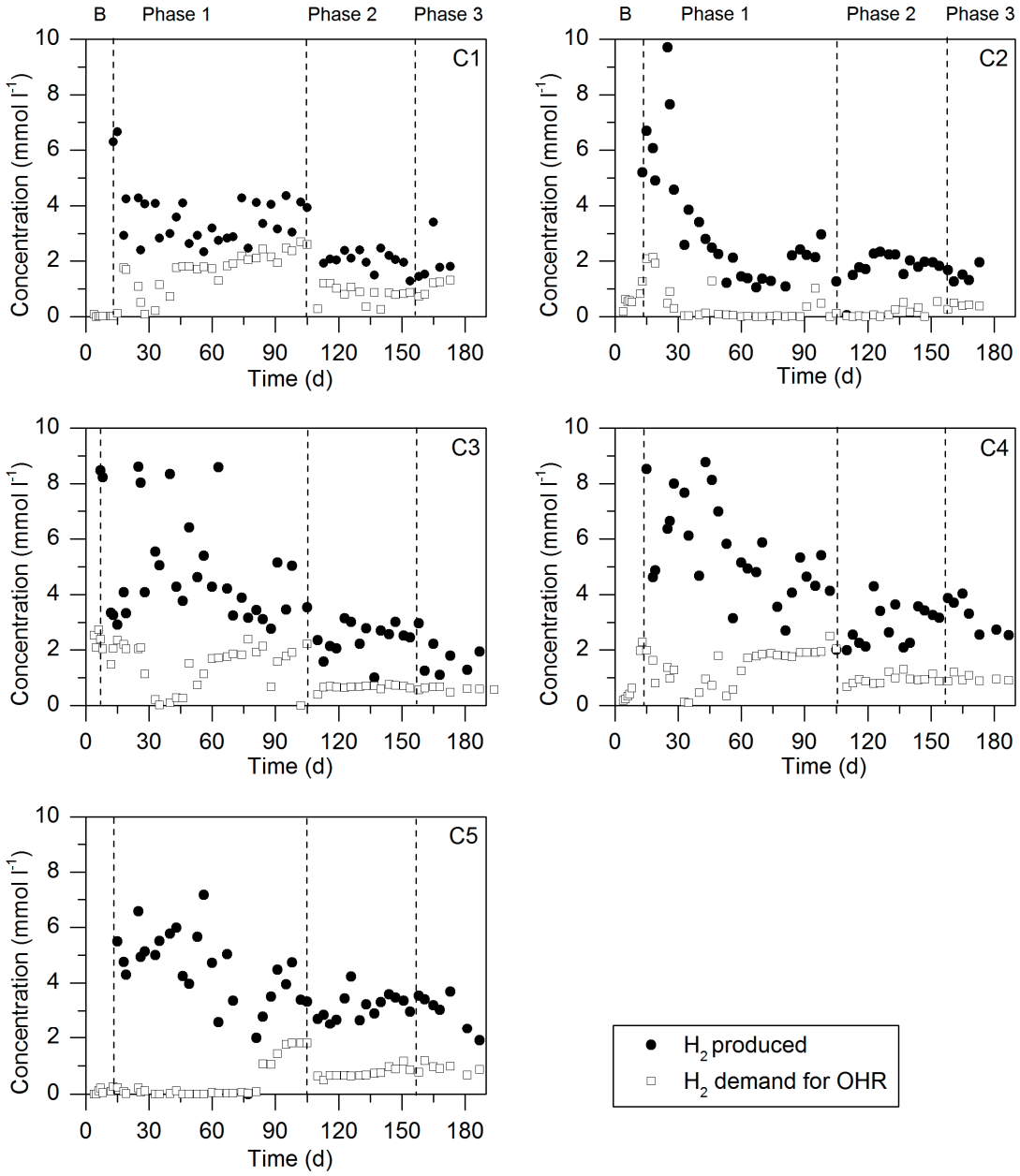

Figure 5.16. Theoretical hydrogen production compared with hydrogen demand by OHRB calculated on the basis of chloroethenes concentration. B: batch phase, C1, C2, C3, C4, C5: columns 1, 2, 3, 4, and 5.

5.4.4.3 Microbial community composition along the flow path

In columns with minerals, a higher bacterial diversity and a higher variation of microbial community composition along the column flow path were observed compared to control columns. These differences could be attributed to the variations of physicochemical conditions along the column. Indeed, in control columns, especially in the positive control, the pore-water composition was constant along the column flow path while in columns amended with minerals, pH and cation concentrations

increased towards the outlet of the column due to mineral dissolution. Different conditions might have selected different microbial populations, which also explained the higher diversity observed.

5.4.4.4 Presence of OHRB in the columns and system performance

A relationship between the extent of PCE dechlorination and the presence of OHRB were observed. Only PCE dechlorination patterns at the very end of the experiment, just prior to column dissection, were considered. In general, the presence of *Dehalococcoides* was related to VC and ethene production. In column 1, where PCE was fully converted to ethene, *Dehalococcoides* spp. were evenly distributed and represented a significant part of the microbial community (13 to 25%) while in column 2, where PCE was only partially converted to *cis*-DCE, the relative abundance of *Dehalococcoides* was lower than 1%. *Dehalococcoides* spp. were also present in high relative abundance in column 4, which had the best PCE degradation performance after column 1. However, no quantitative correlation between VC/ethene production and *Dehalococcoides* spp. relative abundance could be drawn from the results of columns 3 and 5. This result showed that bacterial presence is not always a good indicator of activity. Other parameters, especially pH, seemed to have a higher influence on VC and ethene production kinetic rates than the number of bacterial cells. *Sulfuropirillum* spp., a known OHRB genera able to dechlorinate PCE to *cis*-DCE[126] was detected in the five columns. Its presence was related with the formation of *cis*-DCE in the column effluent at the end of the experiment. Indeed, in column 1, where no *cis*-DCE was observed at the end of the experiment, the *Sulfurospirillum* spp. relative abundance was below 1.8%. In contrast, in the four other columns where *cis*-DCE was detected, higher *Sulfurospirillum* relative abundances were reported. Hence, in columns with a pH around neutral, *Dehalococcoides* spp. seemed to be solely responsible for PCE dechlorination whereas under less favorable pH conditions *Sulfurospirillum* spp. took over the dechlorination of PCE to *cis*-DCE due to its better resistance to variable pH (see Chapter 4).

5.4.4.5 Influence of silicate mineral dissolution on OHRB

Previous experiments realized in batch with silicate minerals and OHRB had raised concerns about the potential toxicity of silicate minerals on *cis*-DCE dechlorination by *Dehalococcoides* (Chapter 4). The result of the present study showed that, in flow-through experiments, mineral dissolution does not inhibit the development of *Dehalococcoides* and transformation of *cis*-DCE to ethene. Lower *Dehalococcoides* abundance and lower PCE dechlorination performances in columns 3 and 5 compared to the positive control were likely the result of non-optimal pH conditions (especially for column 3). The reason for the long lag phase prior to activity in column 5 is unclear but could be the result of non-optimal pH conditions, increase of redox potential due to sulfide precipitation, and competition with iron-reducing bacteria.

5.5 Conclusion

In this study, the long-term buffering capacity of diopside, fayalite and forsterite were evaluated in the presence of active OHRB. Forsterite appeared as the best buffer candidate. Indeed, forsterite dissolution was constant over time during the whole duration of the experiment, no secondary precipitates were formed, and dissolution increased with increasing level of acidity. In addition, forsterite promoted the development of *Dehalococcoides* which were responsible for *cis*-DCE dechlorination. In contrast, despite its promising results in batch experiments (see Chapter 3 and 4), diopside was not a good buffer candidate over the long-term because the formation of a low-reactive leached layer decreased its dissolution rate over time. The buffering capacity of fayalite was limited to pH 6.5 due to the occurrence of iron sulfide precipitation. This study also showed that, at high PCE concentration (0.3 to 0.9 mmol l^{-1}), the *Dehalococcoides* population present in the SDC-9™ consortium is very sensitive to acidic pH conditions with complete inhibition of PCE degradation at pH below 6. Comparison with the study of Vainberg et al.[130] suggests that OHRB are more sensitive to acidic conditions when PCE concentrations are close to saturation.

5.6 Appendix

Table A5.1. Basal medium for growth of SDC-9 consortium in batch and column (LB: low buffered, B: buffered).

Compounds	Final concentration (mmol l^{-1})		
	Medium for batch (mmol l^{-1})	Medium LB for column (mmol l^{-1})	Medium B for column (mmol l^{-1})
Solution A			
KH_2PO_4	2.0	2×10^{-1}	4×10^{-1}
K_2HPO_4	2.0	2×10^{-1}	4×10^{-1}
Solution B			
NH_4Cl	10.0	2.0	2.0
$CaCl_2.2H_2O$	0.5×10^{-1}	1.0×10^{-1}	1.0×10^{-1}
$MgCl_2.6H_2O$	4.9×10^{-1}	1.0×10^{-1}	1.0×10^{-1}
$FeCl_2.4H_2O$	5.1×10^{-3}	1.0×10^{-3}	1.0×10^{-3}
Solution C			
$MnCl_2.4H_2O$	2.5×10^{-2}	5×10^{-3}	5×10^{-3}
H_3BO_3	8.2×10^{-4}	1.6×10^{-4}	1.6×10^{-4}
$ZnCl_2$	3.7×10^{-4}	7.4×10^{-5}	7.4×10^{-5}
$CuCl_2$	2.25×10^{-4}	4.5×10^{-5}	4.5×10^{-5}
$Na_2MoO_4.2H_2O$	4.17×10^{-5}	8×10^{-6}	8×10^{-6}
$CoCl_2.6H_2O$	2.1×10^{-3}	4.25×10^{-4}	4.25×10^{-4}
$NiCl2.6H_2O$	2.1×10^{-3}	4.3×10^{-5}	4.3×10^{-5}
Na_2SeO_3	2.9×10^{-4}	5.9×10^{-5}	5.9×10^{-5}
$Na_2S.9\ H_2O$	2.02	2.02	2.02
$NaHCO_3$	9.6×10^{-1}	1.9×10^{-1}	1.9×10^{-1}
Vitamin B12	1.7×10^{-5}	3.4×10^{-6}	3.4×10^{-6}
Yeast extract (1%)	5×10^{-1} g l^{-1}	1×10^{-1} g l^{-1}	1×10^{-1} g l^{-1}
MOPS	97	-	97
Resazurin	1.5×10^{-3} g l^{-}	1.5×10^{-3} g l^{-1}	1.5×10^{-3} g l^{-1}

Table A5.2. Duration of each phase of the column experiment. The columns 1, 2 ,3 and 4 were mounted on the same day and column 5 was mounted 4 days later. Day 0 corresponds to the day when the 4 first columns were packed (d=day).

	Column 1	Column 2	Column 3	Column 4	Column 5
Packing the column	d0	d0	d0	d0	d4
Circulation of a solution of saturated PCE (t = 24h)	d1	d1	d1	d1	d5
Batch phase	d1- d13	d1- d13	d1- d6	d1- d13	d6 - d13
Phase 1	d13 - d105	d13 - d105	d6 - d105	d13 - d105	d13 - d105
[Lactate] . 16 mmol l^{-1}					
[PCE] : 0.9 mmol l^{-1}					
Phase 2	d105 - d157	d105 - d157	d105 - d157	d105 - d157	d105 - d157
[Lactate] . 5.33 mmol l^{-1}					
[PCE] : 0.33 mmol l^{-1}					
Phase 3	d157-d173	d157- d173	d157- d194	d157-d194	d157-d194
[Lactate] . 5.33 mmol l^{-1}					
[PCE] : 0.33 mmol l^{-1}					
Column slicing	d180	d181	d194	d195	d196

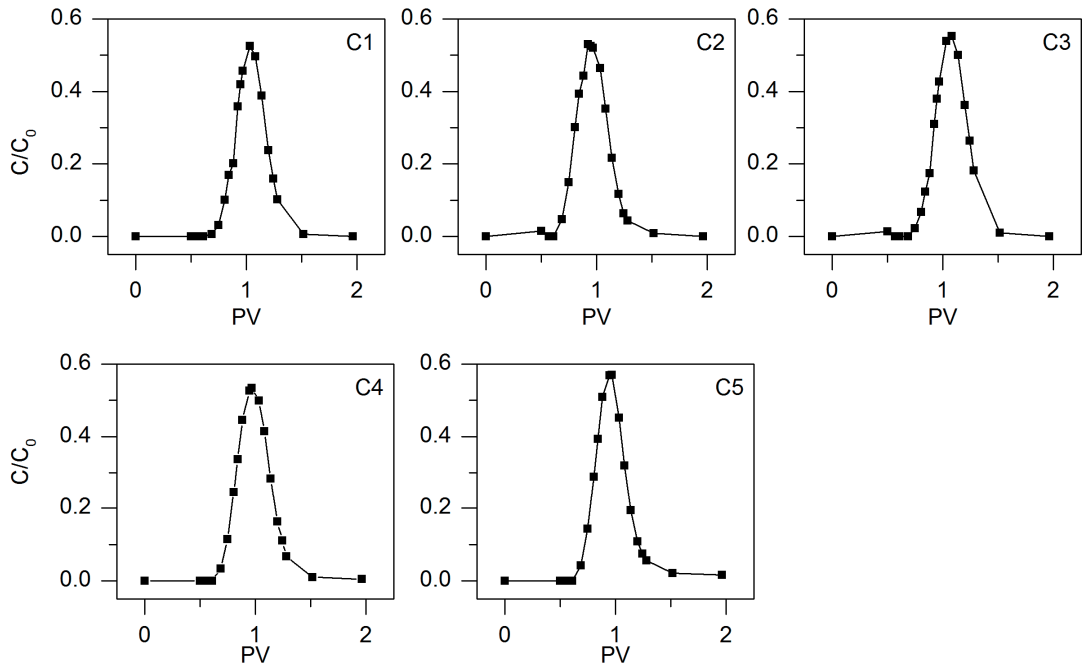

Figure A5.1: Tracer test breakthrough curves for the five columns at the end of experiment (PV: pore volume, calculated with the initial pore water volume and flow rate).

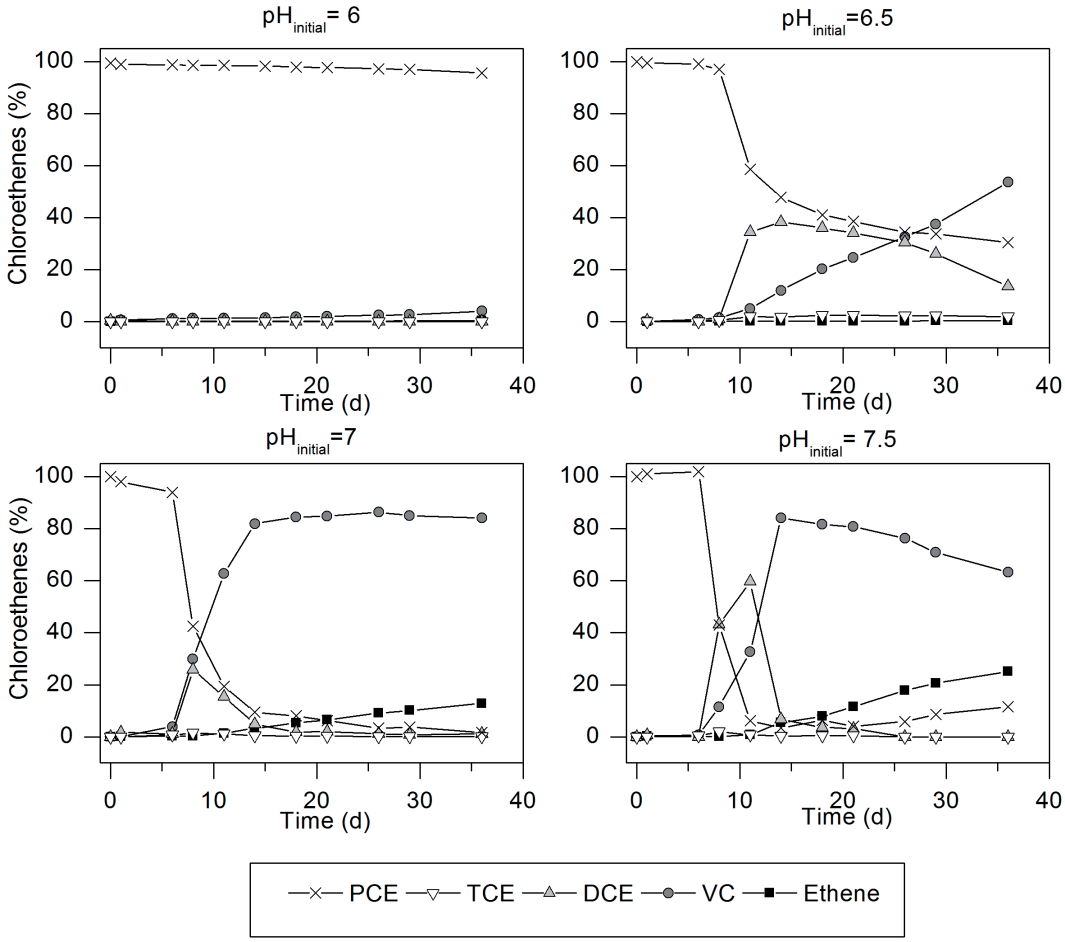

Figure A5.2. Influence of pH on PCE dechlorination by the consortium SDC-9™. This experiment was conducted as described in Chapter 4 section 4.2.3 with the following modifications: the basal medium was the one described in Table A5.1 (batch) and the cultures were amended with 0.9 mmol l^{-1} of PCE dissolved in methanol and 12 mmol l^{-1} of lactate. A pH drift up to 0.5 units was observed at initial pH of 6.5, 7 and 7.5 during the course of the experiment.

Chapter 6

Concluding remarks and outlook

6 Concluding remarks and outlook

6.1 Summary and conclusion

The main objective of this thesis was to develop a novel approach for buffering groundwater pH that relies on the use of silicate minerals as a long-term source of alkalinity. This new method, which provides an alternative to carbonate-based soluble buffer, was developed and tested in the context of *in situ* bioremediation of chloroethenes source zones. The acid- neutralizing potential of silicate mineral powder was demonstrated by a combination of geochemical modeling, batch and flow-through column experiments carried out with various silicate minerals and organohalide-respiring bacterial consortia. The knowledge gained from these different approaches has led to the development of a global methodology to select the most suitable minerals for pH control according to site-specific conditions.

6.1.1 Development of a screening methodology and design tool based on geochemical modeling

To date, approximately 600 different silicate minerals have been identified[84]. Their composition, solubility, and dissolution kinetics are highly variable and only a restricted number may have the potential to act as a buffering agent. In Chapter 2, a screening methodology based on thermodynamic and kinetic considerations was developed for the selection of the most suitable buffering candidates. A compilation of mineral dissolution kinetic parameters from experimental data taken from the literature was performed. Following the approach of Robinson et al.[148], a batch geochemical model including the main microbial processes driving groundwater acidification and silicate mineral dissolution was developed. This model was used to rank the silicate minerals according to their buffering potential and to identify the dominant model parameters. Global sensitivity analyses showed that kinetic rate constants and solubility were the most important parameters. Therefore, accurate characterization of these variables appeared to be crucial for reliable prediction of the acid-neutralizing capacity. The screening methodology was applied to a restricted number of silicate minerals for which kinetic data were available in the literature. In the near future, the quantity of data on silicate dissolution is likely to increase due to the intensive research effort made in the context of geological sequestration of carbon dioxide where silicates play a major role[160]. As more data become available, new potential buffering minerals could be identified using the methodology developed in this study.

6.1.2 Geochemical model validation and optimization

The geochemical model developed in Chapter 2 was improved and validated by abiotic batch experiments conducted with five silicate minerals (nepheline, fayalite, forsterite, diopside and andradite) in Chapter 3. The importance of secondary precipitation, a process not included in the original formulation of the model, was revealed. The most common secondary phases likely to

precipitate such as FeS, $AlPO_4$, ($Ca_5(PO_4)_3OH$) and $Fe_3(PO_4)_2$:$8H_2O$ as well as the degree of saturation at which they formed were reported. Secondary precipitation potentially led to reduction of the porosity, passivation of primary mineral surfaces (i.e., decrease of reactivity), and precipitation of essential nutrients for bacteria (e.g., phosphate). Consequently, formation of secondary precipitation should be avoided or at least limited for an efficient pH control strategy. Abiotic batch experiments also highlighted the influence of pore-water composition on the final mineral solubility and equilibrium pH.

6.1.3 Interaction between OHRB and mineral dissolution

The influence of mineral dissolution on OHRB and fermentative bacteria in batch system was evaluated in Chapter 4. As expected, the five silicate minerals tested were dissolving in response to acidity produced by bacteria and were able to maintain the pH in the tolerance range for the three consortia tested (except for the mineral nepheline). Despite favorable pH conditions, dechlorination of *cis*-DCE by *Dehalococcoides* was completely inhibited in most of the experiments. In contrast, conversion of PCE to *cis*-DCE was not affected by mineral dissolution except in the presence of the Fe(III)-bearing mineral (andradite). The reasons for the inhibition of *Dehalococcoides* activity in batch experiments were not completely elucidated, but two possible explanations were proposed: (i) increase of redox potential due to release of oxidizing compound such as Fe(III) and (ii) accumulation of toxic heavy metals such as chromium, nickel, arsenic, lead, titanium, present in small quantities in the mineral matrix and released upon mineral dissolution. These results showed that compatibility with the bacterial community involved in *in situ* bioremediation has to be carefully evaluated prior to their use for pH control at a specific site. Moreover, additional research should be carried out on the influence of heavy metals on *Dehalococcoides* activity, a topic that has not yet been investigated.

6.1.4 Interaction between OHRB and mineral dissolution in flow-though system and evaluation of long-term buffering potential of silicate minerals

The buffering potential of forsterite, fayalite, and diopside was tested for six and a half months in flow-through column experiments simulating chloroethene source zone conditions. In the flow-through system, silicate mineral dissolution did not inhibit *cis*-DCE transformation contrary to the observations in batch experiments. Production of VC and ethene as well as presence of *Dehalococcoides* were observed in all columns containing minerals suggesting that under field conditions with a sufficient advection rate, inhibition phenomena are less likely to be an issue. However, in terms of buffering potential, the three minerals gave very different results. Diopside, despite its promising results in short-term batch experiments, was not suitable for pH control on the long term. Its dissolution rate and thus buffering potential decreased over time due to the formation of a low-reactive leached layer. The buffering capacity of fayalite, although constant over time, was limited to pH 6.5 by precipitation of iron sulfide. Although, on the time scale of the experiment, no

significant decrease of the fayalite reactivity was observed, secondary precipitation should generally be avoided as explained above. Fayalite could still be considered as a potential buffering agent, provided that sulfide (and sulfate) concentrations are relatively low. Under the experimental conditions of this study, forsterite was the best pH control candidate. In the column amended with forsterite, mineral dissolution was constant over time, pH was maintained between 7.6 and 7.8 throughout the experiment, no secondary precipitates were formed, and the dissolution rate increased in response to acidity production. In addition, significant development of *Dehalococcoides* and good dechlorination performance with production of VC and ethene were observed. The only drawback was that, because of the high solubility of forsterite, the pH might have been slightly above the optimal pH value for dechlorination. Fayalite (Fe_2SiO_4) and forsterite (Mg_2SiO_4) are the end-members of the olivine solid solution series[312]. Olivine minerals have an intermediate composition: $(Mg_xFe_{(1-x)})_2SiO4$ where the relative proportion of Fe and Mg can vary. The result of the present study showed that, under the given experimental conditions, the final pH obtained was slightly too low for fayalite (6.5) and too high for forsterite (7.6). A solution to adjust the pH to the required value (e.g., pH 7) would be to use olivine minerals of intermediate composition.

6.2 Application of pH control with silicate minerals to other groundwater remediation techniques

In this study, utilization of silicate minerals for pH control was evaluated in the context of *in situ* bioremediation of chloroethene source zones. Once validated at field-scale, this method could be extended to other groundwater remediation techniques. For instance, silicate minerals could be used for the remediation of acid mine drainage and coal pile runoff, usually characterized by a pH lower than 3[158,313]. Bioremediation of hydrocarbons[314] and chlorinated organic compounds such as pentachlorophenol[315] and carbon tetrachloride[316] can also benefit from this approach as they are all acid generating processes. Each of these pollutants requires slightly different pH for their degradation. For instance, while chlorinated ethenes are degraded faster at pH between 6.5 and 7.5, *in situ* bioremediation of carbon tetrachloride is optimal at pH 8[316]. Therefore, silicate minerals present a suitable solution since each mineral has a slightly different equilibrium pH. Consequently, mineral selection should be done according to the target optimal pH.

6.3 A methodology for the selection of silicate minerals according to site conditions

A global methodology for design of pH control strategy with silicate minerals according to field conditions was developed based on the knowledge gained from modeling, batch and column experiments. This methodology can be used for the bioremediation of any pollutant requiring close to

neutral pH conditions. The methodology is divided in three major steps, described in detail below and summarized in Figure 6.1.

STEP 1: Site characterization

Prior to design an efficient buffering strategy, a number of site-specific parameters need to be carefully determined.

- **Influence of pH on remediating microbial communities**

The pH tolerance range and optimal pH of the remediating bacteria should be assessed. pH tolerance should be evaluated via microcosm experiments conducted under the same conditions as at the site (i.e. same temperature and contaminant concentration). This latter point is important as the results suggest that, for the case of PCE, tolerance toward acidic pH conditions might be reduced at high contaminant concentrations.

- **Acidity production rate**

An estimation of the rate of acidity production (via production of organic acids and degradation of chlorinated molecules) should be determined to further evaluate the buffering mineral requirement. The concentration of contaminants and electron donors as well as kinetic rates of the bacteria can be inferred from field measurements and from microcosm experiments.

- **Groundwater composition and temperature**

Characterization of groundwater composition is required to define the actual solubility of a given mineral and its equilibrium pH, and to predict the potential formation of secondary phases accurately. Temperature is important as it influences solubility and kinetic rates of silicate mineral dissolution.

- **Aquifer hydrodynamic**

Groundwater flow velocity should also be characterized. As demonstrated in a previous study by Brovelli et al.[152], advection rate controlled acidity build-up and therefore buffer requirement.

STEP 2: Mineral selection

Once the site has been characterized, the following criteria have to be applied to select one or several buffering candidates among available silicate minerals.

- **Criterion 1: Mineral availability and costs**

The minerals should be available locally at affordable costs. Local deposits and availability can be identified from mineralogical databases (e.g., www.mindat.org). Minerals tested in the present study are easily found on the market as they are used in industrial processes as ceramic components, abrasive agents or refractory material. They can be directly purchased from suppliers or recycled from

by-products of industrial processes. Their prices are relatively low, around $300 per tonne for forsterite and $18 per tonne for fayalite.

- **Criterion 2: Mineral composition**

Results of batch and column experiments showed that the composition of the mineral is of critical importance. Silicates are constituted of $(SiO4)^4$ tetrahedra interconnected with cations, the most common ones being Al^{3+}, Ca^{2+}, Mg^{2+}, Na^+, Fe^{2+}, Fe^{3+}, and K^+. From the results of this study, three categories of silicate minerals based on their composition were defined:

- Minerals containing Ca^{2+}, Mg^{2+}, Na^+, or K^+ are suitable for pH control. These cations do not change the redox potential, they are not toxic to bacteria (in the range of concentrations expected) and potential secondary precipitations are limited at neutral pH.
- Fe^{2+}-bearing minerals (such as fayalite) could be used as buffering agents provided that the concentration of sulfide (or sulfate) in the groundwater is low to avoid iron sulfide precipitation.
- Minerals containing Fe^{3+} and Al^{3+} are not suitable for pH control. Indeed, release of Fe^{3+} could result in increase of redox potential[273], stimulation of iron-reducing bacteria that compete with *cis*-DCE dechlorinators[145] and precipitation of phosphate[292,293]. Release of Al^{3+} is an issue due to its precipitation with phosphate at neutral pH[293].

- **Criterion 3: Mineral dissolution rates**

Dissolution rates vary over six orders of magnitude between fast- and slow-dissolving silicate minerals[160]. Only fast-dissolving silicate minerals have a potential for pH control. A general rule established from the result of this study is that mineral dissolution rate at pH 6 and 20°C should be above 10^{-12} mol m^{-2} s^{-1}. Above this value, mineral dissolution will be sufficient to counterbalance the acidity production rate typically observed at contaminated sites undergoing bioremediation (e.g., in the case of chloroethene source zones). For precise design of the pH control strategy, accurate characterization of the mineral dissolution rate in the mildly acidic range should be conducted. In theory, the rate calculation can be done using the compilation of kinetic parameters provided in Table 2.2 (Chapter 2). However, given the discrepancies for kinetic parameters between studies on a given mineral (around 2-3 orders of magnitude), it is recommended to determine the dissolution rate of the selected mineral experimentally. This test should be performed in flow-through mixed reactor operated at constant pH of 5 or 6 under the same conditions (groundwater composition, temperature) as in the contaminated site.

- **Criterion 4: Mineral solubility**

Solubility of the minerals (in mol l^{-1}) and their equilibrium pH under site conditions should be determined. Both variables can easily be computed with geochemical software based on the

equilibrium constants of mineral dissolution, temperature, and the exact groundwater composition. Minerals with low solubility at slightly acidic pH (pH 5) are unlikely to provide sufficient buffering capacity and should be excluded from the selection. Similarly, minerals with high solubility at slightly basic pH (pH 8) can result in pH overshooting. In order to reduce this risk, the equilibrium pH of the selected mineral should be below the inhibiting pH value in the basic range for remediating bacteria (e.g., < 8.5-9 for chloroethene bioremediation). As for kinetic dissolution, it is recommended that, once the mineral has been selected, confirmation of the modeling prediction be carried out using a simple dissolution test such as that described in Chapter 3.

- **Criterion 5: Long-term evolution of dissolution rates**

One of the advantages of using silicate minerals for pH control is their long-term buffering effect, which avoids frequent re-injection and reduces operational costs. *In situ* bioremediation is a relatively slow process usually conducted over a period of several years and thus buffering potential of silicates should last over a similar time frame. However, results of the column studies showed that long-term buffering efficiency varies between the minerals tested. Two processes are likely to decrease mineral reactivity over time, armoring of the mineral surfaces by secondary precipitation and development of a thick less reactive leached layer. While secondary precipitation can be avoided by careful selection of the mineral according to the site geochemistry, prediction of leached layer formation limiting dissolution is more difficult and is still a subject of scientific debate[163,265,296]. In the present study, development of a cation-depleted less reactive leached layer was only observed for diopside and not for forsterite and fayalite. These results are corroborated by the study of Casey et al.[296] suggesting that chain silicates (like diopside) are likely to develop thick, low-reactive leached layers. In contrast, high-resolution transmission electron microscopy studies of olivines (fayalite and forsterite) showed very thin leached layers formation unlikely to limit dissolution[317] and to affect buffering potential. According to these results, olivine minerals are suitable candidates for long-term pH control while diopside should not be used. For other minerals not tested in this study, the potential to present constant mineral dissolution rates should be evaluated based on previous laboratory studies (if available) or by column experiments of at least 100 d.

STEP 3: Designing pH control strategy

Once site characterization and selection of potential buffering minerals are done, a more detailed geochemical simulation should be conducted to estimate the quantity of mineral required (in terms of mass and surface area). To do so, the geochemical model developed in Chapter 2 and improved in Chapter 3 provides a useful tool. Site-specific parameters determined in the first step of the methodology as well as kinetic and thermodynamic mineral parameters would be used as model input. The groundwater flow velocity should also be included in the model, except if the advection rate is really low compared to microbial and mineral dissolution processes.

6.4 Towards field scale applications

An extremely important point for the field application of the pH control approach developed in this study is the delivery of the mineral to the subsurface. This topic was beyond the scope of this thesis but was investigated in a parallel study by Brovelli et al. (2013 in preparation). A 3D-reactive transport model was developed with PHAST to study particle transport filtration and dissolution, and its effect on soil and groundwater geochemistry. The model included particle advection and dispersion, deep-bed filtration, porosity, and hydraulic conductivity changes associated with deposition and mobilization. The results of the numerical simulations showed that, in general, the distance between two injection wells should not exceed 15 m to ensure a sufficiently homogeneous distribution of the silicate minerals. It was further observed that the optimal size of the injected particles is around 5 µm. Larger particles would not be transported sufficiently far from the injection point while smaller colloidal particles present a risk of agglomeration and attachment to the surface. Further research should be conducted to test silicate mineral injection in medium and larger scales experiment (e.g. two-dimensional tank experiments and small field scale studies).

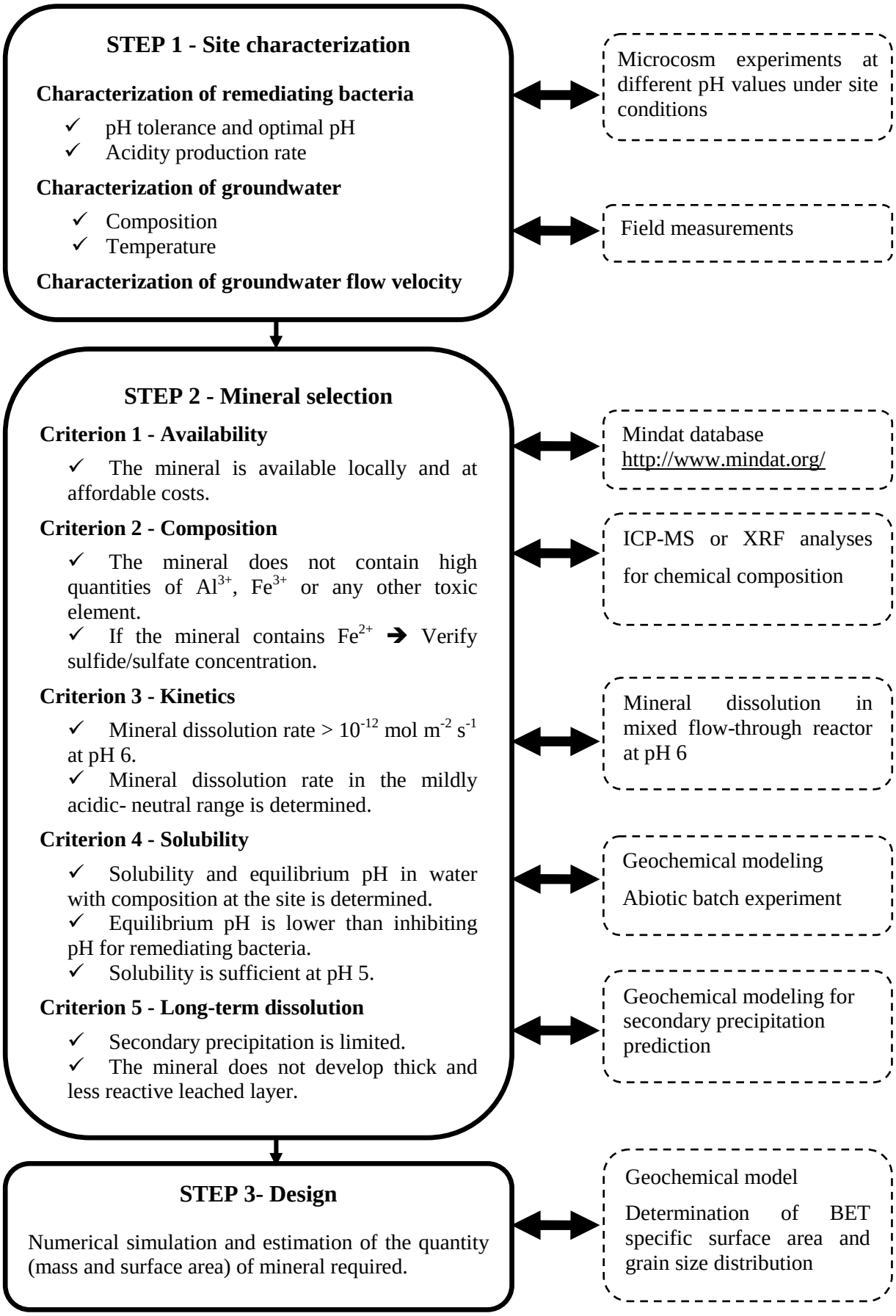

Figure 6.1. Global methodology for pH control strategy using (ground) silicate mineral powders.

References

1 **Gat, J. R., Mook, W. G. & Meijer, H. A.** Environmental isotopes in the hydrological cycle. *Principles and Applications UNESCO/IAEA Series* **2**, 63-67, (2001).

2 **Swiss Federal Office of the Environment (FOEN).** *Groundwater protection.* http://www.bafu.admin.ch. Last access: May 2013.

3 **European Environment Agency (EEA).** *Progress in management of contaminated sites (CSI 015) - Assessment published* . http://www.eea.europa.eu/data-and-maps/indicators/progress-in-management-of-contaminated-sites/progress-in-management-of-contaminated-1, (2007). Last access: May 2013.

4 **Mercer, J. W. & Cohen, R. M.** A review of immiscible fluids in the subsurface: Properties, models, characterization and remediation. *Journal of Contaminant Hydrology* **6**, 107-163, (1990).

5 **Lenhard, R. J., Parker, J. C. & Kaluarachchi, J. J.** A model for hysteretic constitutive relations governing multiphase flow: 3. Refinements and numerical simulations. *Water Resources Research* **25**, 1727-1736, (1989).

6 **Schwille, F. & Pankow, J. F.** *Dense chlorinated solvents in porous and fractured media - Model experiments.* Lewis Publishers. Chelsea, MI, USA, (1988).

7 **Interstate Technology & Regulatory Council (ITRC).** DNAPL Source Reduction: Facing the Challenge. The Interstate Technology & Regulatory Council, Washington, DC, USA, www.itrcweb.org, (2002). Last access: May 2013.

8 **Cohen, R. M. & Mercer, J. M. W.** *DNAPL Site Evaluation.* C.K. Smoley-CRC Press. Boca Raton, Fla, USA, (1993).

9 **Mackay, D. M. & Cherry, J. A.** Groundwater contamination: Pump-and-treat remediation. *Environmental Science & Technology* **23**, 630-636, (1989).

10 **Interstate Technology & Regulatory Council (ITRC).** Overview of In Situ Bioremediation of Chlorinated Ethene DNAPL Source Zones. BIODNAPL-1. Interstate Technology & Regulatory Council, Washington, D.C, USA, www.itrcweb.org, (2005). Last access: May 2013.

11 **Ruder, A. M.** Potential health effects of occupational chlorinated solvent exposure. *Annals of the New York Academy of Sciences* **1076**, 207-227, (2006).

12 **Gribble, G. W.** The natural production of chlorinated compounds. *Environmental Science & Technology* **28**, A310-A319, (1994).

13 **Jordan, A.** Volcanic Formation of Halogenated Organic Compounds in *Natural Production of Organohalogen Compounds* Vol. 3P,*The Handbook of Environmental Chemistry* (ed G. Gribble) Ch. 7,121-139. Springer Berlin, Heidelberg, Germany, (2003).

14 **Jordan, A., Harnisch, J., Borchers, R., Le Guern, F. N. & Shinohara, H.** Volcanogenic halocarbons. *Environmental Science & Technology* **34**, 1122-1124, (2000).

15 **Gribble, G. W.** Naturally occurring organohalogen compounds: A comprehensive update in *Progress in the Chemistry of Organic Natural Products* Vol. 91, (eds A. D. Kinghorn, H. Falk, & J. Kobayashi) Springer Wien New York, USA, (2009).

16 **Gribble, G. W.** The diversity of naturally occurring organobromine compounds. *Chemical Society Reviews* **28**, 335-346, (1999).

17 **Abrahamsson, K., Ekdahl, A., Collen, J. & Pedersen, M.** Marine algae - A source of trichloroethylene and perchloroethylene. *Limnology and Oceanography* **40**, 1321-1326, (1995).

18 **Keppler, F., Borchers, R., Pracht, J., Rheinberger, S. & Scholer, H. F.** Natural formation of vinyl chloride in the terrestrial environment. *Environmental Science & Technology* **36**, 2479-2483, (2002).

19 **Toxics Use Reduction Institute.** Five Chemicals Alternatives Assessment Study. University of Massachusetts Lowell, Lowell, MA, USA, http://www.turi.org/, (2006). Last access: May 2013.

20 **ICIS.** *Chemical profile: Trichloroethylene.* http://www.icis.com/Articles/2005/07/05/689483/chemical-profile-trichloroethylene.html, (2005). Last access: May 2013.

21 **Pant, P. & Pant, S.** A review: Advances in microbial remediation of trichloroethylene (TCE). *Journal of Environmental Sciences* **22**, 116-126, (2010).

22 **Aulenta, F., Majone, M. & Tandoi, V.** Enhanced anaerobic bioremediation of chlorinated solvents: environmental factors influencing microbial activity and their relevance under field conditions. *Journal of Chemical Technology and Biotechnology* **81**, 1463-1474, (2006).

23 **United States Environmental Protection Agency (USEPA).** Common chemicals found at Superfund sites. Washington, DC, USA, http://nepis.epa.gov/, (1994). Last access: May 2013.

24 **Moran, M. J., Zogorski, J. S. & Squillace, P. J.** Chlorinated solvents in groundwater of the United States. *Environmental Science & Technology* **41**, 74-81, (2007).

25 **Squillace, P. J., Scott, J. C., Moran, M. J., Nolan, B. T. & Kolpin, D. W.** VOCs, pesticides, nitrate, and their mixtures in groundwater used for drinking water in the United States. *Environmental Science & Technology* **36**, 1923-1930, (2002).

26 **Pankow, J. F. & Cherry, J. A.** *Dense Chlorinated Solvents and other DNAPLs in Groundwater: History, Behavior, and Remediation.* Waterloo Press. Portland, Oregon, USA, (1996).

27 **United State Environmental Protection Agency (US EPA).** Toxics Release Inventory Public Data Release Report. Office of Environmental Information US EPA, Washington, DC, USA, http://www.epa.gov/, (2003). Last access: May 2013.

28 **Schmidt, R., DeZeeuw, R., Henning, L. & Trippler, D.** State programs to clean up dry cleaners. State coalition for remediation of dry cleaners. United States Environmental Protection Agency (USEPA), http://www.drycleancoalition.org/survey/, (2001). Last access: May 2013.

29 **Stroo, H. F., Leeson, A., Marqusee, J. A., Johnson, P. C., Ward, C. H., Kavanaugh, M. C., Sale, T. C., Newell, C. J., Pennell, K. D. & Lebrón, C. A.** Chlorinated ethene source remediation: lessons learned. *Environmental Science & Technology* **46**, 6438-6447, (2012).

30 **National Research Council. Committee on Source Removal of Contaminants in the Subsurface**. *Contaminants in the Subsurface: Source Zone Assessment and Remediation.* The National Academy Press. Wahington, DC, USA, (2005).

31 **National Research Council**. *Alternatives for Ground Water Cleanup.* The National Academies Press. Wahington, DC, USA, (1994).

32 **MacDonald, J. A. & Kavanaugh, M. C.** Restoring contaminated groundwater: An achievable goal? *Environmental Science & Technology* **28**, 362-368, (1994).

33 **Travis, C. & Doty, C.** ES&T Views: Can contaminated aquifers at superfund sites be remediated? *Environmental Science & Technology* **24**, 1464-1466, (1990).

34 **Christ, J. A., Ramsburg, C. A., Abriola, L. M., Pennell, K. D. & Loffler, F. E.** Coupling aggressive mass removal with microbial reductive dechlorination for remediation of DNAPL source zones: A review and assessment. *Environmental Health Perspectives* **113**, 465-477, (2005).

35 **Stroo, H. F., Unger, M., Ward, C. H., Kavanaugh, M. C., Vogel, C., Leeson, A., Marqusee, J. A. & Smith, B. P.** Peer reviewed: Remediating chlorinated solvent source zones. *Environmental Science and Technology* **37**, 224A-230A, (2003).

36 **Triplett Kingston, J. L., Dahlen, P. R. & Johnson, P. C.** State of the practice review of in situ thermal technologies. *Ground Water Monitoring & Remediation* **30**, 64-72, (2010).

37 **Soga, K., Page, J. W. E. & Illangasekare, T. H.** A review of NAPL source zone remediation efficiency and the mass flux approach. *Journal of Hazardous Materials* **110**, 13-27, (2004).

38 **Sale, T., Newell, C., Stroo, H., Hinchee, R. & Johnson, P.** Frequently asked questions regarding management of chlorinated solvents in soils and groundwater. Environmental Security Technology certification Program Office (Department of Defense), Arlington, VA, USA, http://serdp-estcp.org/, (2008). Last access: May 2013.

39 **McGuire, T. M., McDade, J. M. & Newell, C. J.** Performance of DNAPL source depletion technologies at 59 chlorinated solvent-impacted sites. *Ground Water Monitoring and Remediation* **26**, 73-84, (2006).

40 **McDade, J. M., McGuire, T. M. & Newell, C. J.** Analysis of DNAPL source-depletion costs at 36 field sites. *Remediation Journal* **15**, 9-18, (2005).

41 **Costanza, J. & Pennell, K. D.** Distribution and abiotic degradation of chlorinated solvents in heated field samples. *Environmental Science & Technology* **41**, 1729-1734, (2007).

42 **Davis, E. L.** *Steam Injection for Soil and Aquifer Remediation.* United States Environmental Protection Agency (US EPA). Washington, DC, USA, (1998).

43 **Siegrist, R. L., Urynowicz, M. A., West, O. A., Crimi, M. L. & Lowe, K. S.** *Principles and practices of in situ chemical oxidation using permanganate.* Battelle Press. Columbus, OH, USA, (2001).

44 **Urynowicz, M. A. & Siegrist, R. L.** Chemical degradation of TCE DNAPL by permanganate in *Chemical Oxidation and Reactive Barriers: Remediation of Chlorinated and Recalcitrant Compounds.* Battelle Press, Columbus, OH, USA, (2000).

45 **Krembs, F. J., Siegrist, R. L., Crimi, M. L., Furrer, R. F. & Petri, B. G.** ISCO for groundwater remediation: Analysis of field applications and performance. *Groundwater Monitoring & Remediation* **30**, 42-53, (2010).

46 **Siegrist, R. L., Crimi, M. & Brown, R. A.** *In Situ Chemical Oxidation for Groundwater Remediation.* Springer. New York, NY, USA, (2011).

47 **Fountain, J. C., Starr, R. C., Middleton, T., Beikirch, M., Taylor, C. & Hodge, D.** A controlled field test of surfactant enhanced aquifer remediation. *Groundwater* **34**, 910-916, (1996).

48 **Boving, T. B., Wang, X. & Brusseau, M. L.** Cyclodextrin-enhanced solubilization and removal of residual-phase chlorinated solvents from porous media. *Environmental Science & Technology* **33**, 764-770, (1999).

49 **Boving, T. B., Barnett, S. M., Perez, G., Blanford, W. J. & McCray, J. E.** Remediation with cyclodextrin: Recovery of the remedial agent by membrane filtration. *Remediation Journal* **17**, 21-36, (2007).

50 **Ramakrishnan, V., Ogram, A. V. & Lindner, A. S.** Impacts of co-solvent flushing on microbial populations capable of degrading trichloroethylene. *Environmental Health Perspectives* **113**, 55, (2005).

51 **Dugan, P. J., Siegrist, R. L. & Crimi, M. L.** Coupling surfactants/cosolvents with oxidants for enhanced DNAPL removal: A review. *Remediation Journal* **20**, 27-49, (2010).

52 **Häggblom, M. M. & Bossert, I. D.** *Dehalogenation: Microbial Processes and Environmental Applications.* Kluwer Academic Publishers. Dordrecht, The Netherlands, (2003).

53 **Parsons Corporation.** Principles and Practices of Enhanced Anaerobic Bioremediation of Chlorinated Solvents. US Department of Defense - Air Force Center for Environmental Excellence (AFCEE) and the Environmental Security Technology Certification Program (ESTCP). http://www.dtic.mil/cgi-bin/GetTRDoc?AD=ADA511850, (2004). Last access: May 2013.

54 **Carr, C. S. & Hughes, J. B.** Enrichment of high rate PCE dechlorination and comparative study of lactate, methanol, and hydrogen as electron dopers to sustain activity. *Environmental Science & Technology* **32**, 1817-1824, (1998).

55 **Fennell, D. E. & Gossett, J. M.** Modeling the production of and competition for hydrogen in a dechlorinating culture. *Environmental Science & Technology* **32**, 2450-2460, (1998).

56 **Yang, Y. R. & McCarty, P. L.** Comparison between donor substrates for biologically enhanced tetrachloroethene DNAPL dissolution. *Environmental Science & Technology* **36**, 3400-3404, (2002).

57 **Yang, Y. R. & McCarty, P. L.** Competition for hydrogen within a chlorinated solvent dehalogenating anaerobic mixed culture. *Environmental Science & Technology* **32**, 3591-3597, (1998).

58 **Koenigsberg, S. S. & Farone, W.** *The use of hydrogen release compound (HRC™) for CAH bioremediation.* Battelle Press. Columbus, OH, USA, (1999).

59 **Middeldorp, P. J. M., van Aalst, M. A., Rijnaarts, H. H. M., Stams, F. J. M., de Kreuk, H. F., Schraa, G. & Bosma, T. N. P.** Stimulation of reductive dechlorination for in situ bioremediation of a soil contaminated with chlorinated ethenes. *Water Science and Technology* **37**, 105-110, (1998).

60 **Yu, S. & Semprini, L.** Kinetics and modeling of reductive dechlorination at high PCE and TCE concentrations. *Biotechnology and Bioengineering* **88**, 451-464, (2004).

61 **Nielsen, R. B. & Keasling, J. D.** Reductive dechlorination of chlorinated ethene DNAPLs by a culture enriched from contaminated groundwater. *Biotechnology and Bioengineering* **62**, 160-165, (1999).

62 **Yang, Y. R. & McCarty, P. L.** Biologically enhanced dissolution of tetrachloroethene DNAPL. *Environmental Science & Technology* **34**, 2979-2984, (2000).

63 **Adamson, D. T., Lyon, D. Y. & Hughes, J. B.** Flux and product distribution during biological treatment of tetrachloroethene dense non-aqueous-phase liquid. *Environmental Science and Technology* **38**, 2021-2028, (2004).

64 **Duhamel, M., Wehr, S. D., Yu, L., Rizvi, H., Seepersad, D., Dworatzek, S., Cox, E. E. & Edwards, E. A.** Comparison of anaerobic dechlorinating enrichment cultures maintained on tetrachloroethene, trichloroethene, cis-dichloroethene and vinyl chloride. *Water Research* **36**, 4193-4202, (2002).

65 **Isalou, M., Sleep, B. E. & Liss, S. N.** Biodegradation of high concentrations of tetrachloroethene in a continuous flow column system. *Environmental Science & Technology* **32**, 3579-3585, (1998).

66 **Sleep, B. E. *et al.*** Biological enhancement of tetrachloroethene dissolution and associated microbial community changes. *Environmental Science & Technology* **40**, 3623-3633, (2006).

67 **Amos, B. K., Suchomel, E. J., Pennell, K. D. & Loffler, F. E.** Spatial and temporal distributions of *geobacter lovleyi* and *dehalococcoides* spp. during bioenhanced PCE-NAPL dissolution. *Environmental Science & Technology* **43**, 1977-1985, (2009).

68 **Amos, B. K., Suchomel, E. J., Pennell, K. D. & Loffler, F. E.** Microbial activity and distribution during enhanced contaminant dissolution from a NAPL source zone. *Water Research* **42**, 2963-2974, (2008).

69 **Adamson, D. T., McDade, J. M. & Hughes, J. B.** Inoculation of DNAPL source zone to initiate reductive dechlorination of PCE. *Environmental Science & Technology* **37**, 2525-2533, (2003).

70 **Carr, C. S., Garg, S. & Hughes, J. B.** Effect of dechlorinating bacteria on the longevity and composition of PCE-containing nonaqueous phase liquids under equilibrium dissolution conditions. *Environmental Science & Technology* **34**, 1088-1094, (2000).

71 **Cope, N. & Hughes, J. B. a.** Biologically-enhanced removal of PCE from NAPL source zones. *Environmental Science & Technology* **35**, 2014-2021, (2001).

72 **Glover, K. C., Munakata-Marr, J. & Illangasekare, T. H.** Biologically enhanced mass transfer of tetrachloroethene from DNAPL in source zones: Experimental evaluation and influence of pool morphology. *Environmental Science & Technology* **41**, 1384-1389, (2007).

73 **Bowman, K. S., Moe, W. M., Rash, B. A., Bae, H.-S. & Rainey, F. A.** Bacterial diversity of an acidic Louisiana groundwater contaminated by dense nonaqueous-phase liquid containing chloroethanes and other solvents. *FEMS Microbiology Ecology* **58**, 120-133, (2006).

74 **Interstate Technology & Regulatory Council (ITRC).** In situ bioremediation of chlorinated ethene DNAPL source zones: case studies. Interstate Technology & Regulatory Council, Washington, D.C, USA, www.itrcweb.org, (2007). Last access: May 2013.

75 **de Blanc, P., Brown, C., McKinney, D., Speitel, G. & Pope, G.** Surfactant flushing and bioremediation—striking a balance in *In situ and on-site bioremediation* Vol. 2,565-574. Battelle Press, Columbus, OH, USA, (1997).

76 **Rao, P. S. C., Jawitz, J. W., Enfield, C. G., Falta Jr, R., Annable, M. D. & Wood, A. L.** Technology integration for contaminated site remediation: clean-up goals and performance criteria in *Groundwater quality: Natural and enhanced restoration of groundwater pollution* Vol. 275,571-578. IAHS Press, Wallingford, Oxfordshire, UK, (2001).

77 **Zoller, U. & Rubin, H.** Feasibility of in situ NAPL-contaminated aquifer bioremediation by biodegradable nutrient-surfactant mix. *Journal of Environmental Science and Health, Part A* **36**, 1451-1471, (2001).

78 **Friis, A. K., Heron, G., Albrechtsen, H.-J., Udell, K. & Bjerg, P. L.** Anaerobic dechlorination and redox activities after full-scale Electrical Resistance Heating (ERH) of a TCE-contaminated aquifer. *Journal of Contaminant Hydrology* **88**, 219-234, (2006).

79 **Ramsburg, C. A., Abriola, L. M., Pennell, K. D., Löffler, F. E., Gamache, M., Amos, B. K. & Petrovskis, E. A.** Stimulated microbial reductive dechlorination following surfactant treatment at the Bachman Road site. *Environmental Science & Technology* **38**, 5902-5914, (2004).

80 **Sahl, J. W., Munakata-Marr, J., Crimi, M. L. & Siegrist, R. L.** Coupling permanganate oxidation with microbial dechlorination of tetrachloroethene. *Water Environment Research* **79**, 5-12, (2007).

81 **Adamson, D. T. & Newell, C. J.** Support of source zone bioremediation through endogenous biomass decay and electron donor recycling. *Bioremediation Journal* **13**, 29-40, (2009).

82 **Adamson, D. T., McGuire, T. M., Newell, C. J. & Stroo, H.** Sustained treatment: Implications for treatment timescales associated with source-depletion technologies. *Remediation Journal* **21**, 27-50, (2011).

83 **Suthersan, S., Lutes, C., Palmer, P., Lenzo, F., Payne, F., Liles, D. & Burdick, J.** Technical protocol for using soluble carbohydrates to enhance reductive dechlorination of chlorinated aliphatic hydrocarbons. Air Force Center for Environmental Excellence (AFCEE) and Environmental Security Technology Certification Program (ESTCP), Arlington, VA, USA, http://serdp-estcp.org/, (2002). Last access: May 2013.

84 **Putnis, A.** *An Introduction to Mineral Sciences.* Cambridge University Press. Cambridge, UK. (1992).

85 **Bradley, P. M. & Chapelle, F. H.** Biodegradation of chlorinated ethenes in *In situ Remediation of Chlorinated Solvent Plumes (SERDP and ESTCP RemediationTechnology Monograph Series)* (eds H.F. Stroo & C.H. Ward) 39-67. Springer Science + Business Media, LLC, New York, NY,USA, (2010).

86 **Gantzer, C. J. & Wackett, L. P.** Reductive dechlorination catalyzed by bacterial transition-metal coenzymes. *Environmental Science & Technology* **25**, 715-722, (1991).

87 **Fathepure, B. Z. & Boyd, S. A.** Dependence of tetrachloroethylene dechlorination on methanogenic substrate consumption by *Methanosarcina* sp. strain DCM. *Applied and Environmental Microbiology* **54**, 2976-2980, (1988).

88 **Fathepure, B. Z. & Boyd, S. A.** Reductive dechlorination of perchloroethylene and the role of methanogens. *FEMS Microbiology Letters* **49**, 149-156, (1988).

89 **El Fantroussi, S., Naveau, H. & Agathos, S. N.** Anaerobic dechlorinating bacteria. *Biotechnology Progress* **14**, 167-188, (2008).

90 **Townsend, G. T. & Suflita, J. M.** Influence of sulfur oxyanions on reductive dehalogenation activities in Desulfomonile tiedjei. *Applied and Environmental Microbiology* **63**, 3594-3599, (1997).

91 **Freedman, D. L. & Gossett, J. M.** Biological reductive dechlorination of tetrachloroethylene and trichloroethylene to ethylene under methanogenic conditions. *Applied and Environmental Microbiology* **55**, 2144-2151, (1989).

92 **Terzenbach, D. P. & Blaut, M.** Transformation of tetrachloroethylene to trichloroethylene by homoacetogenic bacteria. *FEMS Microbiology Letters* **123**, 213-218, (1994).

93 **Davis, J. W. & Carpenter, C. L.** Aerobic biodegradation of vinyl chloride in groundwater samples. *Applied and Environmental Microbiology* **56**, 3878-3880, (1990).

94 **Bradley, P. M. & Chapelle, F. H.** Anaerobic mineralization of vinyl chloride in Fe (III)-reducing, aquifer sediments. *Environmental Science & Technology* **30**, 2084-2086, (1996).

95 **Mattes, T. E., Alexander, A. K. & Coleman, N. V.** Aerobic biodegradation of the chloroethenes: pathways, enzymes, ecology, and evolution. *FEMS Microbiology Reviews* **34**, 445-475, (2010).

96 **Vogel, T. M., Criddle, C. S. & McCarty, P. L.** Transformations of halogenated aliphatic-compounds. *Environmental Science & Technology* **21**, 722-736, (1987).

97 **MaymoGatell, X., Chien, Y. T., Gossett, J. M. & Zinder, S. H.** Isolation of a bacterium that reductively dechlorinates tetrachloroethene to ethene. *Science* **276**, 1568-1571, (1997).

98 **Bradley, P. M.** History and ecology of chloroethene biodegradation: A review. *Bioremediation Journal* **7**, 81-109, (2003).

99 **Mohn, W. W. & Tiedje, J. M.** Microbial reductive dehalogenation. *Microbiological Reviews* **56**, 482-507, (1992).

100 **Bouwer, E. J.** Bioremediation of chlorinated solvents using alternate electron acceptors in *Handbook of bioremediation*. (eds RD Norris, RE Hinchee, R Brown, PL McCarty, L Semprini, JT Wilson, DH Kampbell, M Reinhard, Edward J Bouwer, & RC Borden) 149-175. Lewis Publishers, Boca Raton, FL, USA, (1994).

101 **Holliger, C., Schraa, G., Stams, A. J. M. & Zehnder, A. J. B.** A highly purified enrichment culture couples the reductive dechlorination of tetrachloroethene to growth. *Applied and Environmental Microbiology* **59**, 2991-2997, (1993).

102 **Holliger, C., Hahn, D., Harmsen, H., Ludwig, W., Schumacher, W., Tindall, B., Vazquez, F., Weiss, N. & Zehnder, A. J. B.** *Dehalobacter restrictus* gen. nov. and sp. nov., a strictly anaerobic bacterium that reductively dechlorinates tetra- and trichloroethene in an anaerobic respiration. *Archives of Microbiology* **169**, 313-321, (1998).

103 **Loffler, F. E., Tiedje, J. M. & Sanford, R. A.** Fraction of electrons consumed in electron acceptor reduction and hydrogen thresholds as indicators of halorespiratory physiology. *Applied and Environmental Microbiology* **65**, 4049-4056, (1999).

104 **Krumholz, L. R., Sharp, R. & Fishbain, S. S.** A freshwater anaerobe coupling acetate oxidation to tetrachloroethylene dehalogenation. *Applied and Environmental Microbiology* **62**, 4108-4113, (1996).

105 **Krumholz, L. R.** *Desulfuromonas chloroethenica* sp. nov. uses tetrachloroethylene and trichloroethylene as electron acceptors. *International Journal of Systematic Bacteriology* **47**, 1262-1263, (1997).

106 **Scholz-Muramatsu, H., Neumann, A., Messmer, M., Moore, E. & Diekert, G.** Isolation and characterization of *Dehalospirillum multivorans* gen. nov., sp. nov., a tetrachloroethene-utilizing, strictly anaerobic bacterium. *Archives of Microbiology* **163**, 48-56, (1995).

107 **Sharma, P. K. & McCarty, P. L.** Isolation and characterization of a facultatively aerobic bacterium that reductively dehalogenates tetrachloroethene to cis-1,2-dichloroethene. *Applied and Environmental Microbiology* **62**, 761-765, (1996).

108 **Gerritse, J., Renard, V., Gomes, T. P., Lawson, P. A., Collins, M. D. & Gottschal, J. C.** *Desulfitobacterium* sp. strain PCE1, an anaerobic bacterium that can grow by reductive dechlorination of tetrachloroethene or ortho-chlorinated phenols. *Archives of Microbiology* **165**, 132-140, (1996).

109 **Smidt, H. & de Vos, W. M.** Anaerobic microbial dehalogenation. *Annual Review of Microbiology* **58**, 43-73, (2004).

110 **Holliger, C., Wohlfarth, G. & Diekert, G.** Reductive dechlorination in the energy metabolism of anaerobic bacteria. *FEMS Microbiology Reviews* **22**, 383-398, (1998).

111 **Löffler, F. E., Yan, J., Ritalahti, K. M., Adrian, L., Edwards, E. A., Konstantinidis, K. T., Müller, J. A., Fullerton, H., Zinder, S. H. & Spormann, A. M.** *Dehalococcoides mccartyi* gen. nov., sp. nov., obligate organohalide-respiring anaerobic bacteria, relevant to halogen cycling and bioremediation, belong to a novel bacterial class, *Dehalococcoidetes* classis nov., within the phylum *Chloroflexi*. *International Journal of Systematic and Evolutionary Microbiology*, (2012).

112 **Maymo-Gatell, X., Nijenhuis, I. & Zinder, S. H.** Reductive dechlorination of *cis*-1,2-dichloroethene and vinyl chloride by "*Dehalococcoides ethenogenes*". *Environmental Science & Technology* **35**, 516-521, (2001).

113 **He, J., Ritalahti, K. M., Yang, K.-L., Koenigsberg, S. S. & Löffler, F. E.** Detoxification of vinyl chloride to ethene coupled to growth of an anaerobic bacterium. *Nature* **424**, 62-65, (2003).

114 **Sung, Y., Ritalahti, K. M., Apkarian, R. P. & Löffler, F. E.** Quantitative PCR confirms purity of strain GT, a novel trichloroethene-to-ethene-respiring *Dehalococcoides* isolate. *Applied and Environmental Microbiology* **72**, 1980-1987, (2006).

115 **Hendrickson, E. R., Payne, J. A., Young, R. M., Starr, M. G., Perry, M. P., Fahnestock, S., Ellis, D. E. & Ebersole, R. C.** Molecular analysis of *Dehalococcoides* 16S ribosomal DNA from chloroethene-contaminated sites throughout North America and Europe. *Applied and Environmental Microbiology* **68**, 485-495, (2002).

116 **Edwards, E. A. & Cox, E.** Field and laboratory studies of sequential anaerobic-aerobic chlorinated solvent biodegradation in *In situ and on-site bioremediation* Vol. 3,261-265. Battelle Press, Columbus, OH, USA, (1997).

117 **Shani, N.** *Assessing the bacterial ecology of organohalide respiration for the design of bioremediation strategies*. Ph.D. Thesis, Ecole Polytechnique Fédérale de Lausanne, Lausanne, Switzerland. doi: 10.5075/epfl-thesis-5379, (2012).

118 **Flynn, S. J., Löffler, F. E. & Tiedje, J. M.** Microbial community changes associated with a shift from reductive dechlorination of PCE to reductive dechlorination of cis-DCE and VC. *Environmental Science & Technology* **34**, 1056-1061, (2000).

119 **Rouzeau-Szynalski, K., Maillard, J. & Holliger, C.** Frequent concomitant presence of *Desulfitobacterium* spp. and "*Dehalococcoides*" spp. in chloroethene-dechlorinating microbial communities. *Applied Microbiology and Biotechnology* **90**, 361-368, (2011).

120 **Futagami, T., Goto, M. & Furukawa, K.** Biochemical and genetic bases of dehalorespiration. *The Chemical Record* **8**, 1-12, (2008).

121 **Suyama, A., Iwakiri, R., Kai, K., Tokunaga, T., Sera, N. & Furukawa, K.** Isolation and characterization of *Desulfitobacterium* sp strain Y51 capable of efficient dehalogenation of tetrachloroethene and polychloroethanes. *Bioscience Biotechnology and Biochemistry* **65**, 1474-1481, (2001).

122 **Sung, Y., Ritalahti, K. M., Sanford, R. A., Urbance, J. W., Flynn, S. J., Tiedje, J. M. & Löffler, F. E.** Characterization of two tetrachloroethene-reducing, acetate-oxidizing anaerobic bacteria and their description as *Desulfuromonas michiganensis* sp. nov. *Applied and Environmental Microbiology* **69**, 2964-2974, (2003).

123 **Kaplan, A. R., Munakata-Marr, J. & Illangasekare, T. H.** Biodegradation of residual dense nonaqueous-phase liquid tetrachloroethene: Effects on mass transfer. *Bioremediation Journal* **12**, 21-31, (2008).

124 **Heimann, A., Jakobsen, R. & Blodau, C.** Energetic constraints on H_2-dependent terminal electron accepting processes in anoxic environments: A review of observations and model approaches. *Environmental Science & Technology* **44**, 24-33, (2010).

125 **Chapelle, F. H.** Identifying redox conditions that favor the natural attenuation of chlorinated ethenes in contaminated ground-water systems in *Symposium on Natural Attenuation of Chlorinated Organics in Ground Water*. 17-20. U.S. Environmental Protection Agency (US EPA), Washington, DC, USA, (1996).

126 **Neumann, A., Scholzmuramatsu, H. & Diekert, G.** Tetrachloroethene metabolism of *Dehalospirillum multivorans*. *Archives of Microbiology* **162**, 295-301, (1994).

127 **Utkin, I., Woese, C. & Wiegel, J.** Isolation and characterization of *Desulfitobacterium dehalogenans* gen-nov, sp-nov, an anaerobic bacterium which reductively dechlorinates chlorophenolic compounds. *International Journal of Systematic Bacteriology* **44**, 612-619, (1994).

128 **Deweerd, K. A., Mandelco, L., Tanner, R. S., Woese, C. R. & Suflita, J. M.** *Desulfomonile tiedjei* gen-nov and sp-nov, a novel anaerobic, dehalogenating, sulfate-reducing bacterium. *Archives of Microbiology* **154**, 23-30, (1990).

129 **Zhuang, P. & Pavlostathis, S. G.** Effect of temperature, pH and electron-donor on the microbial reductive dechlorination of chloroalkenes. *Chemosphere* **31**, 3537-3548, (1995).

130 **Vainberg, S., Condee, C. W. & Steffan, R. J.** Large-scale production of bacterial consortia for remediation of chlorinated solvent-contaminated groundwater. *Journal of Industrial Microbiology and Biotechnology* **36**, 1189-1197, (2009).

131 **Ise, K., Suto, K. & Inoue, C.** Characterization of an enriched anaerobic culture having ability to dechlorinate TCE in *AIP Conference Proceedings.* 231-234. American Institute of Physics, Melville, NY, USA, (2007).

132 **Rowlands, D.** Development of optimal pH for degradation of chlorinated solvents by the KB-1® anaerobic bacterial culture. Geosyntec Consultants/SiREM, Guelph, Ontario, Canada, (2004).

133 **Li, J. J. Y. X.** *Adaptation of a Dechlorinating Culture, KB-1, to Acidic Environments*. Master Thesis, University of Toronto, Toronto, Ontario, Canada, (2012).

134 **Lu, X., Wilson, J. T. & Kampbell, D. H.** Relationship between geochemical parameters and the occurrence of *Dehalococcoides* DNA in contaminated aquifers. *Water Resources Research* **42**, W08427. doi:08410.01029/02005WR004283, (2006).

135 **Löffler, F. E., Sanford, R. A. & Ritalahti, K. M.** Enrichment, cultivation, and detection of reductively dechlorinating bacteria. *Methods in Enzymology* **397**, 77-111, (2005).

136 **Smatlak, C. R., Gossett, J. M. & Zinder, S. H.** Comparative kinetics of hydrogen utilization for reductive dechlorination of tetrachloroethene and methanogenesis in an anaerobic enrichment culture. *Environmental Science & Technology* **30**, 2850-2858, (1996).

137 **Ballapragada, B. S., Stensel, H. D., Puhakka, J. & Ferguson, J. F.** Effect of hydrogen on reductive dechlorination of chlorinated ethenes. *Environmental Science & Technology* **31**, 1728-1734, (1997).

138 **Fennell, D. E., Gossett, J. M. & Zinder, S. H.** Comparison of butyric acid, ethanol, lactic acid, and propionic acid as hydrogen donors for the reductive dechlorination of tetrachloroethene. *Environmental Science & Technology* **31**, 918-926, (1997).

139 **Wu, W.-M., Nye, J., Jain, M. K. & Hickey, R. F.** Anaerobic dechlorination of trichloroethylene (TCE) to ethylene using complex organic materials. *Water Research* **32**, 1445-1454, (1998).

140 **Yang, Y. & McCarty, P. L.** Biomass, oleate, and other possible substrates for chloroethene reductive dehalogenation. *Bioremediation Journal* **4**, 125-133, (2000).

141 **DiStefano, T. D., Baral, R., Duran, M. & Speece, R. E.** A comparison of complex electron donors for anaerobic dechlorination of PCE. *Bioremediation Journal* **5**, 131-143, (2001).

142 **Hoelen, T. P. & Reinhard, M.** Complete biological dehalogenation of chlorinated ethylenes in sulfate containing groundwater. *Biodegradation* **15**, 395-403, (2004).

143 **Aulenta, F., Canosa, A., Leccese, M., Papini, M. P., Majone, M. & Viottit, P.** Field study of *in situ* anaerobic bioremediation of a chlorinated solvent source zone. *Industrial & Engineering Chemistry Research* **46**, 6812-6819, (2007).

144 **Heimann, A. C., Friis, A. K. & Jakobsen, R.** Effects of sulfate on anaerobic chloroethene degradation by an enriched culture under transient and steady-state hydrogen supply. *Water Research* **39**, 3579-3586, (2005).

145 **Shani, N., Rossi, P. & Holliger, C.** Correlations between environmental variables and bacterial community structures suggest Fe(III) and vinyl chloride reduction as antagonistic terminal electron-accepting processes. *Environmental Science & Technology*, doi: 10.1021/es304017s, (2013).

146 **Luijten, M., Roelofsen, W., Langenhoff, A. A. M., Schraa, G. & Stams, A. J. M.** Hydrogen threshold concentrations in pure cultures of halorespiring bacteria and at a site polluted with chlorinated ethenes. *Environmental microbiology* **6**, 646-650, (2004).

147 **McCarty, P. L., Chu, M. Y. & Kitanidis, P. K. a.** Electron donor and pH relationships for biologically enhanced dissolution of chlorinated solvent DNAPL in groundwater. *European Journal of Soil Biology* **43**, 276-282, (2007).

148 **Robinson, C., Barry, D. A., McCarty, P. L., Gerhard, J. I. & Kouznetsova, I.** pH control for enhanced reductive bioremediation of chlorinated solvent source zones. *Science of the Total Environment* **407**, 4560-4573, (2009).

149 **Chu, M., Kitanidis, P. K. & McCarty, P. L.** Possible factors controlling the effectiveness of bioenhanced dissolution of non-aqueous phase tetrachloroethene. *Advances in Water Resources* **27**, 601-615, (2004).

150 **Appelo, C. A. J. & Postma, D.** *Geochemistry, Groundwater and Pollution.* AA Balkema Publishers. Leiden, The Netherlands, (2005).

151 **Robinson, C. & Barry, D. A.** Design tool for estimation of buffer requirement for enhanced reductive dechlorination of chlorinated solvents in groundwater. *Environmental Modelling & Software* **24**, 1332-1338, (2009).

152 **Brovelli, A., Barry, D. A., Robinson, C. & Gerhard, J.** Analysis of acidity production during enhanced reductive dechlorination using a simplified reactive transport model. *Advances in Water Resources* **43**, 14-27, (2012).

153 **Lee, M. D., Lieberman, M. T., Beckwith, W., Borden, R. C., Haas, P., Becvar, E. S. K., Dobson, K. & Sandlin, G. J.** Vegetable oil pilots to enhance DNAPL sequestration and

reductive dechlorination in *Proceedings of the 8th International In Situ and On-Site Bioremediation Symposium.* 660-667. Battelle Memorial Institute, Columbus, OH, USA, (2005).

154 **Piegat, J. & Newman, W. A.** Maintaining Neutral pH in Deep Soils and Ground Water Utilizing Insoluble Colloidal Buffers in *Sixth International Conference on Remediation of Chlorinated and Recalcitrant Compounds.* Battelle Press, Colombus, OH, USA, (2008).

155 **Delgado, A. G., Parameswaran, P., Fajardo-Williams, D., Halden, R. U. & Krajmalnik-Brown, R.** Role of bicarbonate as a pH buffer and electron sink in microbial dechlorination of chloroethenes. *Microbial Cell Factories* **11**, 128, (2012).

156 **Falatko, D. M., Fam, S. A. & Pon, G.** Applications and benefits of groundwater recirculation for electron donor delivery and pH-adjustment during enhanced anaerobic dechlorination in *Proceedings of the Annual International Conference on Soils, Sediments, Water and Energy.* Berkeley Electronic Press, Berkeley, CA, USA, (2011).

157 **Rust, C. M., Aelion, C. M. & Flora, J. R. V.** Laboratory sand column study of encapsulated buffer release for potential in situ pH control. *Journal of Contaminant Hydrology* **54**, 81-98, (2002).

158 **Aelion, C. M., Davis, H. T., Flora, J. R. V., Kirtland, B. C. & Amidon, M. B.** Application of encapsulation (pH-sensitive polymer and phosphate buffer macrocapsules): A novel approach to remediation of acidic ground water. *Environmental Pollution* **157**, 186-193, (2009).

159 **Liu, L., Baker, B., Flora, J. R. & Aelion, C. M.** Kinetics of acidic macrocapsules in controlling the pH of groundwater. *Environmental Engineering Science* **25**, 1345-1356, (2008).

160 **Marini, L.** *Geological Sequestration of Carbon Dioxide: Thermodynamics, Kinetics, and Reaction Path Modeling.* Elsevier. Amsterdam, The Netherlands, (2007).

161 **Giammar, D. E., Bruant, R. G. & Peters, C. A.** Forsterite dissolution and magnesite precipitation at conditions relevant for deep saline aquifer storage and sequestration of carbon dioxide. *Chemical Geology* **217**, 257-276, (2005).

162 **O'Connor, W. K., Dahlin, D. C., Nilsen, D. N., Rush, G., Walters, R. P. & Turner, P. C.** Carbon dioxide sequestration by direct mineral carbonation: results from recent studies and current status. Albany Research Center (ARC), Albany, OR, USA, (2001).

163 **Weissbart, E. J. & Rimstidt, J. D.** WolLastonite: Incongruent dissolution and leached layer formation. *Geochimica et Cosmochimica Acta* **64**, 4007-4016, (2000).

164 **Kump, L. R., Brantley, S. L. & Arthur, M. A.** Chemical weathering, atmospheric CO_2, and climate. *Annual Review of Earth and Planetary Sciences* **28**, 611-667, (2000).

165 **Sherlock, E. J., Lawrence, R. W. & Poulin, R.** On the neutralization of acid rock drainage by carbonate and silicate minerals. *Environmental Geology* **25**, 43-54, (1995).

166 **Palandri, J. L. & Kharaka, Y. K.** A compilation of rate parameters of water-mineral interaction kinetics for application to geochemical modeling. Open File Report 2004-1068. United States Geological Survey (USGS), Menlo Park, CA, USA, http://pubs.usgs.gov/of/2004/1068/, (2004). Last access: May 2013.

167 **Knauss, K. G. & Wolery, T. J.** Dependence of albite dissolution kinetics on pH and time at 25°C and 70°C. *Geochimica et Cosmochimica Acta* **50**, 2481-2497, (1986).

168 **Blum, A. E. & Stillings, L. L.** Feldspar dissolution kinetics. *Reviews in Mineralogy and Geochemistry* **31**, 291-351, (1995).

169 **Knauss, K. G. & Thomas J, W.** Muscovite dissolution kinetics as a function of pH and time at 70°C. *Geochimica et Cosmochimica Acta* **53**, 1493-1501, (1989).

170 **Nagy, K.** Dissolution and precipitation kinetics of sheet silicates. *Reviews in Mineralogy and Geochemistry* **31**, 173-233, (1995).

171 **Knauss, K. G., Nguyen, S. N. & Weed, H. C.** Diopside dissolution kinetics as a function of pH, CO_2, temperature and time. *Geochimica et Cosmochimica Acta* **57**, 285-294, (1993).

172 **Xie, Z. & Walther, J. V.** Dissolution stoichiometry and adsorption of alkali and alkaline earth elements to the acid-reacted wolLastonite surface at 25°C. *Geochimica et Cosmochimica Acta* **58**, 2587-2598, (1994).

173 **Lartigue, J. E.** *Contribution à l'étude de l'altération des silicates: approche expérimentale en milieu ouvert de la cinétique de dissolution à 25°C d'un pyroxène (Ca-Mg-Fe) en fonction du pH*. Doctoral Thesis, Université d'Aix-Marseille 3, Marseille, France, (1994).

174 **Lasaga, A. C. & Kirkpatrick, R. J.** *Kinetics of geochemical processes.* Mineralogical Society of America. Washington, DC, USA, (1981).

175 **Laidler, K. J.** *Chemical Kinetics.* Harper & Row. New York, USA, (1987).

176 **Bennett, P. C., Rogers, J. R. & Choi, W. J.** Silicates, silicate weathering, and microbial ecology. *Geomicrobiology Journal* **18**, 3-19, (2001).

177 **Vogelsberger, W., Löbbus, M., Sonnefeld, J. & Seidel, A.** The influence of ionic strength on the dissolution process of silica. *Colloids and Surfaces A: Physicochemical and Engineering Aspects* **159**, 311-319, (1999).

178 **Dove, P. M. & Crerar, D. A.** Kinetics of quartz dissolution in electrolyte solutions using a hydrothermal mixed flow reactor. *Geochimica et Cosmochimica Acta* **54**, 955-969, (1990).

179 **Pokrovsky, O. S. & Schott, J.** Kinetics and mechanism of forsterite dissolution at 25° C and pH from 1 to 12. *Geochimica et Cosmochimica Acta* **64**, 3313-3325, (2000).

180 **Stillings, L. L. & Brantley, S. L.** Feldspar dissolution at 25°C and pH 3- Reaction stoichiometry and the effect of cations. *Geochimica et Cosmochimica Acta* **59**, 1483-1496, (1995).

181 **Welch, S. A. & Ullman, W. J.** The effect of organic-acids on plagioclase dissolution rates and stoichiometry. *Geochimica et Cosmochimica Acta* **57**, 2725-2736, (1993).

182 **Stillings, L. L., Drever, J. I., Brantley, S. L., Sun, Y. & Oxburgh, R.** Rates of feldspar dissolution at pH 3 – 7 with 0 – 8 mM oxalic acid. *Chemical Geology* **132**, 79-89, (1996).

183 **Cama, J. & Ganor, J.** The effects of organic acids on the dissolution of silicate minerals: A case study of oxalate catalysis of kaolinite dissolution. *Geochimica et Cosmochimica Acta* **70**, 2191-2209, (2006).

184 **Golubev, S. V., Bauer, A. & Pokrovsky, O. S.** Effect of pH and organic ligands on the kinetics of smectite dissolution at 25°C. *Geochimica et Cosmochimica Acta* **70**, 4436-4451, (2006).

185 **Kleiv, R. A. & Sandvik, K. L.** Using tailings as heavy metal adsorbents - The effect of buffering capacity. *Minerals engineering* **13**, 719-728, (2000).

186 **Likens, G. E., Buso, D. C., Dresser, B. K., Bernhardt, E. S., Hall, R. O., Macneale, K. H. & Bailey, S. W.** Buffering an acidic stream in New Hampshire with a silicate mineral. *Restoration Ecology* **12**, 419-428, (2004).

187 **Fernandez-Caliani, J. C., Barba-Brioso, C. & Perez-Lopez, R.** Long-term interaction of wolLastonite with acid mine water and effects on arsenic and metal removal. *Applied Geochemistry* **23**, 1288-1298, (2008).

188 **Interstate Technology & Regulatory Council, In Situ Chemical Oxidation Team.** Technical and Regulatory Guidance for In Situ Chemical Oxidation of Contaminated Soil and Groundwater, 2nd ed. ISCO-2. Washington, D.C, USA, www.itrcweb.org, (2005). Last access: May 2013.

189 **Czupyrna, G., MacLeon, A. I., Levy, R. D. & Gold, H.** *In situ immobilization of heavy-metal-contaminated soils.* Noyes Data Corporation. Park Ridge, NJ, USA, (1989).

190 **Fetzner, S.** Bacterial dehalogenation. *Applied Microbiology and Biotechnology* **50**, 633-657, (1998).

191 **Zhang, H. & Bloom, P. R.** The pH dependence of hornblende dissolution. *Soil Science* **164**, 624-632, (1999).

192 **Roychowdhury, S., Cox, D. & Levandowsky, M.** production of hydrogen by microbial fermentation. *International Journal of Hydrogen Energy* **13**, 407-410, (1988).

193 **Lee, Y. J., Miyahara, T. & Noike, T.** Effect of pH on microbial hydrogen fermentation. *Journal of Chemical Technology and Biotechnology* **77**, 694-698, (2002).

194 **Payne, F. C., Suthersan, S. S., Nelson, D. K., Suarez, G., Tasker, I. & Akladiss, N.** Enhanced reductive dechlorination of PCE in unconsolidated soils. *Remediation Journal* **17**, 5-21, (2006).

195 **Lozecznik, S., Sparling, R., Oleszkiewicz, J. A., Clark, S. & VanGulck, J. F.** Leachate treatment before injection into a bioreactor landfill: Clogging potential reduction and benefits of using methanogenesis. *Waste Management* **30**, 2030-2036, (2010).

196 **White, A. F. & Brantley, S. L.** *Chemical weathering rates of silicate minerals, Reviews in Mineralogy 31*. Mineralogical Society of America. Washington, DC, USA, (1995).

197 **Bureau de Recherches Géologiques et Minières (BRGM).** *Thermoddem, a database devoted to waste minerals*. http://thermoddem.brgm.fr, (2007). Last access: May 2013.

198 **HydroGeoLogic, Inc & Allison Geoscience Consultants, Inc.** MINTEQA2/PRODEFA2, A geochemical assessment model for environmental systems: User manual supplement for Version 4.0. U.S. Environmental Protection Agency. National Exposure Research Laboratory. Ecosystems Research Division, Athens, Georgia, USA, http://www.epa.gov/osw/hazard/wastetypes/wasteid/hwirwste/pdf/risk/reports/s0536.pdf, (1998). Last access: May 2013.

199 **Parkhurst, D. L. & Appelo, C. A. J.** User's Guide to PHREEQC - A computer program for speciation, reaction-path, 1D-transport, and inverse geochemical calculations. Water-Resources Investigations Report 99-4259. United States Geological Survey (USGS), Denver, Colorado, USA, http://wwwbrr.cr.usgs.gov/projects/GWC_coupled/phreeqc/html/final.html, (1999). Last access: May 2013.

200 **Lawrence Livermore National Laboratory.** *The LLNL thermochemical database. Report URCL-21658*. *http://www.ntis.gov/search/product.aspx?ABBR=DE91017525*, (1990). Last access: May 2013.

201 **Chou, L. & WolLast, R.** Study of the weathering of albite at room-temperature and pressure with a fluidized-bed reactor. *Geochimica et Cosmochimica Acta* **48**, 2205-2217, (1984).

202 **Sverdrup, H.** *The kinetics of base cation release due to chemical weathering.* Lund University Press. Lund, Sweden, (1990).

203 **Tole, M. P., Lasaga, A. C., Pantano, C. & White, W. B.** The kinetics of dissolution of nepheline ($NaAlSiO_4$). *Geochimica et Cosmochimica Acta* **50**, 379-392, (1986).

204 **Kouznetsova, I., Mao, X. M., Robinson, C., Barry, D. A., Gerhard, J. I. & McCarty, P. L.** Biological reduction of chlorinated solvents: Batch-scale geochemical modeling. *Advances in Water Resources* **33**, 969-986, (2010).

205 **Aulenta, F., Pera, A., Rossetti, S., Papini, M. P. & Majone, M.** Relevance of side reactions in anaerobic reductive dechlorination microcosms amended with different electron donors. *Water Research* **41**, 27-38, (2007).

206 **Curtis, G. P.** Comparison of approaches for simulating reactive solute transport involving organic degradation reactions by multiple terminal electron acceptors. *Computers & Geosciences* **29**, 319-329, (2003).

207 **Cupples, A. M., Spormann, A. M. & McCarty, P. L.** Comparative evaluation of chloroethene dechlorination to ethene by *Dehalococcoides*-like microorganisms. *Environmental Science & Technology* **38**, 4768-4774, (2004).

208 **Mussati, M. C., Fuentes, M., Aguirre, P. A. & Scenna, N. J.** A steady-state module for modeling anaerobic biofilm reactors. *Latin American Applied Research* **35**, 255-263, (2005).

209 **Schepers, A. W., Thibault, J. & Lacroix, C.** *Lactobacillus helveticus* growth and lactic acid production during pH-controlled batch cultures in whey permeate/yeast extract medium. Part II: kinetic modeling and model validation. *Enzyme and Microbial Technology* **30**, 187-194, (2002).

210 **Bailey, J. E. & Ollis, D. F.** *Biochemical engineering fundamentals. 2nd edition.* McGraw-Hill. New-York, NY, USA. (1986).

211 **Lasaga, A. C.** Fundamentals approaches in describing mineral dissolution and precipitation rates in *Chemical Weathering Rate of Silicate Minerals, Reviews in Mineralogy 31* (eds A.F. White & S.L. Brantley) 23-86. Mineralogic Society of America, Washington, DC, USA, (1995).

212 **Golubev, S. V., Pokrovsky, O. S. & Schott, J.** Experimental determination of the effect of dissolved CO_2 on the dissolution kinetics of Mg and Ca silicates at 25°C. *Chemical Geology* **217**, 227-238, (2005).

213 **Sverdrup, H. U. & Warfvinge, P.** Estimating field weathering rates using laboratory kinetics of primary silicate minerals in natural soil environment in relation to a chemical weathering model in *Chemical weathering rates of silicates of silicate minerals. Reviews in Mineralogy 31* (eds A. F. White & S. L. Brantley) 485-541. Mineralogic Society of America, Washington, DC, USA, (1995).

214 **Scislewski, A. & Zuddas, P.** Estimation of reactive mineral surface area during water-rock interaction using fluid chemical data. *Geochimica et Cosmochimica Acta* **74**, 6996-7007, (2010).

215 **Gaus, I., Audigane, P., Andre, L., Lions, J., Jacquemet, N., Dutst, P., Czernichowski-Lauriol, I. & Azaroual, M.** Geochemical and solute transport modeling for CO_2 storage, what to expect from it? *International Journal of Greenhouse Gas Control* **2**, 605-625, (2008).

216 **Helgeson, H. C., Murphy, W. M. & Aagaard, P.** Thermodynamic and kinetic constraints on reaction-rates among minerals and aqueous-solution.2. Rate constants, effective surface-area, and the hydrolysis of feldspar. *Geochimica et Cosmochimica Acta* **48**, 2405-2432, (1984).

217 **Brantley, S. L., Kubicki, J. D. & White, A. F.** *Kinetics of water-rock interaction.* Springer. New York, NY, USA, (2008).

218 **Lichtner, P. C.** The quasi-stationary state approximation to coupled mass-transport and fluid-rock interaction in a porous-medium. *Geochimica et Cosmochimica Acta* **52**, 143-165, (1988).

219 **Emmanuel, S. & Berkowitz, B.** Mixing-induced precipitation and porosity evolution in porous media. *Advances in Water Resources* **28**, 337-344, (2005).

220 **Kieffer, B., Jove, C. F., Oelkers, E. H. & Schott, J.** An experimental study of the reactive surface area of the Fontainebleau sandstone as a function of porosity, permeability, and fluid flow rate. *Geochimica et Cosmochimica Acta* **63**, 3525-3534, (1999).

221 **Dixon, D. G. & Hendrix, J. L.** Theoretical basis for variable order assumption in the kinetics of leaching of discrete grains. *AIChE Journal* **39**, 904-907, (1993).

222 **Witkamp, G. J., Vandereerden, J. P. & Vanrosmalen, G. M.** Growth of Gypsum. 1. Kinetics. *Journal of Crystal Growth* **102**, 281-289, (1990).

223 **White, A. F. & Brantley, S. L.** The effect of time on the weathering of silicate minerals: why do weathering rates differ in the laboratory and field? *Chemical Geology* **202**, 479-506, (2003).

224 **White, A. F., Blum, A. E., Schulz, M. S., Bullen, T. D., Harden, J. W. & Peterson, M. L.** Chemical weathering rates of a soil chronosequence on granitic alluvium .1. Quantification of mineralogical and surface area changes and calculation of primary silicate reaction rates. *Geochimica et Cosmochimica Acta* **60**, 2533-2550, (1996).

225 **Metz, V. & Ganor, J.** Stirring effect on kaolinite dissolution rate. *Geochimica et Cosmochimica Acta* **65**, 3475-3490, (2001).

226 **Alkattan, M., Oelkers, E. H., Dandurand, J. L. & Schott, J.** An experimental study of calcite and limestone dissolution rates as a function of pH from -1 to 3 and temperature from 25 to 80 °C. *Chemical Geology* **151**, 199-214, (1998).

227 **Davis, J. A. & Hayes, K. F.** *Geochemical Processes at Mineral Surfaces, American Chemical Society Symposium Series 323.* American Chemical Society. Washington, DC, USA. (1986).

228 **Vangrinsven, J. J. M. & Vanriemsdijk, W. H.** Evaluation of batch and column techniques to measure weathering rates in soils. *Geoderma* **52**, 41-57, (1992).

229 **Zhu, C., Lu, P., Zheng, Z. P. & Ganor, J.** Coupled alkali feldspar dissolution and secondary mineral precipitation in batch systems: 4. Numerical modeling of kinetic reaction paths. *Geochimica et Cosmochimica Acta* **74**, 3963-3983, (2010).

230 **Yaws, C. L.** *Chemical Properties Handbook: Physical, Thermodynamic, Environmental, Transport, Safety, and Health related Properties for Organic and Inorganic Chemicals.* McGraw-Hill. New York, NY, USA, (1999).

231 **Borkovec, M., Wu, Q., Degovics, G., Laggner, P. & Sticher, H.** Surface-area and size distributions of soil particles. *Colloids and Surfaces A: Physicochemical and Engineering Aspects* **73**, 65-76, (1993).

232 **Aagaard, P. & Helgeson, H. C.** Thermodynamic and kinetic constraints on reaction-rates among minerals and aqueous-solutions.1. Theoretical considerations. *American Journal of Science* **282**, 237-285, (1982).

233 **Gautier, J. M., Oelkers, E. H. & Schott, J.** Are quartz dissolution rates proportional to BET surface areas? *Geochimica et Cosmochimica Acta* **65**, 1059-1070, (2001).

234 **Vandevivere, P., Welch, S. A., Ullman, W. J. & Kirchman, D. L.** Enhanced dissolution of silicate minerals by bacteria at near-neutral pH. *Microbial Ecology* **27**, 241-251, (1994).

235 **Ullman, W. J., Kirchman, D. L., Welch, S. A. & Vandevivere, P.** Laboratory evidence for microbially mediated silicate mineral dissolution in nature. *Chemical Geology* **132**, 11-17, (1996).

236 **Barker, W. W., Welch, S. A., Chu, S. & Banfield, J. F.** Experimental observations of the effects of bacteria on aluminosilicate weathering. *American Mineralogist* **83**, 1551-1563, (1998).

237 **Dopson, M., Halinen, A. K., Rahrmen, N., Bostrom, D., Sundkvist, J. E., Riekkola-Vanhanen, M., Kaksonen, A. H. & Puhakka, J. A.** Silicate mineral dissolution during heap bioleaching. *Biotechnology and Bioengineering* **99**, 811-820, (2008).

238 **Lacroix, E., Brovelli, A., Holliger, C. & Barry, D. A.** Evaluation of silicate minerals for pH control during bioremediation: application to chlorinated solvents. *Water, Air and Soil Pollution* **223**, 2663-2684, (2012).

239 **Xiong, Y., Deng, H., Nemer, M. & Johnsen, S.** Experimental determination of the solubility constant for magnesium chloride hydroxide hydrate ($Mg_3Cl(OH)_5$ center dot 4 H_2O, phase 5) at room temperature, and its importance to nuclear waste isolation in geological repositories in salt formations. *Geochimica et Cosmochimica Acta* **74**, 4605-4611, (2010).

240 **Langmuir, D., Mahoney, J. & Rowson, J.** Solubility products of amorphous ferric arsenate and crystalline scorodite ($FeAsO_4{\cdot}2H_2O$) and their application to arsenic behavior in buried mine tailings. *Geochimica et Cosmochimica Acta* **70**, 2942-2956, (2006).

241 **Cooke, R. C. & Kepkay, P. E.** The solubility of aragonite in seawater—I. Effect of pH and water chemistry at one atmosphere. *Geochimica et Cosmochimica Acta* **44**, 1071-1075, (1980).

242 **Bénézeth, P., Saldi, G. D., Dandurand, J. L. & Schott, J.** Experimental determination of the solubility product of magnesite at 50 to 200°C. *Chemical Geology* **286**, 21-31, (2011).

243 **Baron, D. & Palmer, C. D.** Solubility of jarosite at 4–35°C. *Geochimica et Cosmochimica Acta* **60**, 185-195, (1996).

244 **Bhuiyan, M., Mavinic, D. & Beckie, R.** A solubility and thermodynamic study of struvite. *Environmental technology* **28**, 1015-1026, (2007).

245 **Lasaga, A. C.** *Kinetic Theory in the Earth Sciences.* Princeton University Press. Princeton, New Jersey, USA, (1998).

246 **Salmon, S. U. & Malmstrom, M. E.** Quantification of mineral dissolution rates and applicability of rate laws: Laboratory studies of mill tailings. *Applied Geochemistry* **21**, 269-288, (2006).

247 **Fritz, B. & Noguera, C.** Mineral Precipitation Kinetics in *Thermodynamics and Kinetics of Water-Rock Interaction* Vol. 70,*Reviews in Mineralogy and Geochemistry* (eds Eric H. Oelkers & J. Schott) 371-410. Mineralogical Society of America, Chantilly, VA, USA, (2009).

248 **Lindsay, W. L.** *Chemical Equilibria in Soils.* Wiley, J. and Sons. New York, NY, USA, (1979).

249 **Inskeep, W. P. & Silvertooth, J. C.** Kinetics of hydroxayapatite precipitation at pH 7.4 to 8.4. *Geochimica et Cosmochimica Acta* **52**, 1883-1893, (1988).

250 **Stumm, W. & Morgan, J. J.** *Aquatic Chemistry: Chemical Equilibria and Rates in Natural Waters.* Wiley-Interscience. New York, NY, USA, (1996).

251 **Hemingway, B. S., Kittrick, J. A. & Peryea, F. J.** Relative solubilities of corundum, gibbsite, boehmite, and diaspore at standard state conditions- An addendum. *Clays and Clay Minerals* **37**, 566-567, (1989).

252 **Hyun, S. P. & Hayes, K. F.** Feasibility of using *in situ* FeS precipitation for TCE degradation. *Journal of Environmental Engineering-ASCE* **135**, 1009-1014, (2009).

253 **Wolthers, M., Van der Gaast, S. J. & Rickard, D.** The structure of disordered mackinawite. *American Mineralogist* **88**, 2007-2015, (2003).

254 **Morse, J. W. & Rickard, D.** Chemical dynamics of sedimentary acid volatile sulfide. *Environmental Science and Technology* **38**, 131A-136A, (2004).

255 **Tosca, N. J., Macdonald, F. A., Strauss, J. V., Johnston, D. T. & Knoll, A. H.** Sedimentary talc in Neoproterozoic carbonate successions. *Earth and Planetary Science Letters* **306**, 11-22, (2011).

256 **Environmental Security Technology Certification Program (ESTCP).** Bioaugmentation for Groundwater Remediation. Cost and Performance Report-ER-0515. U.S. Department of Defense, Arlington, VA, USA, http://www.clu-in.org/download/techfocus/biochlor/ER-0515-FR.pdf, (2010). Last access: May 2013.

257 **Szynalski, K.** *Ecophysiology and molecular identification of microbial populations involved in the reductive dechlorination of chloroethenes.* Ph.D. thesis, Ecole Polytechnique Fédérale de Lausanne, Lausanne, Switzerland. doi: 10.5075/epfl-thesis-2898, (2003).

258 **Yu, S.** *Kinetics and modeling investigations of the anaerobic reductive dechlorination of chlorinated ethylenes using single and binary mixed cultures and silicon-based organic compounds as slow release substrates*. Ph.D. thesis, Oregon State University, Corvallis, OR, USA, (2003).

259 **Rossi, P., Gillet, F., Rohrbach, E., Diaby, N. & Holliger, C.** Statistical assessment of variability of terminal restriction fragment length polymorphism analysis applied to complex microbial communities. *Applied and Environmental Microbiology* **75**, 7268-7270, (2009).

260 **Smits, T. H. M., Devenoges, C., Szynalski, K., Maillard, J. & Holliger, C.** Development of a real-time PCR method for quantification of the three genera *Dehalobacter*, *Dehalococcoides*, and *Desulfitobacterium* in microbial communities. *Journal of Microbiological Methods* **57**, 369-378, (2004).

261 **Adrian, L., Hansen, S. K., Fung, J. M., Goerisch, H. & Zinder, S. H.** Growth of *Dehalococcoides* strains with chlorophenols as electron acceptors. *Environmental Science & Technology* **41**, 2318-2323, (2007).

262 **Lanthier, M., Villemur, R., Lepine, F., Bisaillon, J. G. & Beaudet, R.** Geographic distribution of *Desulfitobacterium frappieri* PCP-1 and *Desulfitobacterium* spp. in soils from the province of Quebec, Canada. *FEMS Microbiology Ecology* **36**, 185-191, (2001).

263 **Daprato, R. C., Loffler, F. E. & Hughes, J. B.** Comparative analysis of three tetrachloroethene to ethene halorespiring consortia suggests functional redundancy. *Environmental Science & Technology* **41**, 2261-2269, (2007).

264 **Maillard, J., Charnay, M.-P., Regeard, C., Rohrbach-Brandt, E., Rouzeau-Szynalski, K., Rossi, P. & Holliger, C.** Reductive dechlorination of tetrachloroethene by a stepwise catalysis of different organohalide respiring bacteria and reductive dehalogenases. *Biodegradation* **22**, 949-960, (2011).

265 **Schott, J., Berner, R. A. & Sjöberg, E. L.** Mechanism of pyroxene and amphibole weathering—I. Experimental studies of iron-free minerals. *Geochimica et Cosmochimica Acta* **45**, 2123-2135, (1981).

266 **Sanemasa, I. & Katsura, T.** The dissolution of $CaMg(SiO_3)_2$ in acid solutions. *Bulletin of the Chemical Society of Japan* **46**, 3416-3422, (1973).

267 **Chen, Y. & Brantley, S. L.** Diopside and anthophyllite dissolution at 25° and 90°C and acid pH. *Chemical Geology* **147**, 233-248, (1998).

268 **Löffler, F. E., Yan, J., Ritalahti, K. M., Adrian, L., Edwards, E. A., Konstantinidis, K. T., Müller, J. A., Fullerton, H., Zinder, S. H. & Spormann, A. M.** *Dehalococcoides mccartyi* gen. nov., sp. nov., obligately organohalide-respiring anaerobic bacteria relevant to halogen cycling and bioremediation, belong to a novel bacterial class, *Dehalococcoidia* classis nov., order *Dehalococcoidales* ord. nov. and family *Dehalococcoidaceae* fam. nov., within the phylum *Chloroflexi*. *International Journal of Systematic and Evolutionary Microbiology* **63**, 625-635, (2012).

269 **Ulrich, K. U. & Pöthig, R.** Evidence for aluminium precipitation and phosphorus inactivation in acidified watershed-reservoir ecosystems. *Silva Gabreta* **4**, 185-198, (2000).

270 **Dickson, W.** Some effects of the acidification of Swedish lakes in *20 th Congress, Internationale Vereinigung fur Theoretische und Angewandte Limnologie*, (1978).

271 **Tanada, S., Kabayama, M., Kawasaki, N., Sakiyama, T., Nakamura, T., Araki, M. & Tamura, T.** Removal of phosphate by aluminum oxide hydroxide. *Journal of Colloid and Interface Science* **257**, 135-140, (2003).

272 **Seyama, H. & Soma, M.** Fe 2p spectra of silicate minerals. *Journal of Electron Spectroscopy and Related Phenomena* **42**, 97-101, (1987).

273 **Vilcaez, J., Yamada, R. & Inoue, C.** Effect of pH reduction and ferric ion addition on the leaching of chalcopyrite at thermophilic temperatures. *Hydrometallurgy* **96**, 62-71, (2009).

274 **Zhou, S. G., Zhou, L. X. & Fang, D.** Enhancing metal removal by coaddition of Fe^{2+} and S_0 as substrates of *acidithiobacillus ferrooxidans* for sewage sludge bioleaching. *Practice Periodical of Hazardous, Toxic, and Radioactive Waste Management* **12**, 159-164, (2008).

275 **Abdelouas, A., Lu, Y., Lutze, W. & Nuttall, H. E.** Reduction of U(VI) to U(IV) by indigenous bacteria in contaminated ground water. *Journal of Contaminant Hydrology* **35**, 217-233, (1998).

276 **Smidt, H., Akkermans, A. D. L., Van Der Oost, J. & De Vos, W. M.** Halorespiring bacteria-molecular characterization and detection. *Enzyme and Microbial Technology* **27**, 812-820, (2000).

277 **Sandrin, T. R. & Maier, R. M.** Impact of metals on the biodegradation of organic pollutants. *Environmental Health Perspectives* **111**, 1093, (2003).

278 **Pardue, J. H., Kongara, S. & Jones, J. W.** Effect of cadmium on reductive dechlorination of trichloroaniline. *Environmental Toxicology and Chemistry* **15**, 1083-1088, (1996).

279 **Kong, I.-C.** Metal toxicity on the dechlorination of monochlorophenols in fresh and acclimated anaerobic sediment slurries. *Water Science and Technology* **38**, 143-150, (1998).

280 **Gossett, J. M.** Measurement of Henry's law constants for C1 and C2 chlorinated hydrocarbons. *Environmental Science & Technology* **21**, 202-208, (1987).

281 **United States Environmental Protection Agency (US EPA).** HENRYWIN-Estimation Programs Interface Suite™ for Microsoft® Windows, v 4.11., Washington, DC, USA, http://www.epa.gov/opptintr/exposure/pubs/episuite.htm, (2012). Last access: May 2013.

282 **Abraham, M. H., Whiting, G. S., Fuchs, R. & Chambers, E. J.** Thermodynamics of solute transfer from water to hexadecane. *Journal of the Chemical Society-Perkin Transactions 2* **2**, 291-300, (1990).

283 **Agency for Toxic Substances and Disease Registry** Toxicological profile for vinyl chloride (Update). U.S. Department of Health and Human Services Public Health Service, Atlanta, GA, USA, http://www.atsdr.cdc.gov/toxprofiles/tp.asp?id=282&tid=51, (1997). Last access: May 2013.

284 **Grishchenkov, V., Townsend, R., McDonald, T., Autenrieth, R., Bonner, J. & Boronin, A.** Degradation of petroleum hydrocarbons by facultative anaerobic bacteria under aerobic and anaerobic conditions. *Process Biochemistry* **35**, 889-896, (2000).

285 **Toride, N., Leij, F. & Van Genuchten, M. T.** *The CXTFIT Code for Estimating Transport Parameters from Laboratory Or Filed Tracer Experiments.* US Salinity Laboratory Riverside, (1995).

286 **Rupakula, A., Kruse, T., Boeren, S., Holliger, C., Smidt, H. & Maillard, J.** The restricted metabolism of the obligate organohalide respiring bacterium *Dehalobacter restrictus*: lessons from tiered functional genomics. *Philosophical Transactions of the Royal Society B: Biological Sciences* **368**, (2013).

287 **Sun, Y., Wolcott, R. D. & Dowd, S. E.** Tag-encoded FLX amplicon pyrosequencing for the elucidation of microbial and functional gene diversity in any environment in *High-Throughput Next Generation Sequencing* 129-141. Springer, (2011).

288 **Weissbrodt, D. G., Shani, N., Sinclair, L., Lefebvre, G., Rossi, P., Maillard, J., Rougemont, J. & Holliger, C.** PyroTRF-ID: a novel bioinformatics methodology for the affiliation of terminal-restriction fragments using 16S rRNA gene pyrosequencing data. *BMC microbiology* **12**, 306, (2012).

289 **Bae, H.-S., Moe, W. M., Yan, J., Tiago, I., Da Costa, M. S. & Rainey, F. A.** *Propionicicella superfundia* gen. nov., sp. nov., a chlorosolvent-tolerant propionate-forming, facultative anaerobic bacterium isolated from contaminated groundwater. *Systematic and Applied Microbiology* **29**, 404-413, (2006).

290 **Rosso, J. J. & Rimstidt, J. D.** A high resolution study of forsterite dissolution rates. *Geochimica et Cosmochimica Acta* **64**, 797-811, (2000).

291 **Rickard, D.** Kinetics of FeS precipitation: Part 1. Competing reaction mechanisms. *Geochimica et Cosmochimica Acta* **59**, 4367-4379, (1995).

292 **Lijklema, L.** Interaction of orthophosphate with iron (III) and aluminum hydroxides. *Environmental Science & Technology* **14**, 537-541, (1980).

293 **Hsu, P. H.** Comparison of iron (III) and aluminum in precipitation of phosphate from solution. *Water Research* **10**, 903-907, (1976).

294 **Ghassemi, M. & Recht, H. L.** Water Pollution Control Research Series 17010 EKI 09/71: Phosphate Precipitation with Ferrous Iron. United States Environmental Protection Agency (US EPA), Wahington, DC, USA, http://nepis.epa.gov/, (1971). Last access: May 2013.

295 **Schott, J. & Berner, R. A.** Dissolution mechanisms of pyroxenes and olivines during weathering in *The chemistry of weathering* (ed J. I. Drever) Kluwer Academic, Hingham, MA, USA, (1985).

296 **Casey, W. H., Westrich, H. R., Banfield, J. F., Ferruzzi, G. & Arnold, G. W.** Leaching and reconstruction at the surfaces of dissolving chain-silicate minerals. *Nature* **366**, 253-256, (1993).

297 **Bryant, M., Campbell, L. L., Reddy, C. & Crabill, M.** Growth of *Desulfovibrio* in lactate or ethanol media low in sulfate in association with H_2-utilizing methanogenic bacteria. *Applied and Environmental Microbiology* **33**, 1162-1169, (1977).

298 **Seeliger, S., Janssen, P. H. & Schink, B.** Energetics and kinetics of lactate fermentation to acetate and propionate via methylmalonyl-CoA or acrylyl-CoA. *FEMS Microbiology Letters* **211**, 65-70, (2002).

299 **Liu, Y., Balkwill, D. L., Aldrich, H. C., Drake, G. R. & Boone, D. R.** Characterization of the anaerobic propionate-degrading syntrophs *Smithella propionica* gen. nov., sp. nov. and *Syntrophobacter wolinii*. *International Journal of Systematic Bacteriology* **49**, 545-556, (1999).

300 **Imachi, H., Sekiguchi, Y., Kamagata, Y., Hanada, S., Ohashi, A. & Harada, H.** *Pelotomaculum thermopropionicum* gen. nov., sp. nov., an anaerobic, thermophilic, syntrophic propionate-oxidizing bacterium. *International Journal of Systematic and Evolutionary Microbiology* **52**, 1729-1735, (2002).

301 **Oude Elferink, J. W. H. S., Visser, A., Hulshoff Pol, L. W. & Stams, A. J.** Sulfate reduction in methanogenic bioreactors. *FEMS Microbiology Reviews* **15**, 119-136, (1994).

302 **Müller, N., Worm, P., Schink, B., Stams, A. J. & Plugge, C. M.** Syntrophic butyrate and propionate oxidation processes: from genomes to reaction mechanisms. *Environmental Microbiology Reports* **2**, 489-499, (2010).

303 **Akasaka, H., Ueki, A., Hanada, S., Kamagata, Y. & Ueki, K.** *Propionicimonas paludicola* gen. nov., sp. nov., a novel facultatively anaerobic, Gram-positive, propionate-producing bacterium isolated from plant residue in irrigated rice-field soil. *International Journal of Systematic and Evolutionary Microbiology* **53**, 1991-1998, (2003).

304 **Sineriz, F. & Pirt, S. J.** Methane production from glucose by a mixed culture of bacteria in the chemostat: The role of *Citrobacter*. *Journal of General Microbiology* **101**, 57-64, (1977).

305 **Das, D. & Veziroglu, T. N.** Hydrogen production by biological processes: a survey of literature. *International Journal of Hydrogen Energy* **26**, 13-28, (2001).

306 **Bowman, K. S., Rainey, F. A. & Moe, W. M.** Production of hydrogen by *Clostridium* species in the presence of chlorinated solvents. *FEMS Microbiology Letters* **290**, 188-194, (2009).

307 **Schinschel, C. & Simon, H.** Preparation of pyruvate from (R)-lactate with *Proteus* species. *Journal of Biotechnology* **31**, 191-203, (1993).

308 **Jackson, F.** Pyruvate accumulation and development of thiamine deficiency in cultures of *Proteus vulgaris*. *Journal of General Microbiology* **16**, 711-720, (1957).

309 **Wiegel, J., Tanner, R. & Rainey, F. A.** An introduction to the family *Clostridiaceae*. *Prokaryotes* **4**, 654-678, (2006).

310 **Diekert, G. & Wohlfarth, G.** Metabolism of homoacetogens. *Antonie Van Leeuwenhoek* **66**, 209-221, (1994).

311 **Lovley, D. R., Roden, E. E., Phillips, E. & Woodward, J.** Enzymatic iron and uranium reduction by sulfate-reducing bacteria. *Marine Geology* **113**, 41-53, (1993).

312 **Reipurth, B., Jewitt, D. & Keil, K.** *Protostars and Planets V*. University of ARIZONA Press. Tucson, AZ, USA, (2007).

313 **Dubikova, M., Cambier, P., Sucha, V. & Caplovicova, M.** Experimental soil acidification. *Applied Geochemistry* **17**, 245-257, (2002).

314 **Marín, M., Pedregosa, A., Ríos, S., Luisa Ortiz, M. & Laborda, F.** Biodegradation of diesel and heating oil by *Acinetobacter calcoaceticus* MM5: Its possible applications on bioremediation. *International Biodeterioration & Biodegradation* **35**, 269-285, (1995).

315 **Barbeau, C., Deschenes, L., Karamanev, D., Comeau, Y. & Samson, R.** Bioremediation of pentachlorophenol-contaminated soil by bioaugmentation using activated soil. *Applied Microbiology and Biotechnology* **48**, 745-752, (1997).

316 **Criddle, C., DeWitt, J., Grbić-Galić, D. & McCarty, P.** Transformation of carbon tetrachloride by *Pseudomonas* sp. strain KC under denitrification conditions. *Applied and Environmental Microbiology* **56**, 3240-3246, (1990).

317 **Banfield, J. F., Veblen, D. R. & Jones, B. F.** Transmission electron microscopy of subsolidus oxidation and weathering of olivine. *Contributions to Mineralogy and Petrology* **106**, 110-123, (1990).

Curriculum Vitae

Elsa Lacroix

PERSONAL DATA

Private address	Avenue de Tivoli, 4 1007 Lausanne Switzerland
Professional address	Laboratory for Environmental Biotechnology (LBE) ENAC – IIE Ecole Polytechnique Fédérale de Lausanne (EPFL) Station 6, Bâtiment CH CH-1015 Lausanne Switzerland
Tel	+41 (0)21 693 47 21
E-mail	elsa.lacroix@epfl.ch

PROFESSIONAL EXPERIENCE

Since 04/2009	**PhD thesis** Laboratory for Environmental Biotechnology (LBE) & Ecological Engineering Laboratory (ECOL) Ecole Polytechnique Fédérale de Lausanne (EPFL), Lausanne, Switzerland. Thesis directors: Prof. Christof Holliger & Prof. Andrew Barry Thesis title: Using silicate mineral particles for pH control during *in situ* bioremediation of chloroethene source zones.
08/2008-11/2008	**Centre Régional pour l'Eau Potable et l'Assainissement à faible coût (CREPA),** Sokodé, Togo. Internship. Main project: Evaluation of the groundwater table contamination of Sokodé.
01/2007 – 05/2007	**Trébaol Consulting: Environnement & Aquatic Ressources,** Montpellier, France. Internship. Main project: Impact of bivalves fisheries on marine ecosystem in Mauritanie.
07/2006 – 11/2006	**Coastal Marine Group,** Hamilton University, Hamilton, New Zealand. Internship. Main project: Mangrove expansion and their human removal in Tauranga Harbour.

EDUCATION

Since 04/2009	**PhD thesis** Laboratory for Environmental Biotechnology (LBE) & Ecological Engineering Laboratory (ECOL) Ecole Polytechnique Fédérale de Lausanne (EPFL), Lausanne, Switzerland. Thesis directors: Prof. Christof Holliger & Prof. Andrew Barry Thesis title: Using silicate mineral particles for pH control during *in situ* bioremediation of chloroethene source zones.
09/2007 – 07/2008	**Exchange year: Environmental Sciences and Engineering** EPFL (Ecole Polytechnique Fédérale de Lausanne), Lausanne, Switzerland
09/2004 - 06/2006	**Master degree in Engineering: Water Science and Technology** Polytech' Montpellier, France
09/2002 - 06/2004	**DEUG Life Science** (two-year university diploma) University Victor Segalen Bordeaux 2, France

PRESENTATIONS AT SCIENTIFIC CONFERENCES

2012 **Oral presentation** at the 8th International Conference on Remediation of Chlorinated and Recalcitrant Compounds, May 21- 24, Monterey, California, USA. *Utilization of silicate minerals for pH control during in Situ bioremediation of chlorinated solvents.*

2011 **Oral presentation** at the 5th European Bioremediation Conference, July 4-7, Chania, Crete, Greece. *Utilization of silicate minerals for pH control during in situ bioremediation of chlorinated solvents.*

2011 **Poster presentation** at the 4th Swiss Microbial Ecology (SME) Meeting, February 2-4, Engelberg, Switzerland. *Influence of pH on dehalogenating bacteria for bioremediation of chlorinated solvents.*

2010 **Poster presentation** at the Annual Assembly of the Swiss Society of Microbiology (SSM). Zurich, June 24-25. *Buffering agent for pH control during in situ bioremediation of chlorinated solvent source zones.*

PUBLICATIONS

Lacroix, E., Brovelli, A.,Maillard, J., Rohrbach, E., Barry, D. A. & Holliger, C. Evaluation of long-term acid neutralizing capacity of silicate minerals for PCE bioremediation in continuous-flow columns. In preparation.

Lacroix, E., Brovelli, A., Barry, D. A. & Holliger, C. Use of silicate minerals for pH control during reductive dechlorination of chloroethenes in batch cultures of different microbial consortia. Submitted to *Applied and Environmental Microbiology*.

Lacroix, E., Brovelli, A., Holliger, C. & Barry, D. A. Control of groundwater pH during bioremediation: Improvement and validation of a geochemical model to assess the buffering potential of ground silicate minerals. Submitted to *Water, Air and Soil Pollution*.

Lacroix, E., Brovelli, A., Holliger, C. & Barry, D. A. Evaluation of silicate minerals for pH control during bioremediation: application to chlorinated solvents. *Water, Air and Soil Pollution* **223**, 2663-2684, (2012).

AWARDED POSTER PRESENTATION

2013 *Are silicate minerals good buffering agents for in situ bioremediation of perchloroethylene?*
ENAC Research day, EPFL. April 23, Lausanne , Switzerland.
1st Poster Prize

2012 *pH control strategy for in situ bioremediation of chlorinated solvents.*
ENAC Research day, EPFL, June 15, Lausanne, Switzerland.
3rd Poster Prize

2011 *pH control with silicates minerals for in situ bioremediation of chlorinated solvents*.
ENAC Research day, EPFL, June 8, Lausanne, Switzerland.
1st Poster Prize

Remerciements

Je souhaite exprimer mes remerciements à toutes les personnes qui m'ont accompagnée et soutenue durant ces années de doctorat. Je tiens à remercier tout particulièrement mes deux co-directeurs de thèse Christof Holliger et Andrew Barry pour leur excellent encadrement, leurs conseils avisés et pour la grande confiance qu'ils m'ont accordée durant mon parcours au sein des laboratoires LBE (Laboratoire de Biotechnologie Environnementale) et ECOL (Laboratoire de Technologie Ecologique). Le cadre de travail idéal qu'ils m'ont fournit a, sans aucun doute, contribué à faire de ce doctorat une expérience extrêmement enrichissante tant d'un point de vue professionnel que personnel. Je tiens à remercier tout particulièrement Christof Holliger pour son soutien sans faille dans les moments difficiles ainsi que pour sa grande disponibilité et son aide durant les derniers mois de rédaction de la thèse.

Je remercie la présidente de mon jury de thèse, Prof. Kristin Schirmer, ainsi que les rapporteurs, Prof. Phillip Binning, Prof. Marin Schroth et Prof. Tamar Kohn pour avoir pris le temps de lire mon travail et pour leur participation à ma défense de thèse.

Cette thèse est le fruit de diverses collaborations; à ce titre je tiens à remercier chaleureusement Alessandro Brovelli pour son aide précieuse durant toutes les étapes de ce travail, de la conception des expériences à l'écriture des articles. Ce fut un grand plaisir pour moi de travailler avec lui.

Je tiens également à exprimer ma gratitude à Julien Maillard et Emmanuelle Rohrbach pour notre stimulante collaboration et pour leurs conseils avisés dans le domaine de la biologie moléculaire. Un grand merci également à David Weissbrodt pour son aide avec le software pyro-TRF-ID. Je souhaite également remercier Pierre Rossi, pour ses conseils scientifiques ainsi que pour les discussions intéressantes de la pause de midi qui ont, sans conteste, contribué à élargir ma culture générale scientifique. Un merci tout spécial à Nevenka Adler pour sa présence lumineuse et enthousiaste et ses conseils avisés.

Je souhaite exprimer ma profonde gratitude à Jean Pierre Kradolfer, pour son aide technique au labo, son inventivité géniale et sa capacité à trouver une solution à n'importe quel type de problème. Un grand merci également à Marc Deront pour son excellent travail en tant que spécialiste IT. Merci également aux apprentis pour leur excellente assistance, en particulier Guy De Bourbon-Parme et Julie Luche.

Je souhaite également remercier les secrétaires Sonja Desplos, Marie Sudki et Esther von Arx pour leur travail indispensable et leur aide quotidienne.

Enfin, je ne saurais oublier de remercier les étudiants de master et stagiaires qui ont largement contribué aux travaux de recherches présentés dans cette thèse: Nicole Munz, Louise Gilbert, Laurine Monneret, Naomi Dumas et Ilham Sbaiti. Cette thèse n'aurait pas vu le jour sans leur active participation et leur forte implication et je leur souhaite beaucoup de succès dans leur future vie professionnelle.

Dans le cadre des collaborations externes, je souhaite remercier Nicolas Meisser et Jasquelin Pena de l'Université de Lausanne pour leurs précieux conseils et pour avoir partagé avec moi leurs connaissances en minéralogie et géochimie. Merci également à Simon Vainberg de la société Shaw environmental, Inc. pour son aide à distance depuis les Etats Unis. Un grand merci également à toute l'équipe du Laboratoire Central Environnemental, en particulier à Karine Vernez et Elena Rossel.

Ces quatre années au sein du LBE ont été un réel plaisir grâce à la présence d'une équipe de choc, sympathique et dynamique. Je tiens donc à remercier également mes collègues: Nathalie Bachmann, Samuel Lochmatter, Noam Shani, Aamani Rupakula, Magalie Bassan, Stephen Mackay, Eduardo Pereira Gomez, Brian Reinsch, Géraldine Buttet, Gabrielle Hack, Sonia Tarnawski, Mariluz Bagnoud,

Martina Praveckova et tous les autres. Un grand merci à tous pour les moments de détente et la bonne ambiance générale. Je souhaite remercier également mes collègues du laboratoire ECOL, Jonas Margot, Amir Razmi, Sylvain Coutu et les autres.

Sur le plan personnel, je voudrais spécialement remercier tout les habitants de Tivoli 4 qui ont été en quelque sorte une seconde famille pour moi durant ces quatre années. Merci à l'italian team : Léonardo Brizi et Luca Fontanesi pour m'avoir fait découvrir le monde des bosons et l'art de préparer la pasta. Merci également à Michela Canevascini pour avoir apporter feng shui et sérénité dans notre humble demeure. Enfin, un merci tout spécial aux derniers habitants en date : Elsa Jejcic et Thibault Duretz pour m'avoir supportée, soutenue et nourrie pendant la rédaction de la thèse.

Je tiens également à remercier très chaleureusement tout mes amis de Lausanne grâce auxquels ma vie en Suisse a été un vrai plaisir. Merci pour les belles sorties en montagnes, les voyages, les soirées de folie et les barbecues au bord du lac : Merci à Anurag Mangla, Anna Kounine, Evelyne Ruchti, Luis Miguel Fidalgo, Fabio Donati, Jonathan Besuchet, Belinda Bates, Lorric Ziegler, Friedman Zenke, Michael Mattle et tous les autres. Une pensée spéciale pour la famille Brennecke-Angelim et la petite Mélina et un grand merci à Carlos Stein, chef de file du mouvement horizontal, pour son amitié et son soutien dans les périodes de crise.

Je souhaite remercier de tout mon cœur mes parents, Jean Pierre Lacroix et Elisabeth Oules, pour leur soutien indéfectible et leur présence malgré la distance. Une tendre pensée également pour ma grand-mère Nanie qui m'a, à sa manière, transmis l'intérêt pour la protection de l'environnement. Merci également à mes grands parents Irène et André pour leur soutien durant toute mes études.

Pour finir, je voudrais dédier cette thèse à Flo, pour la force et la joie de vivre que tu m'apporte au quotidien et pour l'avenir que je souhaite construire avec toi. Ti voglio bene per davvero…